UNDERSTANDING THE FORMATION OF DISTANT GALAXIES IN THE CONTEXT OF LARGE-SCALE STRUCTURE

by

Yun Huang

A Dissertation

Submitted to the Faculty of Purdue University

In Partial Fulfillment of the Requirements for the degree of

Doctor of Philosophy

Department of Physics and Astronomy

West Lafayette, Indiana

May 2022

THE PURDUE UNIVERSITY GRADUATE SCHOOL
STATEMENT OF COMMITTEE APPROVAL

Dr. Kyoung-Soo Lee, Chair

Department of Physics and Astronomy

Dr. Matthew Lister

Department of Physics and Astronomy

Dr. Dan Milisavljevic

Department of Physics and Astronomy

Dr. Francis Robicheaux

Department of Physics and Astronomy

Approved by:

Dr. Gabor Csathy

Dedicated to my loving family for their love and support.

ACKNOWLEDGMENTS

First, I would like to express my deepest gratitude to my supervisor, Dr. Kyoung-Soo Lee. She is the person who took my hand and led me to the exhilarating world of astronomy. She taught me how to think, work, and write as an independent scientist. She has always been generous to give encouragement, compliments and suggestions. Without her support, I would not have made it. In addition, I would like to thank my committee members, Dr. Matthew Lister, Dr. Dan Milisavljevic, and Dr. Francis Robicheaux, who provided great help and valuable suggestions during my Ph.D. study. Moreover, I extend my gratitude to all faculty members of Purdue astrophysics group for creating such a wonderful academic atmosphere. I developed my knowledge and presentation skills in the weekly astrophysics journal club. Specially thanks to the department secretaries, Sandy Formica and Janice Thomaz who are always there for support.

Also, I am deeply indebted to my collaborators. Dr. Rui Xue, Dr. Nicola Malavasi, and Dr. Ke shi helped me through my most difficult, early graduate years, and continuously offered valuable suggestions for professional improvement on my research works. Thanks to Vandana Ramakrishnan, Dr. Maria Celeste Artale, Kaustub Anand, Eshwar K Puvvada, Sowon Lee, and Lauren Warshaw for insightful discussions on projects.

Most importantly, I would like to thank my friends. I am grateful to Jingshuang Chen, Zhujing Xu, Jijun Chen, Yuqing Zhu, Fan Zhang, Xuejun Zhao, and Yibiao Ying for sharing the enjoyable days at Purdue. Thanks to Yujie Ou, Chi Zhang and Lulu Zhang for long-lasting friendships. Special thanks to Zhe Li for your love and support.

Finally, my greatest appreciation to my family, especially to my parents and my grandparents for their unconditional love and support throughout my life. I could not have done it without you.

TABLE OF CONTENTS

LIST OF TABLES

LIST OF FIGURES

ABSTRACT

Understanding the formation and evolution of galaxies is one of the most fundamental questions in modern astronomy. While it is widely accepted that galaxy formation needs to be understood in the context of cosmic structure formation of dark matter, a complex interplay of different physical processes that drive galaxy formation makes it challenging to elucidate how the large-scale environment of dark matter influences galaxies, particularly in their formative epoch ($z \gtrsim 2$).

As the most luminous nebular emission arising from star formation, Lyα provides a promising and effective tool to study the young universe and nascent galaxies. At $z > 2$, Lyα emission is redshifted into the visible window that is detectable by ground-based telescopes. Existing studies also suggest that strong Lyα-emitting galaxies represent a young and low-mass galaxy population and therefore are the best visible tracers of the large-scale structure of the distant universe.

In this thesis, I present two complementary studies designed to address these questions using Lyα emission as a cosmological tool. In Chapter 2, I investigate the kinematics and spatial distribution of the gas-phase interstellar and circumgalactic media using compact and diffuse Lyα emission in and around distant galaxies. I also carry out a comprehensive characterization of how Lyα properties correlate with other galaxy properties and the environment that galaxies reside in. In Chapter 3, I explore how Lyα-emitting galaxies trace the large-scale structure characterized by other means; I also conduct a detailed investigation of the distribution of different 'types' of galaxies and H I gas in and around the most massive cosmic structure known to date. These investigations are informative in building clear expectations for the ongoing and upcoming experiments – including the Legacy Survey for Space and Time, James Webb Space Telescope, Dark Energy Spectroscopic Instruments, and Hobby-Eberly Telescope Dark Energy eXperiment – in obtaining a detailed picture of galaxy evolution in the context of their environments.

1. INTRODUCTION

The discovery of dark matter and dark energy has profoundly reorganized our understanding of the universe. According to observations, galaxies and baryons represent the tip of the iceberg of the universe. The bulk of the mass-energy content is in the form of 'dark matter' and 'dark energy' that are not observable via traditional optical telescope. Of these, dark matter interacts through gravity and forms the large-scale structure of the universe. Baryons fall into the potential wells and subsequently form stars. Thus, there exists a close connection between galaxy formation and the large-scale structure of the underlying dark matter.

Understanding galaxy formation is one of the biggest questions of modern astronomy. Although the structure formation and merger histories of dark matter can be predicted via N-body simulation, understanding key astrophysical processes governing galaxy formation in this context is challenging. Even the state-of-the-art magnetohydrodynamical simulations are incapable of fully elucidating the complex interplay among the diverse physical mechanisms governing galaxy formation (e.g., [1]).

My thesis work is focused on two observational fronts that are crucial to obtaining a comprehensive picture of how galaxies form and evolve throughout cosmic time. First, I investigate spatial and kinematic structures of the gas-phase interstellar and circumgalactic media in distant galaxies, which has wide-ranging implications on galaxy evolution and cosmic reionization. Second, I conduct a comprehensive census of galaxies residing in a massive cosmic structure and characterized their spatial distribution; the result of my study sheds light on the structural morphology of protoclusters and the environmental effects on physical properties of high-redshift galaxies.

This thesis is organized as follows. In Chapter 1, I introduce key concepts and background context to highlight the current gap in our knowledge. To this end, I will describe the current framework of galaxy- and structure formation; I will also discuss what is currently known about protocluster formation and introduce observational techniques I will utilize to identify high-redshift galaxies. In Chapter 2, I present detailed characterization of the physical properties of galaxies and of the interstellar and circumgalactic media around them. In Chapter 3, I will discuss a comprehensive census of galaxies in and around the most massive

cosmic structures in the context of the large-scale structure. In Chapter 4 I will summarize my work and discuss the future directions in the field of cluster formation.

1.1 Hierarchical Structure Formation

1.1.1 A Brief History of the Universe

The universe began with a hot Big Bang about 13.8 billion years ago. The very first period of the history (10^{-43} s) is called the Planck Epoch. During this epoch, the temperature of the universe was so high that particles could not form, and the four fundamental forces – gravitation, electromagnetism, weak, and strong nuclear force – were all unified. In a short time, gravitation separated from the unification, and inflation happened. The space expanded by a factor of 10^{26} during a time period on the order of 10^{-36} to 10^{-32} seconds [2]–[5]. During this epoch, minuscule density perturbations were generated by quantum effects, which later became the seeds of the structures observed in today's universe.

Inflation caused the temperature of the universe sharply to drop from $> 10^{27}$ K to 10^{15} K. Interactions between quarks became weaker and hadrons started to form. With time, the universe continued expansion and cooling. Protons and neutrons formed a second after the birth of the universe and the history of baryons began. ≈370,000 years later, the universe was cool enough for neutral atoms to form ('recombination' [6]). Photons decoupled from other particles and began to travel freely. For the first time, the universe became transparent. The photons that emerged at this epoch are observable today (cosmic microwave background or CMB [7]).

The universe remained optically dark for hundreds of millions of years in the Dark Ages. The first stars were born $\sim$ 400 million years after the Big Bang and subsequently galaxies emerged. Galaxies grew in size and mass via accretion and mergers and then coalesced into groups and clusters under gravitation. The ultraviolet photons emitted from the first generation of stars and galaxies reionized neutral gas. The universe became transparent to ultraviolet (UV) photons. Since then, astronomical objects continued to form and evolve and shaped the observable universe. The timeline of the evolution of the universe is shown in Figure 1.1.

Baryons – the observable portion of galaxies – only account for $\sim 5\%$ of the total matter-energy content. The majority of the matter in the universe is in the form of 'dark matter'. It is challenging to observe dark matter with a traditional telescope since dark matter does not interact with baryons or radiation except through gravitation. However, dark matter has profound effects on the formation of cosmic structures. Despite its large mass budget, the density perturbations of dark matter were not washed away by the dominant radiation force in the early universe. With time, small density fluctuations grew and formed potential wells which later became the sites of galaxy formation.

As a natural consequence of gravitation, the expansion of the universe is believed to have slowed down. However, the distance-redshift measurements of Type Ia supernovae [8], [9] strongly suggest that the expansion is accelerating. 'Dark energy' is introduced to explain the supply of the expansion as well as the acceleration. The nature of dark energy remains unknown, though the effect can be simplified as a gravitational force with a negative mass density that pushes objects away. Dark energy behaves similarly to the cosmological constant Λ first introduced by Albert Einstein in his theory of general relativity.

Putting things together, the cold dark matter model with cosmological constant Λ (ΛCDM) suggests that the universe consists of 27% dark matter (of which 5% are baryons) and 68% dark energy and is flat (in other words, described by Euclidean geometry) [10]. The expectations for a ΛCDM cosmology are in excellent agreements with observations from Wilkinson Microwave Anisotropy Probe (WMAP) [11], [12].

1.1.2 Structure Formation

In the ΛCDM paradigm, cosmic structure formation occurs in a hierarchical manner. Minuscule quantum fluctuations of matter density provide the seeds of structure formation. Once the overdense regions reach a critical size (mass), gravitation overcomes the expansion of the universe and pulls particles together. The threshold is called Jeans' length (mass) scale [13]. Overdensities grow non-linearly and subsequently collapse into self-gravitating bodies known as dark matter 'halos'. The regions of highest density contrasts collapse earlier than those of lower contrasts. Over time, these dark matter halos gradually grow in mass

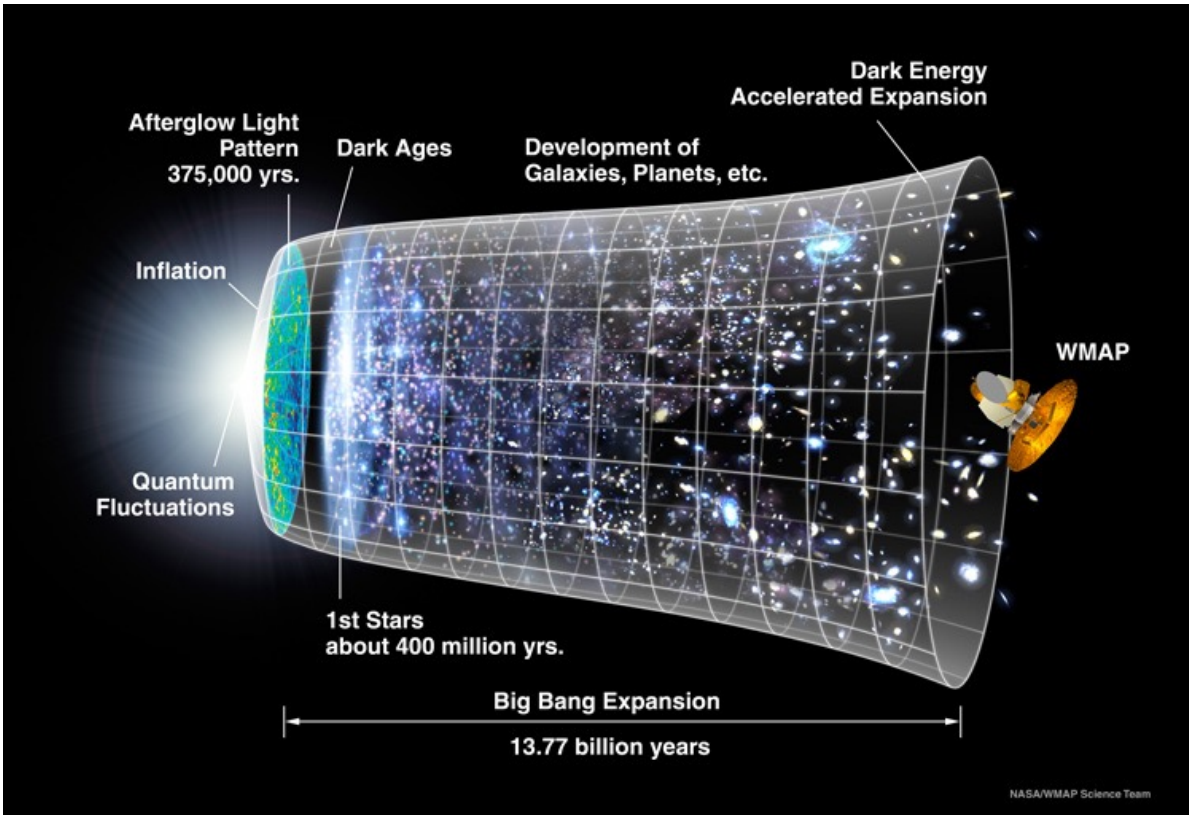

Figure 1.1. A diagram of the universe from the Big Band to the present. Image Credit: NASA/WMAP Science Team.

and size via steady mass accretion from the cosmic web as well as via mergers with other halos [14]–[20].

Since dark matter only interacts via gravity, it is possible to predict the growth and the spatial distribution of dark matter halos using numerical methods. Many cosmological N-body simulations exist to date. These simulations are run assuming dark matter as discrete point particles using the initial conditions informed by the cosmological parameters measured by CMB experiments. As such, these simulations can trace the hierarchical merging history of $\sim 10^{10}$ dark matter 'particles' in a large cosmological volume and can predict the matter distribution in the universe at any redshift, and more crucially, the evolution of the observed universe [21], [22].

Figure 1.2 shows the evolution of a Coma-like dark matter halo over cosmic time, based on Millennium Simulation II [23]. At $z = 6.2$, the mass density is relatively uniform at

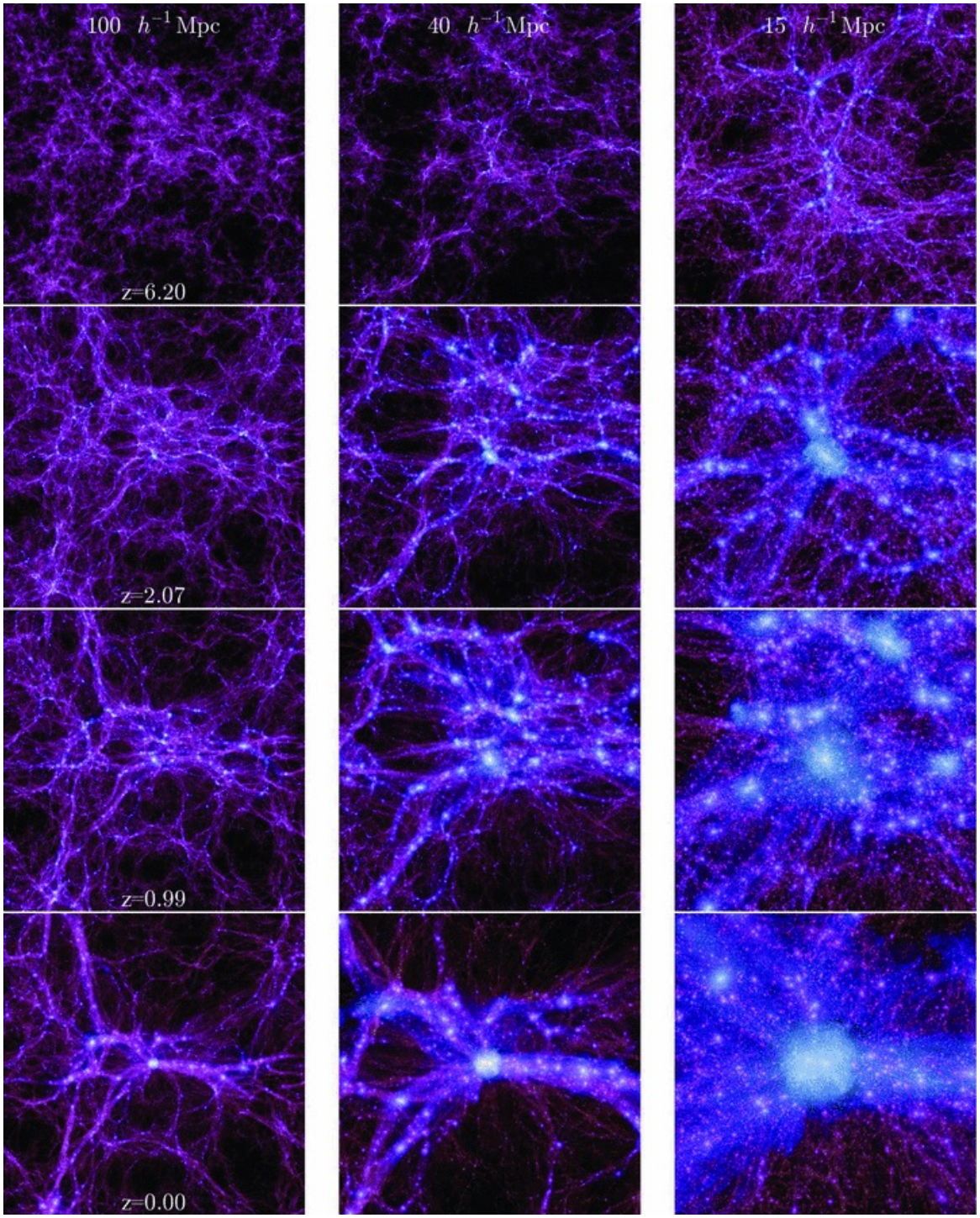

Figure 1.2. The evolution of a massive dark matter halo at $z = 6.2$, 2.07, 0.99, and 0 from top to bottom. At each redshift, subsequent panels are shown at three comoving scales (100, 40, and 15 h^{-1} Mpc from left to right). Figure credit: Millennium Simulation Team [23]).

100 h^{-1} Mpc scale[1] while density contrast is detectable at 15 h^{-1} Mpc scale. Over time, the central overdensity region became increasingly larger in size and more significant in density contrast. The nearby satellite halos also grew in size and density, however, more compact and less pronounced than the parent halo.

1.1.3 Galaxy Formation

In the ΛCDM paradigm, the formation process of galaxies mirrors that of cosmic structures, as the potential wells of dark matter halos serve as the sites where baryons fall in, cool down, and subsequently form stars [18], [24]–[28]. While the basic picture is clearly established within the cosmological framework, how galaxies form and evolve is poorly understood due to the complexity of relevant physical processes. In this section, I will discuss key astrophysical processes essential to understanding galaxy formation.

Gas cooling is a critical step of galaxy formation. As gas flow into dark matter halos, it loses energy primarily through radiative cooling. Atoms that are initially excited or ionized via collisions decay to their ground state or recombine with electrons. Both processes emit photons that carry the energy from the gas. Gas cooling directly results in the loss of the thermal pressure support that prevents gravitational inflow. Therefore, the net effect of cooling is that baryons accumulate as dense, cold gas at the potential wells constructed by dark matter halos.

As gas cools and flows inward, eventually it will collapse under its own gravity and star formation is triggered. The evolutionary paths of stars are predominantly determined by their initial masses, as massive stars are short-lived but exhibit higher brightness, and low-mass stars long-lived and faint. Clear expectations of integrated stellar light in a galaxy can be built based upon stellar population synthesis models, which combine the evolutionary paths of stars in all masses.

One of the key processes governing galaxy formation is referred to as 'feedback'. Supernovae explosions and stellar winds from massive hot stars inject momentum and energy

[1]↑h is the dimensionless Hubble constant. The relation between h and Hubble constant H_0 is expressed as: $H_0 = 100h$ km s^{-1} Mpc^{-1}.

into the interstellar and circumgalactic medium (ISM and CGM: [29]–[34]). The ubiquity of supermassive black holes at the center of local galaxies [35], [36] and a tight correlation between their masses and the velocity dispersion of the bulge of the host galaxy (known as the $M_{\rm BH} - \sigma$ relation: [37]–[40]) strongly suggests that active galactic nuclei (AGN) also play a crucial role by heating the ambient medium and by suppressing the gas inflow. Both stellar and AGN feedback processes can effectively suppress star formation – by heating the gas or ejecting it out of the galaxy – thereby shaping the subsequent evolution of the host galaxy.

Galaxy's large-scale environment also has a profound influence on the formation and evolution of galaxies. In high-density environments, the accretion rates of infalling gas and the incidence of galaxy interactions are expected to be higher than the field average, fostering enhanced star formation activities in galaxies. Existing observations clearly show that older/redder/massive galaxies are hosted by more massive dark matter halos than younger/bluer/less-massive galaxies [41]–[45]. A merger of gas-rich galaxies is expected to efficiently funnel the remaining gas into galaxies' center, triggering a massive starburst [46]–[49] and/or AGN activity [50]–[53], which will ultimately 'quench' star formation and create old massive elliptical galaxies.

1.2 Protocluster and Large-scale Structure

The large-scale environment has profound influence on the formation and evolution of galaxies therein. This is most clearly illustrated in the densest cosmic structures – galaxy clusters. Observations show that local cluster galaxies form a tight red sequence in the color-magnitude diagram (e.g., [54]). The redshift evolution of cluster red sequence suggests that they underwent accelerated formation in the first several billion years followed by swift quenching. Since then, they have been evolving passively [55]–[59]. While this general picture is accepted, it remains a matter of debate how and when the local environment manifested its effect. In order to elucidate the role of environment on the evolution of galaxies, it is

crucial to identify the progenitors of massive clusters, or 'protoclusters', and directly witness the galaxy formation therein.

At the peak epoch of galaxy assembly in clusters ($z \sim 2-4$), the cosmic star formation rate density and the black hole accretion rate density are much higher than today, and a considerable amount of this heightened activity is obscured by dust [60]. Cluster galaxies are also affected by complex physical processes that are enhanced in high-density environments. The accretion rates of infalling gas and the incidence of galaxy interactions are expected to be much higher in cluster environments, which fosters enhanced in-situ star formation in galaxies. Mergers of gas-rich galaxies include an ultra-luminous infrared galaxy (ULIRG, [61]) phase which efficiently converts the majority of their gas into stars over a short timescale. A popular hypothesis is that highly dissipative gas-rich mergers may also help the efficient feeding of gas into the central black hole and trigger an AGN activity, which then ultimately 'quenches' star formation therein and transforms the galaxy into an old and massive cluster elliptical such as that observed today [52]. Depending on the viewing angle and phase of individual galaxies in this 'merger-AGN-quenching' cycle, protocluster galaxies may be observed as a ULIRG (also referred to as submillimeter galaxies, SMG), an X-ray source, a quasar, a Lyα nebula, or a massive quiescent galaxy. Thus, a census of these galaxy 'types' within protoclusters and how these galaxies populate within the large-scale structure are crucial to understanding how the high-density environment drives the evolution.

So far there are $\sim$ 20 confirmed protoclusters at $z > 2$ with a much larger number of candidates from Herschel/Planck/Subaru HSC surveys; the number is expected to grow fast with the Legacy Survey of Space and Time (LSST, [62]). However, the full exploitation of these structures to elucidate a complete and unbiased picture of galaxy formation in protocluster environments and their evolutionary connection to the low-redshift clusters will ultimately require the panchromatic view, which is currently lacking. Currently, there are two primary limitations with existing surveys. First of all, detailed knowledge of the structure identifying different regions (core, outskirts, filaments, voids, and field) is critical not only to quantifying the environmental effects on its constituents but also to determining their descendant ('present-day') masses. Such information is lacking in most of the known systems. Secondly, there is a fundamental disconnection between optical and infrared/mil-

limeter studies of protoclusters. A truly full census of cluster constituents has not been made.

1.2.1 Identifying High-redshift Protoclusters

It is challenging to distinguish galaxies in protoclusters from those in the field due to the absence of a well-defined galaxy red sequence at high redshift. A conventional method of finding protoclusters is by measuring galaxy density in a large cosmic volume. This technique requires deep sensitive observations of galaxies that trace underlying matter distribution and/or extensive spectroscopy to confirm the protocluster status and to identify galaxy membership. Additionally, as structures well before their final virialization, protoclusters are spatially extended and thus span a large cosmic volume [63]. In this section, I will discuss several methods that are used in protocluster searches.

Wide-field Blind Search

Wide-field spectroscopy is a reliable method to identify high-redshift protoclusters. Spectroscopic surveys yield precise spatial positions of galaxies, eliminating chances of misidentifying galaxies with the wrong environmental bin. Additionally, spectra of galaxies carry information of their velocity dispersion, which can shed light on their memberships to the protocluster as well as the true extent of the large-scale structure.

There are a handful successful protocluster searches via blind spectroscopic surveys. The VIMOS Ultra Deep Survey (VUDS: [64]) covers a total of 1 deg^2 in three fields, obtaining redshift measurements on $\gtrsim 6,000$ galaxies at $z > 2$. VUDS discovered three massive protoclusters at $z = 2.9$, $z = 3.3$, and $z = 4.6$ [65]–[67]. [68] identified 42 galaxy groups with $\gtrsim 3,000$ galaxies from zCOSMOS-deep catalog [69], [70]. Combining the two spectroscopic surveys, [71] discovered a proto-supercluster, *Hyperion* at $z \sim 2.45$. The 3D distribution of the spectroscopic members reveal seven density peaks connected by filaments (Figure 1.3), reminiscent of the matter distribution around massive dark matter halos.

Despite the success in blind spectroscopic searches, it is expensive to cover a large cosmic volume with deep spectroscopy. Alternatively, one can identify unbiased galaxy samples

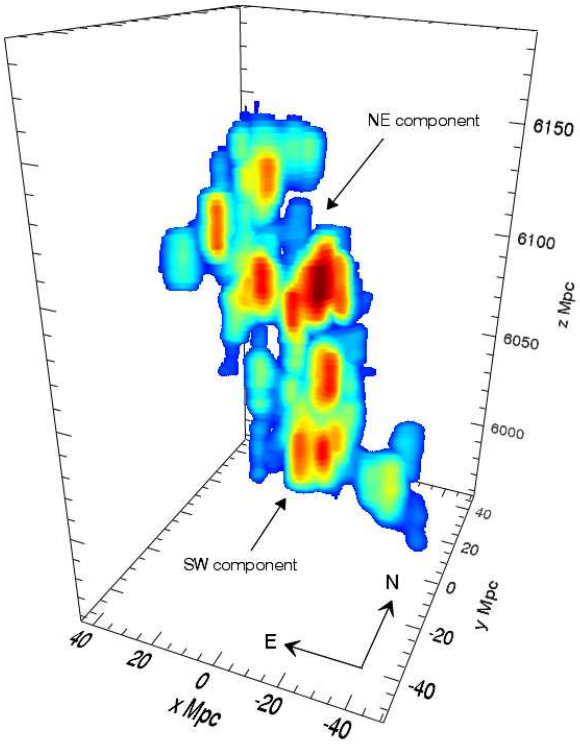

Figure 1.3. 3D structure of the *Hyperion* proto-supercluster. Colors scale with the surface density of spectroscopic galaxies, with red (blue) regions standing for galaxy over- (under-) densities. Figure credit: [71]

using wide-field photometric data, and follow up potential protocluster members with spectroscopy. One successful attempt is the protocluster discovered at $z = 6.01$ [72]. $\gtrsim 200$ galaxies are selected with the Lyman break technique (see next Chapter). Of these, eight galaxies are spectroscopically confirmed as members of a protocluster. Recently, [73] conducted large-scale protocluster search in Canada-France-Hawaii Telescope Legacy Survey (CFHTLS) Deep Fields at $z \sim 3 - 6$. They constructed large Lyman break galaxy (LBG) samples using the deep broad-band images and discovered 21 protocluster candidates that occur as LBG overdensities. Three out of four protocluster candidates at $z = 3 - 4$ are confirmed genuine.

Signposts of Protoclusters

Another search technique is to look for galaxy overdensities around rare sources which may be signposts of protoclusters. One example tracer of protoclusters is the high-redshift radio galaxies that are likely progenitors of local brightest cluster galaxies (BCGs: [74]–[77]). The neighborhoods of radio galaxies have been extensively studied with mixed results [78]–[93].

Other tracers include Lyα blobs (LABs) and submillimeter galaxies (SMGs). LABs are bright, extended Lyα sources with line luminosity $L_{\mathrm{Ly}\alpha} \gtrsim 10^{43}$ erg s^{-1} and physical sizes $\gtrsim 100$ kpc. LABs are expected to trace intergalactic neutral gas in the cosmic web that is illuminated by AGNs or starbursts. Observations targeting the immediate environment of LABs have found their close association with galaxy overdensities [94]–[96]. SMGs, on the other hand, are possible progenitors of local massive elliptical galaxies [97]–[100]. Overdensities of SMGs may be the sites of young clusters whose member galaxies are actively forming stars.

Although these signposts may provide promising avenues for future searches in an efficient manner, it remains unclear how such rare astronomical phenomena are connected to the formation of protoclusters and how well they trace the large-scale environment. More observations are crucially needed to evaluate their usefulness as markers of protocluster sites.

1.2.2 Environmental Effects on Cluster Galaxies

Observations show that the formation of cluster galaxies differ significantly from that of the field galaxies, highlighting the profound effect of environment on galaxies. In the local universe, clusters host a high fraction of early-type (elliptical) galaxies [101] known as the morphology-density relation. [102] found that the fraction of spiral galaxies decreases from $\sim 60\%$ in the lowest density regions to $\lesssim 10\%$ in the densest cores. The redshift evolution of the galaxy red sequence indicates that cluster galaxies ceased star formation ~ 10 Gyr ago [55]–[57], [59]. They are also redder, older, and more massive than their field counterparts [103].

At $0.3 < z < 0.5$, [104] found that there are more blue galaxies residing in clusters than in the local universe. Similarly, morphologies studies with the Hubble Space Telescope (HST) suggested an increase in spiral fraction in cluster environments with increasing redshift [105], [106]. Spectroscopy on intermediate cluster galaxies ($z \sim 0.3 - 0.5$) reveals that they have strong Balmer lines in absorption while no line emission is detected [107], indicating that they had quenched star formation in the last 1-2 Gyr.

At higher redshift ($z > 2$), there is a widespread enhancement of star formation activities found in protoclusters [96], [108], [109]. [96] targeted SFGs in a field containing a massive protocluster at $z = 3.1$. After splitting galaxies into two environment bins according to the local surface density, they found a discernible enhancement in UV and Lyα luminosities, indicating that galaxies are forming stars at higher rates in a dense environment (Figure 1.4).

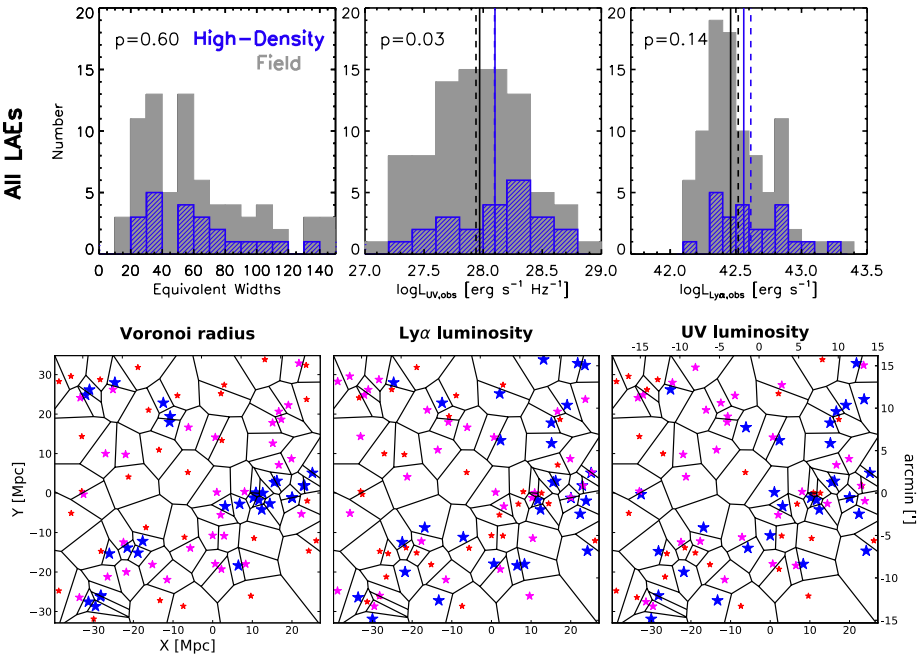

Figure 1.4. Top: number distribution of the key physical properties of LAEs in high-density regions and in the field. Bottom: Voronoi tessellation of the spatial distribution of LAEs. The blue, pink and red stars represent the top, middle and bottom one-third of LAEs with smallest Voronoi radius (left), highest Lyα (middle) and UV luminosities (right). Figure reproduced from [96].

1.3 Lyα Emission in Star Forming Galaxies

1.3.1 Lyman Series in Astronomy

The Lyman series represents the hydrogen transitions between any excited level ($n \geq 2$) and the ground state ($n = 1$). Two spectral features of Lyman series are of great interest to modern astronomy. The first is the hydrogen ionization energy that characterizes the transition $n = 1 \rightarrow \infty$. The rest-frame wavelength (energy) corresponding to the ionization energy is 912 Å (13.6 eV) known as the Lyman limit. A sharp break at the Lyman limit is the strongest feature in the spectra of high-redshift SFGs. Star formation produces a continuous spectral energy distribution (SED), whereas photons that are more energetic than 13.6 eV are absorbed by the surrounding neutral hydrogen gas. Galaxies featured with a break at the Lyman limit are dubbed as 'Lyman break galaxies', or LBGs.

Since LBGs are faint in passbands bluer to the Lyman break while being significantly brighter in longer wavelengths, the conventional approach to select LBGs is to characterize the galaxy spectra over the rest-frame wavelength from 900Å to 1700Å with three broadband filters. The bluest filter samples the wavelength blueward to the Lyman break, where the galaxies should be faint or undetected. The other two filters cover the spectra redward to the Lyman break, where the sources are reasonably bright.

Another useful feature is Lyα emission. A Lyα photon is produced by the $n = 2 \rightarrow 1$ transition, which corresponds to 1215.67 Å (10.2 eV). Lyα photons are ubiquitous in SFGs. Photons emitted by hot (O and B type) stars ionized the surrounding neutral hydrogen atoms, creating ionized bubbles (dubbed as H II regions). These ionized hydrogen subsequently recombine and emit photons with energies corresponding to a series of hydrogen energy transitions. In a typical electron density and temperature expected for such H II regions ('case B recombination': [110]), approximately one-third of the ionizing photons are eventually converted to Lyα photons [111].

Lyα emission has been one of the most useful tools to identify galaxies at the peak epoch of cosmic star formation ($z \sim 2 - 5$: 1-3 Gyr after the Big Bang: [112]–[116]) as Lyα emission is redshifted into the optical window as $\lambda_{\rm obs} = 1215.67(1 + z)$ Å. In practice, observation using a combination of carefully chosen broad- and narrow-band (full-width-at-

half-maximum, or FWHM, $\sim$ 50Å) filters can enable selection of Lyα-emitting galaxies, or Lyα emitters (LAEs), in a narrow pre-determined redshift range. Other broad-band filters sampling a wider spectral range outside the rest-frame Lyα wavelength can further aid in refining the selection. For instance, a bluer filter can be used to straddle the Lyman limit.

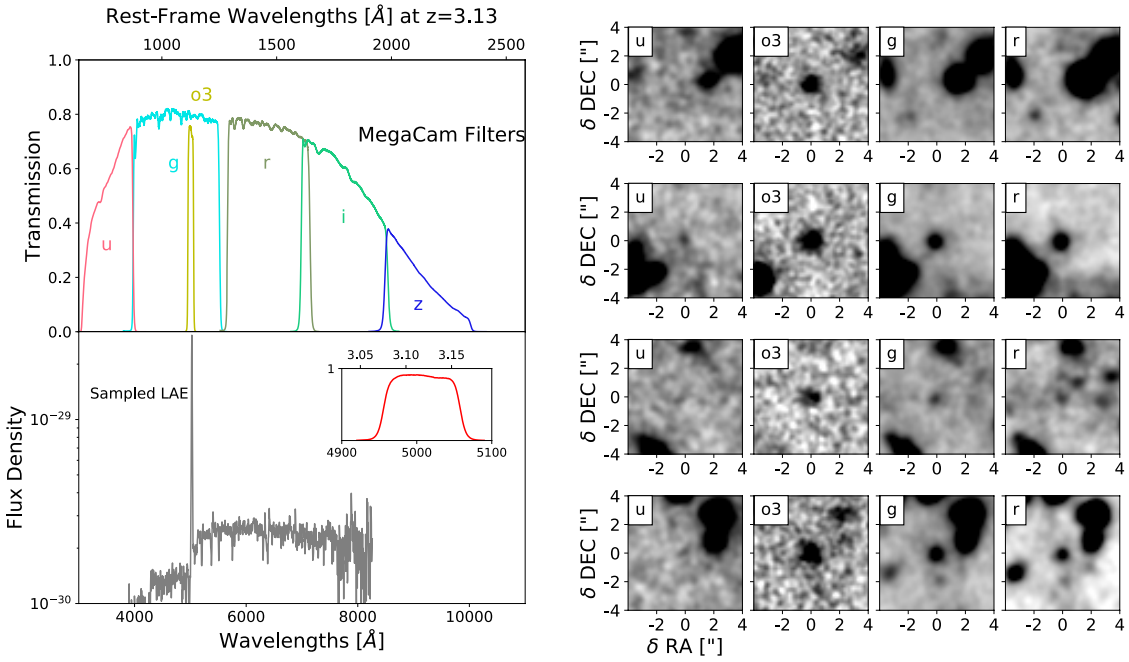

Figure 1.5. Left: transmission curves of the filters used to identify LAEs, and a sampled LAE spectrum [117] shown below. Right: postage-stamp images of four LAE candidates in u, $o3$, g, r bands.

The left panel of Figure 1.5 provides an illustration of the Lyα selection technique. In the top panel, transmission curves of five broad-band filters (u, $o3$, g, r, and z) and of one narrow-band filer $o3$ are shown. The $o3$ filter has a central wavelength of 5024.9 Å, with a FWHM of 55.6 Å, which can sample redshifted Lyα emission in range $z = 3.13 \pm 0.02$. The rest-frame wavelengths sampled by the same filters are shown on the top axis. The lower panel shows a rest-frame UV spectrum of typical SFGs as observed [117].

The postage-stamp images of LAE candidates are shown in the right panel of Figure 1.5. At $z \sim 3.13$, u-band samples $\lambda_{\rm rest} < 912$ Å (Lyman limit), and thus the galaxies are expected to be faint or undetected. The same galaxies should be much brighter in the narrow-band

filter which predominantly samples the Lyα emission than in the broad-band filters sampling mostly the stellar continuum emission.

Existing spectroscopy follow-up of LAE candidates shows that the contamination rate by lower-redshift line emitters such as [O II] or [O III] is very low ($\lesssim 5\%$, the rest-frame wavelengths of the emission lines are 3737 Å and 5007 Å, respectively, [118]). The observed equivalent widths W_0 – defined as the line emission flux relative to the continuum at the same wavelength – of these oxygen lines are typically $W_0 \approx 10$ Å[119], much smaller than the typical equivalent widths cut for an LAE selection. In addition, any given survey samples a much smaller cosmic volume at lower redshift. For example, the above filter set would select line emitters at $z = 3.13$ (Lyα), $z = 0.35$ ([O II]), and $z = 0.0036$ ([O III]). An area of 1 deg^2 corresponds to 1.3×10^4 cMpc^2, 568.7 cMpc^2, and 0.0724 cMpc^2 at these redshift values, respectively.

Since the narrow-band selection technique is practical and efficient in selecting high redshift galaxies with relatively high precision ($\Delta z \lesssim 0.05$), many surveys have carried out deep, wide-field narrow-band observations and have provided rich LAE samples. So far, more than 20,000 LAE candidates have been selected by narrow-band excess, among which $\geq 1,000$ are spectroscopically confirmed [120]. A fraction of LAEs are found at high redshift frontier (e.g., [121] at $z = 8.638$, [122] at $z = 7.506$) providing valuable insights into the epoch of reionization (EoR). The rich LAE sample over a wide range of cosmic time significantly deepens understanding of properties of young galaxies and their evolutionary paths. In the next Chapter, I will discuss the known physical properties of LAEs.

1.3.2 Properties of LAEs

Stellar population

The stellar population of LAEs can be obtained by comparing the spectral energy distributions (SEDs) with those of the stellar population synthesis models. Since LAEs are typically faint in continuum luminosities, one common approach to increase the signal-to-noise ratios (SNR) is to perform image stacking.

The star formation rates (SFRs) of LAEs are estimated from the brightness of the nebular emission lines. Lyα emission originates from the H II regions that are ionized by hot O- and B-type stars. Given that O- and B-type stars are short-lived, Lyα line provides a nearly instantaneous measurement of SFRs that is independent of the star formation history. However, due to the resonant nature of Lyα photons, it is challenging to estimate intrinsic Lyα production efficiency without taking into account their escape fraction (See Chapter 2). Alternatively, one can use Hα as an indicator of intrinsic star formation. Under case B recombination, Hα and Lyα photons originate from the same H II regions, and the ratio of production of the two photons follows $n(\mathrm{Ly}\alpha)/n(\mathrm{H}\alpha) = 8.7$. Assuming solar abundances and Salpeter IMF, the SFR of LAEs is inferred as ([110]):

$$\mathrm{SFR}\ [\mathrm{M}_\odot\ \mathrm{yr}^{-1}] = 7.9 \times 10^{-42}\ \frac{L_{\mathrm{Ly}\alpha}}{8.7}\ [\mathrm{erg\ s}^{-1}] \tag{1.1}$$

Applying SED fitting, multi-wavelength observations have characterized stellar populations of LAEs; they tend to be low-mass ($10^8 - 10^9$ $\mathrm{M}_\odot$), young age ($\sim$ 10 Myr), dust-free SFGs with typical SFR of $\sim 1 - 10$ $\mathrm{M}_\odot$ yr^{-1} [114], [123], [124]. In Figure 1.6, we show the distributions of SFRs, stellar masses, and specific star formation rates (sSFRs) of LAEs, photometrically selected SFGs, and Balmer-break galaxies. Of these, LAEs are characterized with the lowest mass.

Morphology

HST observations showed that the stellar components of LAEs are compact, with a half-light radii of $r \sim 1$ physical kpc on average as measured in rest-frame UV and optical continua [126]–[128]. Recent analysis on the stack Lyα images found that diffuse Lyα emission is ubiquitous around LAEs (e.g., [129], [130], also see Chapter 2.4). Such extensive Lyα emission probably originates from the ISM/CGM that is illuminated by Lyα photons produced by central star formation activities.

Another feature of LAEs is the Lyα spatial offset, $\delta_{Ly\alpha}$, which is defined as the spatial offset between the peaks of Lyα and stellar continuum emission. [131] found some LAEs with $\delta_{Ly\alpha} \sim 2.5 - 4$ kpc, which is significant over statistical errors. They found that $\delta_{Ly\alpha}$ is

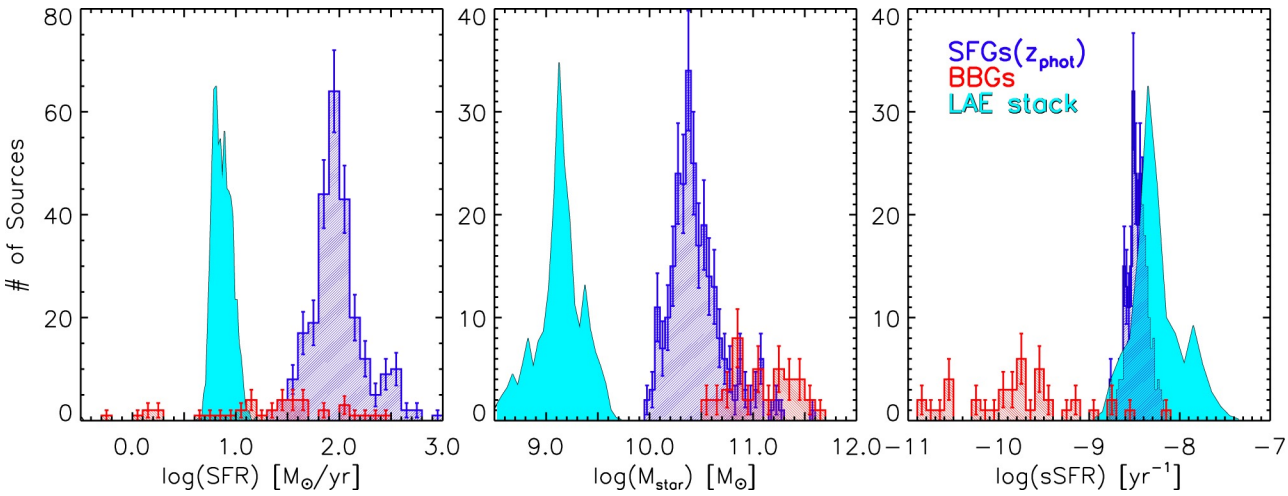

Figure 1.6. The distributions of star formation rate, stellar mass, and specific star formation of LAEs (cyan), SFGs (blue), and BBGs (red). Figure credit: [125]

marginally anti-correlated to the Lyα equivalent widths. Besides, [132] showed that LAEs with spatially-symmetric light profiles tend to exhibit small $\delta_{Ly\alpha}$. These results address the fact that $\delta_{Ly\alpha}$ originates from the inhomogeneous distribution of H I gas that is likely disturbed by mergers or cold stream, resulting in turbulence in Lyα flow. However, [133] suggested the Lyα offsets are unlikely caused by mergers or companion galaxies, whereas they are the products of stellar feedbacks that facilitate Lyα fluorescence in the nearby gas.

Clustering and the Large-Scale Environment

Narrow-band imaging has provided rich LAE samples over a wide range of redshift for mapping out the large-scale distribution of high-redshift galaxies. Spatial distributions of LAEs have been comprehensively studied.

LAEs are found to be weakly clustered. The degree of clustering is quantified by the angular correlation function (ACF) in two dimensions, which describes how the projected actual distribution of galaxies deviates from the expectation. Empirically modeled using ACF, LAEs are predicted with a correlation length $r_0 \approx 2-4$ Mpc at $z = 2-3$, corresponding to a bias factor $b = 1.0-2.0$ [134], [135]. Based on the bias evolution [136], LAEs will evolve to Milky Way-type galaxies at $z = 0$. The ACF of LAEs also shows that LAEs are hosted

by moderately small dark matter halos with $M_{\rm DM} \approx 10^{10-11} M_{\odot}$ [137]. These results suggest that LAEs are less biased by the underlying dark matter distribution, and therefore are good tracers of the large-scale structure.

Because of their redshift precision ($\Delta z \lesssim 0.05$), the Lyα technique is broadly used in protocluster search. Recent LAE surveys around protoclusters showed that the spatial distribution of LAEs bears a striking resemblance to that of cluster-sized halos, revealing the core, infalling groups, and filamentary arms stretching out tens of Mpc surrounded by vast voids (Figure 1.7: [95], [138], [139]). The angular sizes of LAE overdensities are in perfect agreement with those expected for cluster-sized halos at high redshift [63], [140]. These findings strongly suggest that LAEs are the best visible tracers of the underlying matter distribution and large-scale structure.

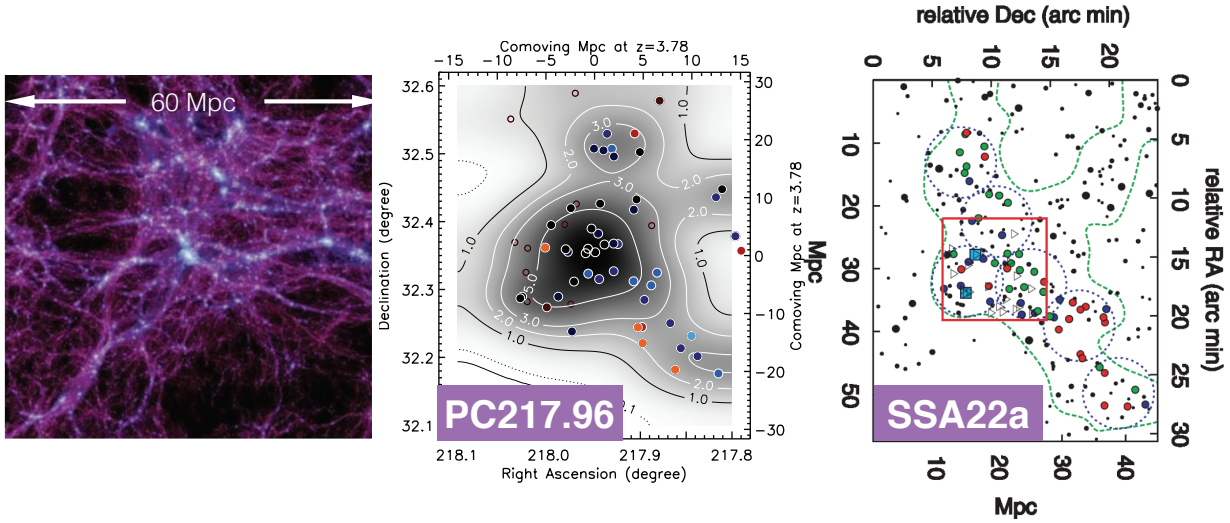

Figure 1.7. Angular distribution of spectroscopic member galaxies within two protoclusters at $z = 3.78$ (middle) and $z = 3.13$ (right) are shown as colored circles. Voids and filamentary arms observed in these structures are reminiscent of the cosmic web expected in and around cluster-sized dark matter halos. Reproduced from [23], [138], [141].

1.3.3 Peering into the ISM and CGM with Lyα

The interstellar and circumgalactic media of a galaxy are continuously shaped by the two dominant factors governing galaxy formation: inflow of gas from the accretion that fuels star formation and outflow that results from feedback effects. Furthermore, stellar and nebular emissions arising from stars are absorbed and modified by interstellar dust and gas. Thus, studying the physical conditions of the ISM and the CGM is of critical importance to make sound interpretations of existing and new observations of galaxies thereby obtaining a comprehensive picture of how galaxy formation has proceeded throughout cosmic time.

Studying the ISM and CGM poses a major observational challenge as the gas therein is very diffuse (surface density 1 to 10^3 atoms/cm^3 in H II regions: [142], [143]). Direct 21 cm imaging of atomic gas is beyond the current capability [144]. While absorption sightlines of a luminous background source (such as QSOs) can probe the CGM [145], [146], inferring the gas distribution from them is nontrivial as such bright sources are rare and thus are limited to discrete sampling. Lyα has recently emerged as a promising alternative to study as I will outline below [147]–[150].

Lyα and LyC Escape Fraction

Star-forming regions emit a copious number of Lyα photons through recombination. In principle, Lyα luminosities are expected to scale linearly with the SFR of the galaxy. However, observations show that such an expectation is rarely fulfilled. This is because, as a resonant line, Lyα photons scatter off neutral hydrogen present in the media, and as a result, have a much shorter mean free path than continuum photons. The likelihood of its escape from the galaxy is determined by the distribution of gas (which scatters them) and dust (which absorbs them), and the kinematic properties (which can get them off resonance frequency) of the gas. Hence, understanding the spatial and kinematic structure of the gas is crucial to interpreting spectroscopic/photometric observations of galaxies.

Understanding how Lyα photons escape the galaxy is also critical to elucidate the cosmic reionization physics. Ionizing Lyman continuum photons (LyC, hereafter) ($E \geq 13.6$ eV) escaping the first generation of galaxies (or 'first galaxies') are currently thought to have

reionized the universe sometime between $z = 7 - 10$ [151]. As low-mass SFGs, LAEs are the best analogs of the first galaxies. Indeed, recent observations show that 'LyC leakers' at $z = 2 - 5$ tend to have similar physical properties to those of LAEs (i.e., blue, high Lyα line equivalent widths, low-mass: [152]–[154]). Even with the James Webb Space Telescope, it will not be possible to directly observe LyC emission from first galaxies as the opacity of the intergalactic H I clouds at such high redshift is much too large; Lyα observations remain the best avenue to probe the reionization epoch.

Lyα Halos

Diffuse Lyα emission, or Lyα halos (LAHs), are extended ($1 - 10$ kpc) Lyα emission ubiquitously found around SFGs. Due to their faint nature, LAHs are hardly detected around individual galaxies (but see [129]). Traditional method for LAH searching is to increase the SNR at large galactic radii via image stacking.

Probing LAHs around distant galaxies recently becomes a promising alternative avenue to study the structures of galaxies well beyond the central regions. Lyα photons can be resonantly scattered by neutral hydrogen gas out to large distances (in the CGM), and thus can appear more extended than the rest-frame UV continuum which samples stellar light. The spatial extent of the LAH is sensitive to the neutral gas density and velocity field of the CGM (e.g., [148]) while the total line luminosity (the sum of that emerging from the galaxy extent and the LAH) can tell the true Lyα escape fraction. Nearly half of the total Lyα luminosity emerges in the CGM as very low surface-brightness diffuse emission [155], which has not been properly taken into account in the literature.

The surface brightness radial profile can also provide useful constraints on other diffuse Lyα producers. These include star formation in ultra-faint satellite galaxies [147], [150], gravitational cooling radiation [156]–[158], AGN fluorescence [159]–[161], or shock-heating by galactic superwinds [162]. [155] investigated these possibilities based on two LAE samples, and concluded that the central star formation is primarily responsible for the LAH while other ancillary mechanisms may play a minor role at large galactocentric radii.

2. THE ROLE OF DUST, UV LUMINOSITY AND LARGE-SCALE ENVIRONMENT ON THE ESCAPE OF Lyα PHOTONS: A CASE STUDY OF A PROTOCLUSTER FIELD AT $z = 3.1$

In this chapter, I study an LAE sample at $z = 3.1$ in a field where a LAE overdensity is observed [96]. I conduct a comprehensive study on the Lyα properties, highlighting the impacts of dust, UV luminosity, and the large-scale environment on the Lyα escape. These results shed light on the physical conditions of the interstellar and circumgalactic media surrounding high-redshift LAEs, providing wide-ranging implications on galaxy evolution and cosmic reionization.

This chapter has been published as Huang et al. (2021) in Astrophysical Journal.

2.1 Abstract

We present a detailed characterization of the Lyα properties for 93 Lyα emitters (LAEs) at $z \sim 3.1$ selected from the D1 field of the Canada-France-Hawaii-Telescope Legacy Survey, including 24 members of a massive protocluster. The median-stacked Lyα image shows an extended Lyα halo (LAH) surrounding the galaxy with the exponential scale length 4.9 ± 0.7 kpc, which accounts for roughly half of the total line flux. Accounting for the LAH contribution, the total Lyα escape fraction, $f_{\rm esc}$, is $40 \pm 26\%$. Combining the dataset with existing measurements, we find a dependence of $f_{\rm esc}$ on the galaxy's UV slope (β) and UV luminosity ($L_{\rm UV}$). The simultaneous use of both parameters allows prediction of $f_{\rm esc}$ within 0.18 dex, a substantial improvement over 0.23 dex when only β is used. The correlation between $f_{\rm esc}$ and E$(B-V)$ suggests that Lyα photons undergo interstellar dust attenuation in a similar manner to continuum photons. Yet, Lyα transmission is typically higher than that expected for continuum photons at similar wavelength by a factor, which depends on UV luminosity, up to 2 in the samples we studied. These results hint at complex geometries and physical conditions of the interstellar medium, which affect the Lyα transmission or production. Alternatively, the dust law may change with luminosity leading to over-or

under-estimation of $f_{\rm esc}$. Finally, we report that protocluster LAEs tend to be bluer and more UV-luminous than their field cousins, resulting in systematically higher $f_{\rm esc}$ values. We speculate that it may be due to the widespread formation of young low-mass galaxies in dense gas-rich environments.

2.2 Introduction

Lyα emission plays a central and multifaceted role in our understanding the formation and evolution of galaxies in the distant universe. Existing studies show that galaxies identified via their strong Lyα emission [Lyα emitters or LAEs, hereafter: see review by 120] tend to be blue, UV-faint, and low-mass galaxies [123], [124], [163], representing a population of galaxies that not only drives the cosmic star formation rate density at $z \gtrsim 2$ [164] but also is the primary building blocks of typical present-day galaxies such as our own Milky Way [e.g., 134].

As a resonant line, the properties of Lyα emission, such as the escape fraction and the spectral shape, offer vital clues to the spatial and kinematic structures of the neutral gas and dust in the interstellar and circumgalactic media [ISM and CGM, respectively: e.g., 148], [149], [165]. Studies found that the escape of Lyα photons strongly and positively correlates with the escape of Lyman continuum (LyC) photons in low-redshift analogs [e.g., 166], [167] and in high-redshift galaxies [e.g., 168], lending credence to the possibility that understanding Lyα emission in galaxies may be key to constraining the reionization of the universe.

Deep narrow-band imaging surveys have recently demonstrated the utility of Lyα emission as tracers of the large-scale structure in the distant universe. Massive protocluster sites are found to be significant overdensities of LAEs [95], [96], [169], [170]. In several protoclusters, filamentary structures traced by LAEs stretch out tens of Mpcs from a protocluster [139], [171], mirroring the expectation of dark matter structures around a cluster-sized halo. [172] noted that, as pre-virialized and highly overdense structures, protoclusters and the galaxies therein play a significant role in driving the cosmic star formation rate density of the universe at high redshift. To better quantify their importance, however, more detailed

understanding of how galaxy formation proceeds in high-density environment is required. Although recent studies are beginning to address these questions, there is no clear consensus yet [see, e.g., 109], [125], [173]–[175].

Together with the current and upcoming deep wide-field optical imaging surveys employing both broad- and narrow-band filters [e.g., the Subaru Strategic Program with the Hyper Suprime Cam, the Legacy Survey of Space and Time with the Vera C. Rubin telescope, SILVERRUSH, and ODIN: 136], [176], [177, also see Section 2.7], these considerations make it likely that Lyα emitting galaxies will continue to play a crucial role in our understanding of the cosmos well into the future.

One crucial diagnostic that is central to elucidating the key questions mentioned above is Lyα escape fraction ($f_{\rm esc}$, hereafter), which encapsulates the prominence of the Lyα relative to the stellar light. Thus far, the intrinsic faintness of most LAEs has limited the $f_{\rm esc}$ measurements only to those residing in a handful of deep surveys [e.g. 178]–[181], resulting in relatively small number statistics and a narrow dynamic range in galaxy properties.

To further complicate matters, there is a growing consensus that the presence of an extended low surface brightness Lyα emission (often referred to as Lyman Alpha Halos or LAHs) is ubiquitous around star-forming galaxies at both low- [e.g., 182] and high redshift [e.g., 94], [129], [130], [135], [155], [183]–[186]. The dominant process responsible for the production the LAH remains elusive as is the relative importance of the LAH in different galaxy types [see 155], [186]. If the LAH phenomenon is produced by the photons originating from the H II regions, the true Lyα escape fraction may be considerably larger than currently known. In this context, the existence of an LAH potentially broadens the scope and the importance of Lyα emission in the galaxy formation research.

In this paper, we study how the Lyα escape fraction of a galaxy changes with its physical properties and large-scale environment. In Section 2.3, we provide a brief description of our primary, ancillary datasets, and the LAE sample selection, and give the definition of the protocluster- and field subsamples. In Section 2.4, we present our LAH measurements and comparison to the literature. In Sections 2.5 ad 2.6, we examine how $f_{\rm esc}$ varies with the galaxy's photometric properties and present an empirical formula that can predict a galaxy's $f_{\rm esc}$ given other parameters; the implications of our results on the physical conditions of the

ISM/CGM are also discussed. Section 2.7 explores how large-scale environment affects $f_{\rm esc}$. We summarize the results in Section 2.8.

Throughout this paper, we adopt the cosmology with $\Omega = 0.27$, $\Omega_\Lambda = 0.73$, $H_0 = 70$ km s^{-1} Mpc^{-1} [187]. Distance scales are given in comoving units unless noted otherwise. All magnitudes are given in the AB system [188].

2.3 Observation and Sample Selection

Our LAE sample at $z = 3.13$ is selected from one of the four Canada-France-Hawaii-Telescope Legacy Survey deep fields [CFHTLS D1 field, $(\alpha, \delta) = (36.316°, -4.493°)$, hereafter: 189]. The details of the imaging dataset and the selection of our LAE sample at $z = 3.13$ are given in [96, hereafter S19], and here we only provide a brief summary. The narrow-band observation is obtained using the Mosaic 3 Camera [190] at the Mayall 4m telescope using the KPNO #k1014 filter ($o3$ filter, hereafter) with a central wavelength of 5024.9Å and a full-width-at-half-maximum (FWHM) of 55.6Å. The final stacked image has a delivered image quality of 1.2″and a limiting magnitude $m_{o3,5\sigma} = 25.2$ measured in a 1.2″ diameter aperture.

To create a multi-wavelength photometric catalog, S19 first homogenized the point spread functions (PSFs) of the 'T0007' version CFHTLS broadband images to match the seeing of the $o3$ image. A Moffat profile was assumed to fit the PSF of the $o3$ image with the seeing-dependent parameter $\beta = 3.0$ and FWHM of 1.2″. By running the code `IDL_ENTROPY`, S19 derived the convolution kernel of each broadband image and convolved it accordingly. We run the `SEXTRACTOR` software [191] using the dual-image mode with the $o3$ image as the detection band while measuring the photomerty in the $ugri$ bands.

Based on our multi-wavelength catalog, LAEs are selected using the following criteria:

$$\begin{aligned} & o3 - g < -0.9 \quad \wedge \quad \mathrm{S/N}(o3) \geq 7 \\ \wedge \quad & [\ u - g > 1.2 \quad \vee \quad \mathrm{S/N}(u) < 2\ ] \end{aligned} \tag{2.1}$$

The $o3-g$ color ensures the rest-frame equivalent width $W_0 \gtrsim 20$Å. The $u-g$ color criterion or non-detection in the u band ensure that the colors of these sources are consistent with being at $z \gtrsim 2.7$.

In total, 93 LAEs are identified over an effective area of 1,156 arcmin^2. Of these, none has an X-ray counterpart in the existing XMM data[1] [192], suggesting that AGN contamination is likely low ($\lesssim 9 \times 10^{-4}$ arcmin^{-2}); however, we cannot rule out X-ray faint AGN in our sample. The brightest source in the sample, labelled as QSO30046 in the S19 catalog, is classified as an active galactic nuclei (AGN) at $z_{\rm spec} = 3.86$ in the VIMOS VLT Deep Survey [193]. The blue $o3-g$ color is likely a result of Lyβ and O IV emission falling into the $o3$ band. QSO30046 is removed from the LAE catalog. The contamination from low-redshift line emitters is expected to be low because the adopted $o3-g$ color cut corresponds to the observer-frame line equivalent width of ≈80Å, and thus should be conservative enough to exclude most [O II] emitters ($W_0 \lesssim 60$Å) at $z = 0.34$ [119], [194].

2.3.1 Protocluster and Field LAEs

Among the 93 LAEs, S19 reported that 24 sources reside in a significant LAE overdensity near a spectroscopically confirmed protocluster at $z = 3.13$ [73]. The observed overdensity parameter is comparable to that measured for several confirmed protoclusters [e.g., 81], [86], [139], [170]. Moreover, a luminous and extended Lyα nebula ($L_{\rm Ly\alpha} \approx 2 \times 10^{43}$ erg s^{-1}, with a half-light radius of 40 kpc) was also discovered near the overdensity, as is the case for several known protoclusters [95], [138], [169]. These findings lend credence to the possibility that these LAEs trace a protocluster structure at $z = 3.13$ which will evolve into a galaxy cluster with a total mass of $(1.0-1.5) \times 10^{15}$M$_\odot$ by $z = 0$.

We use the the protocluster LAE sample defined by S19. Briefly, S19 constructed the LAE surface density map by smoothing the LAE positions by a Gaussian kernel with the FWHM of 5.1′(10 comoving Mpc at $z = 3.13$). The highest overdensity region outlined by an isodensity contour contains 21 LAEs within an area 72.8 arcmin^2 corresponding to a surface overdensity $\delta_\Sigma = 3.3 \pm 0.9$ ($\delta_\Sigma \equiv (\Sigma - \bar{\Sigma})/\bar{\Sigma}$) where $\bar{\Sigma}$ and Σ are mean and local surface

[1]↑The flux limits of the XMM data in the D1 field are 2.5×10^{-15} erg cm^{-2} s^{-1} in the 0.5–2 keV band, and 2×10^{-14} erg cm^{-2} s^{-1} in the 2–10 keV band.

overdensities. Additionally, we include three sources which reside in an LBG overdensity and were later spectroscopically confirmed by [73] to lie at $z = 3.13$; they are also recovered by our LAE selection. Thus, our protocluster LAE sample consists of 24 members; the remainder are referred to as 'field LAEs'. While these definitions are simplistic, they provide us with a rare opportunity to conduct quantitative and fair comparison of the two environmental subsamples. For more details of the protocluster, its galaxy members, and their distribution, we refer interested readers to S19 (their Section 4.1 and Figure 6).

2.3.2 Ancillary Data

We make use of the VANDELS public spectroscopic survey DR2 data [181], [195]. The majority of VANDELS targets are drawn from three categories: bright star-forming galaxies ($i_{AB} \leq 25$) at $z = 2.4 - 5.5$; massive quiescent galaxies at $z = 1.0 - 2.5$ with $H_{AB} \leq 22.5$; and faint star-forming galaxies at higher redshift range ($25 \leq H_{AB} \leq 27$, $i_{AB} \leq 27.5$ at $z = 3 - 7$). To the combined galaxy sample, we apply further selection criteria on the VANDELS galaxies to construct an LAE-like sample, which include: 1) the redshift quality flag value is 3, 4, or 9 yielding $\gtrsim 80\%$ confidence in redshift determination; 2) Lyα line in emission is visible in the 1D spectrum. Our selection results in 18 galaxies at $z = 3.0 - 4.9$.

Starting from the publicly available 1D spectra, we compute Lyα luminosities by integrating the flux density over a wavelength window of 50Å, centered at the redshifted Lyα emission ($\lambda_{\mathrm{Ly}\alpha} = 1215.67(1+z)$Å). The continuum flux density in the window is determined by the interpolation from the flux density blueward and redward to the window, which is then subtracted to obtain the line flux[2].

The power-law slope of the UV spectrum β (where $f_\lambda \propto \lambda^\beta$) and UV continuum luminosity at rest-frame wavelength 1700Å (L_{1700}) are determined from the VANDELS multi-wavelength photometric catalog. For each galaxy, β is computed through the linear fitting of the flux densities of the bands which sample the UV portion of the SED but not Lyα: i.e., the izH bands at $z > 3.2$ and the iz bands at $z \leq 3.2$. Once β is determined, L_{1700} is estimated by interpolating the i band flux density. The rest-frame Lyα equivalent width (W_0)

[2]↑We do not correct for the Lyα flux falling outside the slitlet and therefore the Lyα luminosity is likely underestimated.

is derived from the ratio of Lyα flux to the continuum flux density at the same wavelength. The rest-frame W_0 ranges from 0.4Å to 440Å, with a median of 16Å.

2.4 Characterizing the extended Lyman Alpha Emission

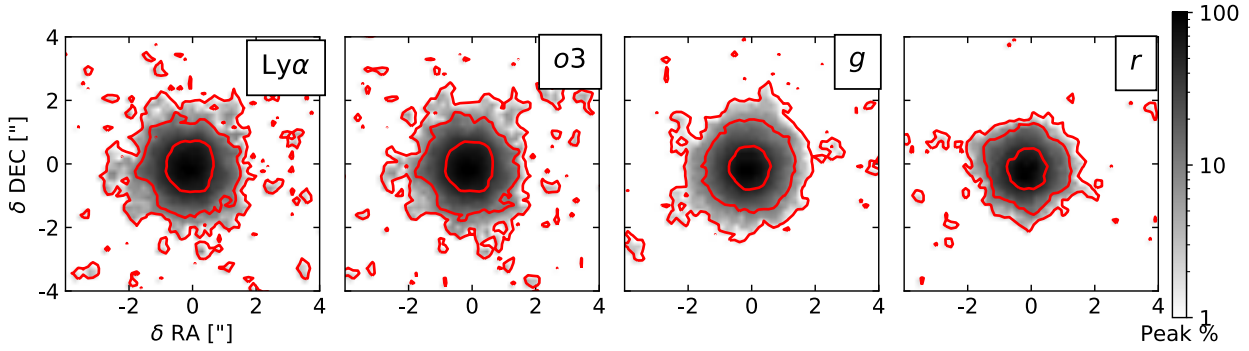

Figure 2.1. Stacked images of LAEs in the D1 field. The Lyα image is constructed from the $o3$ and g band data as described in Section 2.4; both $o3$ and g passbands sample near $\lambda_{\rm rest} \approx 1216$ Å, and thus include the line and continuum emission to a varying degree. The r band samples the UV continuum at $\lambda_{\rm rest} \approx 1700$Å. In each panel, the red contours show the positions at which the surface brightness falls to 50%, 10%, and 1% of the peak brightness.

We investigate their average properties utilizing image stacking analyses. The details of our adopted procedure are given in [155, X17, hereafter]. We create a Lyα line image by subtracting the continuum flux from the $o3$ image. The Lyα flux is determined as $F_{\rm Ly\alpha} = af_{\nu,o3} - bf_{\nu,g}$ where the line flux, $F_{\rm Ly\alpha}$, and the monochromatic flux density, f_ν are given in units of erg s^{-1} cm^{-2} and erg s^{-1} cm^{-2} Hz^{-1}, respectively. a and b are coefficients given in units of Hz, which capture the optical depth of the intergalactic medium [196], which depend on the filter width, redshift, and the UV spectral shape. The detail is given in the Appendix A of X17. For a $z = 3.1$ galaxy with a flat UV spectrum (i.e., $\beta = -2$), $a = 7.3 \times 10^{12}$ Hz and $b = 7.7 \times 10^{12}$ Hz.

We perform image stacking on the PSF-homogenized images in the $o3$, g, r, and Lyα bands. For each LAE, a $1' \times 1'$ cutout is created centered on the galaxy. We run `SEXTRACTOR` for detection and mask out the off-center sources using the output segmentation map. We

visually inspect the cutout images and find that 11 LAEs in our sample have companions within 3″, which can potentially undermine our ability to robustly estimate and remove the local sky background, a step essential to detecting low surface brightness features around galaxies. Additional six sources are clearly extended (with semi-major axis > 2 ″) and elongated. Of these 17 sources, 4 are in the protocluster region and the remainder belong to the field. After removing them, we perform a pixel-to-pixel median image stacking on the final sample of 76 LAEs. Median stacking ensures that our results are robust against being biased by a few high-luminosity outliers.

The sky background in the stacked image is estimated from an annular region of [10″, 20″] from the center and is subtracted to produce a zero-sky image. The inner radius of the sky annulus is chosen not to include any diffuse emission from the galaxy.[3] Using this method, we create the image stacks for our full LAE sample.

In Figure 2.1, we show the resultant stacked images of the full LAE sample in the Lyα, $o3$, g, and r bands. All are normalized at their peak brightness and the contours mark 1, 10, and 50% of the peak brightness. In the bands which primarily sample Lyα emission (Lyα and $o3$), the emission is clearly more extended than in the r band. The fact that the two inner contours in the g-band are similar to those in the r-band is not surprising because the continuum flux is expected to make a larger contribution to the flux density than the line flux at the range of the observed line equivalent width. The outer contour ($\gtrsim 2''$ from the center) closely mirrors those of the Lyα and $o3$ band as the contribution of the Lyα flux increases and the continuum flux falls off rapidly.

2.4.1 Modeling the Surface Brightness Profile of LAH

We measure the physical size of the Lyα and continuum emission from the stacked images. Because the r band only samples the continuum emission, the 1D surface brightness profile of the r band is approximated as an exponentially declining function:

$$I_{\rm obs}(r) = {\rm PSF} * I_c \exp(-r/r_{\rm s,c}) \tag{2.2}$$

[3]↑At $z = 3.13$, 10″ corresponds to 78.4 kpc; even the most extended Lyα emission detected around normal star-forming galaxies are found to be $\lesssim 25$ kpc, in their exponential scale-lengths [e.g., 145].

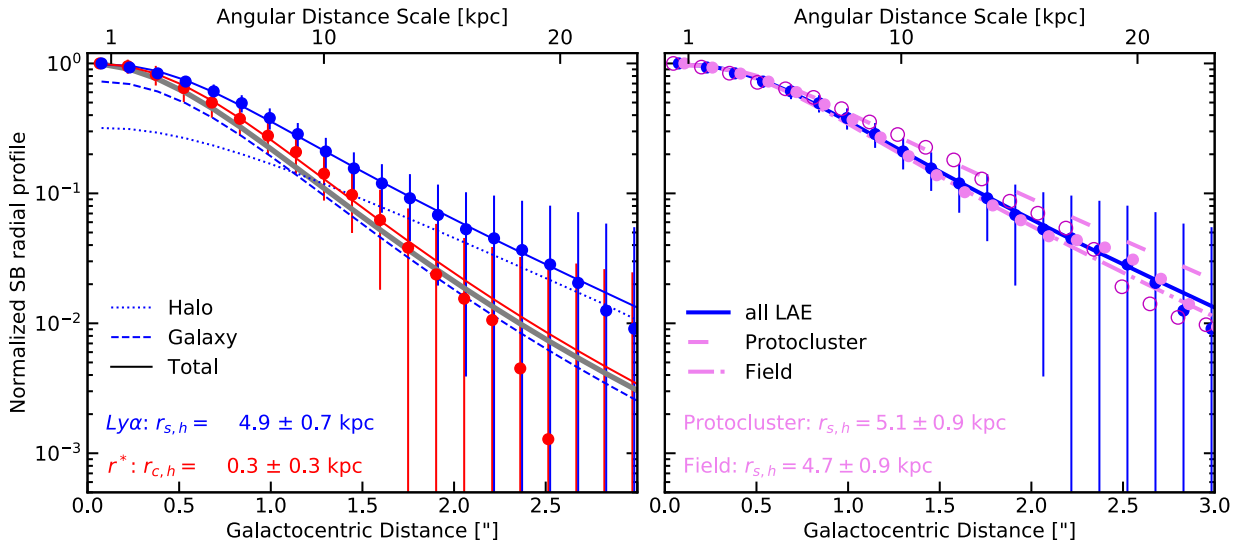

Figure 2.2. *Left:* normalized radial profiles of the stacked images of our LAE sample are shown in the Lyα (blue) and the r band (red). Solid, dashed, and dotted lines of the same color show the best fit exponential profiles for the total, galaxy-, and LAH components, respectively. The exponential scale-lengths are indicated at bottom left corner. The thick grey curve shows the image PSF. Dashed and dotted curves are the continuum and halo components. *Right:* We compare the radial profile of Lyα emission for the full sample (blue) with those for the protocluster (pink open circles) and field subsamples (pink filled circles). For clarity, we do not show the uncertainties of the subsamples, which are $\approx$95% and $\approx$28% larger in the protocluster and field subsamples than those of the full sample. The LAH sizes in protocluster- and field LAEs are indistinguishable.

where the $r_{\rm s,c}$ is the exponential scale length of the galaxy's continuum emission, I_c is the normalized surface brightness, and the symbol $*$ denotes the convolution. We use the PYTHON function `scipy.optimize.curve_fit` and obtain the best fit scale length is 0.3 ± 0.3 kpc: this is consistent with our expectation that our LAEs are unresolved in the r-band. The error accounts for the full variance of the parameter space.

The intrinsic Lyα surface brightness is modeled as a superposition of two exponential functions, representing the emission from the galaxy and the extended halo:

$$S_{\rm Ly\alpha,intrinsic} = S_c \exp(-r/r_{\rm s,c}) + S_h \exp(-r/r_{\rm s,h}); \tag{2.3}$$

The observed Lyα surface brightness is expressed as:

$$S_{\mathrm{Ly}\alpha,\mathrm{obs}}(r) = \mathrm{PSF} * S_{\mathrm{Ly}\alpha,\mathrm{intrinsic}} \tag{2.4}$$

In Equation 2.3, $r_{\mathrm{s,h}}$ is the scale length of the halo component; S_c and S_h normalize the galaxy and halo component, respectively. We determine the best-fit scale length $r_{\mathrm{s,h}}$ while fixing the $r_{\mathrm{s,c}}$ value measured in the r band and obtain $r_{\mathrm{s,h}} = 4.9 \pm 0.7$ kpc.

In the left panel of Figure 2.2, we show the azimuthally averaged radial profiles of the Lyα (blue) and r band (red) together with the best-fit exponential models as solid lines. For the ease of comparison, the profiles are normalized at the innermost angular bin. For the Lyα band, we also show both galaxy and LAH components as a dashed and a dotted line, respectively. The image PSF is indicated by a thick grey line. The uncertainties include both Poisson and bootstrap sampling errors.

In order to explore how the LAH size changes with galaxies' large-scale environment, we repeat the same procedure for the two subsamples. In Figure 2.2 (right), these measurements are shown as pink circles and lines. The uncertainty in the protocluster subsample is ≈95% (≈ 28% in the field) larger than those of the full sample as the number of galaxies in each sample is smaller. When normalized, these measures are consistent with our result for the full sample within uncertainties. The LAH scale-lengths of $r_{s,h} = 5.1 \pm 0.9$ kpc and $r_{s,h} = 4.7 \pm 0.9$ kpc for the protocluster- and field subsample, respectively. Our analysis suggests that the large-scale environment is not a major determinant of LAH sizes, in agreement with the finding of X17.

2.4.2 Lyα Halo Fraction and Aperture Correction

Having separated the total Lyα emission into the halo and galaxy components, we estimate the fractional contribution of the LAH to the total line flux. The halo fraction is defined as:

$$X_{\mathrm{Ly}\alpha} \equiv F_{\mathrm{h}}/F_{\mathrm{tot}} \tag{2.5}$$

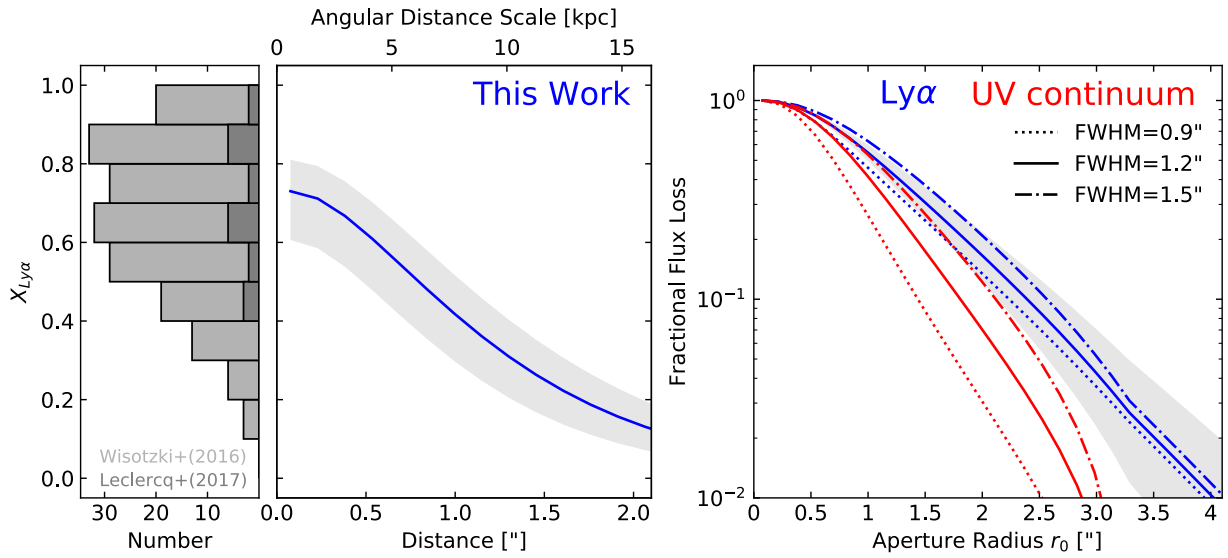

Figure 2.3. *Left:* the number distribution of the fractional contribution of the LAH to the total Lyα flux, $X_{\mathrm{Ly}\alpha}$, as reported by [129, light grey] and [130, dark grey]. *Middle:* $X_{\mathrm{Ly}\alpha}$ as a function of the distance from the galactic center to the inner 'edge' of the LAH (r_{halo}) computed using the Equations 2.5-2.7. The blue line indicates the best-fit model with the grey shade shows the 1σ uncertainties. *Right:* both the intrinsic size of the emission and the image PSF lead to the loss of flux falling outside a given aperture. Using our best-fit profiles, we compute the fractional loss of the UV continuum (red) and Lyα emission (blue) of typical LAEs as a function of aperture size assuming three representative seeing values (full-width-at-half-maximum of $0.9''$, $1.2''$, and $1.5''$shown as dotted, solid, and dashed-dot lines, respectively). For example, at seeing $1.2''$, $\approx$ 30% (20%) of the total Lyα (UV continuum) flux falls outside the $1.5''$ radius circular aperture.

where the halo and total fluxes, F_{h} and F_{tot}, are computed as:

$$F_{\mathrm{h}} = \int_{r_{\mathrm{halo}}}^{\infty} 2\pi r S_h \exp(-r/r_{\mathrm{s,h}}) dr; \tag{2.6}$$

$$F_{\mathrm{tot}} = \int_{0}^{\infty} 2\pi r [S_c \exp(-r/r_{\mathrm{s,c}}) + S_h \exp(-r/r_{\mathrm{s,h}})] dr \tag{2.7}$$

We note that, unlike F_{tot}, the integration interval for F_{h} in Equation 2.6 is set to $[r_{\mathrm{halo}},\infty]$; i.e., F_{h} encloses the observed flux outside the central region where $r = r_{\mathrm{halo}}$ serves as the inner 'edge' of the LAH, or equivalently, the outer edge of the galaxy. This definition is

motivated by the fact that, at a distance comparable to or smaller than the size of the host galaxy, the physical meaning of the LAH (as a component separate from the galaxy emission) becomes ambiguous in all but a mathematical sense. However, our definition of $F_{\rm h}$ would be identical to that used in [129] and [130] if $r_{\rm halo}$ is set to zero.

In the middle panel of Figure 2.3, we show $X_{{\rm Ly}\alpha}$ as a function of $r_{\rm halo}$. The 1σ uncertainties (grey shade) are computed by bootstrapping the radial profile measurements. At $r_{\rm halo} = 0$, our halo fraction is $73^{+8}_{-12}\%$, in good agreement with those estimated by [129] and [130] (light grey and dark grey histograms, respectively, in the left panel of Figure 2.3), and also consistent with the expectation from simulations with a realistic treatment of the ISM [149]. When evaluated at $r_{\rm halo} = 0.5''$ (3.9 kpc at $z = 3.13$) which lies safely outside typical galaxy sizes, the halo fraction decreases to $61^{+9}_{-12}\%$. Our analysis indicates that, for LAEs, the flux from the Lyα halo easily dominates over that originating from the galaxy itself, even in the most conservative estimate.

From the observational viewpoint, it is often useful to know what fraction of the flux falls outside a given aperture. The calculation is similar to that shown in Equation 2.6 except that we integrate the *observed* surface brightness instead of the intrinsic one. In the right panel of Figure 2.3, we show the fractional loss of the Lyα (purple) and continuum r-band (blue) flux as a function of aperture radius, r_0. We start by convolving the best-fit radial profiles with the gaussian kernels with the full-width-at-half-maximum of $0.9''$ (dotted), $1.2''$ (solid), and $1.5''$ (dash-dotted), respectively, to simulate the realistic range of seeing in ground-based observations, which also affect the flux loss.

In a $3''$ aperture in diameter ($r_0 = 1.5''$), the flux loss is $32\% \pm 6\%$ in the Lyα image, much larger than $19.0\% \pm 0.4\%$ in the r band. The aperture radius which encloses 90% of the total flux, r_{90}, is $2.4''\pm$ $0.3''$for the Lyα band, considerably smaller than $r_{90} = 3.7''\pm0.2$ $''$measured for a sample of galaxies with both Hα and Lyα emission [197]. The discrepancy is too large to be explained by the difference in image quality.

The origin of this disagreement is likely intrinsic. Although the galaxies in both samples are both detected with significant Lyα line excess, the Hα-Lyα emitters tend to have larger stellar masses and higher star formation rates (SFRs) than our LAEs. [197] made the stellar mass estimates based on the spectral energy distributing (SED) fitting and reported

$\log(M_{\rm star}/M_\odot) = 8.6 - 11.1$ with a median of 10.3 (see their Table 1). Although we do not have a direct estimate of stellar mass for our LAE sample, photometrically selected LAEs tend to be low-mass galaxies in the range $(10^8 - 10^9)M_\odot$ [114], [123]–[125]. As for the SFR, [197] reported the range $(3 - 50)$ $M_\odot$ yr^{-1} with a median of 20 $M_\odot$ yr^{-1}, once again, much larger than ≈ 5 $M_\odot$ yr^{-1} for our sample by using dust-corrected SFRs generated by observed UV luminosity [125, also see Section 2.5.3]. In Section 2.4.3, we discuss how the LAH sizes change with physical properties.

2.4.3 On the LAH sizes

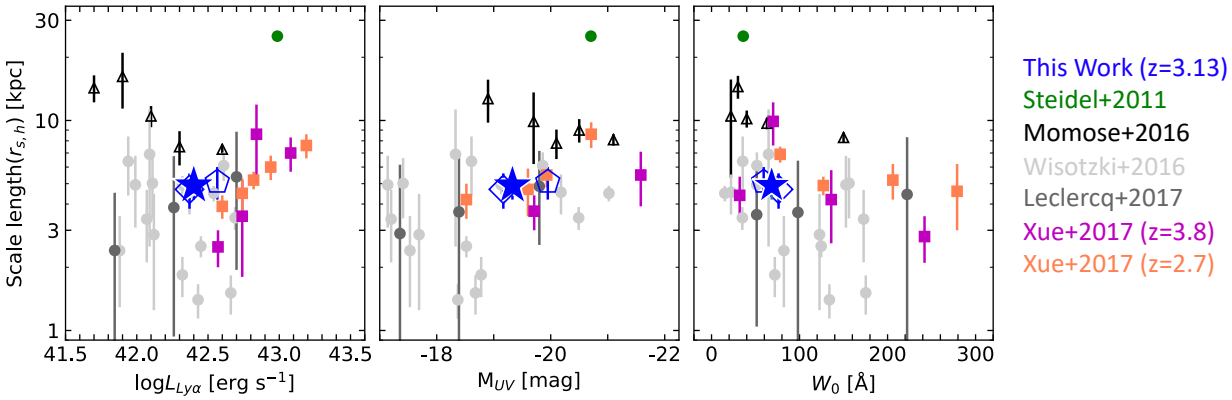

Figure 2.4. LAH sizes as a function of Lyα luminosity, UV luminosity, and Lyα rest-frame equivalent wavelength. Our measurement is shown as blue stars together with the literature measurements including those from [184, green circles], [186, black open triangles], [129, light grey filled circles], X17 (orange filled squares for $z = 3.8$ and purple squares for $z = 2.7$), and [130, dark grey filled circles]. The [130] data are binned and the median value and standard deviation in each bin are displayed. We show the stacked LAH measurements respectively for the LAEs in the protocluster (blue open pentagon) and in the field (blue open diamond).

In Figure 2.4, we show the compilation of Lyα size measurements in the literature as a function of line and continuum luminosity and W_0. The measurements of the full LAE sample, protocluster- and field subsamples are indicated as a blue star, open pentagon and open diamond, respectively. Overlaid are similar measurements based on image stacking for the photometrically selected LAEs at $z \sim 2.7$ and ~ 3.8 (X17, orange and purple,

respectively) and at $z \sim 2.2$ [186, open triangles]. We also show individual measurements for $z \sim 3-6$ star-forming galaxies from deep MUSE observations from [129, light grey circles] and [130, dark grey circles]. The latter measurements are binned[4] for clarity. A green circle in each panel represents the stacked measurement of UV-selected star-forming galaxies [184], with a median equivalent width of 0.9Å (and the range $-27 \leq W_0 \leq 89$Å), the majority of which would not be classified as LAEs. The remainder of the literature samples shown in Figure 2.4 employed the classical definition of LAEs, i.e., $W_0 \geq 20$Å with the exception of the $z \sim 2.7$ sample of X17, which used $W_0 \geq 50$Å.

While limited, our size measurements are in line with the existing data. In particular, the agreement is excellent when compared with the measurements that employed a similar decomposition method which simultaneously fits the galaxy and the LAH component (see Section 2.4.1), namely, those in [130] and X17. Disagreement with the [185] and [184] may be in part due to the difference in the fitting method in that they only considered a single component. For an in-depth discussion of how the size measurement can be affected by the fitting method and image point spread function, we refer interested readers to the Appendix C of X17.

Figure 2.4 showcases the overall trend that the LAH sizes increase with both Lyα luminosity and UV luminosity while showing little correlation with galaxy environment. The very large LAH size [$\approx$ 25 kpc: 184] measured for UV continuum selected star-forming galaxies lies far above these trends, suggesting that a different scaling relation may apply to non-LAEs. The larger LAH sizes for more UV-luminous galaxies imply that the flux loss we estimate in Section 2.4.2 is only applicable to typical LAEs (which are UV-faint, $M_{\rm UV} \gtrsim -20$) and cannot be generalized to all star-forming population.

Discerning how LAH sizes and Lyα surface brightness profiles change with the properties of host galaxies and their large-scale structure can place strong constraints on the dominant physical mechanism that powers the Lyα halo (see, e.g., [94], [186]; X17; [130]). Possible scenarios include resonant scattering of the Lyα photons originating from star formation in the CGM [149], [158], [198], gravitational cooling radiation [150], [156]–[158], and star

[4]↑As for the binning, we used $< 10^{42}$, $10^{42} - 10^{42.5}$, and $> 10^{42.5}$ erg s^{-1} for the line luminosity, > -18, $-(18-19)$, and ≤ -19 mag for the UV absolute magnitude, < 75, 75–150, and ≥ 150 Å for W_0.

formation in ultra-faint satellite galaxies [147], [150]. While the limited nature of our measurement (based on a single stack) prevents us from placing a new meaningful constraint on these scenarios, we stress that the mild disagreement between existing measurements, the large scatter observed in the individual measurements and the apparent dichotomy between LAEs and non-LAEs in LAH sizes seen in Figure 2.4 highlight the incompleteness of the current observational picture. Larger samples spanning a wider range of parameter space (in luminosities and large-scale environment) will be crucial in establishing clearer trends and in discriminating different physical scenarios.

2.5 Lyman α Escape fraction

The escape fraction of Lyα photons is expected to be a sensitive function of not only a galaxy's dust content but also of the distribution of gas and dust therein. In a medium in which the H I gas and dust are uniformly mixed, resonant scattering of Lyα photons renders them to suffer a higher degree of extinction relative to continuum photons at a similar wavelength. As a result, a galaxy selection based on Lyα line equivalent width would be heavily biased towards galaxies with little to no dust. While such an expectation is in line with a majority of LAEs [112], [123], [124], [169], [199], some LAEs are very dusty [e.g., 199]–[204], suggesting that other factors may contribute to the escape of Lyα photons [205]–[207].

The relative distribution of gas and dust is important. [207] showed that the measured Lyα-to-Hα line ratio of local LAE analogs favors a 'clumpy dust screen' scenario in which Lyα-emitting gas is spatially segregated from the dust which exists in clumps. Clumpy dust results in a more porous medium through which Lyα photons can travel with more ease, thereby enhancing their transmission relative to the same amount of gas and dust in a uniform mixture. In the 'clumpy multi-phase' scenario [208], dust coexists with H I gas in clumps embedded in an otherwise warm, ionized medium. Such a configuration would increase Lyα transmission greatly as continuum photons are more prone to dust extinction while Lyα photons scatter off the clump and propagate through the ionized medium.

In this section, we present the Lyα escape fraction, $f_{\rm esc}$, measured for our LAE sample. We also present the *total* escape fraction including the contribution from diffuse Lyα emission, which is not accounted for in the majority of existing measurements [but see 135]. We also evaluate the possible correlation between $f_{\rm esc}$ and other galaxy properties and discuss possible implications of our results on the distribution of gas and dust.

2.5.1 Measuring the Lyman Alpha Escape Fraction

For our analyses in this and subsequent sections, we only consider 62 LAEs for which we have robust measurements of the UV slope β. To this end, we only use the galaxies with $\Delta\beta < 0.9$. A majority of the sources that do not meet this criterion are simply too faint in the images and typically have inferred UV luminosities $\log(L_{1700}) \lesssim 27.3$ erg s^{-1} Hz^{-1}. Following the convention, we compute the Lyα escape fraction as:

$$f_{\rm esc} = \frac{\rm SFR(Ly\alpha)}{\rm SFR(UV) \times 10^{(0.4 k_{1500} E(B-V))}} \tag{2.8}$$

where the color excess $E(B-V)$ is converted from the UV slope β by assuming the [209] extinction law. For the UV- and Lyα-based SFR, we adopt the [110] calibration. k_{1500} denotes the effective dust extinction at rest-frame 1500Å.

The median (mean) value is 60 (101^{+107}_{-101})% for our LAE sample. Of the 62 LAEs, nearly one third (21) have $f_{\rm esc}$ values greater than unity, nine of which lie within the protocluster (see Section 2.3.1). 9 LAEs (2 in the protocluster) do so at a $\geq 1.5\sigma$ level. In comparison, [178] reported 24% for spectroscopically selected LAEs with $f_{\rm esc}$ greater than unity at z=1.9–3.8. Both numbers are based on dust-corrected UV continuum to infer SFRs and thus are subject to similar systematics. Excluding the protocluster LAEs brings down the fraction of LAEs with $f_{\rm esc} \geq 1$ to 27% in a better agreement with [178]. Comparison of field vs protocluster LAEs is given in Section 2.7.

Larger-than-unity $f_{\rm esc}$ values in these two samples may in part arise from photometric scatter, particularly in the bands used for estimating β. To quantify how robustly the estimates of β and $f_{\rm esc}$ can be made for individual galaxies, we create image simulations

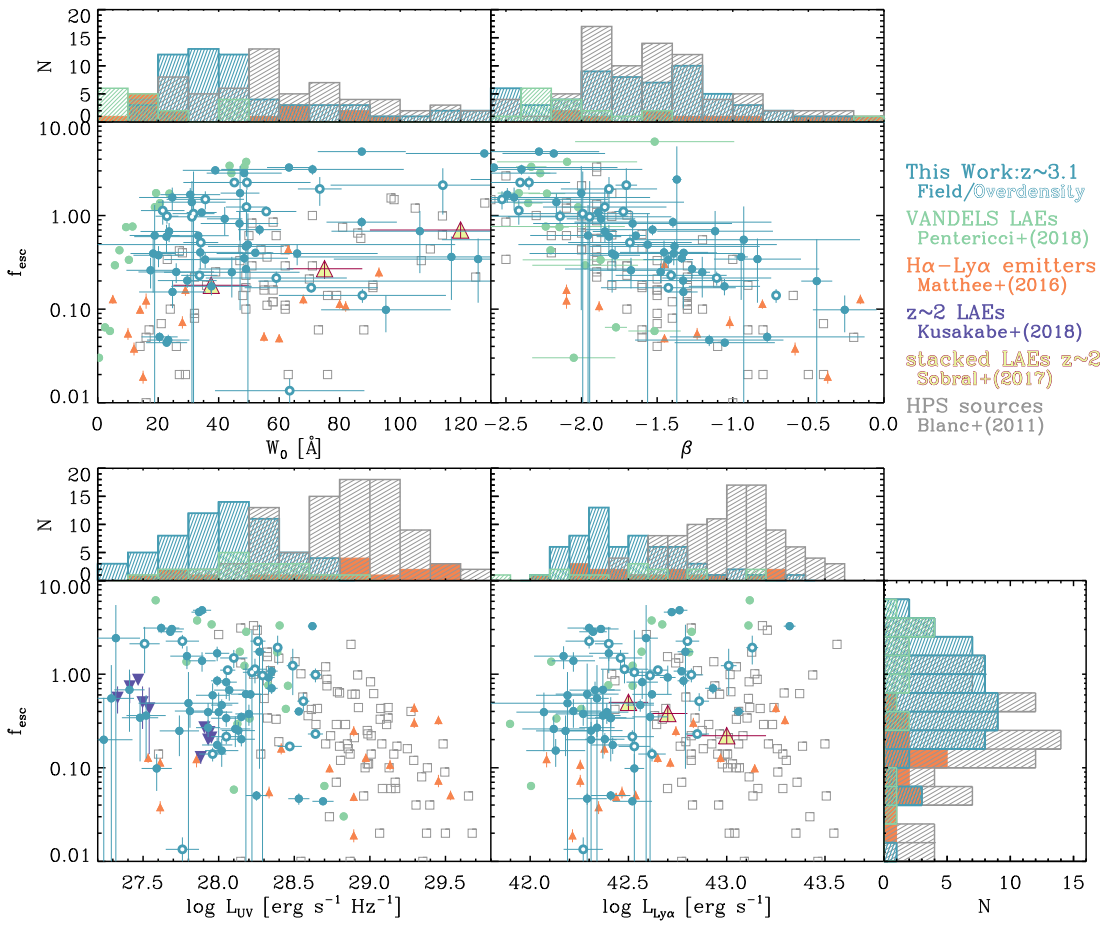

Figure 2.5. Lyα escape fraction as a function of Lyα equivalent width (top left), UV continuum slope β (top right), observed UV and Lyα luminosity (bottom panels) from this work (teal circles) and literature measurements, which include the VANDELS sources [green circles: 181], $z \sim 2$ LAEs [purple downward triangles: 135], the HETDEX Pilot Survey emitters [grey squares: 178], stacked LAEs at $z \sim 2$ [yellow upward triangles: 210], and Hα-Lyα dual emitters [orange upward triangles: 197]. Protocluster (field) LAEs from our sample are shown as open (filled) circles. The histograms show the overall distributions of different samples in each parameter space.

calibrated to closely reflect the brightness and the colors of the real LAEs. While the details of our simulations are given in Appendix 2.9, our result suggests that the photometric recovery of β values is reasonably good at $\beta \approx -2$ (≈ 0.2 dex), as illustrated in Figure 2.11. Photometric scatter tends to result in the recovered β values being more positive than the intrinsic ones, leading to the underestimation – and not overestimation – of $f_{\rm esc}$ values.

Furthermore, many of our LAEs with $f_{\rm esc}> 1$ have relatively small $\Delta\beta$, placing their $f_{\rm esc}$ values $> (2-3)\sigma$ outside the nominal $f_{\rm esc} = 1$ line (see Figure 2.5). Based on these considerations, we argue that, while we cannot rule out the contribution of photometric scatter on $f_{\rm esc} > 1$ sources, it is unlikely to be the sole driver of the $f_{\rm esc} > 1$ sources.

There are multiple physical factors which may result in the larger-than-unity $f_{\rm esc}$. First, radiative transfer through the ISM of complex geometry may cause Lyα emission to have a preferential direction [e.g. 149] unlike continuum emission; in this case, the ratio of Lyα to UV emission would have little physical meaning. While possible, this is unlikely to be the dominant cause given the relatively tight correlation of $f_{\rm esc}$ and other galaxy properties (see Section 2.6). Second, low-level AGN may contaminate our sample. As discussed in Section 2.3, few of our LAEs have spectroscopic observations. It is also possible that the underlying assumptions we make about these galaxies are wrong: they have had relatively continuous and prolonged star formation histories and have solar or moderately sub-solar metallicities. While Lyα luminosity traces instantaneous star formation (< 10 Myr), far-UV continuum luminosity represents the SF activity averaged over the last ≈ 100 Myr [110]. Similarly, substantially subsolar metallicities would result in higher ionizing radiation at a fixed mass. Thus, highly episodic SF activities, extremely young ages, and low metallicities will all lead to a higher Lyα output relative to the UV and can result in seemingly unphysical $f_{\rm esc}$ values [211]–[214].

Alternatively, the dust law we assume to convert measured UV flux density to SFR may not be appropriate. Existing studies [e.g., 215], [216] found that UV-selected star-forming galaxies dominated by younger stellar populations may be better characterized by a Small Magellanic Clouds-like dust law [217]. [218] reached a similar conclusion for a large sample of LAEs. However, an SMC-like dust law would exacerbate the problem at hand. Assuming the SMC law, a given UV slope β would correspond to a smaller color excess E$(B-V)$, leading to an even larger $f_{\rm esc}$ than previously.

2.5.2 Total Escape Fraction of Lyα photons

After excluding the galaxies with $f_{\rm esc} \geq 1$, the median (mean) value of the Lyα escape fraction for our sample is 36 (40$\pm$26)%. Our estimation is in good agreement with other LAE samples in the literature[5], including 29^{+40}_{-29}% [178], 38%$\pm$11% [219] and 37%$\pm$7% [220]. One exception is the Hα-emitting LAE sample [11 $\pm$ 11%: 197], which shows considerably lower $f_{\rm esc}$ values than the rest. As discussed in Section 2.4.2, these Hα-Lyα emitters tend to be more UV-luminous and have larger stellar masses than those identified based on Lyα emission alone, likely signaling that $f_{\rm esc}$ correlates with these physical parameters (see Section 2.5.3).

So far, we have considered the $f_{\rm esc}$ values measured within the galaxy-sized apertures as has been done in the literature. If Lyα emission from the LAH originates from the same H II regions as that from the galaxy, the $f_{\rm esc}$ estimates would need to be revised to account for the additional contribution from the LAH. Using the radial surface brightness profiles of the stacked Lyα and UV images (Section 2.4.2, Figure 2.3), we estimate the total Lyα escape fraction by statistically correcting for the expected flux loss. For the correction, we use the radius of the effective circular aperture, defined as $r_0 = \sqrt{A_{\rm iso}/\pi}$ of each LAE. r_0 ranges from 0.6″–2.0″ with a median of 1.0″ (7.8 kpc). The Lyα flux loss ranges in 6–77% with a median of 54%, mainly due to the extended nature of the halo. While smaller, the UV flux loss due to PSF blurring (seeing 1.2″) is also not negligible, ranging in 10–69% with a median of 40%.

We find the median (mean) value of the *total* Lyα escape fraction, $\langle f_{\rm esc,tot} \rangle$, is 46 (51$\pm$32)% in good agreement with 42 $\pm$ 24% reported by [135], which includes the LAH flux in their estimation. Similar to ours, [135] also defined their LAEs to be galaxies with $W_0 \geq 20$Å. While our value is higher than those in the literature, the relative increase is modest at $\approx$ 29% when the flux loss correction is made consistently for both UV and Lyα fluxes. Additionally, the LAH size for typical LAEs is small enough (4.5 kpc corresponds to 0.57″ at $z = 3.13$) that galaxy-sized apertures can contain much of the flux.

[5]↑The Lyα equivalent width cut is slightly different among the literature, from 20Å [178], 65Å [219], 16Å [220] and 4Å for Hα-detected galaxies studied by [197].

2.5.3 Variations of Lyα Escape Fraction

We explore how $f_{\rm esc}$ values correlate with the galaxies' UV and Lyα properties by combining our own measurements with those in the literature. Since most of these measures do not include the LAH component, we opt to use our $f_{\rm esc}$ values before the LAH correction. Given the modest change that it brings, our conclusion should not change substantially.

In Figure 2.5, we show the correlations of $f_{\rm esc}$ with W_0, UV slope (β), and line and continuum luminosities. In all cases, we show protocluster LAEs with larger symbols than those in the field. Other measurements include 89 galaxies from the HETDEX Pilot Survey [HPS hereafter: 178], 17 LAEs with Hα detection [197], and 18 spectroscopic Lyα detections from VANDELS. The average measurements via stacking analysis of $z \sim 2.2$ LAEs [220] are also shown.

The HPS LAEs span a comparable range of UV slope and W_0 to our sample, but tend to have higher line and UV luminosities; the Hα-Lyα emitters studied by [197] are much more UV-luminous than the rest. The VANDELS sources are comparable to our LAEs in both luminosities but have considerably bluer UV slopes and smaller W_0.

In order to test how these physical properties affect $f_{\rm esc}$, we use two non-parametric ranked correlations, namely, the Kendall's τ and Spearman's ρ rank correlation coefficients [221], [222]. Both tests are run for each parameter shown in Figure 2.5 using two Python scripts `scipy.stats.kendalltau` and `scipy.stats.spearmanr`. To check the consistency, we run these tests on our dataset and the HPS dataset separately then on the combined dataset (our LAEs+HPS and LAEs+HPS+VANDELS). We do not include the [135] measures on our tests because they represent the stacked averages. In Table 2.1, we list the correlation coefficients (τ and ρ) and the probabilities of null hypotheses (p-value). We consider the case with either τ or ρ is larger than 0.6 as a robust correlation while $\approx$0 values in these parameters indicate no correlation.

We find a clear anti-correlation between $f_{\rm esc}$ and the UV continuum slope β, in agreement with existing studies [e.g., 178], [179]. This is not surprising considering that we use the β value as a proxy for dust reddening to correct the SFR$_{\rm UV}$ in our estimation of $f_{\rm esc}$.

Table 2.1. Rank Correlation Coefficients from Kendall's τ and Spearman's ρ Tests

Samples	W_0	β	$L_{\rm UV}$	$L_{{\rm Ly}\alpha}$
Kendall's τ Test: $\tau_{\rm K}$ ($p_{\rm K}$)				
This Work	0.118 (0.174)	0.653 (< 0.001)	0.046 (0.597)	0.189 (0.030)
HPS	0.013 (0.856)	0.704 (< 0.001)	0.518 (< 0.001)	0.120 (0.083)
This Work+HPS	0.037 (0.492)	0.645 (< 0.001)	0.418 (< 0.001)	0.100 (0.060)
This Work+HPS+VANDELS	0.032 (0.522)	0.625(< 0.001)	0.403 (< 0.001)	0.045 (0.372)
Spearman's ρ Test: $\rho_{\rm SR}$ ($p_{\rm SR}$)				
This Work	0.169 (0.188)	0.835 (< 0.001)	0.0786 (0.543)	0.287 (0.023)
HPS	0.048 (0.636)	0.872 (< 0.001)	0.656 (< 0.001)	0.160 (0.113)
This Work+HPS	0.065 (0.410)	0.827 (< 0.001)	0.566 (< 0.001)	0.144 (0.068)
This Work+HPS+VANDELS	0.057 (0.446)	0.807 (< 0.001)	0.544 (< 0.001)	0.069 (0.361)

A weaker correlation with observed UV luminosity is notable: the trend is clear when the combined dataset is considered which spans two orders of magnitude in luminosities. In this parameter space, the Hα-Lyα emitters are no longer significant outliers but part of the correlation at the highest luminosity end. The trend is likely related to the fact that lower-luminosity star-forming galaxies tend to have bluer β values at high redshift [e.g., 151], [223]. We further quantify the luminosity dependence in Section 2.6.2.

No correlation is found with line luminosity or W_0. This is in contrast to the anti-correlation between $L_{\mathrm{Ly}\alpha}$ and f_{esc} reported by [220] which is based on stacking analyses. While their measurements are not inconsistent with the mean values of the combined dataset, the intrinsic scatter is too large to discern any meaningful correlation.

All in all, we conclude that the galaxy's dust reddening and UV luminosity are two primary determinants of the escape fraction of Lyα photons. In the next section, we further quantify these dependencies further to shed light on the physical driver of their escape.

2.6 The Role of Dust and UV Luminosity on f_{esc}

We examine how dust opacity affects the Lyα escape fraction. Following [225], we express the escape fraction as:

$$f_{\mathrm{esc}} = C_{\mathrm{Ly}\alpha} \cdot 10^{-0.4E(B-V)k_{\mathrm{Ly}\alpha}} \tag{2.9}$$

When $C_{\mathrm{Ly}\alpha} = 1$, $k_{\mathrm{Ly}\alpha}$ denotes the effective dust attenuation at Lyα wavelength. Even when $C_{\mathrm{Ly}\alpha} \neq 1$, $k_{\mathrm{Ly}\alpha}$ can still be thought of dust attenuation in a relative sense. As a reference, the escape fraction expected for non-resonant photons at the same wavelength is $k \approx 12$ and $C = 1$ for the [209] dust law.

In Figure 2.6, we show the positions of our LAEs in the $\log f_{\mathrm{esc}}$ – E$(B-V)$ space. There is a clear trend that f_{esc} decreases with increasing dust reddening, in qualitative agreement with existing studies at high redshift [178], [179], [225] and at low redshift [207], [226]–[228].

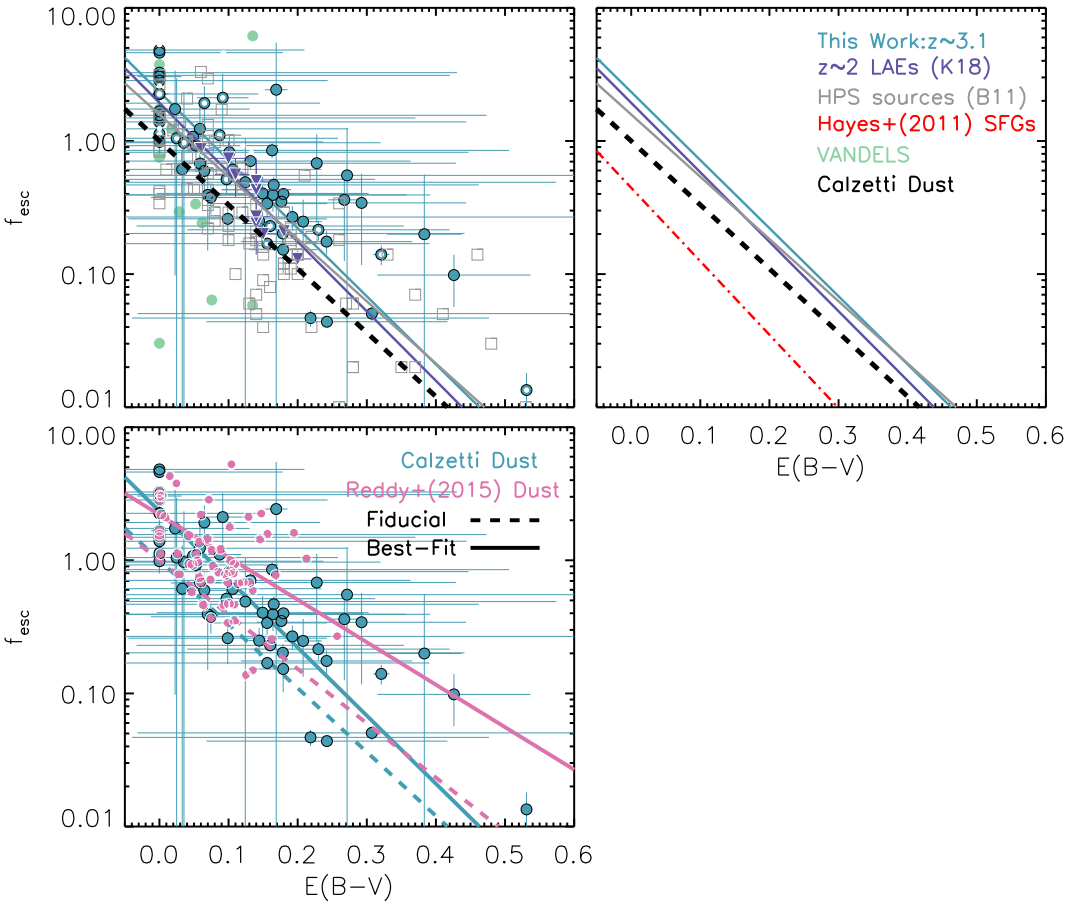

Figure 2.6. *Top-left:* Lyα escape fraction as a function of E$(B-V)$. Teal circles, purple downward triangles, green circles and grey open squares represent measurements of our LAEs, K18, VANDELS and HPS galaxies assuming [209] dust lae. Teal, purple and grey solid curves are the best models fitting to our work, K18 and HPS galaxies, respectively. Black dashed line is the expectation given the [209] law with no resonant scattering. *Top-right:* comparison among the $f_{\rm esc}$ dependence on E$(B-V)$ of different datasets. Red dash-dotted line is the best model for the H11 galaxies, while the remaining lines are identical to those in the top-left panel. *Bottom-left:* comparison between the $f_{\rm esc}$ measurements assuming the [209, teal] and those assuming [224, pink] dust laws of our LAEs. The best models fitting to the two measurements (solid lines) and the expectation given the [209] and [224] law (dashed lines) are also shown.

Using a Python function `scipy.optimize.curve_fit`[6], we determine the best-fit values for both parameters for our full LAE sample. In this figure, $k_{\rm Ly\alpha}$ and $C_{\rm Ly\alpha}$ appear as the

[6]↑The Python function `scipy.optimize.curve_fit` uses a non-linear least squares to fit a function f to a given data. The best-fit model is the one in which the sum of the squared residuals of $f(x_{\rm data}) - y_{\rm data}$ is at its minimum.

slope and the intercept, respectively. By treating $C_{\mathrm{Ly}\alpha}$ as a free parameter, we do not require that the maximum f_{esc} value be unity at zero reddening. As discussed earlier, unphysically high f_{esc} values may result from low-metallicity or young ages. Alternatively, [225] argued that disparate locations from which stellar and nebular emission originate may have caused $C_{\mathrm{Ly}\alpha} \approx 0.45$ at zero reddening of stellar emission for $z \sim 2$ galaxies. Similarly, [229] found $C_{\mathrm{Ly}\alpha}$ much less than unity for $z \sim 0.3$ LAEs.

We apply the same fitting procedure for i) the HPS sources; ii) the stacked averages of the f_{esc} values measured by [135]; and iii) our full LAE sample combined with the HPS sources. Our results are listed in Table 2.2 and indicated as various straight lines in Figure 2.6. All these measures lie well above the best-fit scaling law determined by [225, the orange line in the top right panel of Figure 2.6] at a fixed reddening.

In all samples, we find that $k_{\mathrm{Ly}\alpha} \approx k_{1216}$: i.e., the relative attenuation scales similarly with dust reddening for both Lyα and continuum photons. The trend applies to all samples despite the large spread in $C_{\mathrm{Ly}\alpha}$ among them. Simultaneously, the mean Lyα optical depth – defined as $\tau_{\mathrm{Ly}\alpha} \equiv -2.5\log(f_{\mathrm{esc}})/\mathrm{E}(B-V)$ – is consistently lower than non-resonant photons at similar wavelength in all but the [225] sample. This is visualized in the top right panel of Figure 2.6 where we compare the best-fit scaling laws from the literature to the expectation from the [209] law at $\lambda_{\mathrm{rest}} = 1216$Å (a thick dashed line). Nearly all of our LAEs have f_{esc} values much higher than this expectation (by a factor of $\approx$2, on average: see Table 2.2).

To test how robust our results are against the assumed dust law, we recompute both $\mathrm{E}(B-V)$ and f_{esc} values assuming the [224] dust law (the bottom left panel of Figure 2.6). Once again, we find $k_{\mathrm{Ly}\alpha} = 7.98 \pm 2.11$ reasonably close to $k_{1216,\mathrm{Reddy}} = 10.33$ for continuum photons. The mean Lyα optical depth is significantly lower than that expected from the [209] dust as driven by the large $C_{\mathrm{Ly}\alpha}$. We conclude that Lyα photons – in all LAE samples considered here – suffer *similar* interstellar attenuation to continuum photons regardless of assumed dust law.

Finally, through realistic image simulations, we quantify how well we can constrain an underlying f_{esc}-$\mathrm{E}(B-V)$ scaling law through photometric measurements given the uncertainties expected in estimating line- and continuum luminosities as well as the UV slope.

Table 2.2. The Dependence of Lyα Escape Fraction on Dust Opacity

Sample	$k_{\mathrm{Ly}\alpha}$	$C_{\mathrm{Ly}\alpha}$ Calzetti Dust	χ^2 (DoF[1])	$k_{\mathrm{Ly}\alpha}$ ($f_{\mathrm{esc}} \leq 1$)	$C_{\mathrm{Ly}\alpha}$	$k_{\mathrm{Ly}\alpha}$ ($C_{\mathrm{Ly}\alpha} = 1$)	χ^2 (DoF[1])
This Work	12.79 ± 2.31	2.33 ± 0.10	31.03 (60)	5.82 ± 1.00	0.92 ± 0.10	4.34 ± 2.06	59.16 (61)
blanc2011	10.02 ± 2.00	1.35 ± 0.15	26.79 (87)	8.23 ± 1.07	0.72 ± 0.06	7.35 ± 1.38	28.66 (88)
kusakabe18	13.05 ± 2.11	1.93 ± 0.40	-	-	-	7.41 ± 1.00	-
This Work+HPS	12.21 ± 1.60	1.88 ± 0.12	65.58 (149)	6.72 ± 0.78	0.76 ± 0.05	6.02 ± 1.32	88.68 (150)
c.f. hayes11	13.8	0.445	-	-	-	-	-

[1] Goodness-of-the-fit is given as the total chi-square while the degree of freedom is the number of LAEs included in the fit minus the number of free parameters.

While the details of our simulation are given in Chapter 2.9, Figure 2.12 illustrates that our photometric measurements can reliably determine an underlying scaling relation.

2.6.1 Comparison with ISM models

We consider our result in the context of several ISM models in the literature. First, in a medium composed of uniform mixtures of dust and H I gas, the effective attenuation of Lyα photons should be much higher than continuum photons [e.g., 230] as the former traverse much longer path lengths than the latter, leading to $f_{\rm esc}$ values much lower than the continuum expectation. Our results suggest the opposite.

Alternatively, in a "multi-phase" medium where dust is mostly confined within H I clumps embedded in an otherwise ionized dust-free medium [208], Lyα photons spend most of their time traveling in the intercloud medium while occasionally scattering at cloud surfaces. Thus, $f_{\rm esc}$ primarily depends on cloud albedo (the likelihood of surface absorption by dust) and the number of Lyα scattering before their eventual escape. The consequence is that the dependence of $f_{\rm esc}$ on total dust optical depth is mild at best [231], [232]. In contrast, continuum photons travel through clumps and undergo more severe attenuation. The selective attenuation can enhance Lyα W_0 to, in some cases, above the case B expectation. The degree of W_0 enhancement increases with increasing extinction.

One possible exception would be if star formation mainly occurs deep inside cold H I clouds where dust resides, Lyα photons are decimated by dust absorption before they reach the cloud surface, leaving the role of preferential resonant scattering less consequential [149]. All in all, the strong anti-correlation between $f_{\rm esc}$ and dust reddening, the lack of LAEs with excessively high W_0, and the larger-than-expected $f_{\rm esc}$ are at odds with the multi-phase ISM.

Finally, [207] considered a 'clumpy dust screen' through which Lyα photons take the paths of the least resistance (i.e., escaping through the holes with the lowest opacity between clumps). The process allows $f_{\rm esc}$ to increase while keeping W_0 unchanged without invoking preferential resonant scattering [also see 229]. One defining characteristic of this model is that the relative Lyα enhancement scales with dust extinction, resulting in $k_{\rm Ly\alpha} < k_{1216}$. In Figure 2.6, the effect would manifest itself as a shallower slope. Resonant scattering would

increase Lyα optical depth, bringing the scaling relation closer to the uniform dust screen expectation by steepening the slope $k_{\mathrm{Ly}\alpha}$.

The clumpy dust screen scenario also does not align well with the existing measurements. In all three LAE samples in Table 2.2, we consistently find $k_{\mathrm{Ly}\alpha} \approx k_{1216}$ within uncertainties. There is only one exception: if we only consider sources with $f_{\mathrm{esc}} \leq 1$, the formal fit favors a considerably lower $k_{\mathrm{Ly}\alpha}$ values (≈ 6: column 4 in Table 2.2. A similar reanalysis of the HPS sources, however, results in a marginal change in the slope, from 10.0 to 8.2, suggesting that the dramatic change we observe in our result is caused by a small sample size. Regardless, the removal of those with $f_{\mathrm{esc}} \geq 1$ without a firm physical basis is arbitrary at best. If the underlying assumptions we made in deriving the escape fraction are incorrect (as discussed in Section 2.5.1), the correction needed to recover the true quantities would have to be uniformly applied to all LAEs. Larger sample sizes would improve the measurements, particularly, by getting a better handle on the f_{esc} values of highly reddened LAEs and their intrinsic scatter.

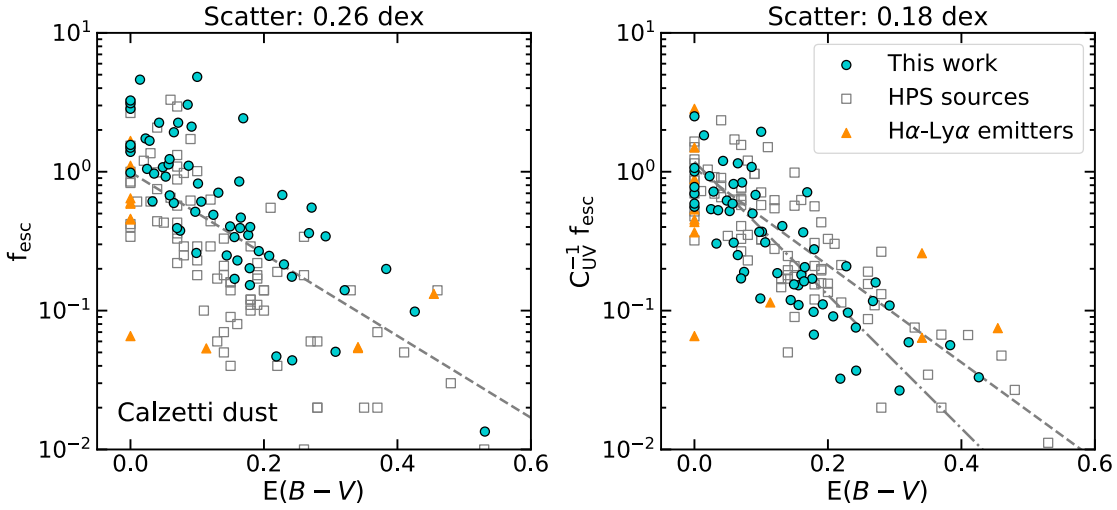

Figure 2.7. Lyα escape fraction as a function of E($B-V$) before (left) and after (right) renormalizing f_{esc}, including measurements from this work (teal circles), HPS sources [grey open squares: 178] and Hα-Lyα emitters [orange triangles: 197]. Dashed lines in both panels are the best-fit models assuming Equation 2.9. Dash-dotted line in the right panel shows the best-fit model assuming the same equation, while fixing the slope $k_{1216} = 12$ according to [209] dust law. Scatters above the figure suggest the root mean square scatters between data points and the best-fit models (dashed lines).

In summary, our results show that Lyα photons undergo interstellar dust attenuation in a similar manner to continuum radiation (i.e., $k_{\mathrm{Ly}\alpha} \approx k_{1216}$). However, the overall Lyα transmission is roughly twice higher than that expected for continuum photons. The constraints derived from one of the largest compilations of LAEs to date appear to favor some form of multi-phase media conducive to the preferential transfer of Lyα photons. Yet, none of the models we have considered is entirely in line with our findings, hinting that the distribution of interstellar gas and dust in distant galaxies is complex. One possibility may be a hybrid of the two aforementioned models in which H I clouds are rendered partially porous due to strong stellar feedback. This would allow for a substantial fraction of Lyα photons to escape from their birth cloud relatively easily and proceed to undergo selective attenuation via resonant scattering. Detailed calculations will require full radiative transfer calculations based on realistic simulations at sub-parsec scale resolution.

2.6.2 Dependence of f_{esc} on UV luminosity

The range of $C_{\mathrm{Ly}\alpha}$ changes substantially from ≈0.45 for the [225] sample to ≈1.4 for the HPS sources to ≈2 for the other LAE samples while the slope $k_{\mathrm{Ly}\alpha}$ remains unchanged: i.e., at a fixed reddening, f_{esc} varies up to ≈4 in these samples. The high $C_{\mathrm{Ly}\alpha}$ is real as the majority of our LAEs lie well above the fiducial Calzetti expectation (Figure 2.6, top right).

We evaluate the goodness-of-the-fit by computing the total chi-square value as: $\chi^2 = \Sigma_{\mathrm{i}}(f_{\mathrm{esc,model}}(\epsilon_{\mathrm{i}}) - f_{\mathrm{esc,i}})^2/\sigma^2_{\mathrm{esc,i}})$ where $f_{\mathrm{esc,i}}$ and σ_{esc} are the estimates of the Lyα escape fraction and its error, ϵ_{i} is the estimated $\mathrm{E}(B-V)$ value for the galaxy i; $f_{\mathrm{esc,model}}$ is computed using Equation 2.9. Although the measurement errors are unlikely to obey a gaussian distribution and therefore χ^2 value does not carry the usual statistical significance, it should still provide us a way to evaluate whether a given model gives a better description of the data over another. When we refit the data while forcing $C_{\mathrm{Ly}\alpha}$ to be unity, we obtain unrealistically shallow slopes $k_{\mathrm{Ly}\alpha}$ with a much poorer agreement with the data with the total χ^2 increasing from $\sim$ 30 to 60. The results for our single-parameter fits are listed in Table 2.

The differences in $C_{\mathrm{Ly}\alpha}$ appear to be linked to galaxies' UV luminosities. Figure 2.5 shows that the HPS sources tend to be more UV-luminous than our LAEs by nearly an

order of magnitude while the W_0 and β distributions of the two samples largely overlap. As for the Hα-Lyα emitters from [197], which have the lowest $f_{\rm esc}$ values, all but four lie at the bright end ($L_{\rm UV} > 10^{28.3}$ erg s^{-1} Hz^{-1}; $M_{\rm UV} < -20.7$), but they too have the W_0 and $L_{{\rm Ly}\alpha}$ range similar to our LAEs. Thus, we conclude that $f_{\rm esc}$ depends not only on the galaxy's dust content but also on its UV luminosity.

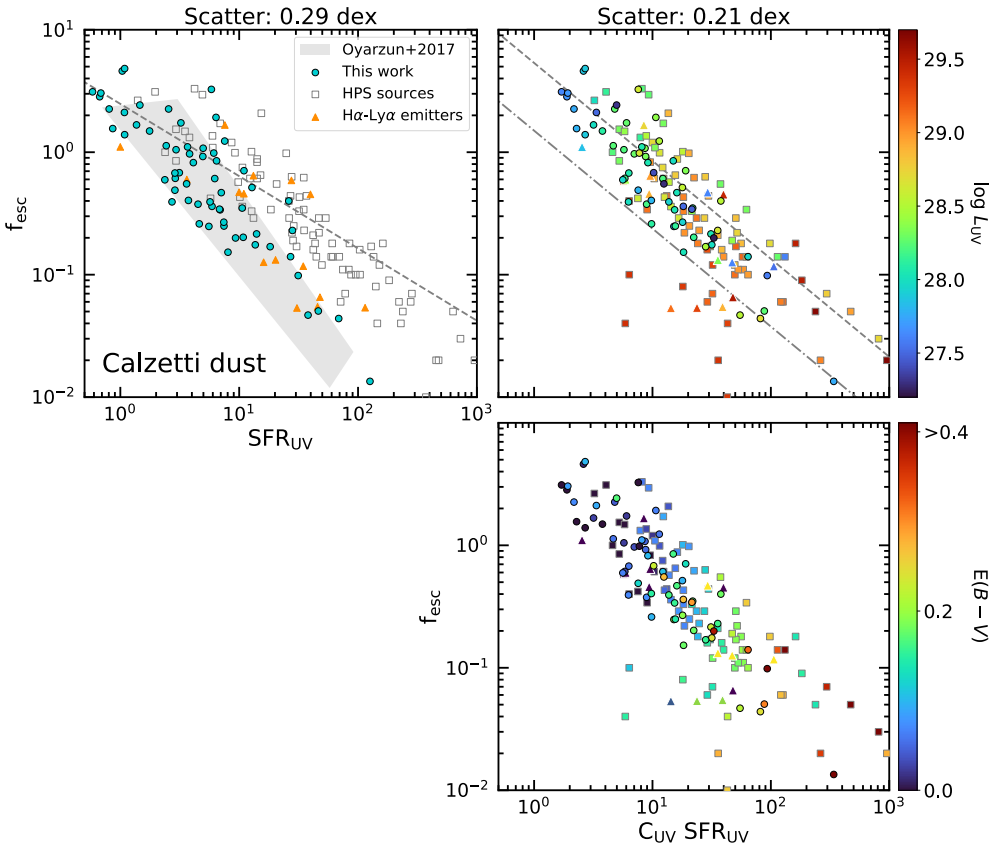

Figure 2.8. *Top-left:* Lyα escape fraction as a function of intrinsic SFR as observed, including the measurements of this work (teal circles), HPS galaxies [grey open squares: 178], and Hα-Lyα emitters [orange triangles: 197]. Grey-shaded area in the top-left panel marks the position of [180] galaxies in parameter space. Dashed lines are the best-fit models assuming power-law correlation between $f_{\rm esc}$ and SFR$_{\rm UV}$. *Top-right:* Lyα escape fraction as a function of renormalized SFR$_{\rm UV}$ (C$_{\rm UV}$SFR$_{\rm UV}$). The symbol shapes are identical to those in the top-left panel, while they are color-coded by galaxies' UV luminosity. Dashed line shows the best model fitting to $f_{\rm esc}$ versus C$_{\rm UV}$SFR$_{\rm UV}$. All the galaxies below the dash-dotted line are identified as outliers which are excluded from calculating the rms scatter. *Bottom-right:* Lyα escape fraction as a function of renormalized SFR (C$_{\rm UV}$SFR$_{\rm UV}$, with the symbols color-coded by E$(B-V)$.

Although we are limited to analyzing the Lyα-emitting population only, our conclusions are in broad agreement with several studies of the general star-forming galaxy population: [233] found an anti-correlation between UV luminosity and Lyα escape fraction in a sample of local Lyman Break Galaxy Analogs. [234] found that the fraction of Lyα-emitting galaxies, X, increases with decreasing UV luminosity among the UV-selected galaxy samples[7]. [180] studied a stellar-mass-selected sample of galaxies z=3.0–4.5 and found that both X and $f_{\rm esc}$ strongly anti-correlate with stellar mass [see also 235]. Given that UV luminosity and stellar mass broadly track each other through the star formation main sequence [236]–[239], the latter correlation is consistent with the $L_{\rm UV}-f_{\rm esc}$ scaling we find. Similarly, [240] found a similar correlation between stellar mass and $f_{\rm esc}$ of [O III] emitters at $z = 1.9 - 2.4$.

Motivated by the dependence of $f_{\rm esc}$ on UV luminosity as shown in Figures 2.5–2.6, we parametrize $f_{\rm esc}$ as:

$$f_{\rm esc} = C_{\rm UV} \cdot 10^{-0.4 k_{\rm Ly\alpha} E(B-V)} \tag{2.10}$$

The equation is identical to Equation 2.9 except for the difference that the normalization, $C_{\rm UV}$, is expressed as $C_{\rm UV} \equiv \log(\frac{L_{\rm UV}}{L_0})^\alpha$ where $L_{\rm UV}$ is given in units of erg s^{-1} Hz^{-1} and α and L_0 are constants. We repeat the fitting procedure using the combined sample of our LAEs and the HPS sources. The best-fit $k_{\rm Ly\alpha} = 7.37 \pm 0.98$, $\alpha = -1.62 \pm 0.20$, and $L_0 = (2.90 \pm 1.15) \times 10^{29}$ erg s^{-1} Hz^{-1}. The α value is firmly in the negative, affirming the fact that the normalization C indeed decreases with increasing luminosity.

In Figure 2.7, we illustrate our result. The left panel shows our measurements *as observed*, while, in the right panel, we 'correct' for the luminosity dependence by showing $f_{\rm esc,renorm} \equiv C_{\rm UV}^{-1} f_{\rm esc}$. Relative to the power law that best describes each set of data points (dashed lines), the scatter decreases from 0.26 dex to 0.18 dex. In short, Equation 2.10 allows us to predict a galaxy's $f_{\rm esc}$ with a $\lesssim$50% accuracy provided that both the UV slope β and $L_{\rm UV}$ are known.

The efficacy of the luminosity-dependent $f_{\rm esc}$ calibration is better illustrated in Figure 2.8, where we combine $L_{\rm UV}$ and E$(B-V)$ into a single parameter, i.e., dust-corrected UV SFR. In the top left panel, we once again show the measurements as observed. A clear separation between our LAEs and the HPS sources is visible. The grey swath marks the correlation

[7]↑The parameter is typically denoted as $X_{\rm Ly\alpha}$ in the literature. Here, we denote it as X to avoid confusion with another parameter defined in Equation 2.5.

reported by [180] for Lyα-emitting galaxies, which shows an excellent agreement with our own measurements. Although their stellar mass range is $\log[M_{\rm star}/M_\odot] = 7.6 - 10.6$, the majority lies below $10^{9.5} M_\odot$ and thus should be well matched to the stellar mass range for LAEs [123], [241]–[243].

In the two right panels, we renormalize the SFR as $\mathrm{SFR_{UV,renorm}} \equiv C_{\rm UV} \cdot \mathrm{SFR_{UV}}$. Both panels show identical data which are color-coded by $L_{\rm UV}$ (top) and $\mathrm{E}(B-V)$ (bottom), respectively. The renormalization moves our LAEs to the right in better alignment with the HPS sources and the Hα-Lyα emitters. Only the former are used in the fitting but the latter are rescaled consistently in the figure.

A small fraction (9%) of galaxies lie significantly outside an otherwise tight sequence formed by the rest, which we demarcate with a dot-dashed line. The outlier group largely consists of high UV-luminosity galaxies ($\gtrsim 10^{29}$ erg s^{-1} Hz^{-1}, or $M_{\rm UV} \lesssim -22.4$) with uncharacteristically blue colors ($\mathrm{E}(B-V) \lesssim 0.2$) and near the EW cutoff (≈ 20 Å). Eight of this group belong to the HPS sample, four are Hα-Lyα emitters and additional three are in our sample (one in the protocluster region and the other two in the field). Given that both HPS sources and our LAE selection target single line emission, we cannot rule out that some are low-redshift interlopers such as [O II] emitters at $z = 0.34$. In Section 2.7, we discuss how the exclusion or inclusion of these three LAE candidates affects our conclusion on the environmental dependence on $f_{\rm esc}$.

After excluding these outliers, we fit the data to a power-law and find that the scatter is reduced from 0.29 dex, for the unaltered data, to 0.21 dex. When we account for the expected effect of photometric scatter using image simulations, the intrinsic scatter in the $f_{\rm esc}$–$C_{\rm UV}\mathrm{SFR}_{UV}$ scaling relation is less than 0.19 dex.

The physical origin of the luminosity-dependent $C_{\rm Ly\alpha}$ is unclear. However, it is worth noting that our result does not mean that $C_{\rm UV}\mathrm{SFR_{UV}}$ is the true SFR; in such a case, $f_{\rm esc}$ ($\equiv \mathrm{SFR_{Ly\alpha}/SFR_{UV}}$) in the abscissa should also scale accordingly, which would undo the alignment.

One possibility is that dust laws change with UV luminosity such that more UV-luminous galaxies obey the [209] law while less luminous ones gradually transition to a law more similar to the SMC law. [218] reported that the average IR luminosity of LAEs at $z = 2.2$ measured

from the *Spitzer*/MIPS and *Herschel*/PACS image stacks lie well below that expected under the [209] extinction as evidence that the LAE population may be better described by the SMC law. Similarly, [244] found that UV-selected star-forming galaxies $z \sim 2$ with young stellar population ages ($\lesssim$100 Myr) appear to obey an SMC-like dust law while older galaxies follow the [209] law.

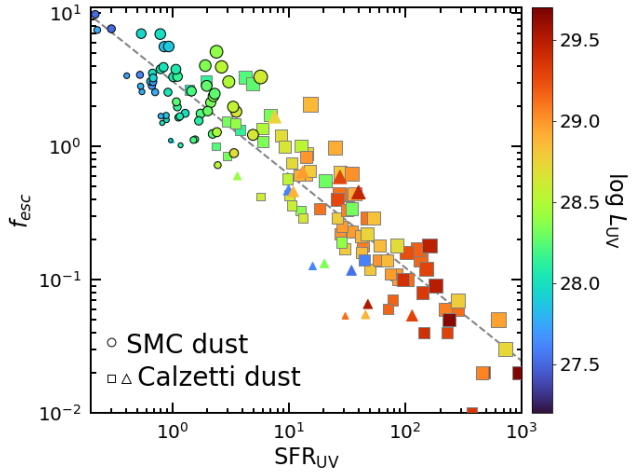

Figure 2.9. Lyα escape fraction as a function of intrinsic SFR_{UV}. Both SFR_{UV} and f_{esc} are computed for our LAEs assuming the SMC dust law, while other datapoints are calculated assuming the [209] dust law. Symbols are color-coded with galaxy's observed UV luminosity, with sizes reflecting their Lyα luminosity and shapes identical to those in Figure 2.8.

In Figure 2.9, we show the same data but this time we apply the SMC law for our LAEs while the HPS sources and the Hα-Lyα emitters still obey the Calzetti law. The tightness of the correlation is comparable to that in Figure 2.8 but with fewer outliers. Modeling a luminosity-dependent change in dust laws could conceivably further tighten the scaling relation. The transformation shown in the figure effectively moves our LAEs (in the top left panel of Figure 2.8) to lower SFR (to the left in the x-axis) and to higher f_{esc} values by the same factor.

One caveat of this interpretation is that it drives already high f_{esc} values even higher. Nearly all of our LAEs would have Lyα escape fractions $\gg$100%. The problem may be mitigated if low UV-luminosity (or SMC laws) go hand in hand with low metallicity, young ages, or level of burstiness in SFHs: these traits either boost the production of ionizing radiation

(and thus Lyα production) or enhances Lyα transmission. A comprehensive study of these properties in LAEs is needed to put to test this hypothesis.

2.7 Environmental Impacts on the Physical Properties of LAEs

As detailed in Section 2.3.1, our sample includes 24 LAEs residing in a protocluster environment ([73]; S19) offering us a rare opportunity to explore how the environment affects the Lyα properties of the galaxies therein.

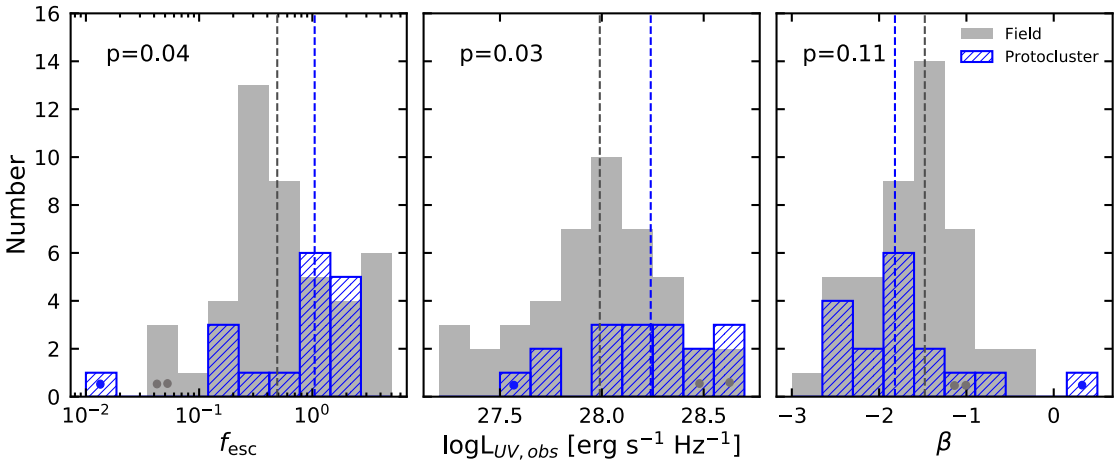

Figure 2.10. Lyα escape fraction, observed UV luminosity, and UV slope β distributions of the protocluster LAEs (blue hatched) and the field LAEs (grey filled). Dashed vertical lines measure the median values of each subsample. Three sources in our sample that are likely [O II] emitters (see Section 2.6.2 and Figure 2.8) are marked as filled circles in the relevant bins. The p values from the K-S tests noted in each panel include these sources. Excluding them makes it more statistically significant that the protocluster- and field LAE distributions are not drawn from the same parent sample.

In Figure 2.10, we show the f_{esc} distribution split into the 'field' (grey) and 'protocluster' (blue hatched) groups. The median values are indicated as dashed lines. The protocluster members not only show higher f_{esc} values than the field LAEs by a factor of $\approx$2 – $\langle f_{esc} \rangle$ = 1.05 vs 0.49 – but also contain a larger fraction of sources exceeding f_{esc}=1: i.e., 65% (11/17) vs 33% (15/45).

The K-S test results in $p = 0.04$ indicating that the two $f_{\rm esc}$ distributions are distinguishable at a $\approx 2\sigma$ (96% confidence) level. Despite small-number statistics, our results support the hypothesis that the galaxies' Lyα properties depend on their large-scale environment. The middle and right panels of Figure 2.10 show the histograms of $L_{\rm UV}$ and β of the same galaxies, the two primary parameters from which $f_{\rm esc}$ is computed. There is a clear tendency towards higher UV luminosities (78%) and bluer slopes ($\Delta\beta \sim 0.3$) for protocluster galaxies compared to the control group. Similarly, the change in Lyα luminosities roughly tracks that of UV luminosities (see Figure 2.5).

A higher UV luminosity in protocluster LAEs (our K-S test yields $p = 0.03$) is consistent with that found for another protocluster [139]. Here we report, for the first time, a statistical difference in the UV slope β for LAEs in different environments. The bluer UV slope, $\Delta\beta \approx 0.3$, corresponds to $\Delta{\rm E}(B-V) \approx 0.07$ assuming the [209] extinction law, leading to a factor of ≈ 1.6 lower extinction given everything else equal. This is roughly consistent with the factor of $\approx$2 enhancement we find in $f_{\rm esc}$. However, the difference in β between the two samples is statistically less significant ($p = 0.11$) than the other two parameters. It may be owing to the intrinsically narrow range in β observed for distant star-forming galaxies[8]. Additionally, photometric estimates of the β are expected to have a higher degree of uncertainty because it requires secure detection in two or more bands relative to $L_{\rm UV}$ measurements, which rely primarily on single-band detection.

As discussed in Section 2.6.2, there are three sources in our LAE sample which are likely to be [O II] emitters. In Figure 2.8, they lie at the low end of the $f_{\rm esc}$ and $E(B-V)$ values and at the high end of the UV luminosity. One belongs to the protocluster and the other two in the field subsample. These sources are indicated in each panel of Figure 2.5 as filled circles at the bottom of the relevant bin. We repeat the statistical tests after excluding them and found that doing so does not significantly impact our conclusion but further strengthens it. The p parameter decreases slightly for $f_{\rm esc}$ values ($p = 0.04 \rightarrow 0.03$), $L_{\rm UV,obs}$ ($p = 0.03 \rightarrow 0.01$), and β ($p = 0.11 \rightarrow 0.08$).

[8]↑UV-selected star-forming galaxies with the luminosity range $L_{\rm UV} = (0.1 - 3.0)L^*$ at $z = 3 - 4$ typically span β in $[-2.5, -1.0]$ [151], [245]

To summarize our results, our data suggest strong evidence for higher UV luminosity, higher line luminosity, and less dust content prevail in galaxies residing in dense protocluster environment. As a result, these galaxies are more efficient producers of Lyα photons and possibly of LyC photons than their field cousins.

It is worth noting that an opposite trend was reported by [67], who, based on a spectroscopic sample of star-forming galaxies, concluded that Lyα emission in nine protocluster galaxies in PCl J1001+0220 – a protocluster at $z = 4.6$ – is suppressed ($\langle f_{\rm esc} \rangle = 1.8^{+0.3}_{-1.7}\%$) relative to that in the field ($4.0^{+1.0}_{-0.8}\%$). However, the galaxies in the [109] sample are significantly more luminous star-formers (with the median brightness $\langle \mathrm{i}^* \rangle \sim 24.5$) than our LAEs (median $\langle \mathrm{i} \rangle \sim 25.8$) and are more massive and dustier than our LAEs. If both results are correct, the implication would be that the environmental trend we observe in our LAEs may be confined to young, low-mass systems and cannot be generalized to more evolved galaxies in the same structure.

2.7.1 Physical origins of enhanced $f_{\rm esc}$ in protoclusters

Higher Lyα escape fraction for the protocluster LAEs is intriguing. Recent absorption-line studies found that the regions of galaxy overdensities are also H I-richer than average fields [170], [246]–[248]. [248] reported a cross-correlation length 4 ± 1 Mpc (comoving) between the LAE overdensity and H I line-of-sight optical depth. These results are broadly consistent with the expectation that both galaxy- and gas overdensities track those of the underlying dark matter. Higher H I column densities at the galaxy scales would result in more frequent random walks of Lyα photons, thereby enhancing the chance of their destruction by dust grains along their paths and thus lowering $f_{\rm esc}$ values. Our result runs counter to this expectation.

One possible explanation is that different ISM conditions for protocluster galaxies facilitate Lyα photons to escape more easily relative to field galaxies. [167] studied local star-forming galaxies and found that the escape fraction (for both Lyα and Lyman continuum photons) negatively correlates with H I covering fraction and dust reddening, favoring the scenario in which low column density channels serve as privileged routes through which

Lyα and LyC photons can escape the galaxy. Such photoionized 'tunnels' can be carved out by supernovae feedback (e.g., [152]) or by the turbulent early phase of the H II regions and the surrounding molecular clouds [249]. In protocluster galaxies embedded in the H I-richer large-scale environment, faster growth brought on by higher star formation efficiency [e.g., 172] may work through these processes to effectively create a more porous ISM relative to their field counterparts. Such a scenario would have a strong implication for the role of protocluster galaxies in cosmic reionization.

Another possibility is that we may be witnessing simultaneous births of young primeval galaxies occurring in high-density regions. Extremely young stellar ages may lead not only to a higher level of turbulence in the ISM creating low-density channels [249] but also to higher ionizing photon production efficiency (thus increasing Lyα production), higher specific SFRs [250], [251], and low dust content. Enhanced sSFRs in galaxies residing in high-density environment have been reported recently [109], [173]. While the positive SFR-density relation is relatively weak for the general population, there is also tentative evidence that LAEs – as young, low-mass galaxies – lie above the $M_{\rm star}$–SFR main sequence ([124], [252]: but see [135] for a contradictory result) in which such effects may manifest more clearly.

Finally, protocluster LAEs may be more metal-poor than the field LAEs, producing hotter stellar photospheres and thus higher ionizing radiation efficiency [253], [254]. While lower metallicity in high-density regions is counter-intuitive, it is plausible if these galaxies are hosted by low-mass ($\lesssim 10^{11} M_{\odot}$) halos undergoing the first major starburst fueled by the H I-rich environment. At $z \sim 3$, the volume of a single protocluster is immense [63] and the chemical enrichment therein is expected to be heterogeneous.

Distinguishing these different but possibly related scenarios would require considerably larger samples of LAEs spanning a range of large-scale environment and deeper imaging data to enable photometric measurements with improved precision. Optical spectroscopy can enable comparative analyses of the Lyα properties (i.e., the shape and velocity offset) and dust content to test if the distribution of H I gas in the galaxy indeed changes with their large-scale structure. Robust measurements of their SFR, stellar masses, and overall shape of the spectral energy distribution will also help discern a significant difference in metallicity

and ages. Deep JWST NIRSPEC observations can place direct constraints on the metallicity of galaxies in a diverse range of environments.

The One-hundred square-degree DECam Imaging in Narrowbands (ODIN) survey will provide the largest samples of LAEs in protocluster and field environments alike, which can serve as the basis of these investigations. As a new NSF's NOIRLab program (Program ID: 2020B-0201), the survey began in early 2021 to image an area of 91 deg^2 with three narrow-band filters sampling redshifted Lyα emission at $z = 4.5$, 3.1, and 2.4 (cosmic ages of 1.3, 2.0, and 2.7 Gyr, respectively), straddling the epoch in which the stellar mass assembly rate of both cluster and field galaxies reached its peak [60]. Within the survey volume of $\approx$0.24 Gpc^3 (comoving), $\approx$100,000 LAEs, $\approx$45 Coma progenitors, and $\approx$600 Virgo progenitor systems are expected. Combined with the existing and upcoming facilities[9], these new datasets will considerably enrich our understanding of the galaxy growth occurring in the largest cosmic structures in direct comparison with that of average galaxies at the same epoch.

2.8 Conclusions

We have conducted a comprehensive investigation of the Lyα properties of the LAEs at $z \sim 3.1$ including the contribution from the extended, low surface brightness Lyα emission. We summarize our results as follows:

1. The average Lyα emission is spatially extended, spanning at least $4''$ across, in contrast to the UV emission of the same galaxies which is unresolved ($\lesssim 1.3''$, Figure 2.1) confirming the ubiquity of the Lyα halo (Section 2.4). The Lyα halo has a scale length of $r_{s,h} = 4.9 \pm 0.7$ kpc (Figure 2.2) and contributes up to 61^{+9}_{-12}% of the total line flux in a typical LAE at $z \sim 3$. Protocluster- and field LAEs have similar LAH sizes, implying that large-scale environment is not a major factor that drives the LAH sizes. We provide a simple diagnostic (Figure 2.3) which can help estimate the expected Lyα flux loss as a function of aperture sizes in a range

[9]↑The ODIN survey fields largely overlap with legacy fields including the Legacy Survey of Space and Time Deep fields, Euclid deep fields, and one of the HETDEX survey fields.

of seeing values typical in ground-based imaging data.

2. We estimate the Lyα escape fraction for 62 individual LAEs (Section 2.5.1), nearly one-third of which show unphysically high $f_{\rm esc}(\gtrsim 100\%)$. Large $f_{\rm esc}$values may be a result of a wide spread in metallicity, age, and star formation histories for the LAEs in our sample; AGN contamination or highly sightline-dependent Lyα emission cannot be ruled out. However, the relative fraction falling into this category is considerably higher for protocluster LAEs than those in the field, hinting at an environmental effect. After excluding the protocluster LAEs, we find $\langle f_{\rm esc}\rangle \sim 40 \pm 26\%$ within galaxy-sized apertures. After correcting the flux loss on the average basis, we obtain $\langle f_{\rm esc,tot}\rangle \sim 51 \pm 31\%$. The modest increase is owing to the compact sizes of the Lyα halo (Section 2.5.2). Despite the ubiquity of extended line emission in this class of objects, its presence does not warrant a substantial revision to the current picture.

3. Using a compilation of existing measurements, we explore how $f_{\rm esc}$ varies with galaxies' photometric properties (Section 2.5.3). Our results suggest that the attenuation of Lyα flux due to interstellar dust is similar to that experienced by continuum photons ($k_{\rm Ly\alpha} \approx k_{1216}$: Section 2.6), but with a clear difference in their overall transmission by the factor, $C_{\rm Ly\alpha}$, which changes with the galaxy's UV luminosity (Figure 2.6). $C_{\rm Ly\alpha}$ is $\approx$2 for our LAEs, but is reduced to $\approx$0.5–1 for more UV-luminous galaxies. These results are incompatible with the expectation of several ISM models we have considered, and may support some form of multi-phase interstellar media that allow preferential escape of Lyα photons through selective attenuation (Section 2.6.1).

4. We empirically calibrate the Lyα escape as a function of $L_{\rm UV}$ and β (Section 2.6.2, Figures 2.7 and 2.8). Doing so allows us to predict the $f_{\rm esc}$ value of individual LAEs within $\sim$50% of the measured value, improving the precision by nearly a factor of 2 compared to the single-parameter (β) model. The luminosity dependence in the $f_{\rm esc}$–β relation may result from a gradual shift of the dust law, from SMC-like extinction for low-mass galaxies to the

[209] or [255] extinction for more evolved, more luminous galaxies.

5. Protocluster LAEs have higher Lyα escape fractions and are bluer than their field counterparts (Section 2.7, Figure 2.10) suggesting that galaxy formation proceeds differently in dense protocluster environments. We consider different physical scenarios which may explain the observations (Section 2.7.1); these include the possibility that heightened SF activity in the protocluster environment is more conducive to creating a more porous medium facilitating the escape of Lyα and LyC photons. Alternatively, we may be witnessing simultaneous births of extremely young and/or low-metallicity galaxies hosted in low-mass halos in the region. Larger samples of protoclusters and their galaxy constituents combined with sensitive observations from upcoming facilities will place stringent constraints on these scenarios.

2.9 Appendix: Robustness of the Dependence of $f_{\rm esc}$ on dust

The escape fraction of Lyα photons is estimated based on three parameters, the reddening parameter (E($B-V$)) and the line- and continuum luminosity ($L_{\rm UV}$ and $L_{\rm Ly\alpha}$) of the galaxy through Equation 2.8. Estimation of these parameters comes with varying degrees of uncertainties which can adversely affect our ability to discern the intrinsic scaling relation from our photometric measurements. In this section, we utilize a galaxy simulation to assess the robustness of our photometric measurements and the conclusions based on them presented in Section 2.6.

We run a simulation containing sources spanning a wide range of relevant parameters. Following the procedure described in S19 and [175], we use the stellar population synthesis model of [256] to create a model galaxy spectrum (20 Myr in age) characterized by a constant star formation history, the [257] initial mass function, and solar metallicity. Since we are mainly interested in photometric measurements, our results are largely insensitive to these assumptions.

To the base spectrum, we assign UV luminosity, UV continuum slope and redshift *at random* within the range appropriate for our LAE sample[10]. The attenuation by the intergalactic media and interstellar dust are corrected using the H I opacity given by [258] and [209] dust reddening law, respectively. A Lyα line is then added to the redshifted galaxy SED, which is approximated as a Gaussian profile peaked at $1215.67(1+z)$Å with an intrinsic FWHM = 3Å and a line luminosity in range $\log L_{\mathrm{Ly}\alpha} \in [42, 44.5]$ erg s^{-1}. We compute AB magnitudes in $o3$-, g-, r-, i- and z-bands by convolving the synthetic SED with the total filter transmission curves. In practice, the line flux falling into a given filter was estimated separately from continuum flux and added to the flux to mitigate the coarse resolution of the [256] galaxy templates. Our parent mock catalog consists of a total of 10,000 galaxies whose properties span the full range of the observed values.

From the base catalog, we randomly draw 200 entries and assign position, morphology (disk/bulge and position angle), and size (half-light radii) to each source. Although we use the size distribution consistent with the literature [e.g., 128], the angular size of LAEs at $z \sim 3$ is small enough such that most can be considered as point sources in a ground-based image with $\approx 1''$ seeing as is the case for the present work. These galaxies are added to the science images after being convolved with the image PSF to add realistic photon noise. Source detection and photometric measurements are performed in the identical manner to the real data. We repeat this procedure 100 times, inserting 20,000 artificial sources to the data. Of these, 14,273 ($\approx 71\%$) are detected in the $o3$ band at S/N$\geq$7. The L_{UV}, $L_{\mathrm{Ly}\alpha}$, β, and f_{esc} of these $o3$-detected galaxies are estimated following the same procedure as described in S19.

Using the mock photometric catalog, we construct a source list that closely matches the distribution of *observed* L_{UV}, $L_{\mathrm{Ly}\alpha}$, and β values of our real LAEs. Doing so is critical to avoid creating a false sense of agreement or disagreement as any photometric measurement is expected to be more accurate for brighter sources. Galaxies are randomly drawn from the catalog with a probability assigned to each source according to its physical parameters. Similar to the real data, only sources with the uncertainty in β value less than 0.9 are retained at this step. The broad correlation between L_{UV} and $L_{\mathrm{Ly}\alpha}$, which stems from the equivalent

[10] $\uparrow \log L_{\mathrm{UV}} \in [27, 30]$ erg s^{-1} Hz^{-1}, $\beta \in [-2.1, -0.4]$, and $z \in [3.11, 3.15]$

width cut, is also mimicked by excluding sources lying outside the region populated by the real LAEs. Our final mock LAE catalog consists of 1,166 galaxies for which both intrinsic and observed values of the key parameters are available for comparison.

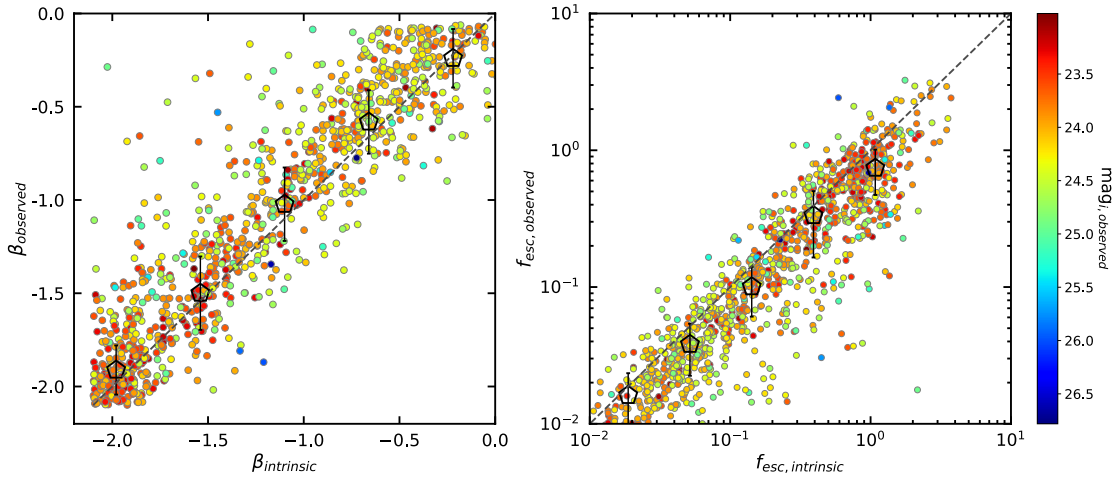

Figure 2.11. The comparisons between the intrinsic and observed values of UV continuum slope β and Lyα escape fraction. The synthetic galaxies are color-coded by their observed i-band magnitude. In each panel, dashed line marks the one-to-one relationship. Open pentagons represent the mean value in each intrinsic $\beta/f_{\rm esc}$ bin after rejecting $> 3\sigma$ outliers.

In Figure 2.11, we show the intrinsic and the recovered values of β and $f_{\rm esc}$. Each galaxy is represented by a circle color-coded by the observed i-band magnitude. The overall agreement is evaluated by calculating the mean and the standard deviation of the mock data after rejecting $> 3\sigma$ outliers and are shown as open pentagons. Most of these catastrophic outliers tend to be i-band faint sources; i-bright outliers may simply be the case in which a simulated source falls too close to a real galaxy in the image. The one-to-one line is shown as a dashed line. The spread in observed β values ($\sigma_\beta \approx 0.15 - 0.20$ in most bins) is primarily due to the photometric scatter in the bands used for the UV slope measurements, which propagates into our $f_{\rm esc}$ determination. The recovered β values have a tendency of upscattering to a larger value (i.e., a redder SED), particularly for continuum-fainter sources. This is likely caused by our $\Delta\beta < 0.9$ cut which, everything else being equal, retains sources which up-scatter to a higher continuum flux while rejecting those which down-scatter. This effect leads to the slight underestimation of $f_{\rm esc}$. However, in most bins, the mean is consistent with the

intrinsic value within the error. The recovery of the continuum- and line luminosities is much better ($\lesssim 0.1$ dex) than the parameters shown in Figure 2.11 because the luminosities are tied to the source brightness in a single band given the narrow redshift range of the LAEs. At the redshift range sampled by the $o3$ filter, the change in luminosity from $z = 3.15$ to 3.10 is less than 4%, much smaller than any measurement uncertainties. All in all, we conclude that our ability to estimate the intrinsic β and $f_{\rm esc}$ values is reasonably good.

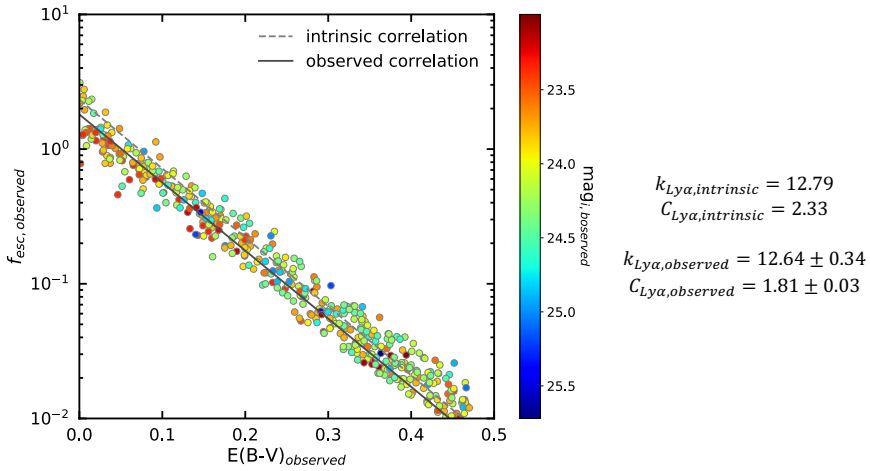

Figure 2.12. Using a sample of mock galaxies which obey an intrinsic scaling law between $f_{\rm esc}$ and E($B-V$), we test our ability to discern such a relation based on photometric measurements. The scaling law is assumed to be what best describes the D1 LAE sample and is shown as a grey dashed line. Recovered quantities are shown as circles color-coded by the i-band brightness for galaxies obeying the scaling law within $\pm$0.15 dex. The best-fit power-law of these measurements is marked by the solid line.

We further test our ability to infer the $f_{\rm esc}$-E($B-V$) scaling relation based on our photometric measurements by defining a subsample of mock LAEs, but this time, only retaining sources whose intrinsic $f_{\rm esc}$ and E($B-V$) values obey the dashed line in Figure 2.12 within $\pm$0.15 dex, which represents the best-fit scaling law (see Table 2.2 and Section 2.6). The recovered values are shown as filled circles, once again color-coded by the observed i-band brightness. We then determine the best-fit power-law model in the identical manner to the real data and obtain $k_{\rm Ly\alpha} = 12.64 \pm 0.34$ and $C_{\rm Ly\alpha} = 1.81 \pm 0.03$ indicated by the solid line in the figure. Because we tend to underestimate $f_{\rm esc}$ the most for the bluest (low E($B-V$)) galaxies, the recovered $C_{\rm Ly\alpha}$ is slightly lower than the intrinsic value, while $k_{\rm Ly\alpha}$

is robustly recovered. However, it is clear that the intrinsic and the observed scaling laws are very similar. Thus, we conclude that our measurements can recover the intrinsic scaling law in a statistically robust manner and that the dependence of $f_{\rm esc}$ on interstellar extinction presented in Section 2.6 is real.

3. EVALUATING LYα EMISSION AS A TRACER OF THE LARGEST COSMIC STRUCTURE AT $z \sim 2.47$

Motivated by the discovery of *Hyperion*, the only-known proto-supercluster at high redshift, I carry out deep narrow-band imaging in the neighborhood of *Hyperion* to select LAEs. In this chapter, I investigate different constituents of the proto-supercluster mapped by different cluster tracers and galactic neutral gas. These results shed light on the formation history of the proto-supercluster and its evolutionary connection to present-day cosmic structures.

This chapter will be submitted to Astrophysical Journal.

3.1 Abstract

The discovery and spectroscopic confirmation of *Hyperion*, a proto-supercluster at $z = 2.45$, provides an unprecedented opportunity to study distant galaxies in the context of the large-scale environment. We carry out deep narrow-band imaging of a $\approx 1^\circ \times 1^\circ$ region around *Hyperion* and select 157 Lyα emitters (LAEs). The inferred LAE overdensity is $\delta_g \approx 40$ within an effective volume of 1.3×10^5 cMpc^3, consistent with the fact that *Hyperion* is composed of multiple protoclusters and will evolve into a super-cluster with a total mass of $M_{tot} \approx 1.4 \times 10^{15}$ M$_\odot$. The LAE positions closely mirror those of spectroscopic members, tracing the cores and extended filamentary arms connected to them, suggesting that they trace the same large-scale structure. By cross-correlating the LAE positions with the H I tomography data, we find that LAEs tend to lie in the regions of moderate H I column density. Lyα transmission is likely suppressed in the highest density regions due to resonant scattering. The *Hyperion* region hosts a large population of active galactic nuclei (AGN), $\approx$12 times more than that in the field. The prevalence of AGN in protocluster regions hints at the possibility that they may be triggered by physical processes that occur more frequently in dense environments, such as galaxy merger. Our study demonstrates LAEs as reliable markers of the largest cosmic structures. When combined with ongoing and upcoming imaging and spectroscopic surveys, wide-field narrow-band imaging has a potential

to advance our knowledge in the formation and evolution of cosmic structures and of their galaxy inhabitants.

3.2 Introduction

In the cold dark matter-dominated universe we live in, the formation of cosmic structures is well explained by the hierarchical theory. Minuscule fluctuations of matter density grow through gravity and subsequently these local overdensity regions collapse into self-gravitating structures which are named dark matter 'halos'. The halos grow in mass and size via accretion from cosmic web or mergers [14], [16]–[20], [259].

Galaxies are formed in a similar manner as dark matter halos [18], [26]–[28]. However, the physics of how baryons respond to the underlying dark matter distribution becomes more complicated since the 'feedback' processes play crucial roles in regulating galaxy formation and evolution. For example, supernova explosions and stellar winds from massive hot stars inject momentum and energy into the interstellar and circumgalactic medium [hereafter, ISM and CGM, 29]–[34]. Studies on supermassive black holes in the center of local galaxies suggest that active galactic nuclei (AGN) can heat the surrounding medium and prevent the gas inflow [37]–[40]. These processes effectively suppress star formation by heating or ejecting the gas in the ISM.

Studies on galaxy clusters may offer insights into both the formation of cosmological structures and the evolution of individual galaxies. Existing surveys found a distinct color-magnitude relation in local cluster galaxies [260], [261], which convincingly suggests that they underwent accelerated formation followed by swift quenching [55], [58], [262]. In order to elucidate the role of the environment on the galaxy forming history, it is critically needed to identify the progenitors of massive clusters – the so-called 'protoclusters' – and witness the galaxy formation therein.

Since immature protoclusters lack the observational characteristics like those of the present-day clusters, it is challenging to identify robust candidates as well as the whole extent of such structures. Early protocluster studies targeted the surroundings of rare galaxies that are possible progenitors of local galaxies or good tracers of cool gas reservoirs, e.g., radio

galaxies [83], [86], [91], [93], quasars [QSOs, 263]–[267] and Lyα blobs [LABs, 95], [268]–[270]. Another technique of protocluster search is to find concentrations of star forming galaxies at high redshift [63], [271]. A reasonable pool of protocluster candidates has been provided by wide-field observation on Hα emitters [HAEs, 89], [93], [272]–[274], Lyman break galaxies [LBGs, 73], [275]–[278], Lyα emitters [LAEs, 96], [139], [141], [171], [279] and sub-millimeter galaxies [SMGs, 280]–[283]. A relative new technique in the field is to detect through neutral hydrogen absorption lines in the spectra of bright background galaxies [e.g., 170], [275], [284], [285].

Narrowband observations targeting Lyα emission can efficiently provide robust protocluster members within a small slice of redshift ($\Delta z \sim 0.1$). At $z \gtrsim 2$, Lyα emission is redshifted into the optical window, which makes it easier to be detected by ground-based telescopes. In addition, LAEs are proven to be hosted by less-massive dark matter halos. As a result, they are less biased by the underlying dark matter distribution [galaxy bias $b \sim 1.5-2.0$, 286]. Recent surveys suggested that the spatial distribution of LAEs resembles that of cluster-sized halos: e.g., both show characteristics of dense cores, filamentary arms, and zone of voids [95], [138], [139] and are comparable in angular sizes [140], [172]. Therefore, LAEs are commonly used in mapping the large-scale structure.

In this paper, we present the first deep wide-field Lyα imaging around a proto-supercluster in the Cosmic Evolution Survey [COSMOS, 287]. The structure, dubbed as *Hyperion*, which was first confirmed by [71] using a combination of the VIMOS Ultra-Deep Survey [VUDS, 64], zCOSMOS Survey [69], [70] and COSMOS2015 photometric catalog [288]. The whole structure extents over a volume of $\sim 60 \times 60 \times 150$ comoving Mpc^3 at $z \sim 2.45$, with at least seven density clumps within $2.4 \leq z \leq 2.5$, each of which was studied in detail with heterogeneous galaxy samples [279], [289]–[292]. We target the Lyα emission around the proto-supercluster with a custom narrowband filter in order to explore the large-scale structure traced by LAEs.

This paper is organized as follows: in Section 3.3, we describe the observation strategy and data reduction. Combined the narrowband image with the existing deep broadband data, we define a sample of LAEs in Section 3.4. We build a sky map of LAEs, and compare it with the distribution of spectroscopic members of the *Hyperion*, photometric galaxies, H I

tomography, and active galactic nuclei (AGN) in Section 3.5. In Section 3.6, we calculate the descendent mass and discuss the future directions in the field of cluster formation. Finally, we summarize the main findings in Section 3.7.

Throughout this paper, we adopt a cosmology with $\Omega_M = 0.286$, $\Omega_\Lambda = 0.714$, $h = 0.696$, $H_0 = 100h$ km s^{-1} Mpc^{-1}. All magnitudes are in the AB system.

3.3 Observations and Data Reduction

3.3.1 New Observations

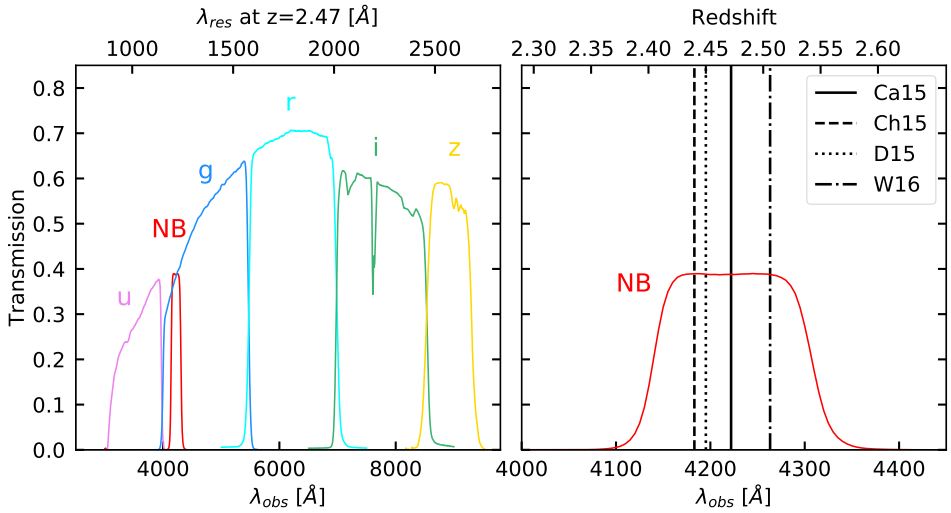

Figure 3.1. Left: total throughput (filter + mirror + optics + CCD response) of the u band filter of CLAUDS, the *NB422* filter, and the g, r, i, z band filters of HSC. **Right:** the zoomed-in view of the *NB422* filter. Vertical lines mark the redshifts of the spectroscopically confirmed protoclusters in *Hyperion* (Ca15: [289], Ch15: [279], D15: [290], W16: [292]).

We obtained deep wide-field narrowband images using the One Degree Imager [ODI: 293], [294] on the WYIN 3.5m telescope. ODI has 30 orthogonal transfer array detectors arranged in a 5×6 configuration, with an intrinsic pixel scale of $0.11''$ pixel^{-1} and a field of view of $40'' \times 48''$. Our custom narrowband filter (hereafter, *NB422*) has a central wavelength of $\lambda_c \approx 4225$ Å and a full-width-at-half-maximum width of 170 Å. The filter is designed to sample redshifted Lyα emission $z = 2.40 - 2.54$, corresponding to a comoving line-of-sight distance of ≈170 cMpc.

The observations were carried out during four separate runs in 2018–2020 using two pointing centers: $\alpha = 10^h01^m25.5^s$, $\delta = +02°15'00''$(cosmosE, hereafter) and $\alpha = 09^h59^m25.5^s$, $\delta = +02°17'24''$(cosmosW), J2000. These pointings overlap 0.14 deg in the east-west direction, and together cover a total area of ~ 1 deg^2 centered at $\alpha = 10^h00^m21.6^s$, $\delta = +02°14'24''$. We adopted the 5ODI 9-Point dithering pattern between successive exposures to fill the gaps between CCDs. We discarded the frames with seeing $> 1.3''$ and the frames that were taken when the guide star was lost during the exposures. Total exposure times are 19 and 16 for the cosmosE and cosmosW pointings, respectively, with the overlapping region receiving the effective exposure of 35 hours. Individual exposures were 10 or 20 minutes long, depending on transparency and cloud coverage.

For broad-band imaging data, we utilize the existing data from the Hyper Suprime-Cam Subaru Strategic Program [HSC-SSP; 295], [296] second data release [297] and the deep u-band data from the CFHT large area U-band deep survey [CLAUDS; 298]. The broadband data covers the entire survey field imaged with $NB422$. Figure 3.1 shows the total throughput of all filters and the filter information is summarized in Table 3.1. The 5σ limiting magnitudes reported by HSC-SSP DR2 [297] are for point sources, which are ~ 0.3 mag deeper than those measured in a $2''$ diameter aperture.

3.3.2 Data Reduction

The raw images of our $NB422$ data are transferred and processed by the ODI pipeline, Portal and Archive (ODI-PPA; [299]) where image bias, dark and pupil ghosts are removed and the images are flat-fielded.

The astrometry is tied to the the *Gaia* second data release [300] using IRAF task `msccmatch`. After correction, The root-mean-square (rms) of astrometry offsets are $0.1''$ for both right ascension and declination. A narrowband image with the best seeing condition is chosen as the reference image. We then resample each image with a pixel scale of $0.3''$ using the tangent point of the reference image using `SWarp` [301]. The scaling factor relative to the reference frame is determined by the IRAF task `mscimatch`. Finally, the rescaled reprojected images are combined into a final mosaic using a median combination method

Table 3.1. Filters used in this survey

Band	Instrument	Limiting magnitude[1]	FWHM
		(5σ, AB)	($''$)
$NB422$	ODI	25.4[2]	1.0
u	MegaCam/CLAUDS	27.1	0.8
g	SUBARU/HSC	26.9	0.7
r	SUBARU/HSC	26.6	0.9
i	SUBARU/HSC	25.3	0.7

[1] 5σ limiting magnitude measured in a $2''$ diameter aperture.
[2] limiting magnitude measured at cosmosW, where the image is the shallowest.

with `SWarp`. Even though median stacking is not an optimal method in maximizing the image depth, it was a necessary choice because long exposures needed for our observations led to strong amplifier glows in ODI. The seeing of the final mosaic image is 1.0″.

To calibrate the photometric zeropoint of the final mosaic, we use the CLAUDS u and HSC-SSP g band images. To estimate continuum emission, we calculate the fractional contribution from the flux densities of u and g (denoted as ug) bands at the central wavelength of *NB422*. The zeropoint of the *NB422* is determined by requiring that the median color excess $NB - ug$ is close to zero for all objects with $0 \leq g - r \leq 1.0$.

3.3.3 Photometry

In order to construct a multi-wavelength photometric catalog, we first calibrate the astrometry of each broadband image with the *Gaia* DR2 data. We also match the pixel scale of all images to that of the *NB422* image 0.3″pix^{-1}; HSC-SSP and CLAUDS have the pixel scale of 0.17″pix^{-1} and 0.186″pix^{-1}, respectively. We homogenize the point spread functions (PSFs) of the broadband data with the seeing of *NB422* image. A Moffat profile is assumed to fit the PSF of each image with a measured seeing and a fixed parameter $\beta = 3$. The convolution kernel is obtained from an IDL routine `MAX_ENTROPY`. Each broadband image is then convolved with the respective kernel to create the PSF-matched image.

We run `SExtractor` [191] on a dual-image mode to create a multi-wavelength catalog where *NB422* image is used for detection (`DETECT_THRESH`=1.1, `MIN_AREA`=10). Photometry is performed in all images. Colors are estimated from isophotal flux (`FLUX_ISO`). A total of 64,690 sources are detected.

3.4 Analysis

3.4.1 Lyα emitter selection

In the right panel of Figure 3.1, we show the *NB422* filter transmission. The redshifts of the four protoclusters in the region are indicated as vertical lines, illustrating that any Lyα-

emitting galaxies that belong to these structures should lie well within the filter transmission. LAEs are selected using the following criteria:

$$\Sigma \geq 2 \ \cap \ \mathrm{S/N}(NB422) \geq 10 \ \cap \ NB422 - \mathrm{g} \leq -0.5 \tag{3.1}$$

where S/N is the signal-to-noise within the isophotal area. The color cut $NB422 - g = -0.5$ corresponds to the rest-frame equivalent width $W_0 = 50$ Å. Σ is the flux density excess measured relative to the 1σ photometric scatter expected for zero $NB422{-}g$ color. In a background-dominated data, a photometric error and Σ is a function of color:

$$m_g - m_{\mathrm{NB}} = -2.5 \log_{10}(1 - \Sigma 10^{-0.4(ZP - m_{\mathrm{NB}})} \sqrt{\sigma_g^2 + \sigma_{\mathrm{NB}}^2}) \tag{3.2}$$

where ZP is the photometric zeropoint of the $NB422$ image. Finally, at $z \sim 2.5$, the Lyman limit is redshifted to $\lambda_{\mathrm{obs}} \sim 3200$Å resulting in the flux deficit in u band. After careful calibration against spectroscopic sources, we require:

$$u - g \geq 0.9 \times (g - r) - 0.2 \tag{3.3}$$

In Figure 3.2, we show the $NB422{-}g$ color vs the narrowband magnitude of all NB-detected sources. The line-excess criterion applied to each field is shown as black curves[1]. 120 galaxies which satisfy the LAE selection criteria are shown as red circles. In addition, we identify 53 spectroscopic sources showing Lyα emission at a lower significance ($\Sigma > 1$). While the majority of these sources (orange triangles) come from the VUDS survey which covers the region uniformly, 10 come from more targeted studies by Ca15 and Ch15.

3.4.2 Multiwavelength and Spectroscopic data

To validate our sample selection and to quantify the rate of contamination, we compile the existing multi-wavelength and spectroscopic data in the field. For spectroscopy, we merge

[1]↑The sky background noise σ_{NB} is estimated separately for the cosmosW ($\alpha < 150.02°$), cosmosE ($\alpha \geq 150.02°$) and the overlapping region, cosmosC. We obtain $\sigma_{f_{NB}}$ is 1.08, 1.01 and 0.81 in cosmosW, cosmosE and cosmosC, respectively.

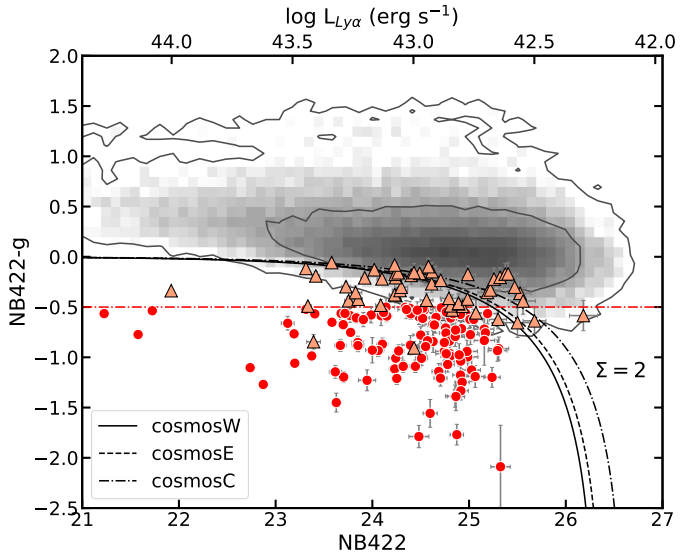

Figure 3.2. *NB422*$-g$ color as a function of *NB422* magnitude. All *NB422* sources are represented by the greyscale and the contour lines. Photometric LAE candidates (pLAEs) selected using Equations 3.1 and 3.3 are shown as circles; triangles indicate the $z_{\rm spec} = 2.40 - 2.52$ sources satisfying the same criteria with a modified line excess $\Sigma > 1$ (sLAEs). The solid, dashed and dash-dotted curves show the $\Sigma = 2$ lines computed for the cosmosW, cosmosE and cosmosC subfields, respectively. The horizontal dashed line marks the color corresponding to a rest-frame $W_0 = 50$Å at $z = 2.45$.

the redshift catalogs from the HETDEX Pilot Survey [HPS: 302], the zCOSMOS survey [69], [70] and the VVDS UltraDeep Survey [VUDS: 64]. We will refer to the merged catalog as the VUDS+zCOSMOS catalog hereafter. The same catalog was originally used in [71].

Sample Contamination At the central wavelength of our *NB422* filter, the dominant contaminants of the LAE selection are likely [O II] emitters at $z = 0.13$ but the contamination is likely low. At $z = 0.13$, the volume covered by our data is negligibly small at ≈0.8% compared to that at $z \sim 2.4$. [119] found that at $z < 0.2$, [O II] emitters have a rest-frame equivalent width of $W_{0,\rm O\ II} = 8 \pm 2$ Å. Our *NB422*$-g$ color cut corresponds to an observed equivalent width of 170 Å and thus excludes most [O II] emitters. Assuming that [O II]λ3727 emitters have an EW distribution similar to that measured by [119], we expect $\lesssim 1$ galaxy at $z < 0.2$.

Low-luminosity AGNs with a broad line emission can also contaminate our LAE sample. We cross-match the LAEs with the source lists from the Chandra COSMOS Legacy Survey [303], [304] and the XMM survey [192] and find that 24 have X-ray detection. Of these, we remove seven sources that have spectroscopic redshifts placing them at $z_{\rm spec} < 2.40$. Their blue *NB422*$-g$ colors are likely a result of broad C IV, Fe II and O II emission lines falling into the *NB422* filter [305]. Sixteen sources lie within the *NB422* redshift range while the remaining one LAE has no spectroscopic match. The distribution of these seventeen LAEs is discussed in Section 3.5.5.

We cross-match the source list against the *Spitzer* MIPS 24 μm catalog and the radio data from the 1.4 GHz VLA survey [306] and find 4 and 8 matches, respectively. At $z \approx 2.5$, 24 μm samples $\lambda_{\rm rest} \approx 7$ μm emission of dust heated by starbursts or AGNs [307]. The radio emission is produced by synchrotron radiation from relativistic jets of supermassive black holes [308], [309]. Two MIPS sources and three radio counterparts are confirmed to be within our redshift range.

Several LAEs are flagged as AGNs by multiple diagnostics. LAE_31446 ($z_{\rm spec} = 2.450$) is detected at X-ray, mid-IR and radio wavelengths. LAE_8845 (MIPS and radio), LAE_20628 (X-ray and MIPS), LAE_3575, LAE_33546, and LAE_34108 (X-ray and radio) also have multiple detections. All lie within the *NB422* redshift range except for LAE_33546 ($z_{\rm spec} = 2.146$). We remove LAE_33546 from our subsequent analyses.

Redshift Distribution We use the same spectroscopic catalog to validate our LAE selection. As for the VUDS/zCOSMOS sources, we only use those with reliability $\gtrsim 75\%$ according to their redshift flag[2]; for the HPS sources, we use all sources in the COSMOS field because no redshift quality flag available [302]. In Figure 3.3, we show the redshift histogram of the LAEs with spectroscopic counterparts. Nearly half (75) of our LAEs have spectroscopic redshifts. Of these, 70 lie within $2.40 \leq z \leq 2.54$, the redshift distribution of which is consistent with

[2]↑redshift reliability flag equal to X2, X3, X4 or X9. $X = 0$ is for galaxies; $X = 1$ is for broad-line AGNs; $X = 2$ and $X = 3$ are the cases where secondary objects fall in the slit and are separable/not separable from the main target [64]

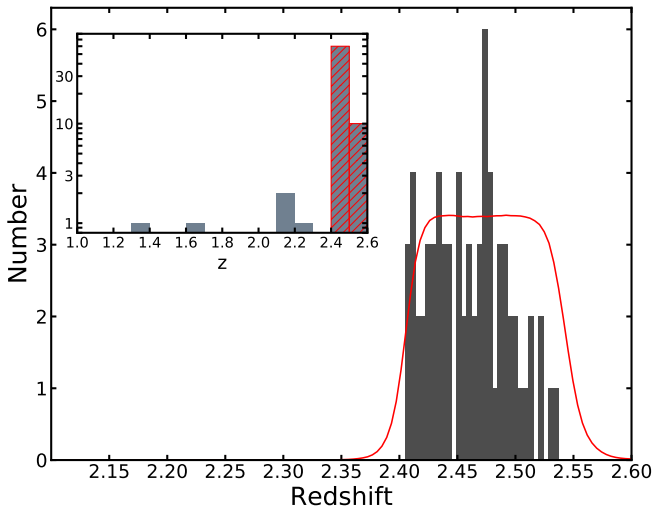

Figure 3.3. The spectroscopic redshift distribution of the 70 LAEs with spectroscopic counterparts in the redshift range is shown. The red curve shows the *NB422* filter transmission with arbitrary normalization. The inset shows the zoomed-out distribution including 5 low-zredshift interlopers. The red-hatched bars highlight those at the *Hyperion* redshift.

the expected filter transmission curve. Among the five lower-redshift interlopers, three are broad-line AGNs, which we remove from our LAE catalog.

The purity of our photometric sample (defined as the fraction of selected sources that fall within the expected redshift range regardless of their spectral types) is 77%. Our contamination rate is comparable to other LAE surveys. [115] confirmed 60% of their LAE candidates at $z = 3.1/3.7$ and 5.7. [118] obtained a success rate of 77% for their LAE selection at $z = 2.2$.

Our final catalog contains 157 LAEs, which include 53 LAEs with spectroscopic redshifts and 104 additional LAEs; we will refer to them as sLAEs and pLAEs, respectively.

3.5 Large-scale Structure Traced by LAEs

3.5.1 The sky distribution of LAEs

Our sample consists of 157 LAEs over the survey area of 3,455 arcmin^2, yielding the mean surface density of $\bar{\Sigma} = (4.5 \pm 0.4) \times 10^{-2}$ arcmin^{-2} where the uncertainty reflects the Poisson noise.

Using this number as the baseline, we quantify the distribution of local over- and under-densities traced by the LAEs. The 2D distribution is constructed using a PYTHON function `hist2D` then smoothed with a Gaussian kernel of a full-width-at-half-maximum (FWHM) 10 comoving Mpc. The kernel size is chosen to maximize the density contrast of a protocluster and is comparable to those adopted in the literature for LAE overdensity identification [95], [96]. The LAE density map is shown in the left panel of Figure 3.4 where both contours and grayscale represent the local surface density relative to the field average. The positions of the pLAEs and sLAEs are shown as circles and triangles.

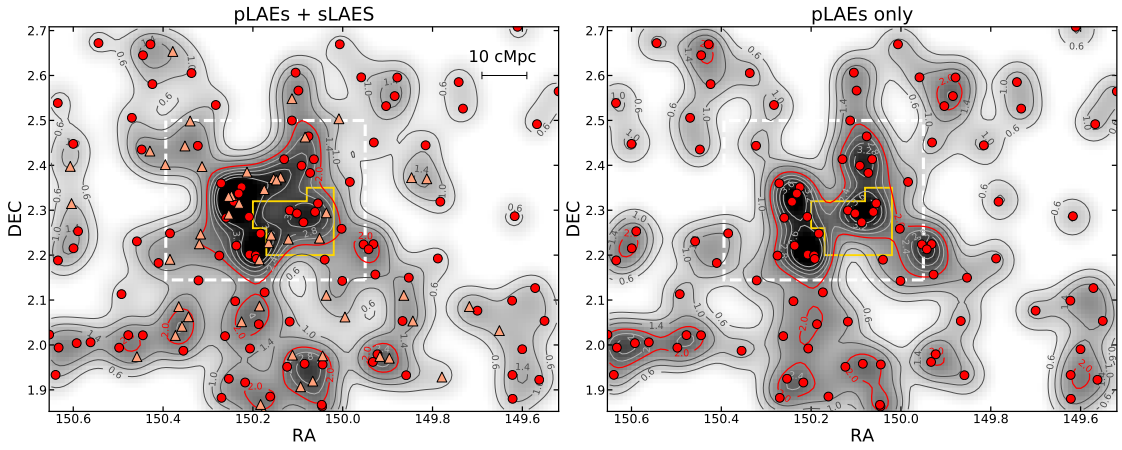

Figure 3.4. Left: smoothed density map of LAE candidates at $z = 2.47$. Red circles and salmon triangles represent pLAEs and sLAEs, respectively. The contours and background grey scale show the surface density levels relative to the field, and the red-highlighted contour ($2.0\bar{\Sigma}$) marks the threshold for protocluster selection. The yellow thick polygon shows the field of view of HPS survey. White dashed rectangle shows the field of view of the CLAMATO survey. **Right:** density map constructed by pLAEs only.

A significant LAE overdensity lies at the center of the field. Taking the $2.0\bar{\Sigma}$ isodensity contour as the boundary, the area of the overdensity is 226.4 arcmin^2 in which 38 LAEs are enclosed. The number density of LAEs in the region is 0.17 ± 0.03 arcmin^{-2}, a factor of 3.7 ± 0.5 times the field average (the overdensity, calculated as $\delta_\Sigma \equiv (\Sigma/\bar{\Sigma} - 1)$, is 2.7 ± 0.5). The likelihood of such an overdensity arising from Poisson fluctuation is $\sim 10^{-11}$. After excluding the overdensity region, we recompute both field LAE density and the central overdensity, which are $\bar{\Sigma} = (3.7 \pm 0.3) \times 10^{-2}$ arcmin^{-2} and $\delta_\Sigma = 3.6 \pm 0.7$, respectively.

Over our survey field, a large fraction of our LAEs have known redshifts from various spectroscopic surveys. Indeed, the number of sLAEs is not negligible compared to that of pLAEs within the central overdensity. To demonstrate that the presence of the overdensity is robust regardless of the inclusion of the spectroscopic sources, we repeat the same procedure but this time only using pLAEs, i.e., the sources which satisfy our LAE criteria (Equation 3.1). Our result, shown in the top right panel of Figure 3.4, suggests that the same general region stands out as a pLAE overdensity. Similar to previously, the $2.0\bar{\Sigma}$ isodensity contour has the effective area of 228.4 arcmin^2 within which 27 pLAEs are found. The central overdensity is $\delta_\Sigma = 3.8 \pm 0.8$ similar to our estimate made including both pLAEs and sLAEs. Both pLAEs and sLAEs broadly trace the same cosmic structure.

3.5.2 LAE overdensity vs Hyperion

In this section, we compare the distribution of LAEs with the large-scale environment quantified by spectroscopic sources. One key question we wish to address is how LAEs are distributed relative to the known members of *Hyperion*, many of which are not LAEs or at least not selected because they are LAEs.

In Figure 3.5, we show the angular positions of spectroscopic sources around *Hyperion* divided to coincide with the redshifts of the protoclusters reported by Ch15 and D15 (z=2.44–2.45: top left), Ca15 (z=2.47: top right), and W16 (z=2.50: bottom left). Galaxy members published in these papers are indicated as triangles while other spectroscopic sources are plotted as squares color-coded by redshift. The LAE distribution – shown as open circles, greyscale, and contours – is identical to that in Figure 3.4. The zCOSMOS coverage of our

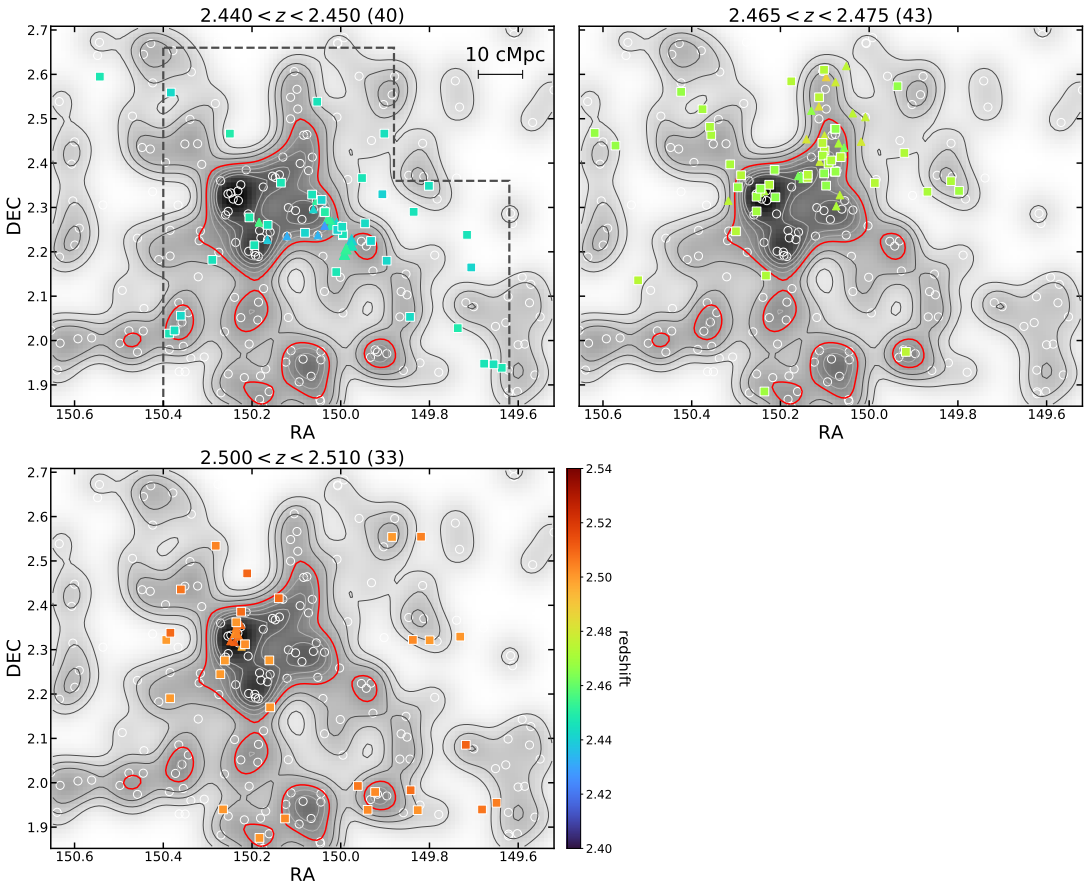

Figure 3.5. The sky distribution of all LAEs (white open circles) and of the known spectroscopic members (triangles) of *Hyperion*: Ch15 and D15 (top left), Ca15 (top right) and W16 (bottom left). VUDS+zCOSMOS galaxies located in the three redshift slices as indicated in the title are plotted as squares. The numbers in the parentheses indicate the total number of spectroscopic galaxies in each redshift slice. The smoothed LAE density maps in the background are identical to that shown in the top left panel of Figure 3.4. The field of view of VUDS is marked as gray dashed polygon. Spectroscopic sources are color-coded by redshift as indicated by the color bar in the bottom-left panel. The galaxy distribution affirms that our LAEs trace the same structures as the known members of *Hyperion*.

survey field is uniform while the spectroscopic coverage of the VUDS survey is marked by a dashed line.

LAEs in Ch15 and D15 structures (z=2.440–2.450)

The protocluster at $z = 2.44$ was first reported by Ch15 as a concentration of nine LAEs from the HPS survey while the $z = 2.45$ structure was initially identified by the zCOSMOS survey as one of the 42 galaxy proto-groups at $z = 1.8 - 3.0$; based on the VLT/FORS2 spectroscopy, D15 reported eleven spectroscopic member galaxies.

Six of the nine Ch15 sources are recovered by our LAE selection. Of the remaining three, two have $NB422 - g > 0.2$ colors and the third has no NB422 detection. Given the large size of the fibers ($4.2''$), these sources may have been mismatched to other galaxies. Alternatively, they may be serendipitous detection of fainter galaxies. None of the D15 sources are LAEs; they are bright at the near-infrared wavelength ($K_s < 24.0$), suggesting that they represent more evolved, more massive galaxies than our LAEs.

The two protoclusters are close in both redshift and angular space and thus are likely a single broad structure. Figure 3.5 (top left) shows that the main structure is a long filament-like alignment stretching in the northeast-southwest direction with a smaller group of galaxies found at ≈10 comoving Mpc east of it. This configuration is closely mirrored by the LAEs which extend even further in the southwestern direction and form a compact group on the eastern end of the overdensity.

LAEs in the Ca15 structure (z=2.465–2.475)

Ca15 reported a serendipitous discovery of an overdensity of dusty star-forming galaxies (DSFGs) at $z = 2.47$. Extensive follow-up spectroscopy revealed 41 galaxy members including 33 LBGs, 7 DSFGs, and one quasar. Only 9 of these members are recovered by our LAE selection, reinforcing the notion that dusty or UV-luminous galaxies tend not to be strong line emitters.

Similar to the D15 structure, the member galaxies form a linear structure stretching out in the north-south direction. However, the full spectroscopy revealed another long array of galaxies in the east, nearly parallel to the main structure. The two join together at the northern end of the LAE overdensity forming a letter 'U'. As such, it appears that the $z \approx 2.47$ structure possibly traces two large overdensities each with filamentary arms. Once again, the LAEs appear to trace the spectroscopic members remarkably well; the contour lines clearly mark the locations of the two filaments stretching northward and the two main

overdensities of the $z \approx 2.47$ structure lie well inside the LAE overdensity.

The W16 structure (z=2.500–2.510)

W16 reported a protocluster at $z \approx 2.50$ observed as a highly significant (11.6σ) overdensity of distant red galaxies. Many are populated in a compact region $\approx 10''$ in diameter ($\approx$80 kpc physical) where weak extended X-ray emission is detected by *Chandra*. Seventeen massive galaxies ($M_{\rm star} \gtrsim 10^{10.5} M_{\odot}$) are confirmed as spectroscopic members via ALMA and near-IR spectroscopy. Though individually plotted, their locations appear as a single symbol in Figure 3.5 (bottom left) due to their proximity.

Unlike the other protoclusters, the region does not exhibit a significant redshift overdensity of optically bright galaxies although there is a mild overdensity in a $\approx$10 cMpc region around it. Although the LAE overdensity peaks near the highest concentration of DSFG members, it remains unclear how many of the LAEs belong to $z \approx 2.50$. Indeed, by cross-matching the positions of LAEs with the VUDS/zCOSMOS catalog, we find that two LAEs are found in the outskirts of the structure at $z \approx 2.53$ while the remainder is at $z \approx 2.47$. Our visual inspection also suggests the least correlation between the spectroscopic sources and the LAEs.

The dearth of LAEs associated with the W16 structure is in stark contrast with all other protoclusters in the region. Given the tentative X-ray detection and the excess of evolved galaxy populations in the region, it is possible that the most massive halo has already formed a hot intracluster medium, suppressing the formation of line-emitters therein. However, the relative lack of LAEs in the extended region around the core is more difficult to explain.

In addition to the association of LAEs to individual protoclusters, we also perform the Spearman's rank correlation test to determine how well LAEs trace the spec-z sources. To this end, we use the `scipy.stats.spearmanr` routine in Python limiting the sources to lie within the region $\alpha_{2000} = 150.00^{\circ} - 150.45^{\circ}$ and $\delta_{2000} = 2.15^{\circ} - 2.50^{\circ}$. The redshift range is chosen to be 2.40–2.54 to reflect the redshift selection function defined by the NB422 transmission (Figure 3.3); only the spectroscopic sources with `zflag` > 2 are used. The resultant galaxy samples are then binned to construct a 2D histogram with each cell $16''$ on

a side. We obtain the Spearman's coefficients $\rho = 0.27$ and $p = 8.09 \times 10^{-31}$ for the full LAE sample: i.e., the two distributions are positively correlated ($\rho > 0$), and the likelihood that the two distributions are not drawn from the same parent sample is extremely low at $1 - p$. Since the sLAEs are selected in part because they lie at this redshift range, we also repeat the test by only using pLAEs and obtain $\rho = 0.06$ and $p = 0.012$. While the significance is lower, the result suggests that the two distributions are correlated at a 3.2σ level. The similarities in the LAE vs spectroscopic sources strongly hint that the LAEs are excellent tracers of the large-scale structure within massive protoclusters.

3.5.3 Environment measured by photometric redshifts

Using the public COSMOS2015 catalog [288], we construct a photometric redshift-based local density map to evaluate the potential to use the photometric redshift technique to isolate massive protoclusters. Although photometric redshift precision is poorer than that achievable by spectroscopy and narrow-band imaging, the catalog provides more than half a million galaxies thereby substantially lowering the Poisson fluctuations of local density measurements. Additionally, the measurements of SFR and stellar masses of each galaxy can elucidate the evolutionary stages of galaxies within the structure. Indeed, several studies used the photo-z technique to identify protoclusters [72], [73], [310] and to study the density-SFR relation [93], [109], [311] at high redshift.

The COSMOS2015 sources are selected based on the UltraVISTA DR2 survey $YJHK_S$ bands. The catalog also includes a suite of deep optical data from CFHT and Subaru and the *Spitzer* IRAC 3.6/4.5μm data from the Spitzer Large Area Survey with Hyper-Suprime-Cam (SPLASH) survey. Although several strips covering 0.6 deg^2 in area were imaged at a greater depth ($K_S = 24.7$ AB, 3σ, $3''$), we limit our analysis to the sources brighter than $K_S = 24$ to ensure uniformity across the field, roughly corresponding to $M_{\rm star} \gtrsim 10^{10} M_\odot$ at $z = 2.5$. When compared against the zCOSMOS and VUDS spectroscopic sources at $z > 1.5$, we find the redshift uncertainty to be $\sigma_{\Delta z/(1+z_s)} \sim 0.03$ and the catastrophic failure ranges in 8% and 13%, respectively.

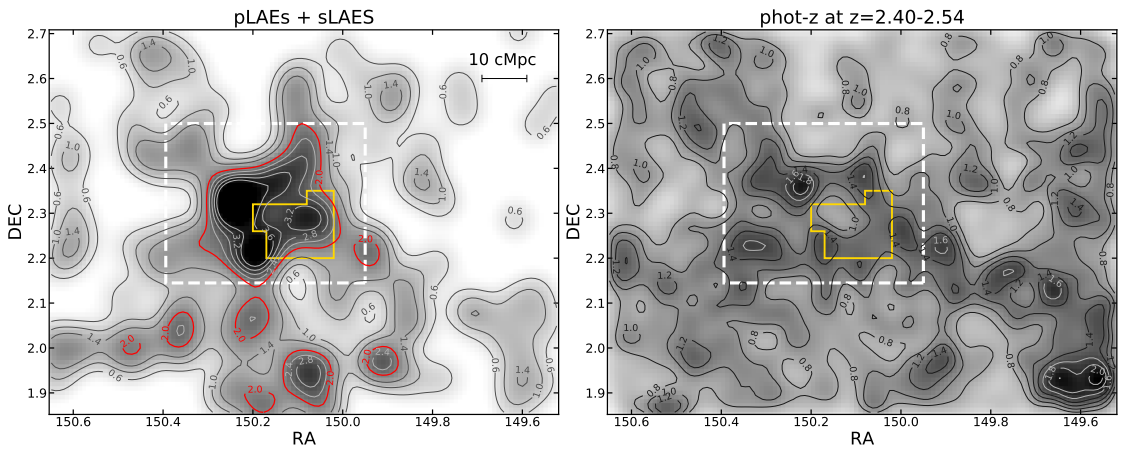

Figure 3.6. Left: smoothed density map of LAE candidates at $z = 2.47$. The contours and background grey scale are identical to the left panel of Figure 3.4. The yellow thick polygon shows the field of view of HPS survey. White dashed rectangle shows the field of view of the CLAMATO survey. **Right:** density map using selected photometric galaxies in COSMOS2015 catalog [288].

To construct the local density map, we treat each galaxy's redshift in a probabilistic manner: i.e., the probability density function (PDF) of a given galaxy obeys a normal distribution centered on z=`zPDF`; the standard deviation is computed as one-half of the distance between the upper and lower 68% confidence level (`zPDF_h68` and `zPDF_l68`). We assign a redshift to each galaxy accordingly but only retain galaxies at z=2.40–2.54, typically resulting in ≈2,000 galaxies in the 1.5 deg^2 UltraVISTA field. Using these galaxies, the local density map is constructed in an identical manner to previously (Section 3.5.1). This procedure is repeated 10,000 times and the final density map is computed as the average over all realizations and is visualized in the bottom left panel of Figure 3.4.

The choice of a smoothing kernel can facilitate identification of a galaxy overdensity. A kernel larger than a typical angular size of cosmic structures can wash out the signal whereas too small a kernel would create numerous density peaks consisting of small overdensities. Another factor to consider is source density, which adds Poisson noise to measured overdensity. Indeed, smoothing scales used by existing studies are similarly motivated. [312] used the median of the distances between galaxies in their samples. [171] chose the kernel

size matching the redshift dispersion due to the peculiar velocity of LAEs. [269] used an adaptive kernel technique to find a kernel that maximizes the overdensity.

In this context, the surface density of phot-z galaxies is $\approx$ 10 times higher (0.58 ± 0.01 arcmin^{-2}) than that of LAEs. To avoid oversmoothing the photo-z density map, we adopt a kernel size of 6 Mpc ($3.5'$) FWHM, smaller than the 10 Mpc kernel used for the LAEs. We generate several density maps using even smaller kernels and find that our results are insensitive to this choice.

The photo-z density map reasonably matches several features present in the LAE overdensity map including the highest galaxy overdensities within *Hyperion* and the voids around it. However, the features reminiscent of 'filaments' present in both LAE and spectroscopic distributions are largely missed by the photo-z density map; this is not surprising given that these regions are intermediate in the density range and thus are more likely to be washed away by the large photo-z uncertainties. We also note that the most significant photo-z overdensity – located at the southwestern corner – has no counterpart in the LAE overdensity. The same structure is identified by [310] constructed from an earlier version of the COSMOS photometric redshift catalog. Although the nature of this galaxy overdensity is currently unknown, it is conceivable that it is an unrelated structure at a slightly lower or higher redshift. In conclusion, a photometric-redshift technique offers a promising avenue of identifying distant protoclusters, its estimate of local density needs to be taken with caution. Additionally, the regions of interest such as filaments connecting to high-density knots may be better traced by line-emitting galaxies.

3.5.4 The distribution of LAEs vs H I gas

We compare the LAE distribution with the H I gas distribution as measured by the COSMOS Lyman-Alpha Mapping and Tomography Observations [CLAMATO: 170] survey; CLAMATO measured Lyα forest absorption in the spectra of background quasars and star-forming galaxies at $z = 2.3-2.8$ in the region surrounding *Hyperion* (see Figure 3.4). The Lyα forest fluctuation is defined as $\delta_F \equiv F/\langle F_z \rangle - 1$ where F is the Lyα transmission relative to the continuum and $\langle F_z \rangle$ denotes the mean transmission as a function of redshift as measured

by [313]. CLAMATO also reconstructed the Lyα forest fluctuation, δ_F^{rec}, calculated from δ_F corrected by the noise covariance matrix with the spatial resolution of 5 comoving Mpc at z=2.05–2.55.

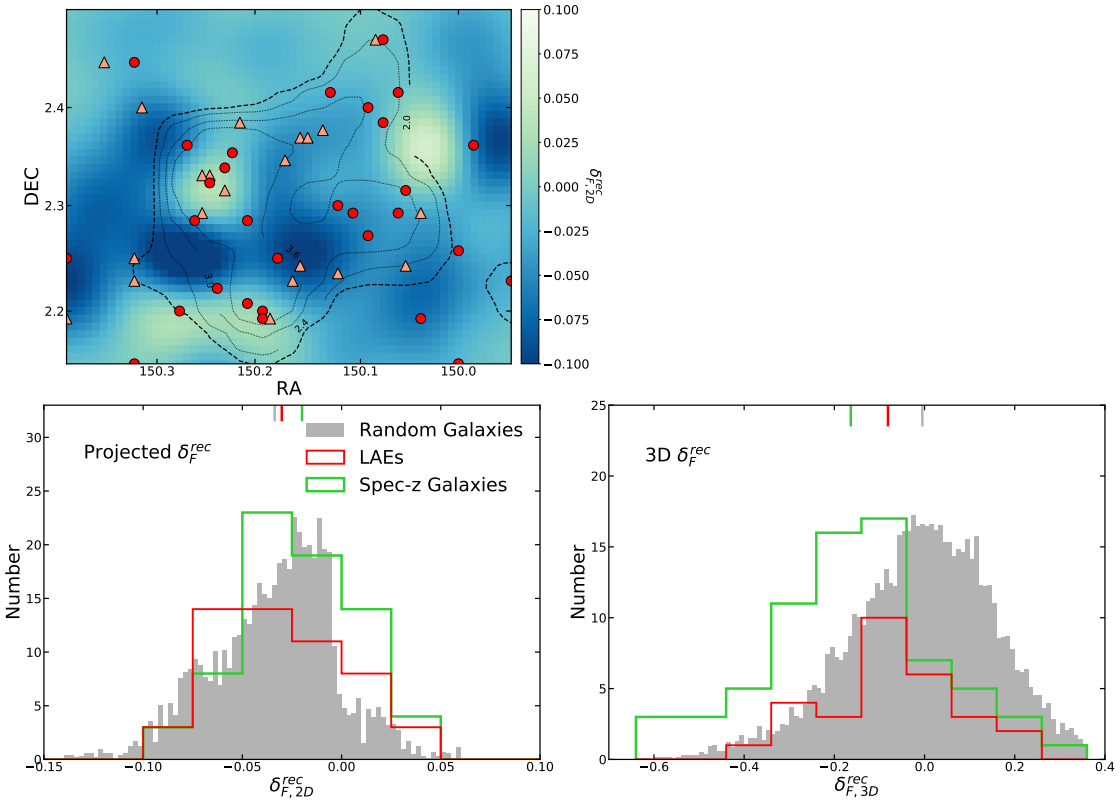

Figure 3.7. Top-left: the sky distribution of the LAEs within the CLAMATO field of view. Red circles and salmon triangles mark the position of pLAEs and sLAEs, respectively. The contours label the galaxy number density, and the dashed contour highlights the central overdensity. The background color map shows the projected Lyα forest fluctuations $\delta_{F,2D}^{rec}$ over redshift $z = 2.40 - 2.54$. **Bottom-left:** histograms of $\delta_{F,2D}^{rec}$ of all LAEs (red steps), spectroscopic members of *Hyperion* (green steps) and random galaxies (gray bars). The mean $\delta_{F,2D}^{rec}$ value of each sample is shown at the top axis. **Bottom-right:** histograms of $\delta_{F,3D}^{rec}$ of the three galaxy samples. The mean $\delta_{F,3D}^{rec}$ value of each sample is marked at the top axis.

To determine the Lyα forest fluctuation at the angular positions of LAEs, we project the 3D CLAMATO data to our survey redshift range z=2.40–2.54. Negative δ_F^{rec} values mean stronger-than-average Lyα absorption (i.e., high hydrogen column density). We denote $\delta_{F,2D}^{rec}$ as the reprojected Lyα forest fluctuation while $\delta_{F,3D}^{rec}$ refers to the 3D CLAMATO data cube.

The top left panel of Figure 3.7 shows the 2D gas density map. The LAE surface density contours are overlaid. In the bottom left panel, we compare the $\delta^{rec}_{F,2D}$ distributions on the positions of LAEs (red) and spectroscopic members of *Hyperion* at $z = 2.40 - 2.52$ (green). We also show the $\delta^{rec}_{F,2D}$ distribution of 100 random positions within the field (grey) as a reference.

The result shows similar mean values: $\delta^{rec}_{F,2D} = -0.03$, -0.02, and -0.03 for the LAEs, spec-z galaxies, and random positions, respectively. This is likely because the 2D projection washes away the density fluctuations occurring at protocluster scales ($\Delta z \sim 0.01$ or $r \sim 10 - 15$ cMpc) as reported by [291]. *NB422* samples much larger line-of-sight distance ≈ 170 cMpc.

We repeat the same analysis but this time using 29 LAEs with known spectroscopic redshifts to examine the 3D distribution. Random points are drawn in the 3D volume. The bottom right panel of Figure 3.7 shows that the locations of LAEs and spec-z galaxies are skewed towards more negative $\delta^{rec}_{F,3D}$ values (-0.08 and -0.16, respectively) suggesting that both are preferentially found in H I-overdensity regions. The random distribution peaks at ≈ 0 as expected. While the $\delta^{rec}_{F,3D}$ distribution peaks at similar values for both LAEs and spec-z sources, the comparison of the mean values suggest that the latter tends to reside in the regions with higher H I column densities than the former. Indeed, LAEs systematically avoid the regions of the highest $\delta^{rec}_{F,2D}$ values (see Figure 3.7, top left).

Existing observations suggest a positive correlation between IGM opacity and galaxy density on Mpc scales [291], [314], [315]. Our result appears to suggest the opposite that LAEs tend to avoid the regions with the highest hydrogen column densities. Our result is consistent with the findings of [316], who measured the cross-correlation function (CCF) between galaxy number density and IGM traced by Lyα forest absorption using the CLAMATO data in conjunction with 19 LAEs at $z_{\rm spec} = 2.125 - 2.225$. They reported a 'flattening' of the positive LAE-IGM correlation at scales $\lesssim$ several cMpc, hinting at the same conclusion that LAEs are not found in the highest gas- and DM density. While more observations are crucially needed to quantify this effect at a higher significance, our result is consistent with the expectation that Lyα transmission via resonant scattering declines precipitously with the gas column density.

3.5.5 The Prevalence of AGN near the LAE overdensity

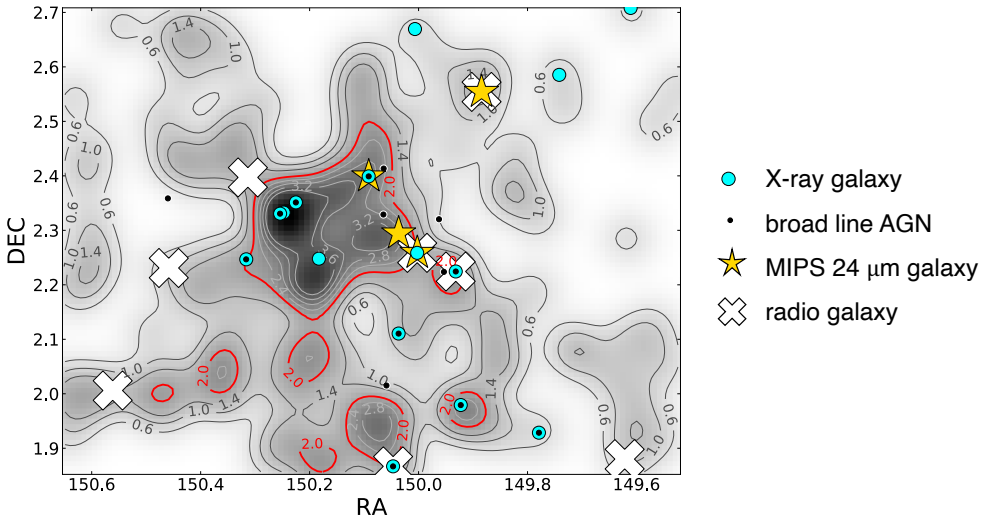

Figure 3.8. Sky positions of LAEs with X-ray (cyan circles), MIPS 24 μm (yellow stars) and VLA (white crosses) detection. The broad line AGNs confirmed by spectroscopic surveys are shown as black dots. The smoothed LAE density map in the background and contours are identical to those shown in the top left panel of Figure 3.4.

It is widely accepted that AGN may play an important role in regulating star formation in galaxies [32], [317]–[319]. At low redshift, existing observations suggest that AGN activity is less pronounced in high-density environment where galaxies tend to be passively evolving [320]–[322]. However, the AGN–galaxy density relation may reverse at higher redshift [323]–[326] following the reversal of the SFR– density relation (e.g., [327], [328]). In this section, we examine the distribution of AGN in relation to the LAE density in and around *Hyperion*.

As discussed in Section 3.4.2, a number of LAEs are classified as AGN based on X-ray, radio, and mid-IR observations. Additionally, existing spectroscopy identified a number of broad-line AGNs in the field at $z = 2.40 - 2.52$. While sources outside the redshift range are removed, we keep those without spectroscopic redshift (1 with X-ray, 2 with mid-IR and 5 with radio detections). Figure 3.8 shows the sky distribution of these AGNs overlaid on the LAE surface density map. These AGNs are preferentially found within the LAE overdensity

or along the filamentary structures connected to them traced by LAEs and spectroscopic sources (see Section 3.5.2).

There is a significant excess of AGNs in the protocluster region. Within our survey field, 9 of the 17 X-ray AGNs lie inside the LAE overdensity, yielding the surface overdensity of $\delta_{\Sigma,X} = 7.8 \pm 3.4$. Similarly, 9 of the 15 broad line AGNs, 3 of the 4 MIPS-detected AGNs and 3 of the 8 radio AGNs reside within the $2.0\bar{\Sigma}$ isodensity contour or near it. When all types of AGNs are combined altogether, the AGN surface overdensity in *Hyperion* rises to $\delta_{\Sigma,all} = 12.3 \pm 4.6$. For comparison, the LAE surface overdensity is $\delta_{\Sigma,\mathrm{LAE}} = 3.6 \pm 0.7$ (Section 3.5.1).

In a region identified as a significant overdensity of LAEs, an overdensity of other types of galaxies is expected. To account for this effect, we calculate the AGN-to-LAE ratio inside and outside the protocluster region and find 0.16 ± 0.07 and 0.09 ± 0.03, respectively, for X-ray-detected AGN. Using the combined AGN sample, the same ratio is 0.37 ± 0.12 and 0.13 ± 0.03. Though limited by large uncertainties, our result suggests that the level of AGN excess in *Hyperion* is a factor of 2–3 higher than expected.

The enhancement in X-ray emitters in dense environment has been reported in the literature. [323] studied galaxies in the SSA22 protocluster region ($z = 3.09$) and reported the enhancement (defined as AGN-to-galaxy ratio in protocluster divided by that measured in field) $4.9^{+11.7}_{-3.9}$% and $7.3^{+17.0}_{-6.2}$% in LBGs and LAEs bright X-ray sources ($\log L_{8-32\mathrm{keV}} = 43.5 - 44.3$ erg s^{-1}). A similar trend was reported by other studies which examined lower redshift protoclusters [324], [326].

The prevalence of AGN in protocluster cores or filaments is consistent with the scenario in which AGNs are triggered due to the major mergers [329], which occur more frequently in dense environment [e.g., 330]. Additionally, it is consistent with the fact that AGN are hosted by more massive halos than other galaxies [e.g., 331]. The same scenario is supported by some observations: [332] estimated the merger fraction of 0.48 ± 0.10 in the SSA22 protocluster relative to 0.33 ± 0.08 in the field. Similarly, [333] found a merger fraction of $0.57^{+0.13}_{-0.14}$ in a $z = 1.62$ protocluster, considerably higher than 0.11 ± 0.03 in the field.

Another phenomenon related to this may be extended Lyα nebulae, or 'Lyα blobs'. Several known protoclusters show an excess number of blobs around galaxy overdensities

[95], [96], [138], [270]. In SSA22, the best studied protocluster system at $z = 3.09$, are found the overdensity of both AGN [identified by X-ray and submillimeter observations: 334] and Lyα blobs [138] at the 'nodes' of filaments traced by LAEs, hinting at the possible link between them. Like AGNs, the clustering strength of blobs indicates that they too are hosted by more massive halos than galaxies [e.g., 269]. Some blobs show direct evidence of being powered by AGN [335]–[337] while others point to cold gas accretion in dense environment [e.g., 338], [339]. These rare sources provide tantalizing evidence of physical processes uniquely occurring in protocluster environments. Placing robust constraints on the physical connection between protoclusters, AGNs, and blobs will require a much larger scale blind surveys of these objects (see Section 3.5.7).

3.5.6 Intrinsic galaxy overdensity of *Hyperion*

The *NB422* filter has a width 170 Å and samples 170 comoving Mpc in the line-of-sight distance at $z \approx 2.4$. This is much greater than the size of a typical protocluster, thus we expect that the spatial overdensity, δ_g, of the structure is greater than the measured surface overdensity, which is diluted by unassociated fore- and background sources. Here, we estimate the true overdensity of the structure traced by our LAEs.

First, we create a field with a mock protocluster positioned at its center. The 'protocluster' region is defined as a rectangle whose area is equal to that enclosed by the $2.0\bar{\Sigma}$ isodensity contour[3] outlined in red in the left panel of Figure 3.4. In the line-of-sight direction, the protocluster redshift range [2.40, 2.54] is divided into 11 bins with an interval Δz=0.013, corresponding to 15 comoving Mpc roughly matching the half-mass diameter of a massive protocluster [63], [140]. In this setup, the true number of galaxies in a protocluster would be $N_{\rm pc} = (1+\delta_g)N_{\rm obs}/(11+\delta_g)$ where $N_{\rm obs}$ is the total number of LAEs found in the protocluster region; $N_{\rm obs} = 40$ in our data. Then we randomly choose a δ_g value in the range 0–50, compute the number of protocluster- and field galaxies (including their Poisson shot noise), and populate them in the 3D space. The surface overdensity δ_Σ is computed from the

[3]↑The transverse size is 18×12 arcmin^2 or 30×20 cMpc^2 at $z = 2.4$.

run, yielding the δ_g–δ_Σ scaling relation given our observational parameters. The procedure is repeated 10,000 times.

The recovered δ_g–δ_Σ is linear and well-behaved. The LAE surface overdensity $\delta_\Sigma = 3.7$ implies $\delta_g = 39.6^{+5.4}_{-5.1}$, much higher than $\delta_g \sim 3 - 10$ expected for a single protocluster [e.g., 66], [125], [340]–[342]. The unphysically high galaxy overdensity is a direct result of our simplistic assumption that there is a *single* protocluster, which is easily disputed by the redshift distribution of our LAEs (Section 3.5.2).

We repeat the procedure, but this time, assuming four protoclusters. For the lack of better information about the relative size of the structures within *Hyperion* and their configuration, we assume that each protocluster is confined in a rectangular region $6'$ on a side (10.2 comoving Mpc at $z = 2.4$) with the identical overdensity. We obtain $\delta_g = 12.2^{+2.8}_{-2.0}$. Similarly, assuming seven protoclusters in the region as was found by [71], each structure is expected to have $\delta_g = 5.9 - 8.3$. While simplistic, our analysis demonstrates that the significance and the angular extent of the LAE overdensity is too great for a single protocluster but instead require at least 3 massive overlapping ones, reinforcing the notion that LAEs provide an effective pathway to find cosmic structures or a complex of structures in distant universe.

Using these δ_g estimates for each protocluster, we can make a crude estimate of the total mass locked in them. The main limitation comes from our lack of knowledge in the relative sizes of individual groups and their configuration; additionally, if a substantial fraction of LAEs trace the filaments connecting which lie the main halos, it would lead to an overestimation of the total mass.

Following the method outlined in [275], the descendant mass of a structure is expressed as:

$$M_{tot} = \bar{\rho} V_{\rm true} (1 + \delta_m) \tag{3.4}$$

where $\bar{\rho}$ is the mean density of the universe, and $V_{\rm true}$ is the true volume that encloses the structure. The matter overdensity, δ_m, is related to galaxy overdensity as $1 + b\delta_m = C(1 + \delta_g)$ where $C \equiv V_{\rm obs}/V_{\rm true}$ is a correction factor for redshift-space distortion arising from peculiar

velocities. In the case of spherical collapse, $C = 1 + \Omega_m^{4/7}(z)[1 - (1 + \delta_m)^{1/3}]$. For $V_{\rm obs}$, we assume the line-of-sight distance 15 cMpc. We adopt a galaxy bias parameter $b = 2$ for LAEs [134], [286]. The total mass enclosed therein is $M_{tot} = 1.4^{+0.2}_{-0.1} \times 10^{15}$ $M_\odot$. The bias value of $b = 2.5$ would decrease the mass by 14% to 1.2×10^{15} $M_\odot$.

Given the simplistic nature of this analysis, our mass estimate is more than double the value reported by [71], $4.8 \times 10^{14} M_\odot$. This difference is not unexpected considering that we have inferred the total mass enclosed in the entire *Hyperion* volume. In comparison, [71] estimated and summed over the mass of each of the protoclusters therein and therefore do not account for the masses of filaments and sheets connecting the protoclusters.

3.5.7 Future outlook: LAEs as beacons of protoclusters

The present study unambiguously demonstrates LAEs as reliable markers of the largest cosmic structures such as protoclusters and groups of protoclusters. Further, their distribution can be used to estimate the size, morphology, and present-day mass of the structure and to reveal regions of interest such as dense core, filaments, and voids. These capabilities will be valuable in any systematic effort to study cosmic structures that lie outside a handful of deep extragalactic fields with extensive spectroscopy.

The One-hundred-square-degree DECam Imaging in Narrowbands (ODIN) survey has been conducting deep imaging of ≈100 deg^2 in area using the Dark Energy Camera [343] to identify LAEs, Lyα nebulae, and forming protoclusters. ODIN targets three cosmic epochs at $z = 4.5$, 3.1, and 2.4, straddling the crucial epoch in which the mass assembly in field and cluster galaxies reached its peak [e.g., 60], [172]. Over seven fields[4], ODIN will sample a total of ≈0.25 Gpc^3 in cosmic volume in which ≈ 130,000 LAEs and ≈45 (600) progenitors of Coma- and Virgo-like clusters ($M_{tot} > 10^{15}$ $M_\odot$and $(3 - 10) \times 10^{14}$ $M_\odot$, respectively) are expected. The details of the survey will be presented in an upcoming paper (K.-S. Lee et al., in preparation).

[4]↑The targeted fields include all four LSST Deep Drilling Fields, two southern Euclid Deep fields, Deep2-3, and HETDEX-SHELA.

When combined with the new generation of wide-field imaging and spectroscopic experiments such as LSST, Roman, LMT/TolTEC, HETDEX, and DESI, ODIN will open up a new window into the formation of cosmic structures and the role of large-scale environment on the galaxy constituents therein. First, the physical connection between protocluster, AGN, Lyα nebulae, and passive galaxies can be quantified and delineated in a statistically meaningful manner. Measurements of their occurrences, preferred locations, and physical properties can be used to place strong constraints on the physical origin and the timescale of these phenomena.

Second, a robust sample of protoclusters with accurate redshifts will facilitate comparative studies of protoclusters. Recently, large samples of protocluster candidates have been identified as LBG overdensities [e.g., 73], [278] and cold dust emission in the far-IR [e.g., 344], [345]. However, the intersectionality between these samples and the selection efficiency and bias of different techniques are poorly understood [but see, e.g., 346], [347]

Finally, a large statistical sample of ODIN protoclusters will allow us to measure the average star formation activity expected in a protocluster and how it scales with their present-day masses over cosmic time. For example, deep wide-field mm surveys such as the LMT/TolTEC Public Legacy survey will not only detect individual high star-formers but also can be used to estimate the total (dust-obscured) SFR per cluster via stacking analysis. Such measurements can resolve or further highlight the large discrepancies that currently exist between observed and predicted level of star formation in protoclusters [e.g. 348].

3.6 Conclusions

In this paper, we carry out a comprehensive study of galaxies inhabiting *Hyperion*, the first spectroscopically confirmed structure that hosts multiple protoclusters at $z = 2.4 - 2.5$, which will likely evolve into a super cluster of galaxies by the present-day universe. To trace its LSS, we obtain deep narrow-band observations of a $\approx 1^\circ \times 1^\circ$ of the region using *NB422* ($\lambda_c \approx 4225$ Å, $\Delta\lambda = 170$ Å) and select 157 LAE candidates at the *Hyperion* redshift (Section 3.4.1). The new data combined with the extensive spectroscopic and photomet-

ric observations available in the field provide a unique opportunity to closely examine how galaxies of different types trace the same LSS. Our main findings are listed below:

1. A significant excess of LAEs occupies the region of *Hyperion* with the surface overdensity $\delta_\Sigma = 3.6$ (Section 3.5.1). This corresponds to the combined spatial galaxy overdensity $\delta_g \approx 40$ within an effective volume of 1.3×10^5 cMpc^3. The level and the extent of the overdensity is too large for a single structure, strongly suggesting that multiple protoclusters must be embedded in *Hyperion*. The LAE overdensity will evolve into a super cluster of galaxies with a total mass of $M_{tot} \approx 1.4 \times 10^{15}$ M$_\odot$ distributed between the main halos hosting each protocluster and the filaments connecting them (Section 3.5.6).

2. Taking advantage of the densely sampled spectroscopic data, we evaluate the feasibility of LAEs as a probe of the LSS in and around *Hyperion* (Section 3.5.2). The distributions of LAEs and spectroscopic sources are remarkably similar, suggesting that LAEs are excellent tracers of the LSS (Figure 3.5). In particular, the LAE distribution clearly marks several long filamentary arms extending from multiple protoclusters. However, we also find tentative evidence that LAEs may be poor tracers of the most evolved systems [e.g., see 292].

3. Using the COSMOS2015 photometric redshift catalog, we construct a local density map at $z = 2.40 - 2.54$. The photo-z map fares reasonably well in finding several strongest features of *Hyperion*, including the highest galaxy overdensities and the lowest-density voids around it; however, lower-density features of interest such as filaments may be better traced by line-emitting galaxies (Figure 3.6).

4. By cross-correlating the LAE positions with the H I tomography data from the CLAMATO survey [291], we find that LAEs tend to lie in the regions of moderate H I overdensities while avoiding the highest H I density regions (Figure 3.7). Our finding is in line with existing studies [e.g., 316] and is consistent with the expectation that the suppression of Lyα transmission may be substantial in the highest-density regions due to resonant scattering.

5. In and around *Hyperion*, we find a significant overdensity of AGN (Section 3.5.5, Figure 3.8) selected based on X-ray/radio/mid-IR emission or broad emission line features including Lyα. When all types of AGN are considered together, the surface overdensity is measured to be $\delta_{\Sigma,all} \approx 12$, i.e., 3.5 times larger than the LAE surface overdensity of the region, $\delta_{\Sigma,\mathrm{LAE}} = 3.6$. The prevalence of AGN in protocluster regions hints at the possibility that they may be triggered by physical processes that occur more frequently in dense environments, such as galaxy merger.

4. SUMMARY AND PROSPECTS

4.1 Summary

At $z > 2$, Lyα emission is redshifted into the visible window which is detectable by ground-based telescopes. Existing studies show that LAEs are younger and less dusty than any known galaxy population and are hosted by moderate-mass dark matter halos. These traits make LAEs the best visible tracer of the underlying matter distribution, enabling a detailed investigation of the large-scale structures of the young universe and the nascent galaxies therein. In this thesis, I have used Lyα emission as a cosmological tool to conduct two complementary investigations which examined how the formation of galaxies is influenced by the large-scale structure of the universe.

In Chapter 2, I study the spatial distribution of Lyα emission to elucidate the kinematic and spatial distribution of the H I gas in the interstellar and circumgalactic media of galaxies residing in average- and high-density environments. A comprehensive study of how Lyα properties correlate with other galaxy properties is conducted. A strong connection between Lyα escape and dust, UV luminosity, and the large-scale environment is found, hinting at a complex condition of the ISM/CGM that affects the Lyα production and transmission. These results have wide-ranging implications on galaxy evolution and cosmic reionization.

My second project is aimed at understanding galaxy formation in *Hyperion*, the most massive cosmic structure known to date. In Chapter 3, I investigate various constituents residing in *Hyperion* including LAEs, SFGs, intergalactic neutral gas, and AGNs. The different components of proto-superclusters shed light on the formation history of *Hyperion* and on the evolutionary path of the proto-supercluster. In addition, my results strongly reinforce the notion that LAEs are indeed the best tracers of the large-scale environment.

4.2 Prospects

Although existing studies offer tantalizing evidence for interesting physical processes uniquely occurring in protocluster environment, many questions remain poorly addressed.

Clean and statistically robust samples of protoclusters are still lacking. As a result, full characterization of protoclusters and their galaxy constituents has not been possible, limiting our ability to understand how the environment influences the formation of galaxies during their peak epoch, and to make their evolutionary connection between present-day clusters. Additionally, rare astrophysical phenomena (e.g., Lyα blobs or AGN) are found associated with protoclusters [94], [95]. A comprehensive study on these sources can pinpoint the sites of the ongoing galaxy and quasar formation and shed light on the accretion of group-sized halos. However, given their extremely low space density, the basic properties of LABs are not yet fully constrained.

I am a coinvestigator inthe One-hundred square-degree DECam Imaging in Narrowbands (ODIN) survey, which will provide the largest-ever LAE sample spanning a range of large-scale environments. The survey will target an area of 91 deg^2 with three customed narrow-band filters sampling Lyα emission at $z = 4.5$, 3.1 and 2.4 (cosmic ages of 1.3, 2.0, and 2.7 Gyr). By the end of the survey, a total of ≈130,000 LAEs, ≈45 (≈600) Coma (Virgo) progenitors and ≈400 LABs down to surface brightness limits of $\approx 10^{-18}$ erg s^{-1} cm^{-2} arcsec^{-2} are expected within the survey volume. Combined with the existing and upcoming broadband data, ODIN survey will provide an unprecedented large sample of galaxies and (proto)clusters to address their formation over cosmic time and the environmental regulation on the evolution of galaxies.

REFERENCES

[1] A. Pillepich, D. Nelson, L. Hernquist, V. Springel, R. Pakmor, P. Torrey, R. Weinberger, S. Genel, J. P. Naiman, F. Marinacci, and M. Vogelsberger, "First results from the IllustrisTNG simulations: the stellar mass content of groups and clusters of galaxies," *Monthly Notices of the RAS*, vol. 475, no. 1, pp. 648–675, Mar. 2018. DOI: 10.1093/mnras/stx3112. arXiv: 1707.03406 [astro-ph.GA].

[2] A. H. Guth, "Inflationary universe: A possible solution to the horizon and flatness problems," *Physical Review D ++*, vol. 23, no. 2, pp. 347–356, Jan. 1981. DOI: 10.1103/PhysRevD.23.347.

[3] A. D. Linde, "A new inflationary universe scenario: A possible solution of the horizon, flatness, homogeneity, isotropy and primordial monopole problems," *Physics Letters B*, vol. 108, no. 6, pp. 389–393, Feb. 1982. DOI: 10.1016/0370-2693(82)91219-9.

[4] A. D. Linde, "Chaotic inflation," *Physics Letters B*, vol. 129, no. 3-4, pp. 177–181, Sep. 1983. DOI: 10.1016/0370-2693(83)90837-7.

[5] A. Albrecht and P. J. Steinhardt, "Cosmology for Grand Unified Theories with Radiatively Induced Symmetry Breaking," *Physical Review Letters*, vol. 48, no. 17, pp. 1220–1223, Apr. 1982. DOI: 10.1103/PhysRevLett.48.1220.

[6] P. J. E. Peebles, "Recombination of the Primeval Plasma," *Astrophysical Journal*, vol. 153, p. 1, Jul. 1968. DOI: 10.1086/149628.

[7] A. A. Penzias and R. W. Wilson, "A Measurement of Excess Antenna Temperature at 4080 Mc/s.," *Astrophysical Journal*, vol. 142, pp. 419–421, Jul. 1965. DOI: 10.1086/148307.

[8] A. G. Riess, A. V. Filippenko, P. Challis, A. Clocchiatti, A. Diercks, P. M. Garnavich, R. L. Gilliland, C. J. Hogan, S. Jha, R. P. Kirshner, B. Leibundgut, M. M. Phillips, D. Reiss, B. P. Schmidt, R. A. Schommer, R. C. Smith, J. Spyromilio, C. Stubbs, N. B. Suntzeff, and J. Tonry, "Observational Evidence from Supernovae for an Accelerating Universe and a Cosmological Constant," *Astronomical Journal*, vol. 116, no. 3, pp. 1009–1038, Sep. 1998. DOI: 10.1086/300499. arXiv: astro-ph/9805201 [astro-ph].

[9] S. Perlmutter, G. Aldering, G. Goldhaber, R. A. Knop, P. Nugent, P. G. Castro, S. Deustua, S. Fabbro, A. Goobar, D. E. Groom, I. M. Hook, A. G. Kim, M. Y. Kim, J. C. Lee, N. J. Nunes, R. Pain, C. R. Pennypacker, R. Quimby, C. Lidman, R. S. Ellis, M. Irwin, R. G. McMahon, P. Ruiz-Lapuente, N. Walton, B. Schaefer, B. J. Boyle, A. V. Filippenko, T. Matheson, A. S. Fruchter, N. Panagia, H. J. M. Newberg, W. J. Couch, and T. S. C. Project, "Measurements of Ω and Λ from 42 High-Redshift Supernovae," *Astrophysical Journal*, vol. 517, no. 2, pp. 565–586, Jun. 1999. DOI: 10.1086/307221. arXiv: astro-ph/9812133 [astro-ph].

[10] Planck Collaboration, P. A. R. Ade, N. Aghanim, C. Armitage-Caplan, M. Arnaud, M. Ashdown, F. Atrio-Barandela, J. Aumont, C. Baccigalupi, A. J. Banday, R. B. Barreiro, and et al, "Planck 2013 results. XVI. Cosmological parameters," *Astronomy and Astrophysics*, vol. 571, A16, A16, Nov. 2014. DOI: 10.1051/0004-6361/201321591. arXiv: 1303.5076 [astro-ph.CO].

[11] D. N. Spergel, L. Verde, H. V. Peiris, E. Komatsu, M. R. Nolta, C. L. Bennett, M. Halpern, G. Hinshaw, N. Jarosik, A. Kogut, M. Limon, S. S. Meyer, L. Page, G. S. Tucker, J. L. Weiland, E. Wollack, and E. L. Wright, "First-Year Wilkinson Microwave Anisotropy Probe (WMAP) Observations: Determination of Cosmological Parameters," *Astrophysical Journal, Supplement*, vol. 148, no. 1, pp. 175–194, Sep. 2003. DOI: 10.1086/377226. arXiv: astro-ph/0302209 [astro-ph].

[12] D. N. Spergel, R. Bean, O. Doré, M. R. Nolta, C. L. Bennett, J. Dunkley, G. Hinshaw, N. Jarosik, E. Komatsu, L. Page, H. V. Peiris, L. Verde, M. Halpern, R. S. Hill, A. Kogut, M. Limon, S. S. Meyer, N. Odegard, G. S. Tucker, J. L. Weiland, E. Wollack, and E. L. Wright, "Three-Year Wilkinson Microwave Anisotropy Probe (WMAP) Observations: Implications for Cosmology," *Astrophysical Journal, Supplement*, vol. 170, no. 2, pp. 377–408, Jun. 2007. DOI: 10.1086/513700. arXiv: astro-ph/0603449 [astro-ph].

[13] J. H. Jeans, "The Stability of a Spherical Nebula," *Philosophical Transactions of the Royal Society of London Series A*, vol. 199, pp. 1–53, Jan. 1902. DOI: 10.1098/rsta.1902.0012.

[14] P. J. E. Peebles, "Large-scale background temperature and mass fluctuations due to scale-invariant primeval perturbations," *Astrophysical Journal, Letters*, vol. 263, pp. L1–L5, Dec. 1982. DOI: 10.1086/183911.

[15] J. R. Bond and A. S. Szalay, "The collisionless damping of density fluctuations in an expanding universe," *Astrophysical Journal*, vol. 274, pp. 443–468, Nov. 1983. DOI: 10.1086/161460.

[16] G. R. Blumenthal, H. Pagels, and J. R. Primack, "Galaxy formation by dissipationless particles heavier than neutrinos," *Nature*, vol. 299, no. 5878, pp. 37–38, Sep. 1982. DOI: 10.1038/299037a0.

[17] G. R. Blumenthal, S. M. Faber, J. R. Primack, and M. J. Rees, "Formation of galaxies and large-scale structure with cold dark matter.," *Nature*, vol. 311, pp. 517–525, Oct. 1984. DOI: 10.1038/311517a0.

[18] S. D. M. White and M. J. Rees, "Core condensation in heavy halos: a two-stage theory for galaxy formation and clustering.," *Monthly Notices of the RAS*, vol. 183, pp. 341–358, May 1978. DOI: 10.1093/mnras/183.3.341.

[19] J. F. Navarro, C. S. Frenk, and S. D. M. White, "A Universal Density Profile from Hierarchical Clustering," *Astrophysical Journal*, vol. 490, no. 2, pp. 493–508, Dec. 1997. DOI: 10.1086/304888. arXiv: astro-ph/9611107 [astro-ph].

[20] B. Moore, F. Governato, T. Quinn, J. Stadel, and G. Lake, "Resolving the Structure of Cold Dark Matter Halos," *Astrophysical Journal, Letters*, vol. 499, no. 1, pp. L5–L8, May 1998. DOI: 10.1086/311333. arXiv: astro-ph/9709051 [astro-ph].

[21] V. Springel, S. D. M. White, A. Jenkins, C. S. Frenk, N. Yoshida, L. Gao, J. Navarro, R. Thacker, D. Croton, J. Helly, J. A. Peacock, S. Cole, P. Thomas, H. Couchman, A. Evrard, J. Colberg, and F. Pearce, "Simulations of the formation, evolution and clustering of galaxies and quasars," *Nature*, vol. 435, no. 7042, pp. 629–636, Jun. 2005. DOI: 10.1038/nature03597. arXiv: astro-ph/0504097 [astro-ph].

[22] V. Springel, T. Di Matteo, and L. Hernquist, "Modelling feedback from stars and black holes in galaxy mergers," *Monthly Notices of the RAS*, vol. 361, no. 3, pp. 776–794, Aug. 2005. DOI: 10.1111/j.1365-2966.2005.09238.x. arXiv: astro-ph/0411108 [astro-ph].

[23] M. Boylan-Kolchin, V. Springel, S. D. M. White, A. Jenkins, and G. Lemson, "Resolving cosmic structure formation with the Millennium-II Simulation," *Monthly Notices of the RAS*, vol. 398, no. 3, pp. 1150–1164, Sep. 2009. DOI: 10.1111/j.1365-2966.2009.15191.x. arXiv: 0903.3041 [astro-ph.CO].

[24] J. Arons and J. Silk, "On the Jean's criterion in relativistic cosmology," *Monthly Notices of the RAS*, vol. 140, p. 331, Jan. 1968. DOI: 10.1093/mnras/140.3.331.

[25] N. Y. Gnedin and L. Hui, "Probing the Universe with the Lyalpha forest - I. Hydrodynamics of the low-density intergalactic medium," *Monthly Notices of the RAS*, vol. 296, no. 1, pp. 44–55, May 1998. DOI: 10.1046/j.1365-8711.1998.01249.x. arXiv: astro-ph/9706219 [astro-ph].

[26] D. Kereš and L. Hernquist, "Seeding the Formation of Cold Gaseous Clouds in Milky Way-Size Halos," *Astrophysical Journal, Letters*, vol. 700, no. 1, pp. L1–L5, Jul. 2009. DOI: 10.1088/0004-637X/700/1/L1. arXiv: 0905.2186 [astro-ph.CO].

[27] A. J. Benson, "Galaxy formation theory," *Physics Reports*, vol. 495, no. 2-3, pp. 33–86, Oct. 2010. DOI: 10.1016/j.physrep.2010.06.001. arXiv: 1006.5394 [astro-ph.CO].

[28] T. Naab and J. P. Ostriker, "Theoretical Challenges in Galaxy Formation," *Annual Review of Astron and Astrophys*, vol. 55, no. 1, pp. 59–109, Aug. 2017. DOI: 10.1146/annurev-astro-081913-040019. arXiv: 1612.06891 [astro-ph.GA].

[29] E. C. Ostriker, C. F. McKee, and A. K. Leroy, "Regulation of Star Formation Rates in Multiphase Galactic Disks: A Thermal/Dynamical Equilibrium Model," *Astrophysical Journal*, vol. 721, no. 2, pp. 975–994, Oct. 2010. DOI: 10.1088/0004-637X/721/2/975. arXiv: 1008.0410 [astro-ph.CO].

[30] B. D. Oppenheimer, R. Davé, D. Kereš, M. Fardal, N. Katz, J. A. Kollmeier, and D. H. Weinberg, "Feedback and recycled wind accretion: assembling the z = 0 galaxy mass function," *Monthly Notices of the RAS*, vol. 406, no. 4, pp. 2325–2338, Aug. 2010. DOI: 10.1111/j.1365-2966.2010.16872.x. arXiv: 0912.0519 [astro-ph.CO].

[31] P. Creasey, T. Theuns, and R. G. Bower, "How supernova explosions power galactic winds," *Monthly Notices of the RAS*, vol. 429, no. 3, pp. 1922–1948, Mar. 2013. DOI: 10.1093/mnras/sts439. arXiv: 1211.1395 [astro-ph.GA].

[32] P. F. Hopkins, D. Kereš, J. Oñorbe, C.-A. Faucher-Giguère, E. Quataert, N. Murray, and J. S. Bullock, "Galaxies on FIRE (Feedback In Realistic Environments): stellar feedback explains cosmologically inefficient star formation," *Monthly Notices of the RAS*, vol. 445, no. 1, pp. 581–603, Nov. 2014. DOI: 10.1093/mnras/stu1738. arXiv: 1311.2073 [astro-ph.CO].

[33] F. Marinacci, R. Pakmor, and V. Springel, "The formation of disc galaxies in high-resolution moving-mesh cosmological simulations," *Monthly Notices of the RAS*, vol. 437, no. 2, pp. 1750–1775, Jan. 2014. DOI: 10.1093/mnras/stt2003. arXiv: 1305.5360 [astro-ph.CO].

[34] P. Girichidis, S. Walch, T. Naab, A. Gatto, R. Wünsch, S. C. O. Glover, R. S. Klessen, P. C. Clark, T. Peters, D. Derigs, and C. Baczynski, "The SILCC (SImulating the LifeCycle of molecular Clouds) project - II. Dynamical evolution of the supernova-driven ISM and the launching of outflows," *Monthly Notices of the RAS*, vol. 456, no. 4, pp. 3432–3455, Mar. 2016. DOI: 10.1093/mnras/stv2742. arXiv: 1508.06646 [astro-ph.GA].

[35] J. Kormendy and D. Richstone, "Inward Bound—The Search For Supermassive Black Holes In Galactic Nuclei," *Annual Review of Astron and Astrophys*, vol. 33, p. 581, Jan. 1995. DOI: 10.1146/annurev.aa.33.090195.003053.

[36] J. Kormendy and L. C. Ho, "Coevolution (Or Not) of Supermassive Black Holes and Host Galaxies," *Annual Review of Astron and Astrophys*, vol. 51, no. 1, pp. 511–653, Aug. 2013. DOI: 10.1146/annurev-astro-082708-101811. arXiv: 1304.7762 [astro-ph.CO].

[37] L. Ferrarese and D. Merritt, "A Fundamental Relation between Supermassive Black Holes and Their Host Galaxies," *Astrophysical Journal, Letters*, vol. 539, no. 1, pp. L9–L12, Aug. 2000. DOI: 10.1086/312838. arXiv: astro-ph/0006053 [astro-ph].

[38] K. Gebhardt, R. Bender, G. Bower, A. Dressler, S. M. Faber, A. V. Filippenko, R. Green, C. Grillmair, L. C. Ho, J. Kormendy, T. R. Lauer, J. Magorrian, J. Pinkney, D. Richstone, and S. Tremaine, "A Relationship between Nuclear Black Hole Mass and Galaxy Velocity Dispersion," *Astrophysical Journal, Letters*, vol. 539, no. 1, pp. L13–L16, Aug. 2000. DOI: 10.1086/312840. arXiv: astro-ph/0006289 [astro-ph].

[39] S. Tremaine, K. Gebhardt, R. Bender, G. Bower, A. Dressler, S. M. Faber, A. V. Filippenko, R. Green, C. Grillmair, L. C. Ho, J. Kormendy, T. R. Lauer, J. Magorrian, J. Pinkney, and D. Richstone, "The Slope of the Black Hole Mass versus Velocity Dispersion Correlation," *Astrophysical Journal*, vol. 574, no. 2, pp. 740–753, Aug. 2002. DOI: 10.1086/341002. arXiv: astro-ph/0203468 [astro-ph].

[40] L. Ferrarese and H. Ford, "Supermassive Black Holes in Galactic Nuclei: Past, Present and Future Research," *Space Science Reviews*, vol. 116, no. 3-4, pp. 523–624, Feb. 2005. DOI: 10.1007/s11214-005-3947-6. arXiv: astro-ph/0411247 [astro-ph].

[41] P. Norberg, C. M. Baugh, E. Hawkins, S. Maddox, J. A. Peacock, S. Cole, C. S. Frenk, J. Bland-Hawthorn, T. Bridges, R. Cannon, M. Colless, C. Collins, W. Couch, G. Dalton, R. De Propris, S. P. Driver, G. Efstathiou, R. S. Ellis, K. Glazebrook, C. Jackson, O. Lahav, I. Lewis, S. Lumsden, D. Madgwick, B. A. Peterson, W. Sutherland, and K. Taylor, "The 2dF Galaxy Redshift Survey: luminosity dependence of galaxy clustering," *Monthly Notices of the RAS*, vol. 328, no. 1, pp. 64–70, Nov. 2001. DOI: 10.1046/j.1365-8711.2001.04839.x. arXiv: astro-ph/0105500 [astro-ph].

[42] I. Zehavi, M. R. Blanton, J. A. Frieman, D. H. Weinberg, H. J. Mo, M. A. Strauss, S. F. Anderson, J. Annis, N. A. Bahcall, M. Bernardi, J. W. Briggs, J. Brinkmann, S. Burles, L. Carey, F. J. Castander, A. J. Connolly, I. Csabai, J. J. Dalcanton, S. Dodelson, M. Doi, D. Eisenstein, M. L. Evans, D. P. Finkbeiner, S. Friedman, M. Fukugita, J. E. Gunn, G. S. Hennessy, R. B. Hindsley, Ž. Ivezić, S. Kent, G. R. Knapp, R. Kron, P. Kunszt, D. Q. Lamb, R. F. Leger, D. C. Long, J. Loveday, R. H. Lupton, T. McKay, A. Meiksin, A. Merrelli, J. A. Munn, V. Narayanan, M. Newcomb, R. C. Nichol, R. Owen, J. Peoples, A. Pope, C. M. Rockosi, D. Schlegel, D. P. Schneider, R. Scoccimarro, R. K. Sheth, W. Siegmund, S. Smee, Y. Snir, A. Stebbins, C. Stoughton, M. SubbaRao, A. S. Szalay, I. Szapudi, M. Tegmark, D. L. Tucker, A. Uomoto, D. Vanden Berk, M. S. Vogeley, P. Waddell, B. Yanny, and D. G. York, "Galaxy Clustering in Early Sloan Digital Sky Survey Redshift Data," *Astrophysical Journal*, vol. 571, no. 1, pp. 172–190, May 2002. DOI: 10.1086/339893. arXiv: astro-ph/0106476 [astro-ph].

[43] M. Giavalisco and M. Dickinson, "Clustering Segregation with Ultraviolet Luminosity in Lyman Break Galaxies at z~3 and Its Implications," *Astrophysical Journal*, vol. 550, no. 1, pp. 177–194, Mar. 2001. DOI: 10.1086/319715. arXiv: astro-ph/0012249 [astro-ph].

[44] K. L. Adelberger, C. C. Steidel, M. Pettini, A. E. Shapley, N. A. Reddy, and D. K. Erb, "The Spatial Clustering of Star-forming Galaxies at Redshifts 1.4 ¡~z ¡~3.5," *Astrophysical Journal*, vol. 619, no. 2, pp. 697–713, Feb. 2005. DOI: 10.1086/426580. arXiv: astro-ph/0410165 [astro-ph].

[45] N. Kashikawa, M. Yoshida, K. Shimasaku, M. Nagashima, H. Yahagi, M. Ouchi, Y. Matsuda, M. A. Malkan, M. Doi, M. Iye, M. Ajiki, M. Akiyama, H. Ando, K. Aoki, H. Furusawa, T. Hayashino, F. Iwamuro, H. Karoji, N. Kobayashi, K. Kodaira, T. Kodama, Y. Komiyama, S. Miyazaki, Y. Mizumoto, T. Morokuma, K. Motohara, T. Murayama, T. Nagao, K. Nariai, K. Ohta, S. Okamura, T. Sasaki, Y. Sato, K. Sekiguchi, Y. Shioya, H. Tamura, Y. Taniguchi, M. Umemura, T. Yamada, and N. Yasuda, "Clustering of Lyman Break Galaxies at z = 4 and 5 in the Subaru Deep Field: Luminosity Dependence of the Correlation Function Slope," *Astrophysical Journal*, vol. 637, no. 2, pp. 631–647, Feb. 2006. DOI: 10.1086/498403. arXiv: astro-ph/0509564 [astro-ph].

[46] D. B. Sanders, B. T. Soifer, J. H. Elias, B. F. Madore, K. Matthews, G. Neugebauer, and N. Z. Scoville, "Ultraluminous Infrared Galaxies and the Origin of Quasars," *Astrophysical Journal*, vol. 325, p. 74, Feb. 1988. DOI: 10.1086/165983.

[47] E. F. Bell, T. Naab, D. H. McIntosh, R. S. Somerville, J. A. R. Caldwell, M. Barden, C. Wolf, H.-W. Rix, S. V. Beckwith, A. Borch, B. Häussler, C. Heymans, K. Jahnke, S. Jogee, S. Koposov, K. Meisenheimer, C. Y. Peng, S. F. Sanchez, and L. Wisotzki, "Dry Mergers in GEMS: The Dynamical Evolution of Massive Early-Type Galaxies," *Astrophysical Journal*, vol. 640, no. 1, pp. 241–251, Mar. 2006. DOI: 10.1086/499931. arXiv: astro-ph/0506425 [astro-ph].

[48] S. Jogee, S. H. Miller, K. Penner, R. E. Skelton, C. J. Conselice, R. S. Somerville, E. F. Bell, X. Z. Zheng, H.-W. Rix, A. R. Robaina, F. D. Barazza, M. Barden, A. Borch, S. V. W. Beckwith, J. A. R. Caldwell, C. Y. Peng, C. Heymans, D. H. McIntosh, B. Häußler, K. Jahnke, K. Meisenheimer, S. F. Sanchez, L. Wisotzki, C. Wolf, and C. Papovich, "History of Galaxy Interactions and Their Impact on Star Formation Over the Last 7 Gyr from GEMS," *Astrophysical Journal*, vol. 697, no. 2, pp. 1971–1992, Jun. 2009. DOI: 10.1088/0004-637X/697/2/1971. arXiv: 0903.3700 [astro-ph.CO].

[49] A. R. Robaina, E. F. Bell, R. E. Skelton, D. H. McIntosh, R. S. Somerville, X. Zheng, H.-W. Rix, D. Bacon, M. Balogh, F. D. Barazza, M. Barden, A. Böhm, J. A. R. Caldwell, A. Gallazzi, M. E. Gray, B. Häussler, C. Heymans, K. Jahnke, S. Jogee, E. van Kampen, K. Lane, K. Meisenheimer, C. Papovich, C. Y. Peng, S. F. Sánchez, R. Skibba, A. Taylor, L. Wisotzki, and C. Wolf, "Less Than 10 Percent of Star Formation in z ~0.6 Massive Galaxies is Triggered by Major Interactions," *Astrophysical Journal*, vol. 704, no. 1, pp. 324–340, Oct. 2009. DOI: 10.1088/0004-637X/704/1/324. arXiv: 0907.3728 [astro-ph.CO].

[50] L. Hernquist, "Tidal triggering of starbursts and nuclear activity in galaxies," *Nature*, vol. 340, no. 6236, pp. 687–691, Aug. 1989. DOI: 10.1038/340687a0.

[51] B. Moore, N. Katz, G. Lake, A. Dressler, and A. Oemler, "Galaxy harassment and the evolution of clusters of galaxies," *Nature*, vol. 379, no. 6566, pp. 613–616, Feb. 1996. DOI: 10.1038/379613a0. arXiv: astro-ph/9510034 [astro-ph].

[52] P. F. Hopkins, L. Hernquist, T. J. Cox, S. N. Dutta, and B. Rothberg, "Dissipation and Extra Light in Galactic Nuclei. I. Gas-Rich Merger Remnants," *Astrophysical Journal*, vol. 679, no. 1, pp. 156–181, May 2008. DOI: 10.1086/587544. arXiv: 0802.0508 [astro-ph].

[53] P. Di Matteo, F. Bournaud, M. Martig, F. Combes, A. .-L. Melchior, and B. Semelin, "On the frequency, intensity, and duration of starburst episodes triggered by galaxy interactions and mergers," *Astronomy and Astrophysics*, vol. 492, no. 1, pp. 31–49, Dec. 2008. DOI: 10.1051/0004-6361:200809480. arXiv: 0809.2592 [astro-ph].

[54] J. P. Stott, K. A. Pimbblet, A. C. Edge, G. P. Smith, and J. L. Wardlow, "The evolution of the red sequence slope in massive galaxy clusters," *Monthly Notices of the RAS*, vol. 394, no. 4, pp. 2098–2108, Apr. 2009. DOI: 10.1111/j.1365-2966.2009.14477.x. arXiv: 0901.1227 [astro-ph.CO].

[55] S. A. Stanford, P. R. Eisenhardt, and M. Dickinson, "The Evolution of Early-Type Galaxies in Distant Clusters," *Astrophysical Journal*, vol. 492, no. 2, pp. 461–479, Jan. 1998. DOI: 10.1086/305050. arXiv: astro-ph/9708037 [astro-ph].

[56] J. P. Blakeslee, M. Franx, M. Postman, P. Rosati, B. P. Holden, G. D. Illingworth, H. C. Ford, N. J. G. Cross, C. Gronwall, N. Benítez, R. J. Bouwens, T. J. Broadhurst, M. Clampin, R. Demarco, D. A. Golimowski, G. F. Hartig, L. Infante, A. R. Martel, G. K. Miley, F. Menanteau, G. R. Meurer, M. Sirianni, and R. L. White, "Advanced Camera for Surveys Photometry of the Cluster RDCS 1252.9-2927: The Color-Magnitude Relation at z = 1.24," *Astrophysical Journal, Letters*, vol. 596, no. 2, pp. L143–L146, Oct. 2003. DOI: 10.1086/379234. arXiv: astro-ph/0309036 [astro-ph].

[57] D. Thomas, C. Maraston, R. Bender, and C. Mendes de Oliveira, "The Epochs of Early-Type Galaxy Formation as a Function of Environment," *Astrophysical Journal*, vol. 621, no. 2, pp. 673–694, Mar. 2005. DOI: 10.1086/426932. arXiv: astro-ph/0410209 [astro-ph].

[58] P. R. M. Eisenhardt, M. Brodwin, A. H. Gonzalez, S. A. Stanford, D. Stern, P. Barmby, M. J. I. Brown, K. Dawson, A. Dey, M. Doi, A. Galametz, B. T. Jannuzi, C. S. Kochanek, J. Meyers, T. Morokuma, and L. A. Moustakas, "Clusters of Galaxies in the First Half of the Universe from the IRAC Shallow Survey," *Astrophysical Journal*, vol. 684, no. 2, pp. 905–932, Sep. 2008. DOI: 10.1086/590105. arXiv: 0804.4798 [astro-ph].

[59] C. L. Mancone, A. H. Gonzalez, M. Brodwin, S. A. Stanford, P. R. M. Eisenhardt, D. Stern, and C. Jones, "The Formation of Massive Cluster Galaxies," *Astrophysical Journal*, vol. 720, no. 1, pp. 284–298, Sep. 2010. DOI: 10.1088/0004-637X/720/1/284. arXiv: 1007.1454 [astro-ph.CO].

[60] P. Madau and M. Dickinson, "Cosmic Star-Formation History," *Annual Review of Astron and Astrophys*, vol. 52, pp. 415–486, Aug. 2014. DOI: 10.1146/annurev-astro-081811-125615. arXiv: 1403.0007 [astro-ph.CO].

[61] D. B. Sanders and I. F. Mirabel, "Luminous Infrared Galaxies," *Annual Review of Astron and Astrophys*, vol. 34, p. 749, Jan. 1996. DOI: 10.1146/annurev.astro.34.1.749.

[62] Ž. Ivezić, S. M. Kahn, J. A. Tyson, B. Abel, E. Acosta, R. Allsman, D. Alonso, Y. AlSayyad, S. F. Anderson, and J. e. a. Andrew, "LSST: From Science Drivers to Reference Design and Anticipated Data Products," *Astrophysical Journal*, vol. 873, no. 2, 111, p. 111, Mar. 2019. DOI: 10.3847/1538-4357/ab042c. arXiv: 0805.2366 [astro-ph].

[63] Y.-K. Chiang, R. Overzier, and K. Gebhardt, "Ancient Light from Young Cosmic Cities: Physical and Observational Signatures of Galaxy Proto-clusters," *Astrophysical Journal*, vol. 779, no. 2, 127, p. 127, Dec. 2013. DOI: 10.1088/0004-637X/779/2/127. arXiv: 1310.2938 [astro-ph.CO].

[64] O. Le Fèvre, L. A. M. Tasca, P. Cassata, B. Garilli, V. Le Brun, D. Maccagni, L. Pentericci, R. Thomas, E. Vanzella, G. Zamorani, E. Zucca, R. Amorin, S. Bardelli, P. Capak, L. Cassarà, M. Castellano, A. Cimatti, J. G. Cuby, O. Cucciati, S. de la Torre, A. Durkalec, A. Fontana, M. Giavalisco, A. Grazian, N. P. Hathi, O. Ilbert, B. C. Lemaux, C. Moreau, S. Paltani, B. Ribeiro, M. Salvato, D. Schaerer, M. Scodeggio, V. Sommariva, M. Talia, Y. Taniguchi, L. Tresse, D. Vergani, P. W. Wang, S. Charlot, T. Contini, S. Fotopoulou, C. López-Sanjuan, Y. Mellier, and N. Scoville, "The VIMOS Ultra-Deep Survey: ~10 000 galaxies with spectroscopic redshifts to study galaxy assembly at early epochs $2 < z \simeq 6$," *Astronomy and Astrophysics*, vol. 576, A79, A79, Apr. 2015. DOI: 10.1051/0004-6361/201423829. arXiv: 1403.3938 [astro-ph.CO].

[65] O. Cucciati, G. Zamorani, B. C. Lemaux, S. Bardelli, A. Cimatti, O. Le Fèvre, P. Cassata, B. Garilli, V. Le Brun, D. Maccagni, L. Pentericci, L. A. M. Tasca, R. Thomas, E. Vanzella, E. Zucca, R. Amorin, P. Capak, L. P. Cassarà, M. Castellano, J. G. Cuby, S. de la Torre, A. Durkalec, A. Fontana, M. Giavalisco, A. Grazian, N. P. Hathi, O. Ilbert, C. Moreau, S. Paltani, B. Ribeiro, M. Salvato, D. Schaerer, M. Scodeggio, V. Sommariva, M. Talia, Y. Taniguchi, L. Tresse, D. Vergani, P. W. Wang, S. Charlot, T. Contini, S. Fotopoulou, C. López-Sanjuan, Y. Mellier, and N. Scoville, "Discovery of a rich proto-cluster at z = 2.9 and associated diffuse cold gas in the VIMOS Ultra-Deep Survey (VUDS)," *Astronomy and Astrophysics*, vol. 570, A16, A16, Oct. 2014. DOI: 10.1051/0004-6361/201423811. arXiv: 1403.3691 [astro-ph.CO].

[66] B. C. Lemaux, O. Cucciati, L. A. M. Tasca, O. Le Fèvre, G. Zamorani, P. Cassata, B. Garilli, V. Le Brun, D. Maccagni, L. Pentericci, R. Thomas, E. Vanzella, E. Zucca, R. Amorín, S. Bardelli, P. Capak, L. P. Cassarà, M. Castellano, A. Cimatti, J. G. Cuby, S. de la Torre, A. Durkalec, A. Fontana, M. Giavalisco, A. Grazian, N. P. Hathi, O. Ilbert, C. Moreau, S. Paltani, B. Ribeiro, M. Salvato, D. Schaerer, M. Scodeggio, V. Sommariva, M. Talia, Y. Taniguchi, L. Tresse, D. Vergani, P. W. Wang, S. Charlot, T. Contini, S. Fotopoulou, R. R. Gal, D. D. Kocevski, C. López-Sanjuan, L. M. Lubin, Y. Mellier, T. Sadibekova, and N. Scoville, "VIMOS Ultra-Deep Survey (VUDS): Witnessing the assembly of a massive cluster at z ~3.3," *Astronomy and Astrophysics*, vol. 572, A41, A41, Dec. 2014. DOI: 10.1051/0004-6361/201423828. arXiv: 1403.4230 [astro-ph.CO].

[67] B. C. Lemaux, O. Le Fèvre, O. Cucciati, B. Ribeiro, L. A. M. Tasca, G. Zamorani, O. Ilbert, R. Thomas, S. Bardelli, P. Cassata, N. P. Hathi, J. Pforr, V. Smolčić, I. Delvecchio, M. Novak, S. Berta, H. J. McCracken, A. Koekemoer, R. Amorín, B. Garilli, D. Maccagni, D. Schaerer, and E. Zucca, "The VIMOS Ultra-Deep Survey: Emerging from the dark, a massive proto-cluster at z 4.57," *Astronomy and Astrophysics*, vol. 615, A77, A77, Jul. 2018. DOI: 10.1051/0004-6361/201730870. arXiv: 1703.10170 [astro-ph.GA].

[68] C. Diener, S. J. Lilly, C. Knobel, G. Zamorani, G. Lemson, P. Kampczyk, N. Scoville, C. M. Carollo, T. Contini, J. .-P. Kneib, O. Le Fevre, V. Mainieri, A. Renzini, M. Scodeggio, S. Bardelli, M. Bolzonella, A. Bongiorno, K. Caputi, O. Cucciati, S. de la Torre, L. de Ravel, P. Franzetti, B. Garilli, A. Iovino, K. Kovač, F. Lamareille, J. .-F. Le Borgne, V. Le Brun, C. Maier, M. Mignoli, R. Pello, Y. Peng, E. Perez Montero, V. Presotto, J. Silverman, M. Tanaka, L. Tasca, L. Tresse, D. Vergani, E. Zucca, R. Bordoloi, A. Cappi, A. Cimatti, G. Coppa, A. M. Koekemoer, C. López-Sanjuan, H. J. McCracken, M. Moresco, P. Nair, L. Pozzetti, and N. Welikala, "Proto-groups at 1.8 ¡ z ¡ 3 in the zCOSMOS-deep Sample," *Astrophysical Journal*, vol. 765, no. 2, 109, p. 109, Mar. 2013. DOI: 10.1088/0004-637X/765/2/109. arXiv: 1210.2723 [astro-ph.CO].

[69] S. J. Lilly, O. Le Fèvre, A. Renzini, G. Zamorani, M. Scodeggio, T. Contini, C. M. Carollo, G. Hasinger, J. .-P. Kneib, A. Iovino, V. Le Brun, C. Maier, V. Mainieri, M. Mignoli, J. Silverman, L. A. M. Tasca, M. Bolzonella, A. Bongiorno, D. Bottini, P. Capak, K. Caputi, A. Cimatti, O. Cucciati, E. Daddi, R. Feldmann, P. Franzetti, B. Garilli, L. Guzzo, O. Ilbert, P. Kampczyk, K. Kovac, F. Lamareille, A. Leauthaud, J. .-F. Le Borgne, H. J. McCracken, C. Marinoni, R. Pello, E. Ricciardelli, C. Scarlata, D. Vergani, D. B. Sanders, E. Schinnerer, N. Scoville, Y. Taniguchi, S. Arnouts, H. Aussel, S. Bardelli, M. Brusa, A. Cappi, P. Ciliegi, A. Finoguenov, S. Foucaud, A. Franceschini, C. Halliday, C. Impey, C. Knobel, A. Koekemoer, J. Kurk, D. Maccagni, S. Maddox, B. Marano, G. Marconi, B. Meneux, B. Mobasher, C. Moreau, J. A. Peacock, C. Porciani, L. Pozzetti, R. Scaramella, D. Schiminovich, P. Shopbell, I. Smail, D. Thompson, L. Tresse, G. Vettolani, A. Zanichelli, and E. Zucca, "zCOSMOS: A Large VLT/VIMOS Redshift Survey Covering 0 ¡ z ¡ 3 in the COSMOS Field," *Astrophysical Journal, Supplement*, vol. 172, no. 1, pp. 70–85, Sep. 2007. DOI: 10.1086/516589. arXiv: astro-ph/0612291 [astro-ph].

[70] S. J. Lilly, V. Le Brun, C. Maier, V. Mainieri, M. Mignoli, M. Scodeggio, G. Zamorani, M. Carollo, T. Contini, J.-P. Kneib, O. Le Fèvre, A. Renzini, S. Bardelli, M. Bolzonella, A. Bongiorno, K. Caputi, G. Coppa, O. Cucciati, S. de la Torre, L. de Ravel, P. Franzetti, B. Garilli, A. Iovino, P. Kampczyk, K. Kovac, C. Knobel, F. Lamareille, J.-F. Le Borgne, R. Pello, Y. Peng, E. Pérez-Montero, E. Ricciardelli, J. D. Silverman, M. Tanaka, L. Tasca, L. Tresse, D. Vergani, E. Zucca, O. Ilbert, M. Salvato, P. Oesch, U. Abbas, D. Bottini, P. Capak, A. Cappi, P. Cassata, A. Cimatti, M. Elvis, M. Fumana, L. Guzzo, G. Hasinger, A. Koekemoer, A. Leauthaud, D. Maccagni, C. Marinoni, H. McCracken, P. Memeo, B. Meneux, C. Porciani, L. Pozzetti, D. Sanders, R. Scaramella, C. Scarlata, N. Scoville, P. Shopbell, and Y. Taniguchi, "The zCOSMOS 10k-Bright Spectroscopic Sample," *Astrophysical Journal, Supplement*, vol. 184, no. 2, pp. 218–229, Oct. 2009. DOI: 10.1088/0067-0049/184/2/218.

[71] O. Cucciati, B. C. Lemaux, G. Zamorani, O. Le Fèvre, L. A. M. Tasca, N. P. Hathi, K. .-G. Lee, S. Bardelli, P. Cassata, B. Garilli, V. Le Brun, D. Maccagni, L. Pentericci, R. Thomas, E. Vanzella, E. Zucca, L. M. Lubin, R. Amorin, L. P. Cassarà, A. Cimatti, M. Talia, D. Vergani, A. Koekemoer, J. Pforr, and M. Salvato, "The progeny of a cosmic titan: a massive multi-component proto-supercluster in formation at z = 2.45 in VUDS," *Astronomy and Astrophysics*, vol. 619, A49, A49, Nov. 2018. DOI: 10.1051/0004-6361/201833655. arXiv: 1806.06073 [astro-ph.CO].

[72] J. Toshikawa, N. Kashikawa, K. Ota, T. Morokuma, T. Shibuya, M. Hayashi, T. Nagao, L. Jiang, M. A. Malkan, E. Egami, K. Shimasaku, K. Motohara, and Y. Ishizaki, "Discovery of a Protocluster at z ~6," *Astrophysical Journal*, vol. 750, no. 2, 137, p. 137, May 2012. DOI: 10.1088/0004-637X/750/2/137. arXiv: 1203.1326 [astro-ph.CO].

[73] J. Toshikawa, N. Kashikawa, R. Overzier, M. A. Malkan, H. Furusawa, S. Ishikawa, M. Onoue, K. Ota, M. Tanaka, Y. Niino, and H. Uchiyama, "A Systematic Survey of Protoclusters at $z \sim 3-6$ in the CFHTLS Deep Fields," *Astrophysical Journal*, vol. 826, no. 2, 114, p. 114, Aug. 2016. DOI: 10.3847/0004-637X/826/2/114. arXiv: 1605.01439 [astro-ph.GA].

[74] P. N. Best, M. S. Longair, and H. J. A. Roettgering, "HST, radio and infrared observations of 28 3CR radio galaxies at redshift $z \sim 1$ - II. Old stellar populations in central cluster galaxies," *Monthly Notices of the RAS*, vol. 295, no. 3, pp. 549–567, Apr. 1998. DOI: 10.1046/j.1365-8711.1998.01245.x. arXiv: astro-ph/9709195 [astro-ph].

[75] A. W. Zirm, M. Dickinson, and A. Dey, "Massive Elliptical Galaxies at High Redshift: NICMOS Imaging of z~1 Radio Galaxies," *Astrophysical Journal*, vol. 585, no. 1, pp. 90–111, Mar. 2003. DOI: 10.1086/346021. arXiv: astro-ph/0211469 [astro-ph].

[76] G. Miley and C. De Breuck, "Distant radio galaxies and their environments," *Astronomy and Astrophysicsr*, vol. 15, no. 2, pp. 67–144, Feb. 2008. DOI: 10.1007/s00159-007-0008-z. arXiv: 0802.2770 [astro-ph].

[77] C. Collet, N. P. H. Nesvadba, C. De Breuck, M. D. Lehnert, P. Best, J. J. Bryant, D. Dicken, H. Johnston, R. Hunstead, and D. Wylezalek, "Defying jet-gas alignment in two radio galaxies at z ~2 with extended light profiles: Similarities to brightest cluster galaxies," *Astronomy and Astrophysics*, vol. 579, A89, A89, Jul. 2015. DOI: 10.1051/0004-6361/201424544. arXiv: 1506.03725 [astro-ph.GA].

[78] S. M. Pascarelle, R. A. Windhorst, S. P. Driver, E. J. Ostrander, and W. C. Keel, "The Serendipitous Discovery of a Group or Cluster of Young Galaxies at z2.40 in Deep Hubble Space Telescope WFPC2 Images," *Astrophysical Journal, Letters*, vol. 456, p. L21, Jan. 1996. DOI: 10.1086/309852. arXiv: astro-ph/9512033 [astro-ph].

[79] O. Le Fevre, J. M. Deltorn, D. Crampton, and M. Dickinson, "Clustering around the Radio Galaxy MRC 0316-257 at Z = 3.14," *Astrophysical Journal, Letters*, vol. 471, p. L11, Nov. 1996. DOI: 10.1086/310319. arXiv: astro-ph/9609020 [astro-ph].

[80] L. Pentericci, J. D. Kurk, H. J. A. Röttgering, G. K. Miley, W. van Breugel, C. L. Carilli, H. Ford, T. Heckman, P. McCarthy, and A. Moorwood, "A search for clusters at high redshift. II. A proto cluster around a radio galaxy at z=2.16," *Astronomy and Astrophysics*, vol. 361, pp. L25–L28, Sep. 2000. arXiv: astro-ph/0008143 [astro-ph].

[81] J. D. Kurk, H. J. A. Röttgering, L. Pentericci, G. K. Miley, W. van Breugel, C. L. Carilli, H. Ford, T. Heckman, P. McCarthy, and A. Moorwood, "A Search for clusters at high redshift. I. Candidate Lyalpha emitters near 1138-262 at z=2.2," *Astronomy and Astrophysics*, vol. 358, pp. L1–L4, Jun. 2000. arXiv: astro-ph/0005058 [astro-ph].

[82] J. Kurk, B. Venemans, H. Röttgering, G. Miley, and L. Pentericci, "Proto-clusters Associated with Radio Galaxies from z=2 to z=4," in *Astrophysics and Space Science Library*, M. Plionis, Ed., ser. Astrophysics and Space Science Library, vol. 301, Jan. 2004, p. 141. DOI: . arXiv: astro-ph/0309675 [astro-ph].

[83] B. P. Venemans, J. D. Kurk, G. K. Miley, H. J. A. Röttgering, W. van Breugel, C. L. Carilli, C. De Breuck, H. Ford, T. Heckman, P. McCarthy, and L. Pentericci, "The Most Distant Structure of Galaxies Known: A Protocluster at z=4.1," *Astrophysical Journal, Letters*, vol. 569, no. 1, pp. L11–L14, Apr. 2002. DOI: 10.1086/340563. arXiv: astro-ph/0203249 [astro-ph].

[84] B. P. Venemans, H. J. A. Röttgering, R. A. Overzier, G. K. Miley, C. De Breuck, J. D. Kurk, W. van Breugel, C. L. Carilli, H. Ford, T. Heckman, P. McCarthy, and L. Pentericci, "Discovery of six Lyα emitters near a radio galaxy at z $\sim$ 5.2," *Astronomy and Astrophysics*, vol. 424, pp. L17–L20, Sep. 2004. DOI: 10.1051/0004-6361:200400041. arXiv: astro-ph/0408520 [astro-ph].

[85] B. P. Venemans, H. J. A. Röttgering, G. K. Miley, J. D. Kurk, C. De Breuck, R. A. Overzier, W. J. M. van Breugel, C. L. Carilli, H. Ford, T. Heckman, L. Pentericci, and P. McCarthy, "Properties of Lyα emitters around the radio galaxy MRC 0316 257," *Astronomy and Astrophysics*, vol. 431, no. 3, pp. 793–812, Mar. 2005. DOI: 10.1051/0004-6361:20042038. arXiv: astro-ph/0501259 [astro-ph].

[86] B. P. Venemans, H. J. A. Röttgering, G. K. Miley, W. J. M. van Breugel, C. de Breuck, J. D. Kurk, L. Pentericci, S. A. Stanford, R. A. Overzier, S. Croft, and H. Ford, "Protoclusters associated with z ¿ 2 radio galaxies . I. Characteristics of high redshift protoclusters," *Astronomy and Astrophysics*, vol. 461, no. 3, pp. 823–845, Jan. 2007. DOI: 10.1051/0004-6361:20053941. arXiv: astro-ph/0610567 [astro-ph].

[87] M. Chiaberge, A. Capetti, F. D. Macchetto, P. Rosati, P. Tozzi, and G. R. Tremblay, "Three Candidate Clusters of Galaxies at Redshift ~1.8: The "Missing Link" Between Protoclusters and Local Clusters?" *Astrophysical Journal, Letters*, vol. 710, no. 2, pp. L107–L110, Feb. 2010. DOI: 10.1088/2041-8205/710/2/L107. arXiv: 1001.2232 [astro-ph.CO].

[88] E. Kuiper, N. A. Hatch, B. P. Venemans, G. K. Miley, H. J. A. Röttgering, J. D. Kurk, R. A. Overzier, L. Pentericci, J. Bland-Hawthorn, and J. Cepa, "Discovery of a high-z protocluster with tunable filters: the case of 6C0140+326 at z= 4.4," *Monthly Notices of the RAS*, vol. 417, no. 2, pp. 1088–1097, Oct. 2011. DOI: 10.1111/j.1365-2966.2011.19324.x. arXiv: 1106.5495 [astro-ph.CO].

[89] N. A. Hatch, C. De Breuck, A. Galametz, G. K. Miley, R. A. Overzier, H. J. A. Röttgering, M. Doherty, T. Kodama, J. D. Kurk, N. Seymour, B. P. Venemans, J. Vernet, and A. W. Zirm, "Galaxy protocluster candidates around z$\sim$ 2.4 radio galaxies," *Monthly Notices of the RAS*, vol. 410, no. 3, pp. 1537–1549, Jan. 2011. DOI: 10.1111/j.1365-2966.2010.17538.x. arXiv: 1008.4588 [astro-ph.CO].

[90] K. Mawatari, T. Yamada, Y. Nakamura, T. Hayashino, and Y. Matsuda, "Characterization of the Distribution of the Lyα Emitters in the 53w002 Field at z = 2.4," *Astrophysical Journal*, vol. 759, no. 2, 133, p. 133, Nov. 2012. DOI: 10.1088/0004-637X/759/2/133. arXiv: 1209.1253 [astro-ph.CO].

[91] M. Hayashi, T. Kodama, K.-i. Tadaki, Y. Koyama, and I. Tanaka, "A Starbursting Proto-cluster in Making Associated with a Radio Galaxy at z = 2.53 Discovered by Hα Imaging," *Astrophysical Journal*, vol. 757, no. 1, 15, p. 15, Sep. 2012. DOI: 10.1088/0004-637X/757/1/15. arXiv: 1207.2614 [astro-ph.CO].

[92] D. Wylezalek, A. Galametz, D. Stern, J. Vernet, C. De Breuck, N. Seymour, M. Brodwin, P. R. M. Eisenhardt, A. H. Gonzalez, N. Hatch, M. Jarvis, A. Rettura, S. A. Stanford, and J. A. Stevens, "Galaxy Clusters around Radio-loud Active Galactic Nuclei at 1.3 ¡ z ¡ 3.2 as Seen by Spitzer," *Astrophysical Journal*, vol. 769, no. 1, 79, p. 79, May 2013. DOI: 10.1088/0004-637X/769/1/79. arXiv: 1304.0770 [astro-ph.CO].

[93] E. A. Cooke, N. A. Hatch, S. I. Muldrew, E. E. Rigby, and J. D. Kurk, "A z = 2.5 protocluster associated with the radio galaxy MRC 2104-242: star formation and differing mass functions in dense environments," *Monthly Notices of the RAS*, vol. 440, no. 4, pp. 3262–3274, Jun. 2014. DOI: 10.1093/mnras/stu522. arXiv: 1403.4259 [astro-ph.GA].

[94] Y. Matsuda, T. Yamada, T. Hayashino, R. Yamauchi, Y. Nakamura, N. Morimoto, M. Ouchi, Y. Ono, M. Umemura, and M. Mori, "Diffuse Lyα haloes around Lyα emitters at z=3: do dark matter distributions determine the Lyα spatial extents?" *Monthly Notices of the RAS*, vol. 425, no. 2, pp. 878–883, Sep. 2012. DOI: 10.1111/j.1365-2966.2012.21143.x. arXiv: 1204.4934 [astro-ph.CO].

[95] T. Bădescu, Y. Yang, F. Bertoldi, A. Zabludoff, A. Karim, and B. Magnelli, "Discovery of a Protocluster Associated with a Lyα Blob Pair at z = 2.3," *Astrophysical Journal*, vol. 845, no. 2, 172, p. 172, Aug. 2017. DOI: 10.3847/1538-4357/aa8220. arXiv: 1708.00447 [astro-ph.GA].

[96] K. Shi, Y. Huang, K.-S. Lee, J. Toshikawa, K. N. Bowen, N. Malavasi, B. C. Lemaux, O. Cucciati, O. Le Fevre, and A. Dey, "How Do Galaxies Trace a Large-scale Structure? A Case Study around a Massive Protocluster at Z = 3.13," *Astrophysical Journal*, vol. 879, no. 1, 9, p. 9, Jul. 2019. DOI: 10.3847/1538-4357/ab2118. arXiv: 1905.06337 [astro-ph.GA].

[97] I. Smail, R. J. Ivison, and A. W. Blain, "A Deep Sub-millimeter Survey of Lensing Clusters: A New Window on Galaxy Formation and Evolution," *Astrophysical Journal, Letters*, vol. 490, no. 1, pp. L5–L8, Nov. 1997. DOI: 10.1086/311017. arXiv: astro-ph/9708135 [astro-ph].

[98] A. J. Barger, L. L. Cowie, D. B. Sanders, E. Fulton, Y. Taniguchi, Y. Sato, K. Kawara, and H. Okuda, "Submillimetre-wavelength detection of dusty star-forming galaxies at high redshift," *Nature*, vol. 394, no. 6690, pp. 248–251, Jul. 1998. DOI: 10.1038/28338. arXiv: astro-ph/9806317 [astro-ph].

[99] D. H. Hughes, S. Serjeant, J. Dunlop, M. Rowan-Robinson, A. Blain, R. G. Mann, R. Ivison, J. Peacock, A. Efstathiou, W. Gear, S. Oliver, A. Lawrence, M. Longair, P. Goldschmidt, and T. Jenness, "High-redshift star formation in the Hubble Deep Field revealed by a submillimetre-wavelength survey," *Nature*, vol. 394, no. 6690, pp. 241–247, Jul. 1998. DOI: 10.1038/28328. arXiv: astro-ph/9806297 [astro-ph].

[100] S. Eales, S. Lilly, W. Gear, L. Dunne, J. R. Bond, F. Hammer, O. Le Fèvre, and D. Crampton, "The Canada-UK Deep Submillimeter Survey: First Submillimeter Images, the Source Counts, and Resolution of the Background," *Astrophysical Journal*, vol. 515, no. 2, pp. 518–524, Apr. 1999. DOI: 10.1086/307069. arXiv: astro-ph/9808040 [astro-ph].

[101] E. Hubble and M. L. Humason, "The Velocity-Distance Relation among Extra-Galactic Nebulae," *Astrophysical Journal*, vol. 74, p. 43, Jul. 1931. DOI: 10.1086/143323.

[102] A. Dressler, "Galaxy morphology in rich clusters: implications for the formation and evolution of galaxies.," *Astrophysical Journal*, vol. 236, pp. 351–365, Mar. 1980. DOI: 10.1086/157753.

[103] M. V. Costa-Duarte, L. Sodré, and F. Durret, "Stellar populations in superclusters of galaxies," *Monthly Notices of the RAS*, vol. 428, no. 1, pp. 906–911, Jan. 2013. DOI: 10.1093/mnras/sts088. arXiv: 1210.0455 [astro-ph.CO].

[104] H. Butcher and J. Oemler A., "The evolution of galaxies in clusters. II. The galaxy content of nearby clusters.," *Astrophysical Journal*, vol. 226, pp. 559–565, Dec. 1978. DOI: 10.1086/156640.

[105] W. J. Couch, R. S. Ellis, R. M. Sharples, and I. Smail, "Morphological Studies of the Galaxy Populations in Distant "Butcher-Oemler" Clusters with HST. I. AC 114 at Z = 0.31 and Abell 370 at Z = 0.37," *Astrophysical Journal*, vol. 430, p. 121, Jul. 1994. DOI: 10.1086/174387.

[106] G. D. Wirth, D. C. Koo, and R. G. Kron, "Hubble Space Telescope Observations of the Distant Cluster CL 0016+16: Quantitative Morphology of Confirmed Cluster Members," *Astrophysical Journal, Letters*, vol. 435, p. L105, Nov. 1994. DOI: 10.1086/187605. arXiv: astro-ph/9409037 [astro-ph].

[107] A. Dressler and J. E. Gunn, "Spectroscopy of galaxies in distant clusters. II. The population of the 3C 295 cluster.," *Astrophysical Journal*, vol. 270, pp. 7–19, Jul. 1983. DOI: 10.1086/161093.

[108] Y. Koyama, T. Kodama, K.-i. Tadaki, M. Hayashi, M. Tanaka, I. Smail, I. Tanaka, and J. Kurk, "Massive starburst galaxies in a z = 2.16 proto-cluster unveiled by panoramic Hα mapping," *Monthly Notices of the RAS*, vol. 428, no. 2, pp. 1551–1564, Jan. 2013. DOI: 10.1093/mnras/sts133. arXiv: 1210.0972 [astro-ph.CO].

[109] B. C. Lemaux, O. Cucciati, O. Le Fèvre, G. Zamorani, L. M. Lubin, N. Hathi, O. Ilbert, D. Pelliccia, R. Amorín, S. Bardelli, P. Cassata, R. R. Gal, B. Garilli, L. Guaita, M. Giavalisco, D. Hung, A. Koekemoer, D. Maccagni, L. Pentericci, B. Ribeiro, D. Schaerer, L. Shen, M. Talia, A. R. Tomczak, E. Vanzella, D. Vergani, and E. Zucca, "The VIMOS Ultra Deep Survey: The Reversal of the Star Formation Rate – Density Relation at $2 < z < 5$," *arXiv e-prints*, arXiv:2009.03324, arXiv:2009.03324, Sep. 2020. arXiv: 2009.03324 [astro-ph.GA].

[110] J. Kennicutt Robert C., "Star Formation in Galaxies Along the Hubble Sequence," *Annual Review of Astron and Astrophys*, vol. 36, pp. 189–232, Jan. 1998. DOI: 10.1146/annurev.astro.36.1.189. arXiv: astro-ph/9807187 [astro-ph].

[111] M. Dijkstra, "Lyα Emitting Galaxies as a Probe of Reionisation," *Publications of the Astron. Soc. of Australia*, vol. 31, e040, e040, Oct. 2014. DOI: 10.1017/pasa.2014.33. arXiv: 1406.7292 [astro-ph.CO].

[112] L. L. Cowie and E. M. Hu, "High-z Lyalpha Emitters. I. A Blank-Field Search for Objects near Redshift Z = 3.4 in and around the Hubble Deep Field and the Hawaii Deep Field SSA 22," *Astronomical Journal*, vol. 115, no. 4, pp. 1319–1328, Apr. 1998. DOI: 10.1086/300309. arXiv: astro-ph/9801003 [astro-ph].

[113] C. Gronwall, R. Ciardullo, T. Hickey, E. Gawiser, J. J. Feldmeier, P. G. van Dokkum, C. M. Urry, D. Herrera, B. D. Lehmer, L. Infante, A. Orsi, D. Marchesini, G. A. Blanc, H. Francke, P. Lira, and E. Treister, "Lyα Emission-Line Galaxies at z = 3.1 in the Extended Chandra Deep Field-South," *Astrophysical Journal*, vol. 667, no. 1, pp. 79–91, Sep. 2007. DOI: 10.1086/520324. arXiv: 0705.3917 [astro-ph].

[114] K. K. Nilsson, G. Östlin, P. Møller, O. Möller-Nilsson, C. Tapken, W. Freudling, and J. P. U. Fynbo, "The nature of $z \sim 2.3$ Lyman-α emitters," *Astronomy and Astrophysics*, vol. 529, A9, A9, May 2011. DOI: 10.1051/0004-6361/201015606. arXiv: 1009.0007 [astro-ph.CO].

[115] M. Ouchi, K. Shimasaku, M. Akiyama, C. Simpson, T. Saito, Y. Ueda, H. Furusawa, K. Sekiguchi, T. Yamada, T. Kodama, N. Kashikawa, S. Okamura, M. Iye, T. Takata, M. Yoshida, and M. Yoshida, "The Subaru/XMM-Newton Deep Survey (SXDS). IV. Evolution of Lyα Emitters from z = 3.1 to 5.7 in the 1 deg^2 Field: Luminosity Functions and AGN," *Astrophysical Journal, Supplement*, vol. 176, no. 2, pp. 301–330, Jun. 2008. DOI: 10.1086/527673. arXiv: 0707.3161 [astro-ph].

[116] J. E. Rhoads, S. Malhotra, A. Dey, D. Stern, H. Spinrad, and B. T. Jannuzi, "First Results from the Large-Area Lyman Alpha Survey," *Astrophysical Journal, Letters*, vol. 545, no. 2, pp. L85–L88, Dec. 2000. DOI: 10.1086/317874. arXiv: astro-ph/0003465 [astro-ph].

[117] A. E. Shapley, C. C. Steidel, M. Pettini, and K. L. Adelberger, "Rest-Frame Ultraviolet Spectra of z~3 Lyman Break Galaxies," *Astrophysical Journal*, vol. 588, no. 1, pp. 65–89, May 2003. DOI: 10.1086/373922. arXiv: astro-ph/0301230 [astro-ph].

[118] K. Nakajima, M. Ouchi, K. Shimasaku, Y. Ono, J. C. Lee, S. Foucaud, C. Ly, D. A. Dale, S. Salim, R. Finn, O. Almaini, and S. Okamura, "Average Metallicity and Star Formation Rate of Lyα Emitters Probed by a Triple Narrowband Survey," *Astrophysical Journal*, vol. 745, no. 1, 12, p. 12, Jan. 2012. DOI: 10.1088/0004-637X/745/1/12. arXiv: 1105.2824 [astro-ph.CO].

[119] R. Ciardullo, C. Gronwall, J. J. Adams, G. A. Blanc, K. Gebhardt, S. L. Finkelstein, S. Jogee, G. J. Hill, N. Drory, U. Hopp, D. P. Schneider, G. R. Zeimann, and G. B. Dalton, "The HETDEX Pilot Survey. IV. The Evolution of [O II] Emitting Galaxies from $z \sim 0.5$ to $z \sim 0$," *Astrophysical Journal*, vol. 769, 83, p. 83, May 2013. DOI: 10.1088/0004-637X/769/1/83. arXiv: 1304.5537.

[120] M. Ouchi, Y. Ono, and T. Shibuya, "Observations of the Lyman-α Universe," *Annual Review of Astron and Astrophys*, vol. 58, pp. 617–659, Aug. 2020. DOI: 10.1146/annurev-astro-032620-021859. arXiv: 2012.07960 [astro-ph.GA].

[121] A. Zitrin, I. Labbé, S. Belli, R. Bouwens, R. S. Ellis, G. Roberts-Borsani, D. P. Stark, P. A. Oesch, and R. Smit, "Lymanα Emission from a Luminous z = 8.68 Galaxy: Implications for Galaxies as Tracers of Cosmic Reionization," *Astrophysical Journal, Letters*, vol. 810, no. 1, L12, p. L12, Sep. 2015. DOI: 10.1088/2041-8205/810/1/L12. arXiv: 1507.02679 [astro-ph.GA].

[122] W. Hu, J. Wang, Z.-Y. Zheng, S. Malhotra, J. E. Rhoads, L. Infante, L. F. Barrientos, H. Yang, C. Jiang, W. Kang, L. A. Perez, I. Wold, P. Hibon, L. Jiang, A. A. Khostovan, F. Valdes, A. R. Walker, G. Galaz, A. Coughlin, S. Harish, X. Kong, J. Pharo, and X. Zheng, "The Lyα Luminosity Function and Cosmic Reionization at z $\sim$ 7.0: A Tale of Two LAGER Fields," *Astrophysical Journal*, vol. 886, no. 2, 90, p. 90, Dec. 2019. DOI: 10.3847/1538-4357/ab4cf4. arXiv: 1903.09046 [astro-ph.GA].

[123] E. Gawiser, P. G. van Dokkum, C. Gronwall, R. Ciardullo, G. A. Blanc, F. J. Castander, J. Feldmeier, H. Francke, M. Franx, L. Haberzettl, D. Herrera, T. Hickey, L. Infante, P. Lira, J. Maza, R. Quadri, A. Richardson, K. Schawinski, M. Schirmer, E. N. Taylor, E. Treister, C. M. Urry, and S. N. Virani, "The Physical Nature of Lyα-emitting Galaxies at z=3.1," *Astrophysical Journal, Letters*, vol. 642, no. 1, pp. L13–L16, May 2006. DOI: 10.1086/504467. arXiv: astro-ph/0603244 [astro-ph].

[124] L. Guaita, V. Acquaviva, N. Padilla, E. Gawiser, N. A. Bond, R. Ciardullo, E. Treister, P. Kurczynski, C. Gronwall, P. Lira, and K. Schawinski, "Lyα-emitting Galaxies at z = 2.1: Stellar Masses, Dust, and Star Formation Histories from Spectral Energy Distribution Fitting," *Astrophysical Journal*, vol. 733, no. 2, 114, p. 114, Jun. 2011. DOI: 10.1088/0004-637X/733/2/114. arXiv: 1101.3017 [astro-ph.CO].

[125] K. Shi, K.-S. Lee, A. Dey, Y. Huang, N. Malavasi, C.-L. Hung, H. Inami, M. Ashby, K. Duncan, R. Xue, N. Reddy, S. Hong, B. T. Jannuzi, M. C. Cooper, A. H. Gonzalez, H. J. A. Röttgering, P. N. Best, and C. Tasse, "A Census of Galaxy Constituents in a Coma Progenitor Observed at z ¿ 3," *Astrophysical Journal*, vol. 871, no. 1, 83, p. 83, Jan. 2019. DOI: 10.3847/1538-4357/aaf85d. arXiv: 1808.07065 [astro-ph.GA].

[126] S. Malhotra, J. E. Rhoads, S. L. Finkelstein, N. Hathi, K. Nilsson, E. McLinden, and N. Pirzkal, "Sizing up Lyα and Lyman Break Galaxies," *Astrophysical Journal, Letters*, vol. 750, no. 2, L36, p. L36, May 2012. DOI: 10.1088/2041-8205/750/2/L36. arXiv: 1106.2816 [astro-ph.CO].

[127] A. Paulino-Afonso, D. Sobral, B. Ribeiro, J. Matthee, S. Santos, J. Calhau, A. Forshaw, A. Johnson, J. Merrick, S. Pérez, and O. Sheldon, "On the UV compactness and morphologies of typical Lyman α emitters from z $\sim$ 2 to z $\sim$ 6," *Monthly Notices of the RAS*, vol. 476, no. 4, pp. 5479–5501, Jun. 2018. DOI: 10.1093/mnras/sty281. arXiv: 1709.04470 [astro-ph.GA].

[128] T. Shibuya, M. Ouchi, Y. Harikane, and K. Nakajima, "Morphologies of $\sim$190,000 Galaxies at z = 0-10 Revealed with HST Legacy Data. III. Continuum Profile and Size Evolution of Lyα Emitters," *Astrophysical Journal*, vol. 871, no. 2, 164, p. 164, Feb. 2019. DOI: 10.3847/1538-4357/aaf64b. arXiv: 1809.00765 [astro-ph.GA].

[129] L. Wisotzki, R. Bacon, J. Blaizot, J. Brinchmann, E. C. Herenz, J. Schaye, N. Bouché, S. Cantalupo, T. Contini, C. M. Carollo, J. Caruana, J. .-B. Courbot, E. Emsellem, S. Kamann, J. Kerutt, F. Leclercq, S. J. Lilly, V. Patrício, C. Sandin, M. Steinmetz, L. A. Straka, T. Urrutia, A. Verhamme, P. M. Weilbacher, and M. Wendt, "Extended Lyman α haloes around individual high-redshift galaxies revealed by MUSE," *Astronomy and Astrophysics*, vol. 587, A98, A98, Mar. 2016. DOI: 10.1051/0004-6361/201527384. arXiv: 1509.05143 [astro-ph.GA].

[130] F. Leclercq, R. Bacon, L. Wisotzki, P. Mitchell, T. Garel, A. Verhamme, J. Blaizot, T. Hashimoto, E. C. Herenz, S. Conseil, S. Cantalupo, H. Inami, T. Contini, J. Richard, M. Maseda, J. Schaye, R. A. Marino, M. Akhlaghi, J. Brinchmann, and M. Carollo, "The MUSE Hubble Ultra Deep Field Survey. VIII. Extended Lyman-α haloes around high-z star-forming galaxies," *Astronomy and Astrophysics*, vol. 608, A8, A8, Nov. 2017. DOI: 10.1051/0004-6361/201731480. arXiv: 1710.10271.

[131] T. Shibuya, M. Ouchi, K. Nakajima, S. Yuma, T. Hashimoto, K. Shimasaku, M. Mori, and M. Umemura, "What is the Physical Origin of Strong Lyα Emission? I. Demographics of Lyα Emitter Structures," *Astrophysical Journal*, vol. 785, no. 1, 64, p. 64, Apr. 2014. DOI: 10.1088/0004-637X/785/1/64. arXiv: 1401.1209 [astro-ph.CO].

[132] L. Jiang, E. Egami, X. Fan, R. A. Windhorst, S. H. Cohen, R. Davé, K. Finlator, N. Kashikawa, M. Mechtley, M. Ouchi, and K. Shimasaku, "Physical Properties of Spectroscopically Confirmed Galaxies at $z \geq 6$. II. Morphology of the Rest-frame UV Continuum and Lyα Emission," *Astrophysical Journal*, vol. 773, no. 2, 153, p. 153, Aug. 2013. DOI: 10.1088/0004-637X/773/2/153. arXiv: 1303.0027 [astro-ph.CO].

[133] B. C. Lemaux, S. Fuller, M. Bradač, L. Pentericci, A. Hoag, V. Strait, T. Treu, C. Alvarez, P. Bolan, P. J. Gandhi, K. .-H. Huang, T. Jones, C. Mason, D. Pelliccia, B. Ribeiro, R. E. Ryan, K. B. Schmidt, E. Vanzella, Y. Khusanova, O. Le Fèvre, L. Guaita, N. P. Hathi, A. Koekemoer, and J. Pforr, "The size and pervasiveness of Ly α-UV spatial offsets in star-forming galaxies at z $\sim$ 6," *Monthly Notices of the RAS*, vol. 504, no. 3, pp. 3662–3681, Jul. 2021. DOI: 10.1093/mnras/stab924. arXiv: 2007.01310 [astro-ph.GA].

[134] E. Gawiser, H. Francke, K. Lai, K. Schawinski, C. Gronwall, R. Ciardullo, R. Quadri, A. Orsi, L. F. Barrientos, G. A. Blanc, G. Fazio, J. J. Feldmeier, J.-s. Huang, L. Infante, P. Lira, N. Padilla, E. N. Taylor, E. Treister, C. M. Urry, P. G. van Dokkum, and S. N. Virani, "Lyα-Emitting Galaxies at z = 3.1: L* Progenitors Experiencing Rapid Star Formation," *Astrophysical Journal*, vol. 671, no. 1, pp. 278–284, Dec. 2007. DOI: 10.1086/522955. arXiv: 0710.2697 [astro-ph].

[135] H. Kusakabe, K. Shimasaku, M. Ouchi, K. Nakajima, R. Goto, T. Hashimoto, A. Konno, Y. Harikane, J. D. Silverman, and P. L. Capak, "The stellar mass, star formation rate and dark matter halo properties of LAEs at z $\sim$ 2," *Publications of the ASJ*, vol. 70, no. 1, 4, p. 4, Jan. 2018. DOI: 10.1093/pasj/psx148. arXiv: 1707.09373 [astro-ph.GA].

[136] M. Ouchi, Y. Harikane, T. Shibuya, K. Shimasaku, Y. Taniguchi, A. Konno, M. Kobayashi, M. Kajisawa, T. Nagao, Y. Ono, A. K. Inoue, M. Umemura, M. Mori, K. Hasegawa, R. Higuchi, Y. Komiyama, Y. Matsuda, K. Nakajima, T. Saito, and S.-Y. Wang, "Systematic Identification of LAEs for Visible Exploration and Reionization Research Using Subaru HSC (SILVERRUSH). I. Program strategy and clustering properties of $\sim$2000 Lyα emitters at z = 6-7 over the 0.3-0.5 Gpc^2 survey area," *Publications of the ASJ*, vol. 70, S13, S13, Jan. 2018. DOI: 10.1093/pasj/psx074. arXiv: 1704.07455 [astro-ph.GA].

[137] M. Ouchi, K. Shimasaku, H. Furusawa, T. Saito, M. Yoshida, M. Akiyama, Y. Ono, T. Yamada, K. Ota, N. Kashikawa, M. Iye, T. Kodama, S. Okamura, C. Simpson, and M. Yoshida, "Statistics of 207 Lyα Emitters at a Redshift Near 7: Constraints on Reionization and Galaxy Formation Models," *Astrophysical Journal*, vol. 723, no. 1, pp. 869–894, Nov. 2010. DOI: 10.1088/0004-637X/723/1/869. arXiv: 1007.2961 [astro-ph.CO].

[138] Y. Matsuda, T. Yamada, T. Hayashino, H. Tamura, R. Yamauchi, M. Ajiki, S. S. Fujita, T. Murayama, T. Nagao, K. Ohta, S. Okamura, M. Ouchi, K. Shimasaku, Y. Shioya, and Y. Taniguchi, "A Subaru Search for Lyα Blobs in and around the Protocluster Region At Redshift z = 3.1," *Astronomical Journal*, vol. 128, no. 2, pp. 569–584, Aug. 2004. DOI: 10.1086/422020. arXiv: astro-ph/0405221 [astro-ph].

[139] A. Dey, K.-S. Lee, N. Reddy, M. Cooper, H. Inami, S. Hong, A. H. Gonzalez, and B. T. Jannuzi, "Spectroscopic Confirmation of a Protocluster at z $\approx$ 3.786," *Astrophysical Journal*, vol. 823, no. 1, 11, p. 11, May 2016. DOI: 10.3847/0004-637X/823/1/11. arXiv: 1604.08627 [astro-ph.GA].

[140] S. I. Muldrew, N. A. Hatch, and E. A. Cooke, "What are protoclusters? - Defining high-redshift galaxy clusters and protoclusters," *Monthly Notices of the RAS*, vol. 452, no. 3, pp. 2528–2539, Sep. 2015. DOI: 10.1093/mnras/stv1449. arXiv: 1506.08835 [astro-ph.CO].

[141] K.-S. Lee, A. Dey, S. Hong, N. Reddy, C. Wilson, B. T. Jannuzi, H. Inami, and A. H. Gonzalez, "Discovery of a Very Large Structure at z = 3.78," *Astrophysical Journal*, vol. 796, no. 2, 126, p. 126, Dec. 2014. DOI: 10.1088/0004-637X/796/2/126. arXiv: 1405.2620 [astro-ph.CO].

[142] K. M. Ferrière, "The interstellar environment of our galaxy," *Reviews of Modern Physics*, vol. 73, no. 4, pp. 1031–1066, Oct. 2001. DOI: 10.1103/RevModPhys.73.1031. arXiv: astro-ph/0106359 [astro-ph].

[143] J. K. Werk, J. X. Prochaska, C. Thom, J. Tumlinson, T. M. Tripp, J. M. O'Meara, and M. S. Peeples, "The COS-Halos Survey: An Empirical Description of Metal-line Absorption in the Low-redshift Circumgalactic Medium," *Astrophysical Journal, Supplement*, vol. 204, no. 2, 17, p. 17, Feb. 2013. DOI: 10.1088/0067-0049/204/2/17. arXiv: 1212.0558 [astro-ph.CO].

[144] C. L. Carilli and S. Rawlings, "Motivation, key science projects, standards and assumptions," *New Astronomy Review*, vol. 48, no. 11-12, pp. 979–984, Dec. 2004. DOI: 10.1016/j.newar.2004.09.001. arXiv: astro-ph/0409274 [astro-ph].

[145] C. C. Steidel, D. K. Erb, A. E. Shapley, M. Pettini, N. Reddy, M. Bogosavljević, G. C. Rudie, and O. Rakic, "The Structure and Kinematics of the Circumgalactic Medium from Far-ultraviolet Spectra of z ~= 2-3 Galaxies," *Astrophysical Journal*, vol. 717, no. 1, pp. 289–322, Jul. 2010. DOI: 10.1088/0004-637X/717/1/289. arXiv: 1003.0679 [astro-ph.CO].

[146] J. Tumlinson, C. Thom, J. K. Werk, J. X. Prochaska, T. M. Tripp, N. Katz, R. Davé, B. D. Oppenheimer, J. D. Meiring, A. B. Ford, J. M. O'Meara, M. S. Peeples, K. R. Sembach, and D. H. Weinberg, "The COS-Halos Survey: Rationale, Design, and a Census of Circumgalactic Neutral Hydrogen," *Astrophysical Journal*, vol. 777, no. 1, 59, p. 59, Nov. 2013. DOI: 10.1088/0004-637X/777/1/59. arXiv: 1309.6317 [astro-ph.CO].

[147] Z. Zheng, R. Cen, D. Weinberg, H. Trac, and J. Miralda-Escudé, "Extended Lyα Emission around Star-forming Galaxies," *Astrophysical Journal*, vol. 739, no. 2, 62, p. 62, Oct. 2011. DOI: 10.1088/0004-637X/739/2/62. arXiv: 1010.3017 [astro-ph.CO].

[148] M. Dijkstra and R. Kramer, "Line transfer through clumpy, large-scale outflows: Ly α absorption and haloes around star-forming galaxies," *Monthly Notices of the RAS*, vol. 424, no. 3, pp. 1672–1693, Aug. 2012. DOI: 10.1111/j.1365-2966.2012.21131.x. arXiv: 1203.3803 [astro-ph.CO].

[149] A. Verhamme, Y. Dubois, J. Blaizot, T. Garel, R. Bacon, J. Devriendt, B. Guiderdoni, and A. Slyz, "Lyman-α emission properties of simulated galaxies: interstellar medium structure and inclination effects," *Astronomy and Astrophysics*, vol. 546, A111, A111, Oct. 2012. DOI: 10.1051/0004-6361/201218783. arXiv: 1208.4781 [astro-ph.CO].

[150] E. Lake, Z. Zheng, R. Cen, R. Sadoun, R. Momose, and M. Ouchi, "On the Diffuse Lyα Halo around Lyα Emitting Galaxies," *Astrophysical Journal*, vol. 806, no. 1, 46, p. 46, Jun. 2015. DOI: 10.1088/0004-637X/806/1/46. arXiv: 1502.01349 [astro-ph.CO].

[151] R. J. Bouwens, G. D. Illingworth, P. A. Oesch, M. Trenti, I. Labbé, M. Franx, M. Stiavelli, C. M. Carollo, P. van Dokkum, and D. Magee, "Lower-luminosity Galaxies Could Reionize the Universe: Very Steep Faint-end Slopes to the UV Luminosity Functions at z ¿= 5-8 from the HUDF09 WFC3/IR Observations," *Astrophysical Journal, Letters*, vol. 752, no. 1, L5, p. L5, Jun. 2012. DOI: 10.1088/2041-8205/752/1/L5. arXiv: 1105.2038 [astro-ph.CO].

[152] T. Kimm and R. Cen, "Escape Fraction of Ionizing Photons during Reionization: Effects due to Supernova Feedback and Runaway OB Stars," *Astrophysical Journal*, vol. 788, no. 2, 121, p. 121, Jun. 2014. DOI: 10.1088/0004-637X/788/2/121. arXiv: 1405.0552 [astro-ph.GA].

[153] X. Ma, D. Kasen, P. F. Hopkins, C.-A. Faucher-Giguère, E. Quataert, D. Kereš, and N. Murray, "The difficulty of getting high escape fractions of ionizing photons from high-redshift galaxies: a view from the FIRE cosmological simulations," *Monthly Notices of the RAS*, vol. 453, no. 1, pp. 960–975, Oct. 2015. DOI: 10.1093/mnras/stv1679. arXiv: 1503.07880 [astro-ph.GA].

[154] X. Ma, P. F. Hopkins, S. Garrison-Kimmel, C.-A. Faucher-Giguère, E. Quataert, M. Boylan-Kolchin, C. C. Hayward, R. Feldmann, and D. Kereš, "Simulating galaxies in the reionization era with FIRE-2: galaxy scaling relations, stellar mass functions, and luminosity functions," *Monthly Notices of the RAS*, vol. 478, no. 2, pp. 1694–1715, Aug. 2018. DOI: 10.1093/mnras/sty1024. arXiv: 1706.06605 [astro-ph.GA].

[155] R. Xue, K.-S. Lee, A. Dey, N. Reddy, S. Hong, M. K. M. Prescott, H. Inami, B. T. Jannuzi, and A. H. Gonzalez, "The Diversity of Diffuse Lyα Nebulae around Star-forming Galaxies at High Redshift," *Astrophysical Journal*, vol. 837, no. 2, 172, p. 172, Mar. 2017. DOI: 10.3847/1538-4357/837/2/172. arXiv: 1611.03510 [astro-ph.GA].

[156] M. A. Fardal, N. Katz, J. P. Gardner, L. Hernquist, D. H. Weinberg, and R. Davé, "Cooling Radiation and the Lyα Luminosity of Forming Galaxies," *Astrophysical Journal*, vol. 562, no. 2, pp. 605–617, Dec. 2001. DOI: 10.1086/323519. arXiv: astro-ph/0007205 [astro-ph].

[157] Z. Haiman, M. Spaans, and E. Quataert, "Lyα Cooling Radiation from High-Redshift Halos," *Astrophysical Journal, Letters*, vol. 537, no. 1, pp. L5–L8, Jul. 2000. DOI: 10.1086/312754. arXiv: astro-ph/0003366 [astro-ph].

[158] M. Dijkstra and A. Loeb, "Lyα blobs as an observational signature of cold accretion streams into galaxies," *Monthly Notices of the RAS*, vol. 400, no. 2, pp. 1109–1120, Dec. 2009. DOI: 10.1111/j.1365-2966.2009.15533.x. arXiv: 0902.2999 [astro-ph.CO].

[159] J. A. Kollmeier, Z. Zheng, R. Davé, A. Gould, N. Katz, J. Miralda-Escudé, and D. H. Weinberg, "Lyα Emission from Cosmic Structure. I. Fluorescence," *Astrophysical Journal*, vol. 708, no. 2, pp. 1048–1075, Jan. 2010. DOI: 10.1088/0004-637X/708/2/1048. arXiv: 0907.0704 [astro-ph.CO].

[160] S. Cantalupo, F. Arrigoni-Battaia, J. X. Prochaska, J. F. Hennawi, and P. Madau, "A cosmic web filament revealed in Lyman-α emission around a luminous high-redshift quasar," *Nature*, vol. 506, no. 7486, pp. 63–66, Feb. 2014. DOI: 10.1038/nature12898. arXiv: 1401.4469 [astro-ph.CO].

[161] E. Borisova, S. Cantalupo, S. J. Lilly, R. A. Marino, S. G. Gallego, R. Bacon, J. Blaizot, N. Bouché, J. Brinchmann, C. M. Carollo, J. Caruana, H. Finley, E. C. Herenz, J. Richard, J. Schaye, L. A. Straka, M. L. Turner, T. Urrutia, A. Verhamme, and L. Wisotzki, "Ubiquitous Giant Lyα Nebulae around the Brightest Quasars at z $\sim$ 3.5 Revealed with MUSE," *Astrophysical Journal*, vol. 831, no. 1, 39, p. 39, Nov. 2016. DOI: 10.3847/0004-637X/831/1/39. arXiv: 1605.01422 [astro-ph.GA].

[162] M. Mori, M. Umemura, and A. Ferrara, "The Nature of Lyα Blobs: Supernova-dominated Primordial Galaxies," *Astrophysical Journal, Letters*, vol. 613, no. 2, pp. L97–L100, Oct. 2004. DOI: 10.1086/425255. arXiv: astro-ph/0408410 [astro-ph].

[163] S. L. Finkelstein, J. E. Rhoads, S. Malhotra, N. Pirzkal, and J. Wang, "The Ages and Masses of Lyα Galaxies at z ~4.5," *Astrophysical Journal*, vol. 660, no. 2, pp. 1023–1029, May 2007. DOI: 10.1086/513462. arXiv: astro-ph/0612511 [astro-ph].

[164] N. A. Reddy and C. C. Steidel, "A Steep Faint-End Slope of the UV Luminosity Function at z ~2-3: Implications for the Global Stellar Mass Density and Star Formation in Low-Mass Halos," *Astrophysical Journal*, vol. 692, no. 1, pp. 778–803, Feb. 2009. DOI: 10.1088/0004-637X/692/1/778. arXiv: 0810.2788 [astro-ph].

[165] T. E. Rivera-Thorsen, M. Hayes, G. östlin, F. Duval, I. Orlitová, A. Verhamme, J. M. Mas-Hesse, D. Schaerer, J. M. Cannon, H. Otí-Floranes, A. Sandberg, L. Guaita, A. Adamo, H. Atek, E. C. Herenz, D. Kunth, P. Laursen, and J. Melinder, "The Lyman Alpha Reference Sample. V. The Impact of Neutral ISM Kinematics and Geometry on Lyα Escape," *Astrophysical Journal*, vol. 805, no. 1, 14, p. 14, May 2015. DOI: 10.1088/0004-637X/805/1/14. arXiv: 1503.01157 [astro-ph.GA].

[166] A. Verhamme, I. Orlitová, D. Schaerer, Y. Izotov, G. Worseck, T. X. Thuan, and N. Guseva, "Lyman-α spectral properties of five newly discovered Lyman continuum emitters," *Astronomy and Astrophysics*, vol. 597, A13, A13, Jan. 2017. DOI: 10.1051/0004-6361/201629264. arXiv: 1609.03477 [astro-ph.GA].

[167] S. Gazagnes, J. Chisholm, D. Schaerer, A. Verhamme, and Y. Izotov, "The origin of the escape of Lyman α and ionizing photons in Lyman continuum emitters," *Astronomy and Astrophysics*, vol. 639, A85, A85, Jul. 2020. DOI: 10.1051/0004-6361/202038096. arXiv: 2005.07215 [astro-ph.GA].

[168] C. C. Steidel, M. Bogosavljević, A. E. Shapley, N. A. Reddy, G. C. Rudie, M. Pettini, R. F. Trainor, and A. L. Strom, "The Keck Lyman Continuum Spectroscopic Survey (KLCS): The Emergent Ionizing Spectrum of Galaxies at z $\sim$ 3," *Astrophysical Journal*, vol. 869, no. 2, 123, p. 123, Dec. 2018. DOI: 10.3847/1538-4357/aaed28. arXiv: 1805.06071 [astro-ph.GA].

[169] C. C. Steidel, K. L. Adelberger, A. E. Shapley, M. Pettini, M. Dickinson, and M. Giavalisco, "Lyα Imaging of a Proto-Cluster Region at <z>=3.09," *Astrophysical Journal*, vol. 532, no. 1, pp. 170–182, Mar. 2000. DOI: 10.1086/308568. arXiv: astro-ph/9910144 [astro-ph].

[170] K.-G. Lee, J. F. Hennawi, C. Stark, J. X. Prochaska, M. White, D. J. Schlegel, A.-C. Eilers, A. Arinyo-i-Prats, N. Suzuki, R. A. C. Croft, K. I. Caputi, P. Cassata, O. Ilbert, B. Garilli, A. M. Koekemoer, V. Le Brun, O. Le Fèvre, D. Maccagni, P. Nugent, Y. Taniguchi, L. A. M. Tasca, L. Tresse, G. Zamorani, and E. Zucca, "Lyα Forest Tomography from Background Galaxies: The First Megaparsec-resolution Large-scale Structure Map at z > 2," *Astrophysical Journal, Letters*, vol. 795, no. 1, L12, p. L12, Nov. 2014. DOI: 10.1088/2041-8205/795/1/L12. arXiv: 1409.5632 [astro-ph.CO].

[171] Y. Matsuda, T. Yamada, T. Hayashino, H. Tamura, R. Yamauchi, T. Murayama, T. Nagao, K. Ohta, S. Okamura, M. Ouchi, K. Shimasaku, Y. Shioya, and Y. Taniguchi, "Large-Scale Filamentary Structure around the Protocluster at Redshift z = 3.1," *Astrophysical Journal, Letters*, vol. 634, no. 2, pp. L125–L128, Dec. 2005. DOI: 10.1086/499071. arXiv: astro-ph/0510762 [astro-ph].

[172] Y.-K. Chiang, R. A. Overzier, K. Gebhardt, and B. Henriques, "Galaxy Protoclusters as Drivers of Cosmic Star Formation History in the First 2 Gyr," *Astrophysical Journal, Letters*, vol. 844, no. 2, L23, p. L23, Aug. 2017. DOI: 10.3847/2041-8213/aa7e7b. arXiv: 1705.01634 [astro-ph.GA].

[173] K. Shi, J. Toshikawa, Z. Cai, K.-S. Lee, and T. Fang, "A Detailed Study of Massive Galaxies in a Protocluster at z = 3.13," *Astrophysical Journal*, vol. 899, no. 1, 79, p. 79, Aug. 2020. DOI: 10.3847/1538-4357/aba626. arXiv: 2007.07055 [astro-ph.CO].

[174] K. Shi, J. Toshikawa, K.-S. Lee, T. Wang, Z. Cai, and T. Fang, "Accelerated galaxy growth and environmental quenching in a protocluster at z=3.24," *arXiv e-prints*, arXiv:2102.06499, arXiv:2102.06499, Feb. 2021. arXiv: 2102.06499 [astro-ph.GA].

[175] N. Malavasi, K.-S. Lee, A. Dey, R. Xue, Y. Huang, and K. Shi, "Lyman Alpha line properties at $z \simeq 3.78$ and their environmental dependence: a case study around a massive proto-cluster," *arXiv e-prints*, arXiv:2103.12750, arXiv:2103.12750, Mar. 2021. arXiv: 2103.12750 [astro-ph.GA].

[176] LSST Science Collaboration, P. A. Abell, J. Allison, S. F. Anderson, J. R. Andrew, J. R. P. Angel, L. Armus, D. Arnett, S. J. Asztalos, T. S. Axelrod, and S. e. a. Bailey, "LSST Science Book, Version 2.0," *arXiv e-prints*, arXiv:0912.0201, arXiv:0912.0201, Dec. 2009. arXiv: 0912.0201 [astro-ph.IM].

[177] H. Aihara, N. Arimoto, R. Armstrong, S. Arnouts, N. A. Bahcall, S. Bickerton, J. Bosch, K. Bundy, P. L. Capak, J. H. H. Chan, M. Chiba, J. Coupon, E. Egami, M. Enoki, F. Finet, H. Fujimori, S. Fujimoto, H. Furusawa, J. Furusawa, T. Goto, A. Goulding, J. P. Greco, J. E. Greene, J. E. Gunn, T. Hamana, Y. Harikane, Y. Hashimoto, T. Hattori, M. Hayashi, Y. Hayashi, K. G. Hełminiak, R. Higuchi, C. Hikage, P. T. P. Ho, B.-C. Hsieh, K. Huang, S. Huang, H. Ikeda, M. Imanishi, A. K. Inoue, K. Iwasawa, I. Iwata, A. T. Jaelani, H.-Y. Jian, Y. Kamata, H. Karoji, N. Kashikawa, N. Katayama, S. Kawanomoto, I. Kayo, J. Koda, M. Koike, T. Kojima, Y. Komiyama, A. Konno, S. Koshida, Y. Koyama, H. Kusakabe, A. Leauthaud, C.-H. Lee, L. Lin, Y.-T. Lin, R. H. Lupton, R. Mandelbaum, Y. Matsuoka, E. Medezinski, S. Mineo, S. Miyama, H. Miyatake, S. Miyazaki, R. Momose, A. More, S. More, Y. Moritani, T. J. Moriya, T. Morokuma, S. Mukae, R. Murata, H. Murayama, T. Nagao, F. Nakata, M. Niida, H. Niikura, A. J. Nishizawa, Y. Obuchi, M. Oguri, Y. Oishi, N. Okabe, S. Okamoto, Y. Okura, Y. Ono, M. Onodera, M. Onoue, K. Osato, M. Ouchi, P. A. Price, T.-S. Pyo, M. Sako, M. Sawicki, T. Shibuya, K. Shimasaku, A. Shimono, M. Shirasaki, J. D. Silverman, M. Simet, J. Speagle, D. N. Spergel, M. A. Strauss, Y. Sugahara, N. Sugiyama, Y. Suto, S. H. Suyu, N. Suzuki, P. J. Tait, M. Takada, T. Takata, N. Tamura, M. M. Tanaka, M. Tanaka, M. Tanaka, Y. Tanaka, T. Terai, Y. Terashima, Y. Toba, N. Tominaga, J. Toshikawa, E. L. Turner, T. Uchida, H. Uchiyama, K. Umetsu, F. Uraguchi, Y. Urata, T. Usuda, Y. Utsumi, S.-Y. Wang, W.-H. Wang, K. C. Wong, K. Yabe, Y. Yamada, H. Yamanoi, N. Yasuda, S. Yeh, A. Yonehara, and S. Yuma, "The Hyper Suprime-Cam SSP Survey: Overview and survey design," *Publications of the ASJ*, vol. 70, S4, S4, Jan. 2018. DOI: 10.1093/pasj/psx066. arXiv: 1704.05858 [astro-ph.IM].

[178] G. A. Blanc, J. J. Adams, K. Gebhardt, G. J. Hill, N. Drory, L. Hao, R. Bender, R. Ciardullo, S. L. Finkelstein, A. B. Fry, E. Gawiser, C. Gronwall, U. Hopp, D. Jeong, R. Kelzenberg, E. Komatsu, P. MacQueen, J. D. Murphy, M. M. Roth, D. P. Schneider, and J. Tufts, "The HETDEX Pilot Survey. II. The Evolution of the Lyα Escape Fraction from the Ultraviolet Slope and Luminosity Function of $1.9 < z < 3.8$ LAEs," *Astrophysical Journal*, vol. 736, 31, p. 31, Jul. 2011. DOI: 10.1088/0004-637X/736/1/31. arXiv: 1011.0430.

[179] M. Song, S. L. Finkelstein, K. Gebhardt, G. J. Hill, N. Drory, M. L. N. Ashby, G. A. Blanc, J. Bridge, T. Chonis, R. Ciardullo, M. Fabricius, G. G. Fazio, E. Gawiser, C. Gronwall, A. Hagen, J.-S. Huang, S. Jogee, R. Livermore, B. Salmon, D. P. Schneider, S. P. Willner, and G. R. Zeimann, "The HETDEX Pilot Survey. V. The Physical Origin of Lyα Emitters Probed by Near-infrared Spectroscopy," *Astrophysical Journal*, vol. 791, 3, p. 3, Aug. 2014. DOI: 10.1088/0004-637X/791/1/3. arXiv: 1406.4503.

[180] G. A. Oyarzún, G. A. Blanc, V. González, M. Mateo, and I. Bailey John I., "A Comprehensive Study of Lyα Emission in the High-redshift Galaxy Population," *Astrophysical Journal*, vol. 843, no. 2, 133, p. 133, Jul. 2017. DOI: 10.3847/1538-4357/aa7552. arXiv: 1706.01886 [astro-ph.GA].

[181] L. Pentericci, R. J. McLure, B. Garilli, O. Cucciati, P. Franzetti, A. Iovino, R. Amorin, M. Bolzonella, A. Bongiorno, A. C. Carnall, M. Castellano, A. Cimatti, M. Cirasuolo, F. Cullen, S. De Barros, J. S. Dunlop, D. Elbaz, S. L. Finkelstein, A. Fontana, F. Fontanot, M. Fumana, A. Gargiulo, L. Guaita, W. G. Hartley, M. J. Jarvis, S. Juneau, W. Karman, D. Maccagni, F. Marchi, E. Marmol-Queralto, K. Nandra, E. Pompei, L. Pozzetti, M. Scodeggio, V. Sommariva, M. Talia, O. Almaini, I. Balestra, S. Bardelli, E. F. Bell, N. Bourne, R. A. A. Bowler, M. Brusa, F. Buitrago, K. I. Caputi, P. Cassata, S. Charlot, A. Citro, G. Cresci, S. Cristiani, E. Curtis-Lake, M. Dickinson, G. G. Fazio, H. C. Ferguson, F. Fiore, M. Franco, J. P. U. Fynbo, A. Galametz, A. Georgakakis, M. Giavalisco, A. Grazian, N. P. Hathi, I. Jung, S. Kim, A. M. Koekemoer, Y. Khusanova, O. Le Fèvre, J. M. Lotz, F. Mannucci, D. T. Maltby, K. Matsuoka, D. J. McLeod, H. Mendez-Hernandez, J. Mendez-Abreu, M. Mignoli, M. Moresco, A. Mortlock, M. Nonino, M. Pannella, C. Papovich, P. Popesso, D. P. Rosario, M. Salvato, P. Santini, D. Schaerer, C. Schreiber, D. P. Stark, L. A. M. Tasca, R. Thomas, T. Treu, E. Vanzella, V. Wild, C. C. Williams, G. Zamorani, and E. Zucca, "The VANDELS ESO public spectroscopic survey: Observations and first data release," *Astronomy and Astrophysics*, vol. 616, A174, A174, Sep. 2018. DOI: 10.1051/0004-6361/201833047. arXiv: 1803.07373.

[182] M. Hayes, G. östlin, D. Schaerer, A. Verhamme, J. M. Mas-Hesse, A. Adamo, H. Atek, J. M. Cannon, F. Duval, L. Guaita, E. C. Herenz, D. Kunth, P. Laursen, J. Melinder, I. Orlitová, H. Otí-Floranes, and A. Sandberg, "The Lyman Alpha Reference Sample: Extended Lyman Alpha Halos Produced at Low Dust Content," *Astrophysical Journal, Letters*, vol. 765, no. 2, L27, p. L27, Mar. 2013. DOI: 10.1088/2041-8205/765/2/L27. arXiv: 1303.0006 [astro-ph.CO].

[183] M. Rauch, M. Haehnelt, A. Bunker, G. Becker, F. Marleau, J. Graham, S. Cristiani, M. Jarvis, C. Lacey, S. Morris, C. Peroux, H. Röttgering, and T. Theuns, "A Population of Faint Extended Line Emitters and the Host Galaxies of Optically Thick QSO Absorption Systems," *Astrophysical Journal*, vol. 681, pp. 856–880, Jul. 2008. DOI: 10.1086/525846. arXiv: 0711.1354.

[184] C. C. Steidel, M. Bogosavljević, A. E. Shapley, J. A. Kollmeier, N. A. Reddy, D. K. Erb, and M. Pettini, "Diffuse Lyα Emitting Halos: A Generic Property of High-redshift Star-forming Galaxies," *Astrophysical Journal*, vol. 736, no. 2, 160, p. 160, Aug. 2011. DOI: 10.1088/0004-637X/736/2/160. arXiv: 1101.2204 [astro-ph.CO].

[185] R. Momose, M. Ouchi, K. Nakajima, Y. Ono, T. Shibuya, K. Shimasaku, S. Yuma, M. Mori, and M. Umemura, "Diffuse Lyα haloes around galaxies at z = 2.2-6.6: implications for galaxy formation and cosmic reionization," *Monthly Notices of the RAS*, vol. 442, pp. 110–120, Jul. 2014. DOI: 10.1093/mnras/stu825. arXiv: 1403.0732.

[186] R. Momose, M. Ouchi, K. Nakajima, Y. Ono, T. Shibuya, K. Shimasaku, S. Yuma, M. Mori, and M. Umemura, "Statistical properties of diffuse Lyα haloes around star-forming galaxies at $z\tilde{2}$," *Monthly Notices of the RAS*, vol. 457, pp. 2318–2330, Apr. 2016. DOI: 10.1093/mnras/stw021. arXiv: 1509.09001.

[187] E. Komatsu, K. M. Smith, J. Dunkley, C. L. Bennett, B. Gold, G. Hinshaw, N. Jarosik, D. Larson, M. R. Nolta, L. Page, D. N. Spergel, M. Halpern, R. S. Hill, A. Kogut, M. Limon, S. S. Meyer, N. Odegard, G. S. Tucker, J. L. Weiland, E. Wollack, and E. L. Wright, "Seven-year Wilkinson Microwave Anisotropy Probe (WMAP) Observations: Cosmological Interpretation," *Astrophysical Journal, Supplement*, vol. 192, no. 2, 18, p. 18, Feb. 2011. DOI: 10.1088/0067-0049/192/2/18. arXiv: 1001.4538 [astro-ph.CO].

[188] J. B. Oke and J. E. Gunn, "Secondary standard stars for absolute spectrophotometry.," *Astrophysical Journal*, vol. 266, pp. 713–717, Mar. 1983. DOI: 10.1086/160817.

[189] S. D. J. Gwyn, "The Canada-France-Hawaii Telescope Legacy Survey: Stacked Images and Catalogs," *Astronomical Journal*, vol. 143, 38, p. 38, Feb. 2012. DOI: 10.1088/0004-6256/143/2/38. arXiv: 1101.1084.

[190] A. Dey, D. Rabinowitz, A. Karcher, C. Bebek, C. Baltay, D. Sprayberry, F. Valdes, B. Stupak, J. Donaldson, W. Emmet, T. Hurteau, B. Abareshi, B. Marshall, D. Lang, M. Fitzpatrick, P. Daly, D. Joyce, D. Schlegel, H. Schweiker, L. Allen, B. Blum, and M. Levi, "Mosaic3: a red-sensitive upgrade for the prime focus camera at the Mayall 4m telescope," in *Ground-based and Airborne Instrumentation for Astronomy VI*, ser. Proceedings of the SPIE, vol. 9908, Aug. 2016, p. 99082C. DOI: 10.1117/12.2231488.

[191] E. Bertin and S. Arnouts, "SExtractor: Software for source extraction.," *Astronomy and Astrophysicss*, vol. 117, pp. 393–404, Jun. 1996. DOI: 10.1051/aas:1996164.

[192] L. Chiappetti, M. Tajer, G. Trinchieri, D. Maccagni, L. Maraschi, L. Paioro, M. Pierre, J. Surdej, O. Garcet, E. Gosset, O. Le Fèvre, E. Bertin, H. J. McCracken, Y. Mellier, S. Foucaud, M. Radovich, V. Ripepi, and M. Arnaboldi, "The XMM-LSS survey. The XMD-S/VVDS 4σ catalogue," *Astronomy and Astrophysics*, vol. 439, no. 1, pp. 413–425, Aug. 2005. DOI: 10.1051/0004-6361:20042583. arXiv: astro-ph/0505117 [astro-ph].

[193] O. Le Fèvre, P. Cassata, O. Cucciati, B. Garilli, O. Ilbert, V. Le Brun, D. Maccagni, C. Moreau, M. Scodeggio, L. Tresse, G. Zamorani, C. Adami, S. Arnouts, S. Bardelli, M. Bolzonella, M. Bondi, A. Bongiorno, D. Bottini, A. Cappi, S. Charlot, P. Ciliegi, T. Contini, S. de la Torre, S. Foucaud, P. Franzetti, I. Gavignaud, L. Guzzo, A. Iovino, B. Lemaux, C. López-Sanjuan, H. J. McCracken, B. Marano, C. Marinoni, A. Mazure, Y. Mellier, R. Merighi, P. Merluzzi, S. Paltani, R. Pellò, A. Pollo, L. Pozzetti, R. Scaramella, L. Tasca, D. Vergani, G. Vettolani, A. Zanichelli, and E. Zucca, "The VIMOS VLT Deep Survey final data release: a spectroscopic sample of 35 016 galaxies and AGN out to $z \sim 6.7$ selected with $17.5 \leq i_{AB} \leq 24.75$," *Astronomy and Astrophysics*, vol. 559, A14, A14, Nov. 2013. DOI: 10.1051/0004-6361/201322179. arXiv: 1307.0545.

[194] D. W. Hogg, J. G. Cohen, R. Blandford, and M. A. Pahre, "The O II Luminosity Density of the Universe," *Astrophysical Journal*, vol. 504, pp. 622–628, Sep. 1998. DOI: 10.1086/306122. eprint: astro-ph/9804129.

[195] R. J. McLure, L. Pentericci, A. Cimatti, J. S. Dunlop, D. Elbaz, A. Fontana, K. Nandra, R. Amorin, M. Bolzonella, and A. Bongiorno, "The VANDELS ESO public spectroscopic survey," *Monthly Notices of the RAS*, vol. 479, no. 1, pp. 25–42, Sep. 2018. DOI: 10.1093/mnras/sty1213. arXiv: 1803.07414 [astro-ph.GA].

[196] A. K. Inoue, I. Shimizu, I. Iwata, and M. Tanaka, "An updated analytic model for attenuation by the intergalactic medium," *Monthly Notices of the RAS*, vol. 442, pp. 1805–1820, Aug. 2014. DOI: 10.1093/mnras/stu936. arXiv: 1402.0677.

[197] J. Matthee, D. Sobral, I. Oteo, P. Best, I. Smail, H. Röttgering, and A. Paulino-Afonso, "The CALYMHA survey: Lyα escape fraction and its dependence on galaxy properties at z = 2.23," *Monthly Notices of the RAS*, vol. 458, pp. 449–467, May 2016. DOI: 10.1093/mnras/stw322. arXiv: 1602.02756.

[198] P. Laursen and J. Sommer-Larsen, "Lyα Resonant Scattering in Young Galaxies: Predictions from Cosmological Simulations," *Astrophysical Journal, Letters*, vol. 657, no. 2, pp. L69–L72, Mar. 2007. DOI: 10.1086/513191. arXiv: astro-ph/0610761 [astro-ph].

[199] K. K. Nilsson, C. Tapken, P. Møller, W. Freudling, J. P. U. Fynbo, K. Meisenheimer, P. Laursen, and G. östlin, "Evolution in the properties of Lyman-α emitters from redshifts $z \sim 3$ to $z \sim 2$," *Astronomy and Astrophysics*, vol. 498, pp. 13–23, Apr. 2009. DOI: 10.1051/0004-6361/200810881. arXiv: 0812.3152.

[200] K. Lai, J.-S. Huang, G. Fazio, L. L. Cowie, E. M. Hu, and Y. Kakazu, "The Stellar Population of Lyα-emitting Galaxies at $z \sim 5.7$," *Astrophysical Journal*, vol. 655, no. 2, pp. 704–713, Feb. 2007. DOI: 10.1086/510285. arXiv: astro-ph/0610572 [astro-ph].

[201] N. Pirzkal, S. Malhotra, J. E. Rhoads, and C. Xu, "Optical-to-Mid-Infrared Observations of Lyα Galaxies at $z \sim 5$ in the Hubble Ultra Deep Field: A Young and Low-Mass Population," *Astrophysical Journal*, vol. 667, no. 1, pp. 49–59, Sep. 2007. DOI: 10.1086/519485. arXiv: astro-ph/0612513 [astro-ph].

[202] K. Lai, J.-S. Huang, G. Fazio, E. Gawiser, R. Ciardullo, M. Damen, M. Franx, C. Gronwall, I. Labbe, G. Magdis, and P. van Dokkum, "Spitzer Constraints on the Stellar Populations of Lyα-Emitting Galaxies at z = 3.1," *Astrophysical Journal*, vol. 674, no. 1, pp. 70–74, Feb. 2008. DOI: 10.1086/524702. arXiv: 0710.3384 [astro-ph].

[203] T. M. A. Webb, T. Yamada, J. .-S. Huang, M. L. N. Ashby, Y. Matsuda, E. Egami, M. Gonzalez, and T. Hayashimo, "Spitzer Observations of Extended Lyman-α Clouds in the SSA22 Field," *Astrophysical Journal*, vol. 692, no. 2, pp. 1561–1570, Feb. 2009. DOI: 10.1088/0004-637X/692/2/1561. arXiv: 0812.0991 [astro-ph].

[204] S. Yuma, K. Ohta, K. Yabe, K. Shimasaku, M. Yoshida, M. Ouchi, I. Iwata, and M. Sawicki, "Stellar Populations of Lyα Emitters at z = 4.86: A Comparison to $z \sim 5$ Lyman Break Galaxies," *Astrophysical Journal*, vol. 720, no. 2, pp. 1016–1029, Sep. 2010. DOI: 10.1088/0004-637X/720/2/1016. arXiv: 1007.2057 [astro-ph.CO].

[205] S. L. Finkelstein, J. E. Rhoads, S. Malhotra, N. Grogin, and J. Wang, "Effects of Dust Geometry in Lyα Galaxies at z = 4.4," *Astrophysical Journal*, vol. 678, pp. 655–668, May 2008. DOI: 10.1086/525272. arXiv: 0708.4226.

[206] S. L. Finkelstein, J. E. Rhoads, S. Malhotra, and N. Grogin, "Lyman Alpha Galaxies: Primitive, Dusty, or Evolved?" *Astrophysical Journal*, vol. 691, no. 1, pp. 465–481, Jan. 2009. DOI: 10.1088/0004-637X/691/1/465. arXiv: 0806.3269 [astro-ph].

[207] C. Scarlata, J. Colbert, H. I. Teplitz, N. Panagia, M. Hayes, B. Siana, A. Rau, P. Francis, A. Caon, A. Pizzella, and C. Bridge, "The Effect of Dust Geometry on the Lyα Output of Galaxies," *Astrophysical Journal, Letters*, vol. 704, no. 2, pp. L98–L102, Oct. 2009. DOI: 10.1088/0004-637X/704/2/L98. arXiv: 0909.3847 [astro-ph.CO].

[208] D. A. Neufeld, "The escape of Lyman-alpha radiation from a multiphase interstellar medium," *Astrophysical Journal, Letters*, vol. 370, pp. L85–L88, Apr. 1991. DOI: 10.1086/185983.

[209] D. Calzetti, L. Armus, R. C. Bohlin, A. L. Kinney, J. Koornneef, and T. Storchi-Bergmann, "The Dust Content and Opacity of Actively Star-forming Galaxies," *Astrophysical Journal*, vol. 533, pp. 682–695, Apr. 2000. DOI: 10.1086/308692. eprint: astro-ph/9911459.

[210] D. Sobral, J. Matthee, B. Darvish, I. Smail, P. N. Best, L. Alegre, H. Röttgering, B. Mobasher, A. Paulino-Afonso, A. Stroe, and I. Oteo, "The nature of luminous Ly α emitters at $z\tilde{2} - 3$: maximal dust-poor starbursts and highly ionizing AGN," *Monthly Notices of the RAS*, vol. 477, pp. 2817–2840, Jun. 2018. DOI: 10.1093/mnras/sty782. arXiv: 1802.10102.

[211] S. Charlot and S. M. Fall, "Lyman-Alpha Emission from Galaxies," *Astrophysical Journal*, vol. 415, p. 580, Oct. 1993. DOI: 10.1086/173187.

[212] S. Malhotra and J. E. Rhoads, "Large Equivalent Width Lyα line Emission at z=4.5: Young Galaxies in a Young Universe?" *Astrophysical Journal, Letters*, vol. 565, no. 2, pp. L71–L74, Feb. 2002. DOI: 10.1086/338980. arXiv: astro-ph/0111126 [astro-ph].

[213] N. Kashikawa, T. Nagao, J. Toshikawa, Y. Ishizaki, E. Egami, M. Hayashi, C. Ly, M. A. Malkan, Y. Matsuda, K. Shimasaku, M. Iye, K. Ota, T. Shibuya, L. Jiang, Y. Taniguchi, and Y. Shioya, "A Lyα Emitter with an Extremely Large Rest-frame Equivalent Width of $\sim$ 900 Åat z = 6.5: A Candidate Population III-dominated Galaxy?" *Astrophysical Journal*, vol. 761, no. 2, 85, p. 85, Dec. 2012. DOI: 10.1088/0004-637X/761/2/85. arXiv: 1210.4933 [astro-ph.CO].

[214] T. Hashimoto, T. Garel, B. Guiderdoni, A. B. Drake, R. Bacon, J. Blaizot, J. Richard, F. Leclercq, H. Inami, A. Verhamme, R. Bouwens, J. Brinchmann, S. Cantalupo, M. Carollo, J. Caruana, E. C. Herenz, J. Kerutt, R. A. Marino, P. Mitchell, and J. Schaye, "The MUSE Hubble Ultra Deep Field Survey. X. Lyα equivalent widths at $2.9 < z < 6.6$," *Astronomy and Astrophysics*, vol. 608, A10, A10, Nov. 2017. DOI: 10.1051/0004-6361/201731579. arXiv: 1711.01747 [astro-ph.GA].

[215] N. A. Reddy, C. C. Steidel, D. Fadda, L. Yan, M. Pettini, A. E. Shapley, D. K. Erb, and K. L. Adelberger, "Star Formation and Extinction in Redshift $z \sim 2$ Galaxies: Inferences from Spitzer MIPS Observations," *Astrophysical Journal*, vol. 644, no. 2, pp. 792–812, Jun. 2006. DOI: 10.1086/503739. arXiv: astro-ph/0602596 [astro-ph].

[216] B. Siana, H. I. Teplitz, R.-R. Chary, J. Colbert, and D. T. Frayer, "Spitzer Observations of the z = 2.73 Lensed Lyman Break Galaxy: MS 1512-cB58," *Astrophysical Journal*, vol. 689, no. 1, pp. 59–67, Dec. 2008. DOI: 10.1086/592682. arXiv: 0808.2465 [astro-ph].

[217] K. D. Gordon, G. C. Clayton, K. A. Misselt, A. U. Land olt, and M. J. Wolff, "A Quantitative Comparison of the Small Magellanic Cloud, Large Magellanic Cloud, and Milky Way Ultraviolet to Near-Infrared Extinction Curves," *Astrophysical Journal*, vol. 594, no. 1, pp. 279–293, Sep. 2003. DOI: 10.1086/376774. arXiv: astro-ph/0305257 [astro-ph].

[218] H. Kusakabe, K. Shimasaku, K. Nakajima, and M. Ouchi, "First Infrared-Based Implications for the Dust Attenuation and Star Formation of Typical Lyα Emitters," *Astrophysical Journal, Letters*, vol. 800, no. 2, L29, p. L29, Feb. 2015. DOI: 10.1088/2041-8205/800/2/L29. arXiv: 1411.1615 [astro-ph.GA].

[219] I. Oteo, D. Sobral, R. J. Ivison, I. Smail, P. N. Best, J. Cepa, and A. M. Pérez-García, "On the nature of Hα emitters at $z \sim 2$ from the HiZELS survey: physical properties, Lyα escape fraction and main sequence," *Monthly Notices of the RAS*, vol. 452, no. 2, pp. 2018–2033, Sep. 2015. DOI: 10.1093/mnras/stv1284. arXiv: 1506.02670 [astro-ph.GA].

[220] D. Sobral, J. Matthee, P. Best, A. Stroe, H. Röttgering, I. Oteo, I. Smail, L. Morabito, and A. Paulino-Afonso, "The CALYMHA survey: Lyα luminosity function and global escape fraction of Lyα photons at z = 2.23," *Monthly Notices of the RAS*, vol. 466, pp. 1242–1258, Apr. 2017. DOI: 10.1093/mnras/stw3090. arXiv: 1609.05897.

[221] M. G. Kendall, "A new measure of rank correlation," *Biometrika*, vol. 30, no. 1/2, pp. 81–93, 1938, ISSN: 00063444. [Online]. Available: http://www.jstor.org/stable/2332226.

[222] C. Spearman, "The proof and measurement of association between two things," *American Journal of Psychology*, vol. 15, pp. 88–103, 1904.

[223] R. J. Bouwens, G. D. Illingworth, P. A. Oesch, I. Labbé, P. G. van Dokkum, M. Trenti, M. Franx, R. Smit, V. Gonzalez, and D. Magee, "UV-continuum Slopes of > 4000 z $\sim 4 - 8$ Galaxies from the HUDF/XDF, HUDF09, ERS, CANDELS-South, and CANDELS-North Fields," *Astrophysical Journal*, vol. 793, no. 2, 115, p. 115, Oct. 2014. DOI: 10.1088/0004-637X/793/2/115. arXiv: 1306.2950 [astro-ph.CO].

[224] N. A. Reddy, M. Kriek, A. E. Shapley, W. R. Freeman, B. Siana, A. L. Coil, B. Mobasher, S. H. Price, R. L. Sanders, and I. Shivaei, "The MOSDEF Survey: Measurements of Balmer Decrements and the Dust Attenuation Curve at Redshifts $z \sim 1.4 - 2.6$," *Astrophysical Journal*, vol. 806, no. 2, 259, p. 259, Jun. 2015. DOI: 10.1088/0004-637X/806/2/259. arXiv: 1504.02782 [astro-ph.GA].

[225] M. Hayes, C. Scarlata, and B. Siana, "Central powering of the largest Lyman-α nebula is revealed by polarized radiation," *Nature*, vol. 476, no. 7360, pp. 304–307, Aug. 2011. DOI: 10.1038/nature10320. arXiv: 1108.3332 [astro-ph.CO].

[226] H. Atek, D. Kunth, M. Hayes, G. östlin, and J. M. Mas-Hesse, "On the detectability of Lyα emission in star forming galaxies. The role of dust," *Astronomy and Astrophysics*, vol. 488, no. 2, pp. 491–509, Sep. 2008. DOI: 10.1051/0004-6361:200809527. arXiv: 0805.3501 [astro-ph].

[227] S. L. Finkelstein, S. H. Cohen, J. Moustakas, S. Malhotra, J. E. Rhoads, and C. Papovich, "Dust Extinction and Metallicities of Star-forming Lyα Emitting Galaxies at Low Redshift," *Astrophysical Journal*, vol. 733, no. 2, 117, p. 117, Jun. 2011. DOI: 10.1088/0004-637X/733/2/117. arXiv: 1012.4010 [astro-ph.CO].

[228] L. L. Cowie, A. J. Barger, and E. M. Hu, "Lyα Emitting Galaxies as Early Stages in Galaxy Formation," *Astrophysical Journal*, vol. 738, no. 2, 136, p. 136, Sep. 2011. DOI: 10.1088/0004-637X/738/2/136. arXiv: 1106.0496 [astro-ph.CO].

[229] H. Atek, D. Kunth, D. Schaerer, J. M. Mas-Hesse, M. Hayes, G. östlin, and J.-P. Kneib, "Influence of physical galaxy properties on Lyα escape in star-forming galaxies," *Astronomy and Astrophysics*, vol. 561, A89, A89, Jan. 2014. DOI: 10.1051/0004-6361/201321519. arXiv: 1308.6577 [astro-ph.CO].

[230] S. Charlot and S. M. Fall, "Attenuation of Lyman-Alpha Emission by Dust in Damped Lyman-Alpha Systems," *Astrophysical Journal*, vol. 378, p. 471, Sep. 1991. DOI: 10.1086/170448.

[231] M. Hansen and S. P. Oh, "Lyman α radiative transfer in a multiphase medium," *Monthly Notices of the RAS*, vol. 367, no. 3, pp. 979–1002, Apr. 2006. DOI: 10.1111/j.1365-2966.2005.09870.x. arXiv: astro-ph/0507586 [astro-ph].

[232] F. Duval, D. Schaerer, G. östlin, and P. Laursen, "Lyman α line and continuum radiative transfer in a clumpy interstellar medium," *Astronomy and Astrophysics*, vol. 562, A52, A52, Feb. 2014. DOI: 10.1051/0004-6361/201220455. arXiv: 1302.7042 [astro-ph.GA].

[233] K. Kim, S. Malhotra, J. E. Rhoads, N. R. Butler, and H. Yang, "The Importance of Star Formation Intensity in Lyα Escape from Green Pea Galaxies and Lyman Break Galaxy Analogs," *Astrophysical Journal*, vol. 893, no. 2, 134, p. 134, Apr. 2020. DOI: 10.3847/1538-4357/ab7895. arXiv: 2002.08961 [astro-ph.GA].

[234] D. P. Stark, R. S. Ellis, K. Chiu, M. Ouchi, and A. Bunker, "Keck spectroscopy of faint 3 ¡ z ¡ 7 Lyman break galaxies - I. New constraints on cosmic reionization from the luminosity and redshift-dependent fraction of Lyman α emission," *Monthly Notices of the RAS*, vol. 408, no. 3, pp. 1628–1648, Nov. 2010. DOI: 10.1111/j.1365-2966.2010.17227.x. arXiv: 1003.5244 [astro-ph.CO].

[235] G. A. Oyarzún, G. A. Blanc, V. González, M. Mateo, I. Bailey John I., S. L. Finkelstein, P. Lira, J. D. Crane, and E. W. Olszewski, "How Lyman Alpha Emission Depends on Galaxy Stellar Mass," *Astrophysical Journal, Letters*, vol. 821, no. 1, L14, p. L14, Apr. 2016. DOI: 10.3847/2041-8205/821/1/L14. arXiv: 1604.03113 [astro-ph.GA].

[236] V. González, I. Labbé, R. J. Bouwens, G. Illingworth, M. Franx, and M. Kriek, "Evolution of Galaxy Stellar Mass Functions, Mass Densities, and Mass-to-light Ratios from $z \sim 7$ to $z \sim 4$," *Astrophysical Journal, Letters*, vol. 735, no. 2, L34, p. L34, Jul. 2011. DOI: 10.1088/2041-8205/735/2/L34. arXiv: 1008.3901 [astro-ph.CO].

[237] K.-S. Lee, H. C. Ferguson, T. Wiklind, T. Dahlen, M. E. Dickinson, M. Giavalisco, N. Grogin, C. Papovich, H. Messias, Y. Guo, and L. Lin, "How Do Star-forming Galaxies at z ¿ 3 Assemble Their Masses?" *Astrophysical Journal*, vol. 752, no. 1, 66, p. 66, Jun. 2012. DOI: 10.1088/0004-637X/752/1/66. arXiv: 1111.1233 [astro-ph.CO].

[238] D. P. Stark, M. A. Schenker, R. Ellis, B. Robertson, R. McLure, and J. Dunlop, "Keck Spectroscopy of 3 ¡ z ¡ 7 Faint Lyman Break Galaxies: The Importance of Nebular Emission in Understanding the Specific Star Formation Rate and Stellar Mass Density," *Astrophysical Journal*, vol. 763, no. 2, 129, p. 129, Feb. 2013. DOI: 10.1088/0004-637X/763/2/129. arXiv: 1208.3529 [astro-ph.CO].

[239] M. Song, S. L. Finkelstein, M. L. N. Ashby, A. Grazian, Y. Lu, C. Papovich, B. Salmon, R. S. Somerville, M. Dickinson, K. Duncan, S. M. Faber, G. G. Fazio, H. C. Ferguson, A. Fontana, Y. Guo, N. Hathi, S.-K. Lee, E. Merlin, and S. P. Willner, "The Evolution of the Galaxy Stellar Mass Function at z = 4-8: A Steepening Low-mass-end Slope with Increasing Redshift," *Astrophysical Journal*, vol. 825, no. 1, 5, p. 5, Jul. 2016. DOI: 10.3847/0004-637X/825/1/5. arXiv: 1507.05636 [astro-ph.GA].

[240] L. H. Weiss, W. P. Bowman, R. Ciardullo, G. R. Zeimann, C. Gronwall, E. Mentuch Cooper, K. Gebhardt, G. J. Hill, G. A. Blanc, D. J. Farrow, S. L. Finkelstein, E. Gawiser, S. Janowiecki, S. Jogee, D. P. Schneider, and L. Wisotzki, "The HETDEX Survey: The Lyα Escape Fraction from 3D-HST Emission-Line Galaxies at z $\sim$ 2," *Astrophysical Journal*, vol. 912, no. 2, 100, p. 100, May 2021. DOI: 10.3847/1538-4357/abedb9. arXiv: 2103.12126 [astro-ph.GA].

[241] N. P. Hathi, O. Le Fèvre, O. Ilbert, P. Cassata, L. A. M. Tasca, B. C. Lemaux, B. Garilli, V. Le Brun, D. Maccagni, L. Pentericci, R. Thomas, E. Vanzella, G. Zamorani, E. Zucca, R. Amorín, S. Bardelli, L. P. Cassarà, M. Castellano, A. Cimatti, O. Cucciati, A. Durkalec, A. Fontana, M. Giavalisco, A. Grazian, L. Guaita, A. Koekemoer, S. Paltani, J. Pforr, B. Ribeiro, D. Schaerer, M. Scodeggio, V. Sommariva, M. Talia, L. Tresse, D. Vergani, P. Capak, S. Charlot, T. Contini, J. G. Cuby, S. de la Torre, J. Dunlop, S. Fotopoulou, C. López-Sanjuan, Y. Mellier, M. Salvato, N. Scoville, Y. Taniguchi, and P. W. Wang, "The VIMOS Ultra Deep Survey: Lyα emission and stellar populations of star-forming galaxies at 2 ¡ z ¡ 2.5," *Astronomy and Astrophysics*, vol. 588, A26, A26, Apr. 2016. DOI: 10.1051/0004-6361/201526012. arXiv: 1503.01753 [astro-ph.GA].

[242] S. Santos, D. Sobral, J. Matthee, J. Calhau, E. da Cunha, B. Ribeiro, A. Paulino-Afonso, P. Arrabal Haro, and J. Butterworth, "The evolution of rest-frame UV properties, Ly α EWs, and the SFR-stellar mass relation at z $\sim$ 2-6 for SC4K LAEs," *Monthly Notices of the RAS*, vol. 493, no. 1, pp. 141–160, Mar. 2020. DOI: 10.1093/mnras/staa093. arXiv: 1910.02959 [astro-ph.GA].

[243] P. Arrabal Haro, J. M. Rodríguez Espinosa, C. Muñoz-Tuñón, D. Sobral, A. Lumbreras-Calle, M. Boquien, A. Hernán-Caballero, L. Rodríguez-Muñoz, and B. Alcalde Pampliega, "Differences and similarities of stellar populations in LAEs and LBGs at z $\sim$ 3.4-6.8," *Monthly Notices of the RAS*, vol. 495, no. 2, pp. 1807–1824, Jun. 2020. DOI: 10.1093/mnras/staa1196. arXiv: 2004.11175 [astro-ph.GA].

[244] N. Reddy, M. Dickinson, D. Elbaz, G. Morrison, M. Giavalisco, R. Ivison, C. Papovich, D. Scott, V. Buat, D. Burgarella, V. Charmandaris, E. Daddi, G. Magdis, E. Murphy, B. Altieri, H. Aussel, H. Dannerbauer, K. Dasyra, H. S. Hwang, J. Kartaltepe, R. Leiton, B. Magnelli, and P. Popesso, "GOODS-Herschel Measurements of the Dust Attenuation of Typical Star-forming Galaxies at High Redshift: Observations of Ultraviolet-selected Galaxies at $z \sim 2$," *Astrophysical Journal*, vol. 744, no. 2, 154, p. 154, Jan. 2012. DOI: 10.1088/0004-637X/744/2/154. arXiv: 1107.2653 [astro-ph.CO].

[245] R. J. Bouwens, G. D. Illingworth, M. Franx, R. .-R. Chary, G. R. Meurer, C. J. Conselice, H. Ford, M. Giavalisco, and P. van Dokkum, "UV Continuum Slope and Dust Obscuration from $z \sim 6$ to $z \sim 2$: The Star Formation Rate Density at High Redshift," *Astrophysical Journal*, vol. 705, no. 1, pp. 936–961, Nov. 2009. DOI: 10.1088/0004-637X/705/1/936. arXiv: 0909.4074 [astro-ph.CO].

[246] K.-G. Lee, A. Krolewski, M. White, D. Schlegel, P. E. Nugent, J. F. Hennawi, T. Müller, R. Pan, J. X. Prochaska, A. Font-Ribera, N. Suzuki, K. Glazebrook, G. G. Kacprzak, J. S. Kartaltepe, A. M. Koekemoer, O. Le Fèvre, B. C. Lemaux, C. Maier, T. Nanayakkara, R. M. Rich, D. B. Sanders, M. Salvato, L. Tasca, and K.-V. H. Tran, "First Data Release of the COSMOS Lyα Mapping and Tomography Observations: 3D Lyα Forest Tomography at 2.05 < z < 2.55," *Astrophysical Journal, Supplement*, vol. 237, no. 2, 31, p. 31, Aug. 2018. DOI: 10.3847/1538-4365/aace58. arXiv: 1710.02894 [astro-ph.CO].

[247] Z. Cai, X. Fan, S. Peirani, F. Bian, B. Frye, I. McGreer, J. X. Prochaska, M. W. Lau, N. Tejos, S. Ho, and D. P. Schneider, "Mapping the Most Massive Overdensity Through Hydrogen (MAMMOTH) I: Methodology," *Astrophysical Journal*, vol. 833, no. 2, 135, p. 135, Dec. 2016. DOI: 10.3847/1538-4357/833/2/135. arXiv: 1512.06859 [astro-ph.GA].

[248] Y. Liang, N. Kashikawa, Z. Cai, X. Fan, J. X. Prochaska, K. Shimasaku, M. Tanaka, H. Uchiyama, K. Ito, R. Shimakawa, K. Nagamine, I. Shimizu, M. Onoue, and J. Toshikawa, "Statistical correlation between the distribution of Lyα emitters and IGM HI at $z \sim 2.2$ mapped by Subaru/Hyper Suprime-Cam," *arXiv e-prints*, arXiv:2008.01733, arXiv:2008.01733, Aug. 2020. arXiv: 2008.01733 [astro-ph.GA].

[249] K. Kakiichi and M. Gronke, "Lyman Radiation Hydrodynamics of Turbulent H II Regions in Molecular Clouds: A Physical Origin of LyC Leakage and the Associated Lyα Spectra," *arXiv e-prints*, arXiv:1905.02480, arXiv:1905.02480, May 2019. arXiv: 1905.02480 [astro-ph.GA].

[250] C. Clarke and M. S. Oey, "Galactic porosity and a star formation threshold for the escape of ionizing radiation from galaxies," *Monthly Notices of the RAS*, vol. 337, no. 4, pp. 1299–1308, Dec. 2002. DOI: 10.1046/j.1365-8711.2002.05976.x. arXiv: astro-ph/0208442 [astro-ph].

[251] R. Endsley, D. P. Stark, J. Chevallard, S. Charlot, B. Robertson, R. J. Bouwens, and M. Stefanon, "MMT Spectroscopy of Lyman-alpha at z≃7: Evidence for Accelerated Reionization Around Massive Galaxies," *arXiv e-prints*, arXiv:2010.03566, arXiv:2010.03566, Oct. 2020. arXiv: 2010.03566 [astro-ph.GA].

[252] A. Hagen, G. R. Zeimann, C. Behrens, R. Ciardullo, H. S. Grasshorn Gebhardt, C. Gronwall, J. S. Bridge, D. B. Fox, D. P. Schneider, J. R. Trump, G. A. Blanc, Y.-K. Chiang, T. S. Chonis, S. L. Finkelstein, G. J. Hill, S. Jogee, and E. Gawiser, "HST Emission Line Galaxies at $z \sim 2$: Comparing Physical Properties of Lyman Alpha and Optical Emission Line Selected Galaxies," *Astrophysical Journal*, vol. 817, no. 1, 79, p. 79, Jan. 2016. DOI: 10.3847/0004-637X/817/1/79. arXiv: 1512.03063 [astro-ph.GA].

[253] A. Sternberg, T. L. Hoffmann, and A. W. A. Pauldrach, "Ionizing Photon Emission Rates from O- and Early B-Type Stars and Clusters," *Astrophysical Journal*, vol. 599, no. 2, pp. 1333–1343, Dec. 2003. DOI: 10.1086/379506. arXiv: astro-ph/0312232 [astro-ph].

[254] C. Leitherer, P. A. Ortiz Otálvaro, F. Bresolin, R.-P. Kudritzki, B. Lo Faro, A. W. A. Pauldrach, M. Pettini, and S. A. Rix, "A Library of Theoretical Ultraviolet Spectra of Massive, Hot Stars for Evolutionary Synthesis," *Astrophysical Journal, Supplement*, vol. 189, no. 2, pp. 309–335, Aug. 2010. DOI: 10.1088/0067-0049/189/2/309. arXiv: 1006.5624 [astro-ph.SR].

[255] N. A. Reddy, C. C. Steidel, M. Pettini, and M. Bogosavljević, "Spectroscopic Measurements of the Far-Ultraviolet Dust Attenuation Curve at $z \sim 3$," *Astrophysical Journal*, vol. 828, no. 2, 107, p. 107, Sep. 2016. DOI: 10.3847/0004-637X/828/2/107. arXiv: 1606.00434 [astro-ph.GA].

[256] G. Bruzual and S. Charlot, "Stellar population synthesis at the resolution of 2003," *Monthly Notices of the RAS*, vol. 344, no. 4, pp. 1000–1028, Oct. 2003. DOI: 10.1046/j.1365-8711.2003.06897.x. arXiv: astro-ph/0309134 [astro-ph].

[257] E. E. Salpeter, "The Luminosity Function and Stellar Evolution.," *Astrophysical Journal*, vol. 121, p. 161, Jan. 1955. DOI: 10.1086/145971.

[258] P. Madau, "Radiative transfer in a clumpy universe: The colors of high-redshift galaxies," *Astrophysical Journal*, vol. 441, pp. 18–27, Mar. 1995. DOI: 10.1086/175332.

[259] J. R. Bond, A. S. Szalay, and M. S. Turner, "Formation of Galaxies in a Gravitino-Dominated Universe," *Physical Review Letters*, vol. 48, no. 23, pp. 1636–1640, Jun. 1982. DOI: 10.1103/PhysRevLett.48.1636.

[260] N. Visvanathan and A. Sandage, "The color - absolute magnitude relation for E and S0 galaxies. I. Calibration and tests for universality using Virgo and eight other nearby clusters.," *Astrophysical Journal*, vol. 216, pp. 214–226, Aug. 1977. DOI: 10.1086/155464.

[261] R. G. Bower, J. R. Lucey, and R. S. Ellis, "Precision photometry of early-type galaxies in the Coma and Virgo clusters : a test of the universality of the colour-magnitude relation - II. Analysis.," *Monthly Notices of the RAS*, vol. 254, p. 601, Feb. 1992. DOI: 10.1093/mnras/254.4.601.

[262] P. G. van Dokkum and R. P. van der Marel, "The Star Formation Epoch of the Most Massive Early-Type Galaxies," *Astrophysical Journal*, vol. 655, no. 1, pp. 30–50, Jan. 2007. DOI: 10.1086/509633. arXiv: astro-ph/0609587 [astro-ph].

[263] M. Wold, L. Armus, G. Neugebauer, T. H. Jarrett, and M. D. Lehnert, "Overdensities of Extremely Red Objects in the Fields of High-Redshift Radio-Loud Quasars," *Astronomical Journal*, vol. 126, no. 4, pp. 1776–1786, Oct. 2003. DOI: 10.1086/378362. arXiv: astro-ph/0307224 [astro-ph].

[264] N. Kashikawa, T. Kitayama, M. Doi, T. Misawa, Y. Komiyama, and K. Ota, "The Habitat Segregation between Lyman Break Galaxies and Lyα Emitters around a QSO at $z \sim 5$," *Astrophysical Journal*, vol. 663, no. 2, pp. 765–773, Jul. 2007. DOI: 10.1086/518410. arXiv: 0704.2238 [astro-ph].

[265] J. A. Stevens, M. J. Jarvis, K. E. K. Coppin, M. J. Page, T. R. Greve, F. J. Carrera, and R. J. Ivison, "An excess of star-forming galaxies in the fields of high-redshift QSOs," *Monthly Notices of the RAS*, vol. 405, no. 4, pp. 2623–2638, Jul. 2010. DOI: 10.1111/j.1365-2966.2010.16641.x. arXiv: 1003.2166 [astro-ph.CO].

[266] R. F. Trainor and C. C. Steidel, "The Halo Masses and Galaxy Environments of Hyperluminous QSOs at $z \simeq 2.7$ in the Keck Baryonic Structure Survey," *Astrophysical Journal*, vol. 752, no. 1, 39, p. 39, Jun. 2012. DOI: 10.1088/0004-637X/752/1/39. arXiv: 1204.3636 [astro-ph.CO].

[267] J. F. Hennawi, J. X. Prochaska, S. Cantalupo, and F. Arrigoni-Battaia, "Quasar quartet embedded in giant nebula reveals rare massive structure in distant universe," *Science*, vol. 348, no. 6236, pp. 779–783, May 2015. DOI: 10.1126/science.aaa5397. arXiv: 1505.03786 [astro-ph.GA].

[268] Y. Yang, A. Zabludoff, C. Tremonti, D. Eisenstein, and R. Davé, "Extended Lyα Nebulae at $z \simeq 2.3$: An Extremely Rare and Strongly Clustered Population?" *Astrophysical Journal*, vol. 693, no. 2, pp. 1579–1587, Mar. 2009. DOI: 10.1088/0004-637X/693/2/1579. arXiv: 0811.3446 [astro-ph].

[269] Y. Yang, A. Zabludoff, D. Eisenstein, and R. Davé, "Strong Field-to-field Variation of Lyα Nebulae Populations at z ~= 2.3," *Astrophysical Journal*, vol. 719, no. 2, pp. 1654–1671, Aug. 2010. DOI: 10.1088/0004-637X/719/2/1654. arXiv: 1008.2776 [astro-ph.CO].

[270] M. K. M. Prescott, N. Kashikawa, A. Dey, and Y. Matsuda, "The Overdense Environment of a Large Lyα Nebula at z $\approx$ 2.7," *Astrophysical Journal, Letters*, vol. 678, no. 2, p. L77, May 2008. DOI: 10.1086/588606. arXiv: 0803.4230 [astro-ph].

[271] R. A. Overzier, "The realm of the galaxy protoclusters. A review," *Astronomy and Astrophysics Reviews*, vol. 24, no. 1, 14, p. 14, Nov. 2016. DOI: 10.1007/s00159-016-0100-3. arXiv: 1610.05201 [astro-ph.GA].

[272] J. D. Kurk, L. Pentericci, H. J. A. Röttgering, and G. K. Miley, "A search for clusters at high redshift. III. Candidate Hα emitters and EROs in the PKS 1138-262 proto-cluster at z = 2.16," *Astronomy and Astrophysics*, vol. 428, pp. 793–815, Dec. 2004. DOI: 10.1051/0004-6361:20040075. arXiv: astro-ph/0410202 [astro-ph].

[273] R. Shimakawa, T. Kodama, K. .-I. Tadaki, I. Tanaka, M. Hayashi, and Y. Koyama, "Identification of the progenitors of rich clusters and member galaxies in rapid formation at z ¿ 2.," *Monthly Notices of the RAS*, vol. 441, pp. L1–L5, Jun. 2014. DOI: 10.1093/mnrasl/slu029. arXiv: 1402.3568 [astro-ph.GA].

[274] X. Z. Zheng, Z. Cai, F. X. An, X. Fan, and D. D. Shi, "MAMMOTH: confirmation of two massive galaxy overdensities at z = 2.24 with Hα emitters," *Monthly Notices of the RAS*, vol. 500, no. 4, pp. 4354–4364, Jan. 2021. DOI: 10.1093/mnras/staa2882. arXiv: 2009.08068 [astro-ph.GA].

[275] C. C. Steidel, K. L. Adelberger, M. Dickinson, M. Giavalisco, M. Pettini, and M. Kellogg, "A Large Structure of Galaxies at Redshift Z approximately 3 and Its Cosmological Implications," *Astrophysical Journal*, vol. 492, no. 2, pp. 428–438, Jan. 1998. DOI: 10.1086/305073. arXiv: astro-ph/9708125 [astro-ph].

[276] H. T. Intema, B. P. Venemans, J. D. Kurk, M. Ouchi, T. Kodama, H. J. A. Röttgering, G. K. Miley, and R. A. Overzier, "Large-scale structure of Lyman break galaxies around a radio galaxy protocluster at z $\sim$ 4," *Astronomy and Astrophysics*, vol. 456, no. 2, pp. 433–437, Sep. 2006. DOI: 10.1051/0004-6361:20064812. arXiv: astro-ph/0606298 [astro-ph].

[277] R. A. Overzier, R. J. Bouwens, G. D. Illingworth, and M. Franx, "Clustering of i_{775} Dropout Galaxies at $z \sim 6$ in GOODS and the UDF," *Astrophysical Journal, Letters*, vol. 648, no. 1, pp. L5–L8, Sep. 2006. DOI: 10.1086/507678. arXiv: astro-ph/0607398 [astro-ph].

[278] J. Toshikawa, H. Uchiyama, N. Kashikawa, M. Ouchi, R. Overzier, Y. Ono, Y. Harikane, S. Ishikawa, T. Kodama, Y. Matsuda, Y.-T. Lin, M. Onoue, M. Tanaka, T. Nagao, M. Akiyama, Y. Komiyama, T. Goto, and C.-H. Lee, "GOLDRUSH. III. A systematic search for protoclusters at z $\sim$ 4 based on the ¿100 deg^2 area," *Publications of the ASJ*, vol. 70, S12, S12, Jan. 2018. DOI: 10.1093/pasj/psx102. arXiv: 1708.09421 [astro-ph.GA].

[279] Y.-K. Chiang, R. A. Overzier, K. Gebhardt, S. L. Finkelstein, C.-T. Chiang, G. J. Hill, G. A. Blanc, N. Drory, T. S. Chonis, G. R. Zeimann, A. Hagen, D. P. Schneider, S. Jogee, R. Ciardullo, and C. Gronwall, "Surveying Galaxy Proto-clusters in Emission: A Large-scale Structure at z = 2.44 and the Outlook for HETDEX," *Astrophysical Journal*, vol. 808, no. 1, 37, p. 37, Jul. 2015. DOI: 10.1088/0004-637X/808/1/37. arXiv: 1505.03877 [astro-ph.CO].

[280] C. De Breuck, F. Bertoldi, C. Carilli, A. Omont, B. Venemans, H. Röttgering, R. Overzier, M. Reuland, G. Miley, R. Ivison, and W. van Breugel, "A multi-wavelength study of the proto-cluster surrounding the z = 4.1 radio galaxy TN J1338-1942," *Astronomy and Astrophysics*, vol. 424, pp. 1–12, Sep. 2004. DOI: 10.1051/0004-6361:20035885. arXiv: astro-ph/0405339 [astro-ph].

[281] H. Dannerbauer, J. D. Kurk, C. De Breuck, D. Wylezalek, J. S. Santos, Y. Koyama, N. Seymour, M. Tanaka, N. Hatch, B. Altieri, D. Coia, A. Galametz, T. Kodama, G. Miley, H. Röttgering, M. Sanchez-Portal, I. Valtchanov, B. Venemans, and B. Ziegler, "An excess of dusty starbursts related to the Spiderweb galaxy," *Astronomy and Astrophysics*, vol. 570, A55, A55, Oct. 2014. DOI: 10.1051/0004-6361/201423771. arXiv: 1410.3730 [astro-ph.GA].

[282] E. E. Rigby, N. A. Hatch, H. J. A. Röttgering, B. Sibthorpe, Y. K. Chiang, R. Overzier, R. Herbonnet, S. Borgani, D. L. Clements, H. Dannerbauer, C. De Breuck, G. De Lucia, J. Kurk, F. Maschietto, G. Miley, A. Saro, N. Seymour, and B. Venemans, "Searching for large-scale structures around high-redshift radio galaxies with Herschel," *Monthly Notices of the RAS*, vol. 437, no. 2, pp. 1882–1893, Jan. 2014. DOI: 10.1093/mnras/stt2019. arXiv: 1310.5710 [astro-ph.CO].

[283] Y. Harikane, M. Ouchi, Y. Ono, S. Fujimoto, D. Donevski, T. Shibuya, A. L. Faisst, T. Goto, B. Hatsukade, N. Kashikawa, K. Kohno, T. Hashimoto, R. Higuchi, A. K. Inoue, Y.-T. Lin, C. L. Martin, R. Overzier, I. Smail, J. Toshikawa, H. Umehata, Y. Ao, S. Chapman, D. L. Clements, M. Im, Y. Jing, T. Kawaguchi, C.-H. Lee, M. M. Lee, L. Lin, Y. Matsuoka, M. Marinello, T. Nagao, M. Onodera, S. Toft, and W.-H. Wang, "SILVERRUSH. VIII. Spectroscopic Identifications of Early Large-scale Structures with Protoclusters over 200 Mpc at z $\sim$ 6-7: Strong Associations of Dusty Star-forming Galaxies," *Astrophysical Journal*, vol. 883, no. 2, 142, p. 142, Oct. 2019. DOI: 10.3847/1538-4357/ab2cd5. arXiv: 1902.09555 [astro-ph.GA].

[284] P. J. Francis, B. E. Woodgate, S. J. Warren, P. Møller, M. Mazzolini, A. J. Bunker, J. D. Lowenthal, T. B. Williams, T. Minezaki, Y. Kobayashi, and Y. Yoshii, "A Group of Galaxies at Redshift 2.38," *Astrophysical Journal*, vol. 457, p. 490, Feb. 1996. DOI: 10.1086/176747. arXiv: astro-ph/9511040 [astro-ph].

[285] C. W. Stark, M. White, K.-G. Lee, and J. F. Hennawi, "Protocluster discovery in tomographic Ly α forest flux maps," *Monthly Notices of the RAS*, vol. 453, no. 1, pp. 311–327, Oct. 2015. DOI: 10.1093/mnras/stv1620. arXiv: 1412.1507 [astro-ph.CO].

[286] L. Guaita, E. Gawiser, N. Padilla, H. Francke, N. A. Bond, C. Gronwall, R. Ciardullo, J. J. Feldmeier, S. Sinawa, G. A. Blanc, and S. Virani, "Lyα-emitting Galaxies at z = 2.1 in ECDF-S: Building Blocks of Typical Present-day Galaxies?" *Astrophysical Journal*, vol. 714, no. 1, pp. 255–269, May 2010. DOI: 10.1088/0004-637X/714/1/255. arXiv: 0910.2244 [astro-ph.CO].

[287] N. Scoville, H. Aussel, M. Brusa, P. Capak, C. M. Carollo, M. Elvis, M. Giavalisco, L. Guzzo, G. Hasinger, C. Impey, J. .-P. Kneib, O. LeFevre, S. J. Lilly, B. Mobasher, A. Renzini, R. M. Rich, D. B. Sanders, E. Schinnerer, D. Schminovich, P. Shopbell, Y. Taniguchi, and N. D. Tyson, "The Cosmic Evolution Survey (COSMOS): Overview," *Astrophysical Journal, Supplement*, vol. 172, no. 1, pp. 1–8, Sep. 2007. DOI: 10.1086/516585. arXiv: astro-ph/0612305 [astro-ph].

[288] C. Laigle, H. J. McCracken, O. Ilbert, B. C. Hsieh, I. Davidzon, P. Capak, G. Hasinger, J. D. Silverman, C. Pichon, J. Coupon, H. Aussel, D. Le Borgne, K. Caputi, P. Cassata, Y. .-Y. Chang, F. Civano, J. Dunlop, J. Fynbo, J. S. Kartaltepe, A. Koekemoer, O. Le Fèvre, E. Le Floc'h, A. Leauthaud, S. Lilly, L. Lin, S. Marchesi, B. Milvang-Jensen, M. Salvato, D. B. Sanders, N. Scoville, V. Smolcic, M. Stockmann, Y. Taniguchi, L. Tasca, S. Toft, M. Vaccari, and J. Zabl, "The COSMOS2015 Catalog: Exploring the 1 ¡ z ¡ 6 Universe with Half a Million Galaxies," *Astrophysical Journal, Supplement*, vol. 224, no. 2, 24, p. 24, Jun. 2016. DOI: 10.3847/0067-0049/224/2/24. arXiv: 1604.02350 [astro-ph.GA].

[289] C. M. Casey, A. Cooray, P. Capak, H. Fu, K. Kovac, S. Lilly, D. B. Sanders, N. Z. Scoville, and E. Treister, "A Massive, Distant Proto-cluster at z = 2.47 Caught in a Phase of Rapid Formation?" *Astrophysical Journal, Letters*, vol. 808, no. 2, L33, p. L33, Aug. 2015. DOI: 10.1088/2041-8205/808/2/L33. arXiv: 1506.01715 [astro-ph.GA].

[290] C. Diener, S. J. Lilly, C. Ledoux, G. Zamorani, M. Bolzonella, D. N. A. Murphy, P. Capak, O. Ilbert, and H. McCracken, "A Protocluster at z = 2.45," *Astrophysical Journal*, vol. 802, no. 1, 31, p. 31, Mar. 2015. DOI: 10.1088/0004-637X/802/1/31. arXiv: 1411.0649 [astro-ph.CO].

[291] K.-G. Lee, J. F. Hennawi, M. White, J. X. Prochaska, A. Font-Ribera, D. J. Schlegel, R. M. Rich, N. Suzuki, C. W. Stark, O. Le Fèvre, P. E. Nugent, M. Salvato, and G. Zamorani, "Shadow of a Colossus: A z = 2.44 Galaxy Protocluster Detected in 3D Lyα Forest Tomographic Mapping of the COSMOS Field," *Astrophysical Journal*, vol. 817, no. 2, 160, p. 160, Feb. 2016. DOI: 10.3847/0004-637X/817/2/160. arXiv: 1509.02833 [astro-ph.CO].

[292] T. Wang, D. Elbaz, E. Daddi, A. Finoguenov, D. Liu, C. Schreiber, S. Martín, V. Strazzullo, F. Valentino, R. van der Burg, A. Zanella, L. Ciesla, R. Gobat, A. Le Brun, M. Pannella, M. Sargent, X. Shu, Q. Tan, N. Cappelluti, and Y. Li, "Discovery of a Galaxy Cluster with a Violently Starbursting Core at z = 2.506," *Astrophysical Journal*, vol. 828, 56, p. 56, Sep. 2016. DOI: 10.3847/0004-637X/828/1/56. arXiv: 1604.07404.

[293] D. R. Harbeck, T. Boroson, M. Lesser, J. Rajagopal, A. Yeatts, C. Corson, W. Liu, I. Dell'Antonio, R. Kotulla, D. Ouellette, E. Hooper, M. Smith, R. Bredthauer, P. Martin, G. Muller, P. Knezek, and M. Hunten, "The WIYN one degree imager 2014: performance of the partially populated focal plane and instrument upgrade path," in *Ground-based and Airborne Instrumentation for Astronomy V*, S. K. Ramsay, I. S. McLean, and H. Takami, Eds., ser. Society of Photo-Optical Instrumentation Engineers (SPIE) Conference Series, vol. 9147, Jul. 2014, 91470P. DOI: 10.1117/12.2056651.

[294] D. R. Harbeck, M. Lesser, W. Liu, B. Stupak, R. George, R. Harris, G. Poczulp, J. Rajagopal, R. Kotulla, D. Ouellette, E. J. Hooper, M. Smith, D. Mason, P. Onaka, G. Chin, E. Hunting, and R. Christensen, "The WIYN one degree imager in 2018: an extended 30-detector focal plane," in *Ground-based and Airborne Instrumentation for Astronomy VII*, C. J. Evans, L. Simard, and H. Takami, Eds., ser. Society of Photo-Optical Instrumentation Engineers (SPIE) Conference Series, vol. 10702, Jul. 2018, p. 1 070 229. DOI: 10.1117/12.2311528. arXiv: 1806.01913 [astro-ph.IM].

[295] S. Miyazaki, Y. Komiyama, S. Kawanomoto, Y. Doi, H. Furusawa, T. Hamana, Y. Hayashi, H. Ikeda, Y. Kamata, H. Karoji, M. Koike, T. Kurakami, S. Miyama, T. Morokuma, F. Nakata, K. Namikawa, H. Nakaya, K. Nariai, Y. Obuchi, Y. Oishi, N. Okada, Y. Okura, P. Tait, T. Takata, Y. Tanaka, M. Tanaka, T. Terai, D. Tomono, F. Uraguchi, T. Usuda, Y. Utsumi, Y. Yamada, H. Yamanoi, H. Aihara, H. Fujimori, S. Mineo, H. Miyatake, M. Oguri, T. Uchida, M. M. Tanaka, N. Yasuda, M. Takada, H. Murayama, A. J. Nishizawa, N. Sugiyama, M. Chiba, T. Futamase, S.-Y. Wang, H.-Y. Chen, P. T. P. Ho, E. J. Y. Liaw, C.-F. Chiu, C.-L. Ho, T.-C. Lai, Y.-C. Lee, D.-Z. Jeng, S. Iwamura, R. Armstrong, S. Bickerton, J. Bosch, J. E. Gunn, R. H. Lupton, C. Loomis, P. Price, S. Smith, M. A. Strauss, E. L. Turner, H. Suzuki, Y. Miyazaki, M. Muramatsu, K. Yamamoto, M. Endo, Y. Ezaki, N. Ito, N. Kawaguchi, S. Sofuku, T. Taniike, K. Akutsu, N. Dojo, K. Kasumi, T. Matsuda, K. Imoto, Y. Miwa, M. Suzuki, K. Takeshi, and H. Yokota, "Hyper Suprime-Cam: System design and verification of image quality," *Publications of the ASJ*, vol. 70, S1, S1, Jan. 2018. DOI: 10.1093/pasj/psx063.

[296] Y. Komiyama, Y. Obuchi, H. Nakaya, Y. Kamata, S. Kawanomoto, Y. Utsumi, S. Miyazaki, F. Uraguchi, H. Furusawa, T. Morokuma, T. Uchida, H. Miyatake, S. Mineo, H. Fujimori, H. Aihara, H. Karoji, J. E. Gunn, and S.-Y. Wang, "Hyper Suprime-Cam: Camera dewar design," *Publications of the ASJ*, vol. 70, S2, S2, Jan. 2018. DOI: 10.1093/pasj/psx069.

[297] H. Aihara, Y. AlSayyad, M. Ando, R. Armstrong, J. Bosch, E. Egami, H. Furusawa, J. Furusawa, A. Goulding, Y. Harikane, C. Hikage, P. T. P. Ho, B.-C. Hsieh, S. Huang, H. Ikeda, M. Imanishi, K. Ito, I. Iwata, A. T. Jaelani, R. Kakuma, K. Kawana, S. Kikuta, U. Kobayashi, M. Koike, Y. Komiyama, X. Li, Y. Liang, Y.-T. Lin, W. Luo, R. Lupton, N. B. Lust, L. A. MacArthur, Y. Matsuoka, S. Mineo, H. Miyatake, S. Miyazaki, S. More, R. Murata, S. V. Namiki, A. J. Nishizawa, M. Oguri, N. Okabe, S. Okamoto, Y. Okura, Y. Ono, M. Onodera, M. Onoue, K. Osato, M. Ouchi, T. Shibuya, M. A. Strauss, N. Sugiyama, Y. Suto, M. Takada, Y. Takagi, T. Takata, S. Takita, M. Tanaka, T. Terai, Y. Toba, H. Uchiyama, Y. Utsumi, S.-Y. Wang, W. Wang, and Y. Yamada, "Second data release of the Hyper Suprime-Cam Subaru Strategic Program," *Publications of the ASJ*, p. 106, Oct. 2019. DOI: 10.1093/pasj/psz103. arXiv: 1905.12221 [astro-ph.IM].

[298] M. Sawicki, S. Arnouts, J. Huang, J. Coupon, A. Golob, S. Gwyn, S. Foucaud, T. Moutard, I. Iwata, C. Liu, L. Chen, G. Desprez, Y. Harikane, Y. Ono, M. A. Strauss, M. Tanaka, N. Thibert, M. Balogh, K. Bundy, S. Chapman, J. E. Gunn, B.-C. Hsieh, O. Ilbert, Y. Jing, O. LeFèvre, C. Li, Y. Matsuda, S. Miyazaki, T. Nagao, A. J. Nishizawa, M. Ouchi, K. Shimasaku, J. Silverman, S. de la Torre, L. Tresse, W.-H. Wang, C. J. Willott, T. Yamada, X. Yang, and H. K. C. Yee, "The CFHT large area U-band deep survey (CLAUDS)," *Monthly Notices of the RAS*, vol. 489, no. 4, pp. 5202–5217, Nov. 2019. DOI: 10.1093/mnras/stz2522. arXiv: 1909.05898 [astro-ph.GA].

[299] A. Gopu, S. Hayashi, M. D. Young, D. R. Harbeck, T. Boroson, W. Liu, R. Kotulla, R. Shaw, R. Henschel, J. Rajagopal, E. Stobie, P. Knezek, R. P. Martin, and K. Archbold, "ODI - Portal, Pipeline, and Archive (ODI-PPA): a web-based astronomical compute archive, visualization, and analysis service," in *Software and Cyberinfrastructure for Astronomy III*, ser. Proceedings of the SPIE, vol. 9152, Jul. 2014, 91520E. DOI: 10.1117/12.2057123.

[300] Gaia Collaboration, T. Prusti, J. H. J. de Bruijne, A. G. A. Brown, A. Vallenari, C. Babusiaux, C. A. L. Bailer-Jones, U. Bastian, M. Biermann, D. W. Evans, and et al., "The Gaia mission," *Astronomy and Astrophysics*, vol. 595, A1, A1, Nov. 2016. DOI: 10.1051/0004-6361/201629272. arXiv: 1609.04153 [astro-ph.IM].

[301] E. Bertin, Y. Mellier, M. Radovich, G. Missonnier, P. Didelon, and B. Morin, "The TERAPIX Pipeline," in *Astronomical Data Analysis Software and Systems XI, ASP Conference Proceedings, Vol. 281. Edited by David A. Bohlender, Daniel Durand, and Thomas H. Handley. ISBN: 1-58381-124-9. ISSN: 1080-7926. San Francisco: Astronomical Society of the Pacific, 2002, p. 228.* D. A. Bohlender, D. Durand, and T. H. Handley, Eds., ser. Astronomical Society of the Pacific Conference Series. 2002, vol. 281, p. 228.

[302] J. J. Adams, G. A. Blanc, G. J. Hill, K. Gebhardt, N. Drory, L. Hao, R. Bender, J. Byun, R. Ciardullo, M. E. Cornell, S. L. Finkelstein, A. Fry, E. Gawiser, C. Gronwall, U. Hopp, D. Jeong, A. Kelz, R. Kelzenberg, E. Komatsu, P. J. MacQueen, J. Murphy, P. S. Odoms, M. Roth, D. P. Schneider, J. R. Tufts, and C. P. Wilkinson, "The HETDEX Pilot Survey. I. Survey Design, Performance, and Catalog of Emission-line Galaxies," *Astrophysical Journal, Supplement*, vol. 192, no. 1, 5, p. 5, Jan. 2011. DOI: 10.1088/0067-0049/192/1/5. arXiv: 1011.0426 [astro-ph.CO].

[303] F. Civano, S. Marchesi, A. Comastri, M. C. Urry, M. Elvis, N. Cappelluti, S. Puccetti, M. Brusa, G. Zamorani, G. Hasinger, T. Aldcroft, D. M. Alexand er, V. Allevato, H. Brunner, P. Capak, A. Finoguenov, F. Fiore, A. Fruscione, R. Gilli, K. Glotfelty, R. E. Griffiths, H. Hao, F. A. Harrison, K. Jahnke, J. Kartaltepe, A. Karim, S. M. LaMassa, G. Lanzuisi, T. Miyaji, P. Ranalli, M. Salvato, M. Sargent, N. J. Scoville, K. Schawinski, E. Schinnerer, J. Silverman, V. Smolcic, D. Stern, S. Toft, B. Trakhtenbrot, E. Treister, and C. Vignali, "The Chandra Cosmos Legacy Survey: Overview and Point Source Catalog," *Astrophysical Journal*, vol. 819, no. 1, 62, p. 62, Mar. 2016. DOI: 10.3847/0004-637X/819/1/62. arXiv: 1601.00941 [astro-ph.GA].

[304] S. Marchesi, F. Civano, M. Elvis, M. Salvato, M. Brusa, A. Comastri, R. Gilli, G. Hasinger, G. Lanzuisi, T. Miyaji, E. Treister, C. M. Urry, C. Vignali, G. Zamorani, V. Allevato, N. Cappelluti, C. Cardamone, A. Finoguenov, R. E. Griffiths, A. Karim, C. Laigle, S. M. LaMassa, K. Jahnke, P. Ranalli, K. Schawinski, E. Schinnerer, J. D. Silverman, V. Smolcic, H. Suh, and B. Trakhtenbrot, "The Chandra COSMOS Legacy survey: optical/IR identifications," *Astrophysical Journal*, vol. 817, no. 1, 34, p. 34, Jan. 2016. DOI: 10.3847/0004-637X/817/1/34. arXiv: 1512.01105 [astro-ph.GA].

[305] D. E. Vanden Berk, G. T. Richards, A. Bauer, M. A. Strauss, D. P. Schneider, T. M. Heckman, D. G. York, P. B. Hall, X. Fan, G. R. Knapp, S. F. Anderson, J. Annis, N. A. Bahcall, M. Bernardi, J. W. Briggs, J. Brinkmann, R. Brunner, S. Burles, L. Carey, F. J. Castander, A. J. Connolly, J. H. Crocker, I. Csabai, M. Doi, D. Finkbeiner, S. Friedman, J. A. Frieman, M. Fukugita, J. E. Gunn, G. S. Hennessy, Ž. Ivezić, S. Kent, P. Z. Kunszt, D. Q. Lamb, R. F. Leger, D. C. Long, J. Loveday, R. H. Lupton, A. Meiksin, A. Merelli, J. A. Munn, H. J. Newberg, M. Newcomb, R. C. Nichol, R. Owen, J. R. Pier, A. Pope, C. M. Rockosi, D. J. Schlegel, W. A. Siegmund, S. Smee, Y. Snir, C. Stoughton, C. Stubbs, M. SubbaRao, A. S. Szalay, G. P. Szokoly, C. Tremonti, A. Uomoto, P. Waddell, B. Yanny, and W. Zheng, "Composite Quasar Spectra from the Sloan Digital Sky Survey," *Astronomical Journal*, vol. 122, no. 2, pp. 549–564, Aug. 2001. DOI: 10.1086/321167. arXiv: astro-ph/0105231 [astro-ph].

[306] E. Schinnerer, M. T. Sargent, M. Bondi, V. Smolčić, A. Datta, C. L. Carilli, F. Bertoldi, A. Blain, P. Ciliegi, A. Koekemoer, and N. Z. Scoville, "The VLA-COSMOS Survey. IV. Deep Data and Joint Catalog," *Astrophysical Journal, Supplement*, vol. 188, no. 2, pp. 384–404, Jun. 2010. DOI: 10.1088/0067-0049/188/2/384. arXiv: 1005.1641 [astro-ph.CO].

[307] K. Coppin, A. Pope, K. Menéndez-Delmestre, D. M. Alexander, J. S. Dunlop, E. Egami, J. Gabor, E. Ibar, R. J. Ivison, J. E. Austermann, A. W. Blain, S. C. Chapman, D. L. Clements, L. Dunne, S. Dye, D. Farrah, D. H. Hughes, A. M. J. Mortier, M. J. Page, M. Rowan-Robinson, D. Scott, C. Simpson, I. Smail, A. M. Swinbank, M. Vaccari, and M. S. Yun, "Mid-infrared Spectroscopy of Candidate Active Galactic Nuclei-dominated Sub-millimeter Galaxies," *Astrophysical Journal*, vol. 713, no. 1, pp. 503–519, Apr. 2010. DOI: 10.1088/0004-637X/713/1/503. arXiv: 1003.0447 [astro-ph.CO].

[308] R. D. Blandford and D. G. Payne, "Hydromagnetic flows from accretion disks and the production of radio jets.," *Monthly Notices of the RAS*, vol. 199, pp. 883–903, Jun. 1982. DOI: 10.1093/mnras/199.4.883.

[309] A. H. Bridle and R. A. Perley, "Extragalactic Radio Jets," *Annual Review of Astron and Astrophys*, vol. 22, pp. 319–358, Jan. 1984. DOI: 10.1146/annurev.aa.22.090184.001535.

[310] Y.-K. Chiang, R. Overzier, and K. Gebhardt, "Discovery of a Large Number of Candidate Protoclusters Traced by $\sim$ 15 Mpc-scale Galaxy Overdensities in COSMOS," *Astrophysical Journal, Letters*, vol. 782, no. 1, L3, p. L3, Feb. 2014. DOI: 10.1088/2041-8205/782/1/L3. arXiv: 1312.4747 [astro-ph.CO].

[311] Y. Koyama, I. Smail, J. Kurk, J. E. Geach, D. Sobral, T. Kodama, F. Nakata, A. M. Swinbank, P. N. Best, M. Hayashi, and K.-i. Tadaki, "On the evolution and environmental dependence of the star formation rate versus stellar mass relation since z $\sim$ 2," *Monthly Notices of the RAS*, vol. 434, no. 1, pp. 423–436, Sep. 2013. DOI: 10.1093/mnras/stt1035. arXiv: 1302.5315 [astro-ph.CO].

[312] T. Saito, Y. Matsuda, C. G. Lacey, I. Smail, A. Orsi, C. M. Baugh, A. K. Inoue, I. Tanaka, T. Yamada, K. Ohta, C. De Breuck, T. Kodama, and Y. Taniguchi, "The environments of Ly α blobs - I. Wide-field Ly α imaging of TN J1338-1942, a powerful radio galaxy at $z \simeq 4.1$ associated with a giant Ly α nebula," *Monthly Notices of the RAS*, vol. 447, no. 4, pp. 3069–3086, Mar. 2015. DOI: 10.1093/mnras/stu2538. arXiv: 1403.5924 [astro-ph.GA].

[313] C.-A. Faucher-Giguère, J. X. Prochaska, A. Lidz, L. Hernquist, and M. Zaldarriaga, "A Direct Precision Measurement of the Intergalactic Lyα Opacity at 2 ¡= z ¡= 4.2," *Astrophysical Journal*, vol. 681, no. 2, pp. 831–855, Jul. 2008. DOI: 10.1086/588648. arXiv: 0709.2382 [astro-ph].

[314] K. L. Adelberger, C. C. Steidel, A. E. Shapley, and M. Pettini, "Galaxies and Intergalactic Matter at Redshift $z \sim 3$: Overview," *Astrophysical Journal*, vol. 584, no. 1, pp. 45–75, Feb. 2003. DOI: 10.1086/345660. arXiv: astro-ph/0210314 [astro-ph].

[315] A. B. Newman, G. C. Rudie, G. A. Blanc, D. D. Kelson, S. Rhoades, T. Hare, V. Pérez, A. J. Benson, A. Dressler, V. Gonzalez, J. A. Kollmeier, N. P. Konidaris, J. S. Mulchaey, M. Rauch, O. Le Fèvre, B. C. Lemaux, O. Cucciati, and S. J. Lilly, "LATIS: The Lyα Tomography IMACS Survey," *Astrophysical Journal*, vol. 891, no. 2, 147, p. 147, Mar. 2020. DOI: 10.3847/1538-4357/ab75ee. arXiv: 2002.10676 [astro-ph.CO].

[316] R. Momose, K. Shimasaku, N. Kashikawa, K. Nagamine, I. Shimizu, K. Nakajima, Y. Terao, H. Kusakabe, M. Ando, K. Motohara, and L. Spitler, "Environmental Dependence of Galactic Properties Traced by Lyα Forest Absorption: Diversity among Galaxy Populations," *Astrophysical Journal*, vol. 909, no. 2, 117, p. 117, Mar. 2021. DOI: 10.3847/1538-4357/abd2af. arXiv: 2002.07335 [astro-ph.GA].

[317] R. S. Somerville and R. Davé, "Physical Models of Galaxy Formation in a Cosmological Framework," *Annual Review of Astron and Astrophys*, vol. 53, pp. 51–113, Aug. 2015. DOI: 10.1146/annurev-astro-082812-140951. arXiv: 1412.2712 [astro-ph.GA].

[318] R. S. Beckmann, J. Devriendt, A. Slyz, S. Peirani, M. L. A. Richardson, Y. Dubois, C. Pichon, N. E. Chisari, S. Kaviraj, C. Laigle, and M. Volonteri, "Cosmic evolution of stellar quenching by AGN feedback: clues from the Horizon-AGN simulation," *Monthly Notices of the RAS*, vol. 472, no. 1, pp. 949–965, Nov. 2017. DOI: 10.1093/mnras/stx1831. arXiv: 1701.07838 [astro-ph.GA].

[319] S. J. Penny, K. L. Masters, R. Smethurst, R. C. Nichol, C. M. Krawczyk, D. Bizyaev, O. Greene, C. Liu, M. Marinelli, S. B. Rembold, R. A. Riffel, G. d. S. Ilha, D. Wylezalek, B. H. Andrews, K. Bundy, N. Drory, D. Oravetz, and K. Pan, "SDSS-IV MaNGA: evidence of the importance of AGN feedback in low-mass galaxies," *Monthly Notices of the RAS*, vol. 476, no. 1, pp. 979–998, May 2018. DOI: 10.1093/mnras/sty202. arXiv: 1710.07568 [astro-ph.GA].

[320] G. R. Gisler, "Clusters of galaxies and the statistics of emission-line galaxies.," *Monthly Notices of the RAS*, vol. 183, pp. 633–643, Jun. 1978. DOI: 10.1093/mnras/183.4.633.

[321] A. von der Linden, V. Wild, G. Kauffmann, S. D. M. White, and S. Weinmann, "Star formation and AGN activity in SDSS cluster galaxies," *Monthly Notices of the RAS*, vol. 404, no. 3, pp. 1231–1246, May 2010. DOI: 10.1111/j.1365-2966.2010.16375.x. arXiv: 0909.3522 [astro-ph.CO].

[322] W. Mo, A. Gonzalez, D. Stern, M. Brodwin, B. Decker, P. Eisenhardt, E. Moravec, S. A. Stanford, and D. Wylezalek, "The Massive and Distant Clusters of WISE Survey. IV. The Distribution of Active Galactic Nuclei in Galaxy Clusters at z $\sim$ 1," *Astrophysical Journal*, vol. 869, no. 2, 131, p. 131, Dec. 2018. DOI: 10.3847/1538-4357/aaef83. arXiv: 1811.01826 [astro-ph.GA].

[323] B. D. Lehmer, D. M. Alexander, J. E. Geach, I. Smail, A. Basu-Zych, F. E. Bauer, S. C. Chapman, Y. Matsuda, C. A. Scharf, M. Volonteri, and T. Yamada, "The Chandra Deep Protocluster Survey: Evidence for an Enhancement of AGN Activity in the SSA22 Protocluster at z = 3.09," *Astrophysical Journal*, vol. 691, no. 1, pp. 687–695, Jan. 2009. DOI: 10.1088/0004-637X/691/1/687. arXiv: 0809.5058 [astro-ph].

[324] J. A. Digby-North, K. Nandra, E. S. Laird, C. C. Steidel, A. Georgakakis, M. Bogosavljević, D. K. Erb, A. E. Shapley, N. A. Reddy, and J. Aird, "Excess AGN activity in the z = 2.30 Protocluster in HS 1700+64," *Monthly Notices of the RAS*, vol. 407, no. 2, pp. 846–853, Sep. 2010. DOI: 10.1111/j.1365-2966.2010.16977.x. arXiv: 1005.1833 [astro-ph.CO].

[325] S. Alberts, A. Pope, M. Brodwin, S. M. Chung, R. Cybulski, A. Dey, P. R. M. Eisenhardt, A. Galametz, A. H. Gonzalez, B. T. Jannuzi, S. A. Stanford, G. F. Snyder, D. Stern, and G. R. Zeimann, "Star Formation and AGN Activity in Galaxy Clusters from z=1-2: a Multi-Wavelength Analysis Featuring Herschel/PACS," *Astrophysical Journal*, vol. 825, no. 1, 72, p. 72, Jul. 2016. DOI: 10.3847/0004-637X/825/1/72. arXiv: 1604.03564 [astro-ph.GA].

[326] C. Krishnan, N. A. Hatch, O. Almaini, D. Kocevski, E. A. Cooke, W. G. Hartley, G. Hasinger, D. T. Maltby, S. I. Muldrew, and C. Simpson, "Enhancement of AGN in a protocluster at z = 1.6," *Monthly Notices of the RAS*, vol. 470, no. 2, pp. 2170–2178, Sep. 2017. DOI: 10.1093/mnras/stx1315. arXiv: 1705.10799 [astro-ph.GA].

[327] M. C. Cooper, J. A. Newman, B. J. Weiner, R. Yan, C. N. A. Willmer, K. Bundy, A. L. Coil, C. J. Conselice, M. Davis, S. M. Faber, B. F. Gerke, P. Guhathakurta, D. C. Koo, and K. G. Noeske, "The DEEP2 Galaxy Redshift Survey: the role of galaxy environment in the cosmic star formation history," *Monthly Notices of the RAS*, vol. 383, no. 3, pp. 1058–1078, Jan. 2008. DOI: 10.1111/j.1365-2966.2007.12613.x. arXiv: 0706.4089 [astro-ph].

[328] R. Shimakawa, T. Kodama, M. Hayashi, J. X. Prochaska, I. Tanaka, Z. Cai, T. L. Suzuki, K.-i. Tadaki, and Y. Koyama, "MAHALO Deep Cluster Survey I. Accelerated and enhanced galaxy formation in the densest regions of a protocluster at z = 2.5," *Monthly Notices of the RAS*, vol. 473, no. 2, pp. 1977–1999, Jan. 2018. DOI: 10.1093/mnras/stx2494. arXiv: 1708.06369 [astro-ph.GA].

[329] M. Volonteri, F. Haardt, and P. Madau, "The Assembly and Merging History of Supermassive Black Holes in Hierarchical Models of Galaxy Formation," *Astrophysical Journal*, vol. 582, no. 2, pp. 559–573, Jan. 2003. DOI: 10.1086/344675. arXiv: astro-ph/0207276 [astro-ph].

[330] O. Fakhouri and C.-P. Ma, "Environmental dependence of dark matter halo growth - I. Halo merger rates," *Monthly Notices of the RAS*, vol. 394, no. 4, pp. 1825–1840, Apr. 2009. DOI: 10.1111/j.1365-2966.2009.14480.x. arXiv: 0808.2471 [astro-ph].

[331] N. Cappelluti, V. Allevato, and A. Finoguenov, "Clustering of X-Ray-Selected AGN," *Advances in Astronomy*, vol. 2012, 853701, p. 853 701, Jan. 2012. DOI: 10.1155/2012/853701. arXiv: 1201.3920 [astro-ph.CO].

[332] N. K. Hine, J. E. Geach, D. M. Alexander, B. D. Lehmer, S. C. Chapman, and Y. Matsuda, "An enhanced merger fraction within the galaxy population of the SSA22 protocluster at z = 3.1," *Monthly Notices of the RAS*, vol. 455, no. 3, pp. 2363–2370, Jan. 2016. DOI: 10.1093/mnras/stv2448. arXiv: 1506.05115 [astro-ph.GA].

[333] J. M. Lotz, C. Papovich, S. M. Faber, H. C. Ferguson, N. Grogin, Y. Guo, D. Kocevski, A. M. Koekemoer, K.-S. Lee, D. McIntosh, I. Momcheva, G. Rudnick, A. Saintonge, K.-V. Tran, A. van der Wel, and C. Willmer, "Caught in the Act: The Assembly of Massive Cluster Galaxies at z = 1.62," *Astrophysical Journal*, vol. 773, no. 2, 154, p. 154, Aug. 2013. DOI: 10.1088/0004-637X/773/2/154.

[334] H. Umehata, M. Fumagalli, I. Smail, Y. Matsuda, A. M. Swinbank, S. Cantalupo, C. Sykes, R. J. Ivison, C. C. Steidel, A. E. Shapley, J. Vernet, T. Yamada, Y. Tamura, M. Kubo, K. Nakanishi, M. Kajisawa, B. Hatsukade, and K. Kohno, "Gas filaments of the cosmic web located around active galaxies in a protocluster," *Science*, vol. 366, no. 6461, pp. 97–100, Oct. 2019. DOI: 10.1126/science.aaw5949. arXiv: 1910.01324 [astro-ph.GA].

[335] R. A. Overzier, N. P. H. Nesvadba, M. Dijkstra, N. A. Hatch, M. D. Lehnert, M. Villar-Martín, R. J. Wilman, and A. W. Zirm, "Resolving the Optical Emission Lines of Lyα Blob "B1" at z = 2.38: Another Hidden Quasar," *Astrophysical Journal*, vol. 771, no. 2, 89, p. 89, Jul. 2013. DOI: 10.1088/0004-637X/771/2/89. arXiv: 1305.2926 [astro-ph.CO].

[336] D. M. Alexander, J. M. Simpson, C. M. Harrison, J. R. Mullaney, I. Smail, J. E. Geach, R. C. Hickox, N. K. Hine, A. Karim, M. Kubo, B. D. Lehmer, Y. Matsuda, D. J. Rosario, F. Stanley, A. M. Swinbank, H. Umehata, and T. Yamada, "ALMA observations of a z $\approx$ 3.1 protocluster: star formation from active galactic nuclei and Lyman-alpha blobs in an overdense environment," *Monthly Notices of the RAS*, vol. 461, no. 3, pp. 2944–2952, Sep. 2016. DOI: 10.1093/mnras/stw1509. arXiv: 1601.00682 [astro-ph.GA].

[337] R. Momose, T. Goto, Y. Utsumi, T. Hashimoto, C.-Y. Chiang, S.-J. Kim, N. Kashikawa, K. Shimasaku, and S. Miyazaki, "Possible evolution of the circum-galactic medium around QSOs with QSO age and cosmic time revealed by Ly α haloes," *Monthly Notices of the RAS*, vol. 488, no. 1, pp. 120–134, Sep. 2019. DOI: 10.1093/mnras/stz1707. arXiv: 1809.10916 [astro-ph.GA].

[338] E. Daddi, F. Valentino, R. M. Rich, J. D. Neill, M. Gronke, D. O'Sullivan, D. Elbaz, F. Bournaud, A. Finoguenov, A. Marchal, I. Delvecchio, S. Jin, D. Liu, V. Strazzullo, A. Calabro, R. Coogan, C. D'Eugenio, R. Gobat, B. S. Kalita, P. Laursen, D. C. Martin, A. Puglisi, E. Schinnerer, and T. Wang, "Three Lyman-α-emitting filaments converging to a massive galaxy group at z = 2.91: discussing the case for cold gas infall," *Astronomy and Astrophysics*, vol. 649, A78, A78, May 2021. DOI: 10.1051/0004-6361/202038700. arXiv: 2006.11089 [astro-ph.GA].

[339] E. Daddi, R. M. Rich, F. Valentino, S. Jin, I. Delvecchio, D. Liu, V. Strazzullo, J. Neill, R. Gobat, A. Finoguenov, F. Bournaud, D. Elbaz, B. S. Kalita, D. O'Sullivan, and T. Wang, "Evidence for the cold-stream to hot-accretion transition as traced by Lya emission from groups and clusters at 2¡z¡3.3," *arXiv e-prints*, arXiv:2202.03715, arXiv:2202.03715, Feb. 2022. arXiv: 2202.03715 [astro-ph.CO].

[340] O. Cucciati, G. Zamorani, B. C. Lemaux, S. Bardelli, A. Cimatti, O. Le Fèvre, P. Cassata, B. Garilli, V. Le Brun, D. Maccagni, L. Pentericci, L. A. M. Tasca, R. Thomas, E. Vanzella, E. Zucca, R. Amorin, P. Capak, L. P. Cassarà, M. Castellano, J. G. Cuby, S. de la Torre, A. Durkalec, A. Fontana, M. Giavalisco, A. Grazian, N. P. Hathi, O. Ilbert, C. Moreau, S. Paltani, B. Ribeiro, M. Salvato, D. Schaerer, M. Scodeggio, V. Sommariva, M. Talia, Y. Taniguchi, L. Tresse, D. Vergani, P. W. Wang, S. Charlot, T. Contini, S. Fotopoulou, C. López-Sanjuan, Y. Mellier, and N. Scoville, "Discovery of a rich proto-cluster at z = 2.9 and associated diffuse cold gas in the VIMOS Ultra-Deep Survey (VUDS)," *Astronomy and Astrophysics*, vol. 570, A16, A16, Oct. 2014. DOI: 10.1051/0004-6361/201423811. arXiv: 1403.3691 [astro-ph.CO].

[341] M. W. Topping, A. E. Shapley, C. C. Steidel, S. Naoz, and J. R. Primack, "Understanding Large-scale Structure in the SSA22 Protocluster Region Using Cosmological Simulations," *Astrophysical Journal*, vol. 852, no. 2, 134, p. 134, Jan. 2018. DOI: 10.3847/1538-4357/aa9f0f. arXiv: 1709.06572 [astro-ph.GA].

[342] W. Hu, J. Wang, L. Infante, J. E. Rhoads, Z.-Y. Zheng, H. Yang, S. Malhotra, L. F. Barrientos, C. Jiang, J. González-López, G. Prieto, L. A. Perez, P. Hibon, G. Galaz, A. Coughlin, S. Harish, X. Kong, W. Kang, A. A. Khostovan, J. Pharo, F. Valdes, I. Wold, A. R. Walker, and X. Zheng, "A Lyman-α protocluster at redshift 6.9," *Nature Astronomy*, vol. 5, pp. 485–490, Jan. 2021. DOI: 10.1038/s41550-020-01291-y. arXiv: 2101.10204 [astro-ph.GA].

[343] B. Flaugher, H. T. Diehl, K. Honscheid, T. M. C. Abbott, O. Alvarez, R. Angstadt, J. T. Annis, M. Antonik, O. Ballester, L. Beaufore, and D. et al, "The Dark Energy Camera," *The Astronomical Journal*, vol. 150, no. 5, 150, p. 150, Nov. 2015. DOI: 10.1088/0004-6256/150/5/150. arXiv: 1504.02900 [astro-ph.IM].

[344] Planck Collaboration, N. Aghanim, B. Altieri, M. Arnaud, M. Ashdown, J. Aumont, C. Baccigalupi, A. J. Banday, R. B. Barreiro, N. Bartolo, E. Battaner, and A. e. a. Beelen, "Planck intermediate results. XXVII. High-redshift infrared galaxy overdensity candidates and lensed sources discovered by Planck and confirmed by Herschel-SPIRE," *Astronomy and Astrophysics*, vol. 582, A30, A30, Oct. 2015. DOI: 10.1051/0004-6361/201424790. arXiv: 1503.08773 [astro-ph.GA].

[345] Planck Collaboration, P. A. R. Ade, N. Aghanim, M. Arnaud, J. Aumont, C. Baccigalupi, A. J. Banday, R. B. Barreiro, N. Bartolo, E. Battaner, and K. e. a. Benabed, "Planck intermediate results. XXXIX. The Planck list of high-redshift source candidates," *Astronomy and Astrophysics*, vol. 596, A100, A100, Dec. 2016. DOI: 10.1051/0004-6361/201527206. arXiv: 1508.04171 [astro-ph.GA].

[346] M. Negrello, J. Gonzalez-Nuevo, G. De Zotti, M. Bonato, Z. .-Y. Cai, D. Clements, L. Danese, H. Dole, J. Greenslade, A. Lapi, and L. Montier, "On the statistics of proto-cluster candidates detected in the Planck all-sky survey," *Monthly Notices of the Royal Astronomical Society*, vol. 470, no. 2, pp. 2253–2261, Sep. 2017. DOI: 10.1093/mnras/stx1367. arXiv: 1706.00116 [astro-ph.GA].

[347] C. Gouin, N. Aghanim, H. Dole, M. Polletta, and C. Park, "Questioning Planck-selected star-forming high-redshift galaxy protoclusters and their fate," *arXiv e-prints*, arXiv:2203.16276, arXiv:2203.16276, Mar. 2022. arXiv: 2203.16276 [astro-ph.CO].

[348] S. Lim, D. Scott, A. Babul, D. J. Barnes, S. T. Kay, I. G. McCarthy, D. Rennehan, and M. Vogelsberger, "Is there enough star formation in simulated protoclusters?" *Monthly Notices of the Royal Astronomical Society*, vol. 501, no. 2, pp. 1803–1822, Feb. 2021. DOI: 10.1093/mnras/staa3693. arXiv: 2010.02259 [astro-ph.GA].